REPORT NO.
UCB/EERC-80/40
OCTOBER 1980

INELASTIC BUCKLING OF STEEL STRUTS UNDER CYCLIC LOAD REVERSALS

by
R. GARY BLACK
W.A. BILL WENGER
EGOR P. POPOV

Report to Sponsors:
National Science Foundation
American Iron and Steel Institute

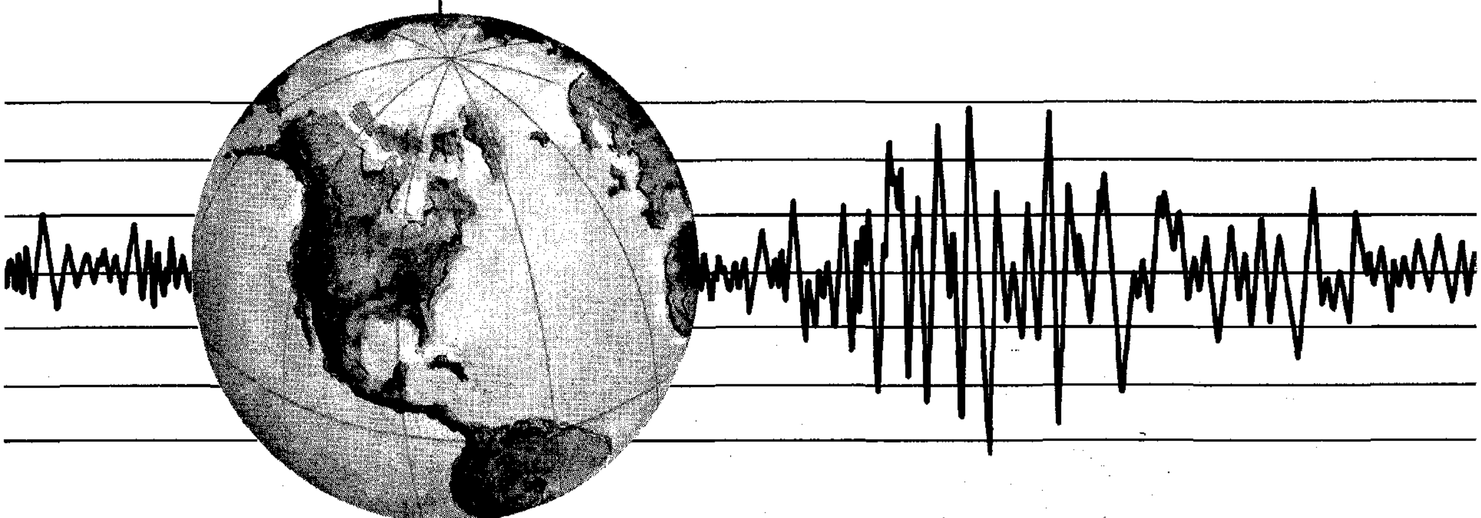

COLLEGE OF ENGINEERING
UNIVERSITY OF CALIFORNIA · Berkeley, California

For sale by the National Technical Information Service, U.S. Department of Commerce, Springfield, Virginia 22161.

See back of report for up to date listing of EERC reports.

50272-101

REPORT DOCUMENTATION PAGE	1. REPORT NO. NSF/RA-800299	2.	3. Recipient's Accession No. PB81 154312

4. Title and Subtitle
Inelastic Buckling of Steel Struts Under Cyclic Load Reversals

5. Report Date
October 1980

6.

7. Author(s)
R. Gary Black, W. A. Bill Wenger and Egor P. Popov

8. Performing Organization Rept. No.
UCB/EERC-80/40

9. Performing Organization Name and Address
Earthquake Engineering Research Center
University of California, Berkeley
Richmond Field Station
47th Street & Hoffman Blvd.
Richmond, Calif. 94804

10. Project/Task/Work Unit No.

11. Contract(C) or Grant(G) No.
(C) ENV 7604263
(G) PFR 7908984

12. Sponsoring Organization Name and Address
National Science Foundation
1800 G Street, N.W.
Washington, D.C. 20550

American Iron & Steel Institute
1000 - 16th Street, N.W.
Washington, D.C. 20036

13. Type of Report & Period Covered

14.

15. Supplementary Notes

16. Abstract (Limit: 200 words)

Cyclic axial loading experiments simulating severe seismic conditions are described for twenty-four structural steel struts of sizes and shapes typically employed as braces in small to moderately large steel buildings. The cross-sectional geometries of the specimens were also chosen to model the larger, heavier struts. Six of the twenty-four members were pinned at one end and fixed at the other, while the remaining eighteen were pinned at both ends. The range of cross-sectional shapes included wide flanges, double-angles, double-channels, structural tees, thin and thick-walled pipes, and thin and thick-walled square tubes.

The responses of the specimens are evaluated and special attention paid to the effects of cross-sectional shape, end conditions, and slenderness ratio using hysteretic envelopes. While investigating the major parameters that influence a member's performance under cyclic loading, some important properties were recognized and quantified. Reduction factors were developed, which can account for the Bauschinger effect and initial curvature of struts. These factors can be used with an AISC code determined load to estimate the deteriorating compressive capacity of a strut during a few consecutive cycles of full inelastic load reversals.

Some design recommendations are made for built-up members likely to experience severe load reversals.

18. Availability Statement:
Release Unlimited

19. Security Class (This Report)

20. Security Class (This Page)

21. No. of Pages

22. Price

(See ANSI-Z39.18) See Instructions on Reverse

OPTIONAL FORM 272 (4-77)
(Formerly NTIS-35)
Department of Commerce

INELASTIC BUCKLING OF STEEL STRUTS UNDER CYCLIC LOAD REVERSALS

R. Gary Black
Research Assistant

W. A. (Bill) Wenger
Research Assistant

Egor P. Popov
Professor of Civil Engineering
University of California, Berkeley

Report to Sponsors
National Science Foundation
American Iron and Steel Institute

Report No. UCB/EERC-80/40
Earthquake Engineering Research Center
College of Engineering
University of California
Berkeley, California

October 1980

ABSTRACT

Cyclic axial loading experiments simulating severe seismic conditions are described for twenty-four structural steel struts. The size and shape of the specimens were those typically employed as braces in small to moderately large steel buildings. The cross-sectional geometries of the specimens were chosen, however, so as to also model the larger, heavier struts. Six of the twenty-four members were pinned at one end and fixed at the other, while the remaining eighteen were pinned at both ends. The range of cross-sectional shapes included wide flanges, double-angles, double-channels, structural tees, thin and thick-walled pipes, and thin and thick-walled square tubes.

The responses of the specimens are compared and evaluated with special attention paid to the effects of cross-sectional shape, end conditions, and slenderness ratio using hysteretic envelopes. While investigating the major parameters that influence a member's performance under cyclic loading, some important properties were recognized and quantified. These findings resulted in the development of reduction factors which can account for the Bauschinger effect and initial curvature of struts. These factors can be used with an AISC code determined load to estimate the deteriorating compressive capacity of a strut during a few consecutive cycles of full inelastic load reversals.

Based on these experiments some design recommendations are made for built-up members likely to experience severe load reversals. It is suggested that these recommendations be considered for inclusion in seismic codes.

ACKNOWLEDGEMENTS

The writers gratefully acknowledge NSF support under Grants ENV 7604263 and PFR 7908984 with some support from AISI which made this work possible. Any opinions, findings, and conclusions or recommendations expressed in this report are those of the authors and do not necessarily reflect the views of the sponsors. A number of graduate students and members of the laboratory staff participated in the project. Willy Yau was particularly helpful with the experimental work, as were Bruce Fong, Perry Chin, Keith Hjelmstad, Victor Zayas, and Barry Lotz. Benson Shing was largely responsible for the data reduction. Their help is greatly appreciated.

TABLE OF CONTENTS

LIST OF SYMBOLS

A	Cross-sectional area
b	Breadth or width of compression element
c	Distance from neutral axis to extreme fiber
d	Depth of member
E	Modulus of elasticity
E_r	Reduced modulus
E_t	Tangent modulus
e	Load eccentricity
F.S.	Factor of safety
K	Effective length factor for a column
ℓ	Actual unbraced length of a column
P	Applied axial load
P_{cr}	Critical buckling load
P_{cr}^{exp}	Experimentally determined buckling load
P_{cr}^{calc}	Calculated or theoretical buckling load
P_y	Axial yield Load
Q_s	Axial stress reduction factor where width-thickness ratio of unstiffened elements exceeds AISC limiting values
R_B	Reduction factor due to the Bauschinger effect
R_E	Reduction factor due to specimen curvature or load eccentricity
r	Radius of gyration
s	Core radius equal to r/c
t	Thickness
e/s	Eccentricity ratio
$K\ell/r$	Effective slenderness ratio
ℓ/r	Slenderness ratio

Δ	Lateral displacement of a strut
δ	Axial displacement of a strut
δ_y	Axial yield displacement
ε	Axial strain
ε_p	Inelastic (plastic) strain
$\Sigma\varepsilon_p$	Cumulative inelastic (plastic) strain
ε_y	Axial yield strain
σ_{cr}	Critical buckling stress
σ_{cr}^{calc}	Calculated critical buckling stress
σ_{cr}^{exp}	Experimental buckling stress
σ_y	Axial yield stress

1. INTRODUCTION

1.1 General

Moment-resisting structural steel frames are widely used in the design of buildings in seismically active regions. Their past performance in well designed structures appears to be satisfactory. However, some of the more recent experience during severe earthquakes suggests that stiffer buildings possessing good ductility, perform particularly well, developing limited non-structural damage [1]*. Further, it is often economically infeasible to use moment-resisting frames to resist lateral forces along the narrow widths of a building. In such applications the use of diagonally braced steel frames provides a practical alternative. However, the information on the behavior of braces under severe load reversals is very limited, and for this reason there is hesitancy on the part of some engineers to employ them. This investigation tries to provide some of the needed data. No attempt is made to consider other framing systems, such as eccentric bracing [2], which can be used as alternative solutions.

Since the overall performance of a conventionally braced frame depends mainly on the performance of the brace, the focus of this report is on the bracing member itself. During a severe earthquake the lateral deflections of the frame cause the brace to alternately stretch and buckle. It is this action, the hysteretic behavior of the brace, that is responsible for the energy absorption and dissipation, and in large measure for the performance of a frame.

---

*Bracketed numbers indicate references listed at the end.

1.2 Objective

This research program experimentally evaluates the hysteretic behavior of axially loaded steel struts having cross-sectional shapes and slenderness ratios frequently encountered in practice. All test specimens were made from commercially available steel such as used in building construction. The results of this investigation are compared with conventional design procedures for axially loaded members based on current code [3]. Some suggestions for analytic prediction of deteriorating capacity of struts due to severe cyclic loading are advanced.

1.3 Scope

A total of twenty-four specimens were subjected to cyclic quasi-statically applied axial loads simulating earthquake effects. The structural shapes tested were wide-flanges, double-angles, double-channels, and both thick and thin round and square tubes. The specimen sections were representative of those used in smaller structures, and were so selected that they simulated some frequently used sections of larger members. The material for all rolled sections conformed to ASTM specifications for A36 steel; for pipes, to A53 Grade B steel; for square tubes, to A501 steel. Eighteen of the specimens were pinned at both ends and had slenderness ratios of 40, 80 and 120; the remaining six specimens, pinned at one end and fixed at the other, had slenderness ratios of 40 and 80.

2. SPECIMEN SELECTION

Each of the twenty-four test specimens was selected from structural steel shapes which are frequently used as brace elements in design. Since the efficiency of a brace under compressive load is reduced by a tendency to buckle locally, a typical brace element is a compact section and design was generally consistent with this criterion. As a group, the specimens represent typical braces of smaller sizes used in practice. In addition, they serve as models for the larger sections.

2.1 Selection

Individual specimens were chosen from standard structural steel shapes primarily on the basis of two criteria: first, that the slenderness ratios of the test specimens be appropriate to those used in practice; and second, that a group of member shapes and proportions be selected which adequately represent the great variety of brace and strut members in current use.

Since the effective slenderness ratio $K\ell/r$ of a compression member has been shown to be the single most important parameter in determining its hysteretic behavior [4,5,6,7,8 and 9], care was taken that the chosen $K\ell/r$'s allow the specimens to be compared with one another as well as with members used in practice. A common slenderness ratio of 80 was used for specimens within each structural shape category to allow for a direct comparison of results due to variation in shape. In addition, slenderness ratios of 40, close to the range of plastic action, and 120, very near the elastic buckling range, were assigned to both wide-flange and double-angle sections.

On the basis of its frequency and importance in applications, the wide flange section was chosen as the basic test shape and is consequently represented by nine of the twenty-four specimens. Eight of the nine were selected to be compact sections as defined by the AISC specifications [3], whereas one, a W 6x15.5, was expected to exhibit local plate buckling. Four of the wide flange struts were W 6x20's. All were cut from the same piece of mill stock; three of them had a slenderness ratio of 80 and one a $K\ell/r$ of 40. The W 6x20 shape was emphasized among the wide-flange specimens because its proportions are similar to those of the widely used larger W 10 and W 14 sections. The $K\ell/r$'s for the W 6×15.5 and W×625 shapes were 40. The three sizes W 6×25, W 6×20 and W 6×15.5 together comprise a complete AISC weight group and, either themselves or as models, define a desirable range of wide-flange strut sections.

Three additional wide-flange specimens were selected, a W 8×20 ($K\ell/r$ of 120), a W 6×16 ($K\ell/r$ of 120) and a W 5×16 ($K\ell/r$ of 80). The first two have low b/d ratios resulting in narrow cross-sections and slender members which, though lower in the initial buckling load than sections of the same weight which are square, might be expected to exhibit elastic behavior over a larger number of cycles than the more compact shapes.

The fabricated double-angle and double-channel sections are traditionally two of the most common of all brace shapes. Placed back-to-back and usually spaced apart by the width of a gusset plate, the two individual angles or channels are fastened, or "stitched" together at intervals so that the pair of elements act as a single member. Whether or not the action of such a member as a whole, or the action of the angles or channels as individual components, controls the behavior, makes the built-up section one of particular interest.

Five built-up specimens were selected: four double-angles and one double-channel. The largest double-angle specimens, 2-L 6x3½x3/8 with long legs back-to-back, and the only double-channel section, 2-C 8x11.5, had virtually the same cross-sectional area, but were assigned slenderness ratios of 80 and 120, respectively. Among the double-angle specimens, the two 2-L 6x3½x3/8 members were chosen as representative of the more slender (defined by the ratio of long leg length to short leg length) double-angle sections most commonly in use, and were expected to buckle about the Y-axis (AISC coordinate system). The second kind of a double-angle specimen, 2-L 5x3½x3/8 with long legs back-to-back and a $K\ell/r$ of 40, also was to buckle about its Y-axis. The third kind of a double-angle specimen selected 2-L 4x3½x3/8 with long legs back-to-back, and a $K\ell/r$ of 80, represents a section which is more square, and which would buckle about the X-axis. All five of these specimens, double-angle and double-channel alike, were made of plates thick enough to require, according to the AISC specifications [3], little or no axial stress reduction. Thus, they were expected to exhibit little or no local plate buckling under the initial compression loading. All double-angle and double-channels were placed back-to-back and fastened, or "stitched" together at intervals. For Strut 8 a "stitch" was placed at mid-length; for all other members the stitches were located at third-points.

Similar in overall cross-sectional shape to the double-angle, but more economical of material and fabrication time, the structural tee is becoming increasingly popular for brace and strut applications. Two tee specimens were selected, both split from W sections, both of the same area, and both with a $K\ell/r$ of 80. The primary difference between the two was that the first specimen shape, a WT 5x22.5, is relatively square in cross-section and would buckle naturally about the X-axis, while the other tee shape, a WT 8x22.5, is more slender in shape (the web plate much taller than the flange width requiring an axial stress reduction factor of $Q_s = 0.908$), and would be expected to buckle about the Y-axis. Most structural tees in use today can be expected to fall somewhere between these two extremes.

Like the built-up sections above, tubular members are also traditionally popular choices for brace and strut applications. Consequently, the fourth and last group of specimens selected were tubular in shape, five round and three square. Two identical circular tube specimens of 4 in. (100 mm) standard weight pipe were chosen to allow for comparisons based on different loading histories. The third specimen, a 4 in. (100 mm) extra strong pipe was chosen for its thicker wall, and a 3½ in. (89 mm) standard weight pipe was used for the fixed-pinned specimen. All three square tubular specimens were 4 x 4 in. (100 x 100 mm). Two of them had a ¼ in. (6 mm) wall-thickness, and one ½ in. (13 mm). These specimens were chosen to illustrate the general behavior of tubes in cyclic loading in comparison with the specimens of other shapes.

The complete program consisted of testing twenty-four specimens: nine wide-flanges, four double-angles, one double-channel, two structural tees, and five circular and three square tubes. Table 1 lists each specimen by structural shape, slenderness ratio, overall length and end conditions. The structural sizes were as selected, and the specimen lengths were implicit within the selected slenderness ratios. All rolled sections were of A36 steel, whereas all pipes were of A53 Grade B steel, and tubes of A501 steel.

A companion report, Ref. 10, details the behavior under cyclic loading of thin-walled circular tubes with the diameter to wall-thickness ratios of 33 and 48. Pipes of such geometry are generally used in fixed offshore platform construction.

2.2 Design of Specimens

Eighteen of the test specimens were designed to be pinned at both ends to correspond to the fundamental case of boundary conditions for a column (Table 1). To obtain some insight on the effect of other boundary conditions, six additional test specimens were pinned at one end and fixed at the other. Five of the specimens had a $K\ell/r$ of 40, fifteen had a $K\ell/r$ of 80, and 4 had a $K\ell/r$ of 120.

The basic specimens were made-up as shown in Figs. 1, 2 and 3 with the test sections welded to 1½ to 2½ in. (38 to 64 mm) thick end plates by means of full-penetration welds. Members made-up of double angles and channels had 3/8 in. (9.5 mm) thick welded on spacers at third-points of a member's length.* The end plates of the strut assembly were attached either to the clevises or to the test fixture by means of high strength bolts as shown diagrammatically in Fig. 4. In a fully assembled strut, the pins were oriented perpendicularly to the plane of buckling. A detail of a pinned connection is shown in Fig. 5. Further details may be seen from Fig. 6. Note that the large pins rotate inside large roller bearings.

Since in relation to a test section the end plates and clevises are very large, these regions can be considered as infinitely rigid. However, as can be shown using a solution given by von Karman and Biot [11], this effect on the buckling load capacity of an elastic column is small providing the regions of large column stiffness at the ends are small. With this in mind, the clevises were made as short as possible with a dimension of 7 in. (180 mm) from the center of a pin to the face of a mating flange. With this precaution the anticipated error from this source was considered to be negligible. Similarly, because of the conservative choice of bolt sizes in the connecting joint, it was estimated that generally less than 4% error would be introduced during the tensile part of a cycle. Four or six 1¼ in. (32 mm) diameter A490 high-strength bolts were used in the joints corresponding to the number of holes shown in the end plates in Figs. 1, 2 and 3.

*One spacer at mid-length was used for Strut 8.

3. TESTING PROCEDURE

The testing arrangement was designed for performing a series of quasi-static, cyclic tests of axially loaded members. The main considerations were to provide for an adequate testing capacity in terms of both load and geometry, to have a convenient system for monitoring a specimens' behavior, and to establish a testing routine that would require only minimal adjustment from specimen to specimen. These considerations translate, in terms of the actual testing requirements into three distinct concerns: equipment and its arrangements, instrumentation and data acquisition, and the testing procedure.

3.1 Testing Equipment

The testing equipment can be subdivided by its function into three types: the loading system, the monitoring devices and ancillary recording equipment (discussed in 3.2), and the specimen support and system alignment devices.

The general testing arrangement for the struts with pinned ends is shown in Fig. 7, and for those with one end pinned and the other fixed in Fig. 8. In either case, a specimen was loaded at the "head" end by a Sheffer heavy duty hydraulic cylinder with a 14 in. (356 mm) bore and a 7 in. (176 mm) rod diameter. The cylinder was actuated by a 3000 psi (20 MPa) oil pressure which enabled the cylinder to develop a maximum tensile force of 345 kips (1.53 MN) and a compressive force of 460 kips (2.05 MN). The rated speed of cylinder travel was approximately 0.33 in./sec (8.4 mm/sec) on the tension stroke, and about 0.43 in./sec (11 mm/sec) on the compression stroke. These travel speeds were seldom approached during the testing.

In either arrangement the loading cylinder was pin-mounted to the inner side of a massive concrete reaction block. Because of the vertical pin mounting at the stationary end of the cylinder, the cylinder was free to swivel in the horizontal plane; the vertical movement was restrained. At the active end of the cylinder, a 450 kip (2.00 MN) load cell was attached to the head clevis.

The head clevis was laterally restrained by a yoke attached to a sidearm which extended to a reaction frame where it was held by a pin. The orientation of the sidearm was roughly perpendicular to the initial direction of the cylinder axis. For struts with pinned ends (Fig. 7), the foot clevis was bolted either to a steel foot frame or directly to a heavy steel girder attached to the concrete reaction block, depending on the overall length requirements of the particular specimen to be tested. For the fixed-pinned struts (Fig. 8), the fixed end of a specimen was bolted directly to either a steel foot frame or to a steel girder. This arrangement of the apparatus and the design of the specimens caused buckling of the struts to occur predominantly in the horizontal plane.

All steel to concrete connections were made using high strength prestressing rods. All steel to steel connections were made with high strength structural bolts, 1¼ in. (32 mm) diameter A490 bolts in the testing train and smaller A325 bolts elsewhere.

3.2 Instrumentation

The instrumentation consisted of two basic categories: those measuring the response of a specimen and those recording the information. On a macro level, linearly variable displacement transducer (LVDT) was used to measure axial displacement, and a potentiometer (a position transducer) was used to monitor horizontal lateral displacement at the theoretical locations of plastic hinges, Fig. 9. On some of the fixed-pinned specimens, where out of plane buckling was a possibility, vertical lateral displacement was also measured. The axial load, and in the case of the fixed-pinned members, the axial and shear forces were measured via load cells attached to the loading ram and to the horizontal sidearm. The location of these devices is shown in Figs. 7, 8 and 9. On a macro scale photogrammetry was also employed. Self adhering aluminum foil targets were evenly spaced longitudinally on the top of members along their centroidal axes (Fig. 10), and a camera was stationed on an overhead crane approximately twenty feet above the specimen. To reduce temperature and moisture effects glass plate film was used. Pictures were taken at predetermined points in a loading cycle. After developing the plates, they were read on a X-Y comparator, and, through the use of a CDC 6400 computer and a Cal Comp plotter, both the actual and the normalized deflected shapes were plotted. These data were obtained to provide some insight with regards to plastic hinge development and information on member curvature.

In an effort to better grasp the fundamental behavior of these members under cyclic loading, and to provide useful data for future finite element modeling, the specimens were also gaged for micro level measurements. For this purpose SR-4 strain gages, as many as twenty-five on some specimens, were placed at strategic points along the member. For example, as can be seen from Fig. 4 for Strut 20, a high concentration of strain gages was provided at the locations of the theoretical plastic hinges. In every case at least two gages were placed on either side of the specimen at the anticipated hinge location and usually additional gages were attached adjacent to the probable hinge. Strain gage data were expected to yield information regarding: strain histories of specific points, plastic hinge formation and possible migration, determination of overall and local buckling phenomena, and section curvature histories.

The recording equipment required calibration and constant attention to insure good accuracy of the results. The instruments were calibrated both before and after each test and comparisons were made. The differences were found to be within the tolerances of the recording or measuring systems themselves (LVDT: $\pm$ 0.0006 in. (15 μmm), Load Cell: $\pm$ 0.5%) indicating that no adjustments in the data were necessary. The information obtained from the axial load cell and all LVDT's was plotted directly by X-Y recorders, with axial load as the ordinate and either axial or lateral displacement at the abcissa. These plots constituted the raw hysteretic loop data for the specimens.

In addtion to the X-Y recorders, a high speed data acquisition system was employed. Leads from all LVDT's, load cells and strain gages were connected to a consol and an operator could constantly monitor the developing information. Upon command, instantaneous readings were stored on a high speed disk to be transferred to magnetic tape at a later date. During the test,selected channels were displayed on a cathode ray viewing screen which told an observer at a glance the condition of the test specimen and related equipment. After testing, plots of one channel vs. another were displayed on the screen and decisions could be made regarding the most desirable plots.

Unlike the X-Y recorders, which can record continuously, the photogrammetric and high speed scanner data can be obtained only at discrete points. This necessitated recording with the scanner data points at approximately every 25 kips (100 kN) along the elastic portions of the hysteresis curve, and every 0.02 in. (0.5 mm) axial displacement during the buckling and every 0.1 in. (2.5 mm) axial displacement in the post buckling region. Figure 11 shows an X-Y continuous recorder plot for one cycle together with dots obtained from the scanner data. As can be seen, the agreement between the two methods at obtaining data is quite satisfactory.

The intention of the photogrammetric phase of an experiment was to capture the overall deflected shape of a member. The photographs were taken at pre-selected points when the application of an axial force was temporarily halted. These points are identified in Fig. 12 and are referenced in the upper right hand corner of Figs. 13 and 14, where the results of a typical sequence of deflected shapes for a fixed-pinned specimen are given. The important observation to make from this data is the large member curvatures (camber or sweep) which develop during the course of testing.

3.3 Testing

The tests were done in such a way as to allow for comparison among the twenty four specimens, while at the same time, maintaining a realistic representation of the loading histories which a brace may experience in an actual structure. All specimens were subjected to a series of quasi-static, axially applied, displacement and load reversal cycles, or what has become known for its graphic description, as a "push-pull" test . Most of the specimens were given a compressive load first, but for comparison purposes some received an initial tensile load. All members experienced an elastic cycle initially, the purpose of which was twofold: it allowed for an instrumentation calibration check using Young's modulus as a basis, and it provided a logical point for making a final review of the specimen and set-up before beginning. As a written explaination of the testing procedure is given in the text, it may be helpful to refer from time to time to Figs. 12 and 15. Figure 15 gives the pre-selected loading history for Strut 21 and is typical of all specimens. Assuming a compressive cycle initially, the test would run as follows: Starting at zero load (point A in Fig. 12) a picture would be taken and a scanner reading recorded. Following this, a compressive load would be applied, with the jack on a displacement control, until the initiation of buckling (point B) is reached. If a photograph were scheduled it would be taken at this time. The specimen would then continue to be compressed until the pre-selected maximum displacement was reached. Once again, if a photograph were scheduled it would be taken. At this point, the jack direction would be reversed allowing the load to relax to a condition of zero load (point D) following a maximum negative displacement. Next, the specimen would be loaded in tension to a positive displacement equal to the negative one. At this position (point E) the load once again is relaxed to zero (point F) completing the cycle. The approach of having the maximum positive (tensile) displacement equal the maximum negative (compressive) displacement was adhered to in this series of experiments.

The resulting axial load vs. axial displacement P-δ curves, as well as the axial load vs. lateral displacement P-Δ curves, are given for all specimens in Appendix B. Photographs shown in Figs. 16 and 17 show some typical tests in progress; Figs. 18, 19 and 20 show selected specimens after testing.

4. MATERIAL PROPERTIES

The actual behavior of a structural element is highly dependent on the properties of the material from which it is made. It is appropriate, therefore, to precede the discussion of the experimental results with an examination of the material properties of the steels used in these experiments. The steels employed in the test specimens conformed to the following ASTM specifications: A36 for rolled shapes, A 53 Grade B for pipes, and A501 for square tubes.

4.1 Monotonic Tests

Tension tests of coupons taken from the specimen stubs were performed for all specimen types. For both the round and square tubes, coupons were taken from positions 90° and 180° from the weld line, whereas three coupons were extracted from the wide flange specimens, one from the web and one from each diametrically opposed flange. For the remaining specimens one coupon was taken from the web and one from the flange. Details and locations of the coupons are shown in Figs. 21 and 22. A clip gage fitted with two LVDT's and having a gage length of 2 in. (50 mm) was attached to the gage portion of the coupon. The entire set-up (coupon with a clip gage) was inserted into a 120 kip (530 kN) capacity Baldwin testing machine and pulled to failure. The corresponding stress-strain curve was plotted on X-Y recorders, and the results for each shape used are displayed in Appendix A.

The most notable observations to be made are concerned with the yield strength and the distinctness of the yield point. Keeping in mind that all specimens were of what is commonly referred to as mild steel, the variability in these parameters is considerable. Wide flanges, double-angles and double-channels indicated yield values from 40 to 50 ksi (275 to 345 MPa), while the tubes varied from a low of 24 ksi (165 MPa) to a high of 82 ksi (565 MPa).* Variability in the sharpness of the yield plateaus are equally striking. The majority of wide flanges, double-angles and double-channels exhibit clearly defined yield points, whereas, the tubes do not show a well defined yield but indicate a gradual transition into the plastic range. As will be shown later, such variability in material properties can significantly affect the initial buckling load of the specimen.

4.2 Cyclic Tests

For determining buckling loads under cyclic loading it is necessary to have hysteretic properties of the material. Two cyclic tests were conducted, one with a coupon from a W 6x20 and another from a 4x4x½ square tube. Details of the coupon for these tests are given in Fig. 21, and the resulting stress-strain curves are shown in Figs. 23 and 24. The most significant observation is the progressive lowering of the tangent modules E_t upon repeated cycling. Note particularly that even following the first load reversal E_t is dramatically smaller than the elastic modulus E and continues to degrade with increased cycles. This phenomenon, the well-known Bauschinger effect, holds true regardless of the intitial sense of the applied stress Fig. 25 [12], and has important implications for the behavior of a brace subjected to cyclic inelastic buckling.

*Yield points for pipes and tubes based on the 0.2% offset method.

5. HYSTERETIC PROPERTIES OF STRUTS

The most sought after results from cyclic experiments involving struts subjected to repeated buckling and stretching relate the applied axial force P to the axial displacement δ. The P-δ curves, which trace out the hysteretic loops for each member are shown in Appendix B. In this chapter the performance of specimens will be examined relative to the AISC specifications as well as to each other. In addition, the bases for determining the maximum compressive value that a specimen can reach in any one cycle will be pointed out.

One primary observation for design consideration is the fact that once a strut buckles inelastically, during subsequent cycles the same capacity of a member in compression cannot be reached. This can be noted repeatedly from the curves of Appendix B, and can be extended to include a statement that during the consecutive inelastic cycles the maximum compressive loads tend to decrease. This is in sharp contrast with the ability of a member to resist tension, which remains essentially constant regardless of previous cyclic history.

5.1 Initial Buckling Loads

In relating experiment with design, the major issue is the comparison of the carrying capacity of a strut to existing codes and specifications. For predicting the initial buckling capacity, Eq. 1.5-1 of the AISC Specifications [3], without the factor of safety, was used. The results of this comparison for all struts are given in Table 2. Since in practice, the yield stress for the steels used in these experiments would usually be assumed to be 36 ksi (250 MPa), a comparison of the specimens based on this value is included. A comparison of the strut buckling capacities using the AISC formula with the experimentally determined yield strengths is also given. Some of the yield strengths were found from the coupon tests, others from observing the first tensile yield in a strut test. Whereas the buckling capacity of most of the struts on either one of the above bases exceed the capacity predicted by the AISC formula, there are notable exceptions. The reduced capacities of struts can be attributed to two principal causes:

(a) Excessive initial curvature. This applies to Struts 1, 2, 10 and 11, and

(b) Non-classical material properties. The steel for tubes and especially for pipes tends to exhibit a poorly defined yield point and the truly elastic region is limited in its extent. Instead, the characteristic stress-strain curves are rounded. Very similar behavior is observed for steel on specimens initially subjected to a tensile yield. These effects contributed to the lowering of the buckling capacities of Struts 5, 7, 17, 22 and 24.

On making the necessary adjustments to account for the above two effects a good agreement between the experimental and the calculated buckling capacities of struts was obtained. A procedure for making a correction for the initial bow in a strut will be discussed in the next chapter. The reduction in the initial column capacity due to the non-classical material properties of mild steel will be commented upon here. Specimen 24 made of a 3½ in. (90 mm) standard steel pipe was selected to illustrate this behavior.

Figure 26 shows the results of a monotonic tension test for a coupon cut from Strut 24. Instead of a definite yield point, the behavior of this material is similar to that of a steel with a previous strain history (see Figs. 23 through 25) in that the tangent modulus E_t progressively attains ever smaller values than the elastic modulus E. For a theoretical investigation this suggests the use of the tangent modulus in the generalized Euler formula for predicting the initial buckling load. Using this approach, the predicted buckling load for Strut 24 is found to be 81 kips (360 kN) (Fig. 27). This result compares favorably with the experimentally determined load. The same approach can be used to explain the low value of the initial buckling load for Strut 5. While Struts 3 and 4, identical to Strut 5, were able to attain their predicted load capacities, Strut 5 reached only about 75% of the expected buckling load. The difference among these members resulted from the fact that Strut 5 was caused to yield in tension prior to the application of the initial compressive force. This induced the development of the Bauschinger effect in the material, resulting in a stress-strain diagram resembling that shown in Fig. 26. By applying the tangent modulus approach to this case, the predicted (adjusted) capacity of the strut comes near to its experimentally determined value. A procedure for applying this approach for cyclic loadings to account for the effect of material properties will be discussed in the next chapter.

5.2 Normalized Hysteretic Curves

To make comparisons among the large variety of specimens used in these experiments, as well as to determine the influence of the two kinds of boundary conditions employed, the P-δ curves were normalized for the purposes of a persual. Appendix C contains such curves for all but Strut 1. To obtain them, the applied force P for a given member was divided by its tensile yield capacity, P_y, and the axial displacement δ by the displacement δ_y at yield. In the form of equations, the normalizing quantities are

$$P_y = \sigma_y A \tag{1}$$

and

$$\delta_y = \varepsilon_y \ell_s \tag{2}$$

For a given member, the values of the yield stress σ_y and yield strain ε_y were obtained by averaging the coupon test data. Where yield plateaus were not clearly defined, a 0.2% offset was used to determine the required quantities. In Eq.1, A defines the cross-sectional area of a member; in Eq. 2, ℓ_s is the length of a member between the heavy end plates, i.e., it corresponds to the length of a strut which contributes most to the axial deformation. As is customary, the ratios P/P_y were used as ordinates, and δ/δ_y as abscissas.

The normalized hysteretic curves exhibit the results in a very meaningful manner by eliminating the effects of variations in material property, cross-sectional area, and specimen length. These graphs clearly bring out the striking effect of large slenderness ratios in reducing the compressive capacity of a strut in relation to its tensile strength.

5.3 Normalized Hysteretic Envelopes

Because of an infinite variety of cyclic patterns that may be applied to a strut, it is convenient to make use of envelopes for a family of hysteretic loops obtained in an experiment. For a general comparison, envelopes for normalized hysteric loops are particularly useful. Although, for identical struts subjected only to different loading patterns, the use of normalized hysteretic loops is not essential. Since, however, in this discussion comparisons include the effects of boundary conditions, cross-sectional shapes, and slenderness ratios, for uniformity all comparisons are made using normalized plots.

As an example, consider the envelope for the normalized hysteretic loops for two identical Struts 3 and 4 shown in Fig. 28. As can be seen from this diagram, the shape of the envelope appears to be unaffected by the different loading histories of the two struts. This is true, however, only because the specimens experienced similar loading patterns. Both specimens were initially compressed, and each initially attained the maximum buckling load, which was in agreement with the conventional AISC formula. By contrast, an identical strut, which initially was caused to yield in tension, reached only about 75% of this capacity, Fig. 29. This is directly attributable to the Bauschinger effect as a result of which the stress-strain diagram in compression is significantly rounded, reducing the elastic range. The maximum compressive load of 152 kips (676 kN) with the associated axial displacement for Strut 5 falls outside the envelope of Fig. 28. This is due to the fact that the envelope drawn there was established from the tests which began with the application of a compressive cycle. Moreover, at the beginning of a second hysteretic loop (such as at point c in Fig. 29), the specimen's cumulative plastic strain was equal to the distances ab plus bc along the abcissa. By contrast, at point d, the beginning of the second cycle for Specimen 5, the cumulative plastic strain is given by the much smaller distance ad. If these differences in the history of loading are taken into account, the maximum first cycle compression load for Strut 5 can be made to lie on the envelope for Struts 3 and 4. The deterioration of the buckling capacity of a strut due to previous plastic working of the material is directly tied in with the Bauschinger effect. An approximate procedure for predicting the buckling capacity of struts subjected to random loadings is discussed in the next chapter.

Another illustration of an envelope for two 4 in. (100 mm) standard steel pipes subjected to similar cyclic loading is shown in Fig. 30.

5.4 Effect of Slenderness Ratio on Hysteretic Loops

An examination of the hysteretic loops for different struts given in the Appendices B and C very clearly shows the dominant influence of the slenderness ratio on the shape of the hysteretic loops. The areas enclosed by such loops, a measure of the energy absorption and dissipation capacity of a member, is superior for the stocky members. In the limit, i.e., for small values of $K\ell/r$, such loops resemble those of the material itself; the slender members generate hysteretic loops that are strongly biased (see the loops for Struts 6 and 11). The same conclusions were reached by a number of other investigators [4,5,6,7,8]. These conclusions can be highlighted by referring to Figs. 31 and 32 where normalized hysteretic envelopes for selected struts are superposed. Whether one considers the struts with pinned ends, or the ones with fixed-pinned conditions at the boundaries, the struts with the smaller slenderness ratios perform better.

It is important to note that the more slender a strut, the larger is the ratio between its capacity in tension to that in compression. As can be seen from Fig. 31, this effect is more pronounced in the later cycles. For example, the initial buckling capacities of Struts 2 and 3 were very nearly alike, but upon repeated load reversals the maximum compressive loads for the more slender Strut 3 deteriorated more rapidly. The same observation can be made regarding Struts 19 and 23 whose normalized hysteretic loops are shown in Fig. 32.

5.5 Effect of Boundary Conditions

Virtually all available analytical and experimental information on the effect of boundary conditions on the buckled shapes of struts pertains to their behavior in the elastic range. The classical elastic buckled shapes for the two cases studied in this investigation are shown in Fig. 33. It is well-known that the effective buckling length for a strut with fixed-pinned end conditions is reduced in comparison to the same length strut having pinned ends. The concept of an effective length $K\ell$, which relates a strut with pinned ends to a strut with any boundary conditions, plays a dominant role in such considerations. It is important to determine if this approach applies to struts cyclically loaded into the inelastic range. The effect of the boundary conditions on the hysteretic behavior of struts also needs further clarification. Both of these problems are discussed in this section.

As noted in the chapter on the testing procedure, photogrammetric pictures were taken of the targets attached along the tops of the test specimens. Some results from this data in normalized form are shown in Figs. 34, 35, and 36. From these plots it can be concluded that in general the buckled shapes in the inelastic range resemble the initial elastic shapes, but there are some differences. As the number of inelastic cycles increases, the curvature tends to concentrate more in the regions of plastic hinges, but points of inflection coincide with the elastic predictions. Further, the buckled shape (compare Figs. 35 and 36) does not appear to be a function of a slenderness ratio. Based on these observations, one can conclude that it appears reasonable to adhere to the effective length concept even in the inelastic range of material behavior for cyclically loaded members.

The effect of boundary conditions on the hysteretic behavior of struts may be again conveniently examined using normalized envelopes. The concept of the effective length, implicitly included in the slenderness ratio parameter, is adopted in this comparison. For comparison purposes, six specimens were selected; two wide flange members with $K\ell/r$ ratios of 40, Fig. 37, two round tubes with $K\ell/r$ ratios of 80, Fig. 38, and two double angles with $K\ell/r$ ratios of 80, Fig. 39.

These graphs indicate a slightly better performance for the fixed-pinned specimens. The hysteretic envelopes for the wide flange members and pipes enclose larger areas, whereas those for the double-angle struts are virtually identical.

The somewhat inferior performance of the fixed-pinned double angle strut in comparison with the other two cases cited, may be attributed to the tendency of this member for developing lateral-torsional buckling. This appears to be a characteristic of thin-walled members whose cross-sections have a single axis of symmetry [13]. Some evidence of this behavior may be noted from Fig. 40 where vertical deflections at the location of the potential plastic hinge are shown.

Based on the results for the two kinds of boundary conditions, and the good correlation found using the effective slenderness ratio concept, the extension of this approach to other boundary conditions for inelastic cyclic loadings seems plausible.

5.6 Effect of Cross-Sectional Shape on Hysteretic Behavior

In the preceding section, it was concluded that through the use of an effective length concept, consideration of the boundary conditions may be eliminated in comparing cyclic behavior of struts. Therefore, in this section, in discussing the effect of cross-sectional shape on hysteretic behavior, only the hysteretic envelopes for struts with pinned ends will be compared. For this purpose, six specimens with pinned ends and $K\ell/r$'s of 80 having different cross-sectional shapes were selected. These included a wide flange member (Strut 3), a structural tee (Strut 13), two pipes (Struts 14 and 16), one tube (Strut 17) and a built-up double angle member (Strut 8). Normalized hysteretic envelopes for these struts are shown in Figs. 41 and 42. Based on the enclosed areas of the hysteretic envelopes some shapes proved to be more efficient than others. A careful scrutinizing of the results indicates the following order in progressively poorer performance:

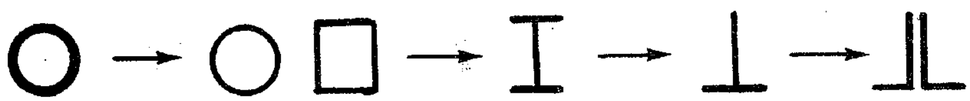

Strut 16 Struts 14 & 17 Strut 3 Strut 13 Strut 8

The characteristic properties of the cross-sectional shapes can account for the observed results. These contribute to the three discernible effects: local buckling, lateral-torsional buckling and local buckling between stiches in built-up members. A discussion of these factors on cyclic buckling capacity of struts is given next.

Some lateral-torsional buckling was observed in some structural tee and double-angle members. It is due to the fact that when a singly symmetrical section buckles in the plane of its axis of symmetry, two modes of failure are possible. Either the specimen buckles in a purely flexural mode, or it buckles in a flexural-torsional mode. The relevant parameters are a function of a specimen's geometric properties [13]. When, however, a singly symmetrical section buckles in the direction perpendicular to its axis of symmetry, flexural and lateral-torsional buckling take place simultaneously, and the critical load is lower than that for a purely flexural buckling mode [13]. Since one of the structural tees and three of the double-angle specimens tested in this sequence of experiments had proportions such that buckling in the direction perpendicular to their axes of symmetry was critical, some lateral-torsional buckling was to be expected, and was confirmed by the tests.

Another manner in which an open section such as a tee or a double-angle can fail is for an outstanding leg to buckle prior to the load which causes failure of the whole section. This type of local failure is primarily dependent upon the b/t ratio of the unstiffened element, and often occurs in conjunction with lateral-torsional buckling [3].

The AISC approach for resolving this problem consists of introducing Q factors which, if necessary, reduce the allowable capacity of a member. When these provisions were followed, the calculated first buckling loads for double-angles and tees were found to be in good agreement with the experimental results (see Table 2). Since the geometry of the cross-section is seen to affect the initial buckling load, it is reasonable to assume the same to be true for the subsequent loading cycles. It is very likely that the reduced cyclic capacity of the singly symmetrical open sections is at least partly due to lateral-torsional and/or local buckling of unstiffened legs.

For Strut 19, a wide-flange specimen, an accurate determination of local buckling was made with the aid of SR-4 strain gages. The location of such gages is shown in Figs. 4 and 43. The sharp deviations from linearly varying read-outs for the selected gages, as is clearly apparent from Fig. 43, indicates the onset of local buckling. For the top gages 5 and 6 this occurred just following the first general buckling of the member; the bottom gages showed local buckling at the bottom flange early in the second cycle. After the development of these first buckles, softening and deterioration in the capacity of the plastic hinge develops during the subsequent cycles.

It should be noted that local buckling was observed for all members, with the exception of those made from thick-walled pipe. Such buckling, however, occurred in very late stages of cyclic load applications at extremely large lateral displacements, Fig. 44.

The most significant effect responsible for the poorest performance of the double-angle struts, which is likely to apply to other built-up members, is local buckling of the individual members between the stitches. Struts 8, 9 and 20 which had the propensity to buckle at right angle to their cross-sectional axes of symmetry, and thereby also developing some torsion-buckling, were particularly poor. The double-angle Strut 8 had only one stitch at its mid-length; whereas Strut 9 had two located at third- points. In conformity with AISC requirements, the slenderness ratio of the individual angles between the fillers did not exceed the governing slenderness ratio of the built-up member. During the initial application of the compressive load, both of these struts behaved well and their buckling capacities at first buckling load were good (see Table 2). However, as severe cyclic load excursions were applied, the angles tended to buckle locally between the stitches. An illustration of this behavior in advanced stages of loading for Strut 8 is shown in Fig. 45 (a), and for Strut 9 in Figs. 19 (b) and 45 (b). From these examples it is apparent that as cyclic load applications proceeded, the flexural straining was concentrated in the middle of a specimen, and the webs tended to approach each other. This behavior was particularly pronounced in Strut

9. In this strut this effect alone raises the slenderness ratio at the critical section by about 10%, and partially accounts for the loss of buckling capacity during severe cycling. Cyclic plastic working of a strut in a hinge region softens the material due to the Bauschinger effect contributing further to its deterioration.

A more extreme case of built-up strut deterioration in advanced stages of cyclic loading is shown in Fig. 46, where a complete failure of the stitches can be seen. Here the spacers, located at third-points of a strut's length, were 2½ in. (64 mm) wide, and were welded to the angles with 5/16 in. (8 mm) fillet welds (see Fig. 3).

An examination of the three cases cited on the bahavior of double-angle stitched members suggests the following. The use of closer spacing or stronger stitches should help but cannot obviate the problem. It would appear that for important applications in seismic design where severe cyclic loading of a compression member can be anticipated, built-up members should be either avoided or very thoroughly stitched together.

6. ANALYTICAL PREDICTIONS OF CYCLIC BUCKLING LOADS

In the analysis of diagonally braced frames for seismic excitations, the inelastic buckling behavior of struts must be mathematically modeled. A number of proposals for accomplishing this have been made [4,6,8,9,14,15], and the subject continues to be an active field of current research. Perhaps the ultimate in accuracy can be achieved using a nonlinear finite element approach, providing an accurate constitutive relation for the material behavior under random cyclic loading becomes available. As yet, the reliability of such constitutive relations is questionable. Alternatively, the experimental evidence on the behavior of struts subjected to inelastic cyclic buckling can be examined, and analytical procedures developed which predict with a reasonable degree of accuracy the magnitudes of the quantities sought. Some aspects of this problem using the latter approach are considered here in detail.

It has been noted earlier that there are two main causes which contribute to the often dramatic decrease in the column capacity for inelastic cyclic loadings. These are the Bauschinger effect, exhibited by the steel subjected to inelastic load reversals, and the effect due to the residual camber or bowing of a specimen resulting from plastic hinge rotations during previous cycles. Each one of these effects can be approximately accounted for by means of reduction factors applied to the theoretical initial carrying capacity of a straight column.

6.1 Reduction Factor due to Bauschinger Effect

In Section 5.1 an example was given showing that following the well-established procedures, the initial buckling load of a strut can be accurately estimated by using the tangent modulus in the generalized Euler formula. The stress-strain diagram for the example strut had a monotonically decreasing tangent modulus (Fig. 26). The same kind of material behavior is clearly exhibited by steels in the post-yield range during cyclic loadings (see Figs. 23, 24, and 25). This observation suggests the possibility of extending the tangent or the reduced (double) modulus approach to cyclic loading. To do so, however, requires that some approximations be introduced.

In establishing the initial buckling load for an ideal strut, a strut is assumed to be perfectly straight. As predicted by the tangent modulus theory, just before reaching the buckling load a uniform axial compressive stress develops throughout the member acting on the material having the same mechanical properties throughout. Such is not the case in cyclically buckled struts. As can be noted from the shapes of the inelastically buckled struts, Figs. 34 and 35, sharp curvatures develop at plastic hinges. Elsewhere the curvatures are moderate, indicating that large portions of a strut are less severely stressed in flexure. Further evidence of local inelastic activity at a plastic hinge may be noted from the strain gage data such as shown in Fig. 43. During inelastic cyclic loading the strain histories vary both along the length of a member and across its sections. However, the behavior at a plastic hinge is dominant in affecting the overall performance of a strut. Therefore, the strains at a centroidal fiber at a hinge can be assumed [10] to be decisive on the behavior of a strut as a whole as far as its buckling characteristics are concerned. It is recognized that this is a drastic simplification of the problem. Significantly different strain histories do occur elsewhere. Nevertheless, because of the key importance of plastic hinges on the buckling behavior of a strut, the proposed simplifying assumption seems reasonable.

An inelastic cyclic coupon test of the strut material defines its mechanical properties, and each loading branch can be considered to represent a monotonic test on a material with a previous inelastic history. This history dependence can be conveniently approximated and defined by the absolute cumulative plastic strain at the beginning of a loading cycle. For example, the tensile loading curve for cycle 2 from a coupon test for the W 6×20 section shown in Fig. 23 is reproduced in Fig. 47. At the beginning of this loading cycle the absolute cumulative plastic strain $\Sigma\varepsilon_p$ at zero stress is 0.0055 in./in. (m/m). This is the sum of strains along the abscissa from a to b to c and then to d. Similar curves can be isolated and identified with different amounts of cumulative plastic strain for the other loading branches of the coupon test.

After establishing a stress-strain curve identified with a particular absolute cumulative plastic strain, as has been done in Fig. 47, the tangent moduli related to the corresponding stresses can be determined. With this information one can make use of the generalized Euler formula to calculate the buckling slenderness ratios $K\ell/r$. The Euler formula in the appropriate form for this purpose reads

$$K\ell/r = \sqrt{\pi^2 E_t/\sigma_{cr}} \qquad (3)$$

where E_t and σ_{cr} are the matching values of these quantities found from a stress-strain diagram such as Fig. 47. The calculated slenderness ratios $K\ell/r$ can then be plotted versus the critical buckling stress σ_{cr}. One of the resulting curves obtained in this manner corresponding to the data given in Fig. 47 ($\Sigma\varepsilon_p = 0.0055$) is shown in Fig. 48.

The family of curves in Fig. 48 identified with different amounts of cumulative plastic strain has been generated in the above manner. However, the curve corresponding to $\Sigma\varepsilon_p = 0$ was found using the AISC column formulas with no factor of safety. The corresponding theoretical curve based on the simplifying assumption of ideal elastic-plastic behavior is known to be inaccurate in the relevant range [16], and the two available experimental points were considered to be insufficient to define the required curve. With this data, for a selected slenderness ratio of a strut, its capacity for a given cumulative plastic strain $\Sigma\varepsilon_p \neq 0$ divided by the capacity at $\Sigma\varepsilon_p = 0$ gives the reduction factor R_B accounting for the Bauschinger effect.

Since all of the struts in this series of experiments tended to develop a residual camber because of a residual curvature at the plastic hinges, it appears more appropriate to apply the reduced modulus theory rather than the tangent modulus theory for determining the buckling loads. The rationale for this contention rests in the belief that in a slightly curved member the unloading process of the fibers on the convex side of a strut is likely to occur earlier than it does in an initially straight member.

By limiting the application of the reduced modulus approach to the wide flange sections used in these experiments, the procedure is very direct. Since all of these members buckled around their X-axes, on neglecting the contribution of the web, the reduced modulus E_r can be taken as one for a rectangular section given by [16]

$$E_r = \frac{4\ E\ E_t}{(\sqrt{E} + \sqrt{E_t})^2} \tag{4}$$

Whence on exchanging E_t by E_r in Eq. 3, the procedure of establishing the column buckling curves as has been done in Fig. 48 can be repeated.

A family of curves based on the reduced modulus approach for different amounts of cumulative plastic strain is shown in Fig. 49. Note that for normalizing the results the curve for $\Sigma\varepsilon_p = 0$ has again been generated using the AISC column formulas with no factor of safety.

Curves giving the reduction factors arrived at on the above two bases to account for the Bauschinger effect as a function of the cumulative plastic strain are shown in Fig. 50. These are established with the aid of Figs. 48 and 49. In general, the tangent modulus approach indicates a larger reduction in the capacity of a strut than that predicted by the reduced modulus theory. However, based on the reduced modulus approach, there appears to be no significant change in the strut capacities for the stockier members with a $K\ell/r$ of 40. As will be shown at the end of this chapter, the reduction factors due to the Bauschinger effect based on the reduced modulus approach generally lead to somewhat better agreement with the experimental results than those based on the tangent modulus theory.

6.2 Reduction Factor due to Specimen Curvature

The second major cause for the observed decrease in column capacity during cyclic loading is due to the fact that after an initial inelastic buckling cycle a specimen develops a residual curvature which generally is not removed by the subsequent tensile yielding. This phenomenon can be clearly seen by examining the P-Δ curves for the struts in Appendix B. On completion of a cycle, at zero axial force, a residual lateral deflection Δ remains. This corresponds to point F shown on the P-δ plot in Fig. 12. Therefore, an inelastically cycled member must be treated in the analysis as having an initial curvature or a camber. This effect can be approximated by solutions available in the literature [16,17] for eccentrically loaded elasto-plastic columns. Here the solutions obtained by Westergaard and Osgood based on von Karman's concept for inelastic buckling of eccentrically loaded columns are utilized. Some of the column buckling curves obtained by them for eccentrically loaded struts [17] are reproduced in Fig. 51. In this figure e denotes an eccentricity of the co-axial forces with respect to a column's centroidal axis, and s is the ratio of a cross-section's section modulus to its cross-sectional area (core radius). The ratio of e to s defines the eccentricity ratio.

As an approximation to the problem being considered here, the experimentally determined maximum effective* lateral deflection Δ of a strut at the beginning of a compression cycle can be taken as e. Adopting this approximation, the curves of Fig. 51 provide nec-

* See Fig. 33(b)

essary information for obtaining graphs for the reduction factor R_E as a function of the eccentricity ratio $e/s \simeq \Delta/s$. Such graphs can be constructed in the following manner. For a selected slenderness ratio such as 80, read off the values of the critical stresses on the e/s curves in Fig. 51, and normalize these results to the capacity of a straight column (e/s = 0). A continuous curve connecting these points gives an R_E plot for the selected column slenderness ratio, as a function of the eccentricity ratio. Graphs of this kind are shown in Fig. 52. Note how rapidly the capacity of a column decreases with an increasing eccentricity ratio $e/s \simeq \Delta/s$. This fact has been repeatedly observed in experiments.

6.3 Comparison of Analytical and Experimental Results

With the aid of the reduction factors due to the Bauschinger effect and the effect of strut curvature, estimates of the critical buckling loads for members subjected to inelastic cyclic loading can be made. The variation of the reduction factors with cumulative plastic strain to account for the Bauschinger effect for selected slenderness ratios of struts, applicable to the material for the W 6 x 20 members used in these experiments, is plotted in Fig. 50. Either an R_B based on the tangent modulus approach, or on the reduced modulus, can be found from this diagram for a particular amount of the cumulative plastic strain $\Sigma\varepsilon_p$. The variation of the reduction factors R_E due to the curvature of a strut for selected slenderness ratios of members can be estimated from Fig. 52.

By multiplying the initial buckling loads for a straight virgin column by the appropriate reduction factors R_B and R_E, a buckling load for the new conditions are found. Some such calculations are summarized in Table 3, where the results for the first three consecutive cycles for Struts 2, 3, 4, 5, and 19 are given. For the purposes of illustration, it was assumed that for Strut 2 the R_B factors could be based on the graph of Fig. 50, although no cyclic coupon tests were made for the material of this strut.

The calculated buckling stresses for the first cycle of the struts listed in Table 3 were determined using an AISC formula [3] without the corresponding factor of safety and using experimentally determined yield strengths. However, since Strut 2 had an initial bow in excess of that permitted by the specifications, a reduction factor R_E was applied. Further, since Strut 5 was initially subjected to a tensile force causing the member to yield, a reduction factor R_B was employed. In these two cases, as well as in all others, the experimental data were used to find Δ and $\Sigma\varepsilon_p$. By applying in a similar manner the required reduction factors to the second and third cycles, the corresponding estimates of the buckling stresses were found. As can be seen from the table, with the use of these factors, the estimated buckling loads are in reasonably good agreement with the experimental results.

It would appear that the use of the reduction factor R_B based on the reduced modulus concept in most cases leads to better results than those based on the tangent modulus approach. However, it is noteworthy that for Strut 5 better results for the first buckling load are obtained by using R_B based on the tangent modulus procedure. This result can be anticipated, since Strut 5 initially was caused to yield in tension, and it was straight prior to the application of a compressive load.

Considering the complexity of the problem, the predictions of buckling loads using the above approach may be said to be satisfactory, and may prove useful in developing algorithms for determining the deterioration of the cyclic buckling capacity of struts.

7. SUMMARY AND CONCLUSIONS

7.1 Summary

An experimental study of the inelastic hysteretic behavior of axially loaded steel members has been presented in this report. Tests were made on twenty-four commercially available steel struts commonly used as bracing members. The sizes of the specimens were sufficiently large to be representative of the members used in practice. A large variety of shapes were tested including wide flanges, structural tees, double-angles, double-channels, and thick and thin-walled square and round tubes. The boundary conditions were of two types, fixed-pinned and pinned-pinned, while the effective slenderness ratios were either 40, 80, or 120. The primary concern of this report was to investigate the effects of loading patterns, end conditions, cross-sectional shapes, and slenderness ratios on the hysteresis response of members. In addition, an explanation of the fundamental mechanisms responsible for the observed degradation in the buckling load capacity during inelastic cycling was advanced.

A reader interested in cyclic behavior of thin-walled circular tubes having diameter to wall-thickness ratios typical of the pipes used in offshore construction by the oil industry may wish to examine a companion report (Ref. 10).

7.2 Conclusions

Based on this investigation of inelastic buckling of struts of various cross-sections several conclusions may be reached which have important design implications.

1. Cyclic buckling of struts showed that:

   a) The conventional definition of an effective slenderness ratio $K\ell/r$ deduced on an elastic basis carries over into the inelastic range. The points of inflection on a deflected curve remain relatively fixed.

   b) The effective slenderness ratio of a member appears to be the single most important parameter in determining the hysteretic behavior. The stockier members generate fuller loops than the more slender ones. The use of normalized hysteretic curves in comparisons is particularly advantageous because a number of variables are removed from consideration by this process.

   c) Hysteretic envelopes provide a convenient means for comparing specimens with different loading histories. They can be very useful considering random loading effects on a brace during a severe earthquake. The use of normalized hysteretic envelopes is convenient for general formulations and studies.

   d) The hysteretic performance of a member is somewhat influenced by its cross-sectional shape. The major determining factors appear to be related to a members' susceptibility toward lateral-torsional buckling, local buckling of outstanding legs, and web buckling between stitches in built-up members.

   e) Stitching of built-up critical compression members for service under severe load reversals as currently specified in standard codes [3] is unconservative. In the region of plastic hinges, the individual parts of a member due to softening of the material have a greater propensity to buckle than envisioned by the codes. Requiring the slenderness ratio ℓ/r for the individual parts of members between stitches to be less than that of the member as a whole and specifying minimum fastener strengths would help in the problem. Just this kind of a provision was contained in the 1959 AISC Specifications [19] and can also be found in the current German ones [20]. However, it would appear that for important applications in seismic design, where severe cyclic loading of a compression member can be anticipated, built-up members should be either avoided or very thoroughly stitched together in the regions of potential plastic hinges.*

2. Significant reduction in buckling loads occurs during inelastic cyclic loadings. The hysteretic loops displayed in this report can serve as an aid for developing and verifying computer models of strut behavior. The use of reduction factors discussed in the report may prove useful in such formulations. The reduction factors are based on rational theory and model the major parameters responsible for a specimen's deterioration in hysteretic behavior. The first one of these reduction factors, R_B, accounts for the material property changes associated with the Bauschinger effect that could occur in the plastic hinge regions of a member. The second cause for the observed decrease in the column capacity results from the

*AISC Spec. Sect. 1.5.1.4.1(1) would satisfy this requirement.

residual curvature that remains in a member following previous inelastic compressive cycles. This can be accounted for by the reduction factor R_E which is based on solutions for eccentrically loaded columns [17].

3. Designers should be aware of the variability in the mechanical properties of commercially available steel used in building construction. The yield strengths for rolled sections used in these experiments made of A36 steel varied from about 36 ksi (250 MPa) to 50 ksi (340 MPa). The materials for these sections exhibited a characteristic yield plateau in their stress-strain diagrams. However, for pipes made of A53 Grade B steel no distinct yield points were apparent. Instead, the stress-strain curves showed a gradual transition into the plastic range. In determining the initial buckling capacity of struts in such cases the tangent modulus approach led to satisfactory results, whereas the buckling loads computed by code formulas were erratic. The nominal yield strengths, determined by noting the attained yield plateau during the tensile phase of a cyclic strut test or by the 0.2% offset method, for pipes and tubes varied from 24 ksi (165 MPa) to a high of over 80 ksi (550 MPa).

8. REFERENCES

1. Sozen, M.A. and Roesset, J., "Structural Damage Caused by the 1976 Guatemala Earthquake," Structural Research Series No. 426, University of Illinois, Urbana/Champaign, March 1976.

2. Roeder, C.W. and Popov, E.P., "Eccentrically Braced Steel Frames for Earthquakes," Journal of the Structural Division, ASCE, Vol. 104, No. ST3, March 1978, pp. 391-412.

3. Manual of Steel Construction, 8th ed., American Institute of Steel Construction, Chicago, Ill., 1980.

4. Wakabayashi, M., Nonaka, T., Nakamura, T., Morino, S., and Yoshida, N., "Experimental Studies on the Behavior of Steel Bars under Repeated Axial Loading," Disaster Prevention Research Institute Annals, Kyoto University, No. 16B, 1973, pp. 113-125.

5. Igarashi, S., and Inoue, I., "Memorandum on the Study of Braced Frames," Quarterly Column, No. 49, October, 1973.

6. Kahn, L.F. and Hanson, R.D., "Inelastic Cycles of Axially Loaded Steel Members," Journal of the Structural Division, ASCE, Vol. 102, No. ST5, May 1976, pp. 947-959.

7. Morino, S., "An Experimental Study of the Hysteresis Behavior of Steel Braces Under Repeated Loading," IABSE Final Report, Symposium on Resistance and Ultimate Deformability of Structures Acted on by Well Defined Repeated Loads, Vol. 14, Lisbon, 1973, pp. 31-37.

8. Ashok, K. J., Goel, S.C., Hanson, R. D., "Hysteresis Behavior of Bracing Members and Seismic Response of Braced Frames with Different Proportions," Univeristy of Michigan Research Report, UMEE 78 , University of Michigan, Ann Arbor, Michigan, 1978.

9. Popov, E. P., Takanashi, K., and Roeder, C.W., "Structural Steel Bracing Systems: Behavior under Cyclic Loading," Report No. EERC 76-17, Earthquake Engineering Research Center, University of California, Berkeley, CA, June 1976.

10. Zayas, V.A., Popov, E.P., and Mahin, S.A., "Cyclic Inelastic Buckling of Tubular Steel Braces," Report No. UCB/EERC-80/16, Earthquake Engineering Research Center, University of California, Berkeley, CA, June, 1980.

11. Karman, V.T., and Biot, M.A., Mathematical Methods in Engineering, McGraw-Hill Book Co., New York, N.Y., 1940, 320 p.

12. Popov, E.P., and Petersson, H., "Cyclic Metal Plasticity: Experiments and Theory," Journal of the Engineering Mechanics Division, ASCE, Vol. 104, No. EM6, 1978, pp. 1371-1388.

13. Chajes, A., Winter, G., "Torsional-flexural Buckling of Thin-Walled Members," Journal of the Structural Division, ASCE, Vol. 91, No. ST4, August, 1965.

14. Niforoushan, R., "Seismic Behavior of Multi-Story K-Braced Frame Structures," University of Michigan Research Report UMEE 73R9, University of Michigan, Ann Arbor, Michigan, Nov., 1973.

15. Maison, B.F. and Popov, E.P., "Cyclic Response Prediction for Braced Steel Frames," Journal of the Structural Division, ASCE, Vol. 106, No. ST7, July 1980, pp. 1401-1416.

16. Timoshenko, S.P., and Gere, J.M., Theory of Elastic Stability Second edition, McGraw-Hill Book Co., New York, N.Y., 1961, p. 200.

17. Westergaard, H.M. and Osgood, W.R., "Strength of Steel Columns," A.S.M.E. Transactions, 1927-28, APM-50-9.

18. Popov, E.P., "Inelastic Behavior of Steel Braces Under Cyclic Loading," Proceedings, Second U.S. National Conference on Earthquake Engineering Research Institute, Stanford University, Stanford, CA, Aug. 22-24, 1979, pp. 923-932.

19. Steel Construction Manual, 5th ed., American Institute of Steel Construction, New York, N.Y. 1959, p. 293.

20. DIN 4114 (German Industrial Standards), Stabilitatsfalle, Stahlbau-Handbuch, Industrie und Handelsverlag, Walter Dorn GMBH, 1952, pp. 572-657.

TABLE 1 LIST OF TEST SPECIMENS

STRUT NO.	SHAPE	$K\ell/r$	LENGTH (ft)	(m)
Struts pinned at both ends:				
1	W 8 x 20	120	12.50	3.81
2	W 6 x 25	40	5.10	1.55
3	W 6 x 20	80	10.07	3.07
4	W 6 x 20	80	10.07	3.07
5	W 6 x 20	80	10.07	3.07
6	W 6 x 16	120	9.67	2.95
7	W 6 x 15.5	40	4.87	1.48
8	2-L 6 x 3-1/2 x 3/8*	80	9.27	2.83
9	2-L 5 x 3-1/2 x 3/8*	40	4.87	1.48
10	2-L 4 x 3-1/2 x 3/8*	120	12.50	3.81
11	2-C 8 x 11.5*	120	9.83	3.00
12	WT 5 x 22.5	80	8.33	2.54
13	WT 8 x 22.5	80	10.47	3.19
14	Pipe 4 Std.	80	10.07	3.07
15	Pipe 4 Std.	80	10.07	3.07
16	Pipe 4 X-Strong	80	9.87	3.01
17	TS 4 x 4 x .250	80	10.00	3.05
18	TS 4 x 4 x .500	80	9.07	2.76
Struts pinned at one end and fixed at the other end:				
19	W 6 x 20	40	7.19	2.19
20	2-L 6 x 3-1/2 x 3/8*	80	13.24	4.04
21	Pipe 4 X-Strong	40	7.19	2.19
22	TS 4 x 4 x .500	80	12.95	3.95
23	W 5 x 16	80	12.00	3.66
24	Pipe 3-1/2 Std.	80	12.76	3.89

* 3/8 in. (9.5 mm) back to back of angles and channels; for double angles the shorter legs are turned out.

TABLE 2 COMPARISON OF EXPERIMENTAL AND PREDICTED INITIAL BUCKLING LOADS

STRUT NO.	EXPERIMENTAL σ_y (ksi)	P_{cr}^{exp}(kips)	P_{cr}^{exp} / P_{cr}^{calc*}		
			Based on σ_y=36ksi	Based on Exper. σ_y	Refined Estimate
1	40.4[a]	95	0.81	0.81	0.98[d]
2	42.2[b]	263	1.05	0.90	1.07[e]
3	40.2[b]	202	1.19	1.09	-
4	40.2[b]	201	1.19	1.09	-
5	40.2[b]	152	0.90	0.83	0.96[f]
6	44.7[b]	112	1.19	1.21	-
7	50.0[c]	201	1.28	0.95	-
8	40.8[b]	197	1.08	0.98	-
9	43.6[b]	292	1.43	1.17	-
10	41.6[c]	97	0.92	0.92	1.06[g]
11	35.5[c]	105	0.79	0.79	1.05[h]
12	39.5[b]	186	0.98	0.91	-
13	41.8[a]	196	1.11	0.99	-
14	47.5[c]	114	1.25	1.03	-
15	47.5[c]	110	1.21	0.99	-
16	24.0[c]	87	0.69	0.95	-
17	59.0[c]	123	1.21	0.88	0.98[f]
18	82.0[b]	272	1.54	1.00	-
19	40.2[b]	240	1.19	1.07	-
20	40.8[b]	180	0.98	0.89	-
21	24.0[c]	107	0.99	1.05	-
22	82.0[b]	239	1.35	0.88	-
23	35.7[c]	165	1.22	1.23	-
24	46.3[c]	85	1.10	0.92	1.05[f]

* $P_{cr}^{calc} = Q_s \left[1 - \frac{(K\ell/r)^2}{2C_c^2}\right] \sigma_y A$

[a] *0.2% offset in coupon test*

[b] *Average yield from coupon tests*

[c] First yield in strut test

[d] Initial max Δ=0.094 in.

[e] Initial max Δ = 0.16 in.

[f] Tangent modulus theory

[g] Initial max Δ = 0.05 in.

[h] Initial max Δ = 0.10 in.

NOTE: 1 ksi = 6.89 MPa; 1 kip = 4.45 kN; 1 in. = 25.4 mm

Preceding page blank

Preceding page blank

TABLE 3 EXPERIMENTAL AND PREDICTED STRESSES AT FIRST THREE CONSECUTIVE BUCKLING CYCLES

STRUT NO.	2			3			4			5			19	
SHAPE	W 6x25			W 6x20			W 6x20			W 6x20			W 6x20	
$K\ell/r$	40			80			80			80			40	
CYCLE NO.	1	2	3	1	2	3	1	2	3	1	2	3	1	2
σ_{cr}^{exp} (ksi)	36.0	32.7	31.5	34.1	16.3	13.8	34.1	26.8	24.6	25.8	12.7	13.5	40.8	33.3
Δ/s	0.21	0.10	0.21	0	0.67	1.11	0	0	0	0	1.33	0.80	0	0.20
R_E	0.85	0.91	0.85	1.00	0.54	0.48	1.00	1.00	1.00	1.00	0.46	0.51	1.00	0.86
$\Sigma\ \epsilon_p \times 10^{-3}$	0	8.70	16.7	0	7.67	14.8	0	6.46	14.8	1.10	4.48	11.0	0	10.9
R_B for E_t	1.00	0.92	0.87	1.00	0.71	0.65	1.00	0.74	0.65	0.86	0.78	0.68	1.00	0.91
R_B for E_r	1.00	1.00	1.00	1.00	0.88	0.80	1.00	0.91	0.80	0.97	0.92	0.84	1.00	1.00
* σ_{cr}^{calc} for E_t	33.8	33.3	29.4	31.2	12.0	9.73	31.2	23.1	20.3	26.8	11.2	10.8	37.9	29.7
* σ_{cr}^{calc} for E_r	33.8	36.2	33.8	31.2	14.8	12.0	31.2	28.4	25.0	30.3	13.2	13.4	37.9	32.6
$\sigma_{cr}^{exp}/\sigma_{cr}^{calc}$ for E_t	1.07	0.98	1.07	1.09	1.36	1.42	1.09	1.16	1.21	0.96	1.13	1.25	1.07	1.12
$\sigma_{cr}^{exp}/\sigma_{cr}^{calc}$ for E_r	1.07	0.90	0.93	1.09	1.10	1.15	1.09	0.94	0.98	0.85	0.96	1.01	1.07	1.02

$$* \quad \sigma_{cr}^{calc} = \left[1 - \frac{(K\ell/r)^2}{2C_c^2}\right] \sigma_y\, R_E\, R_B \quad \text{(ksi)}$$

Note: 1 ksi = 6.89 MPa

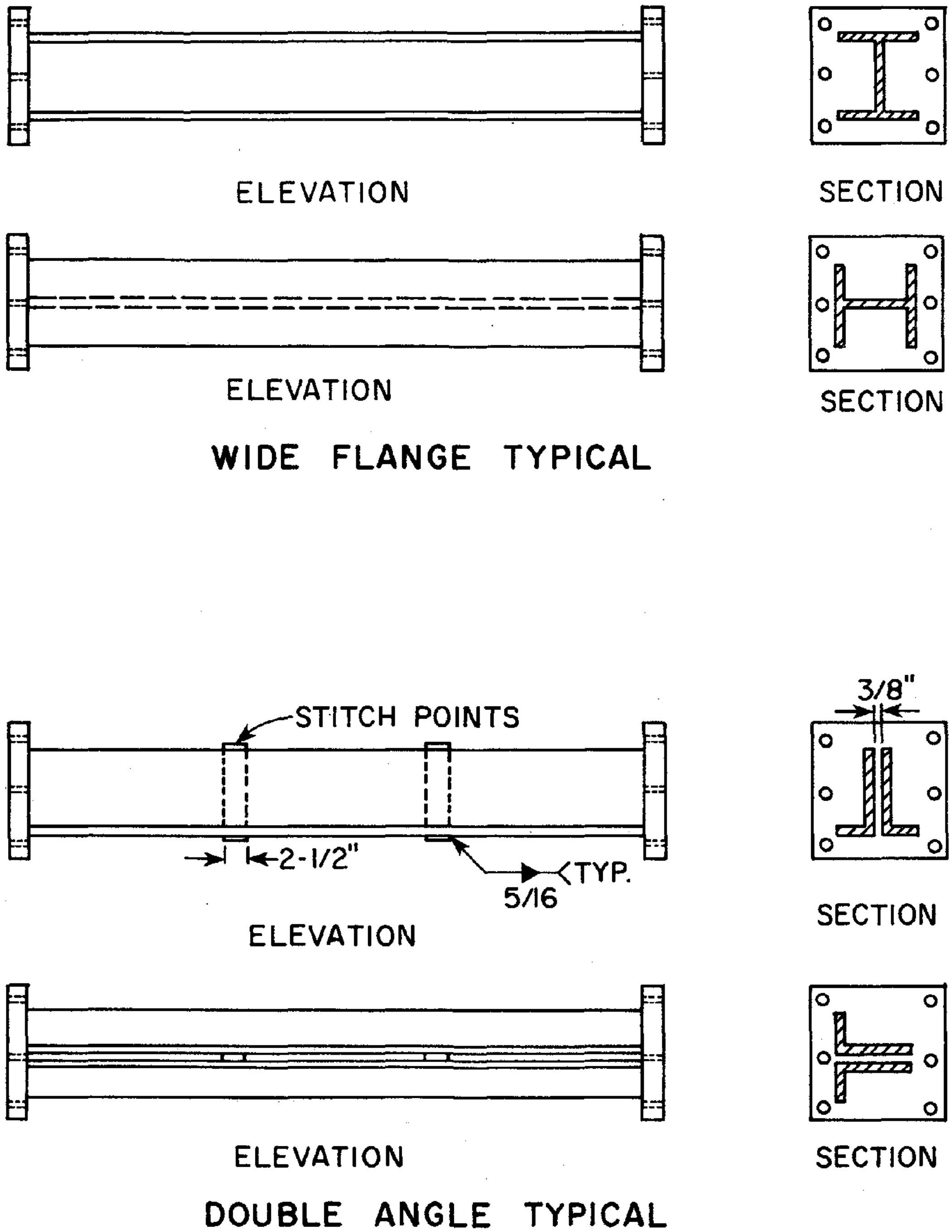

FIG. 1 TYPICAL TEST STRUTS - WIDE FLANGES AND DOUBLE ANGLES

Preceding page blank

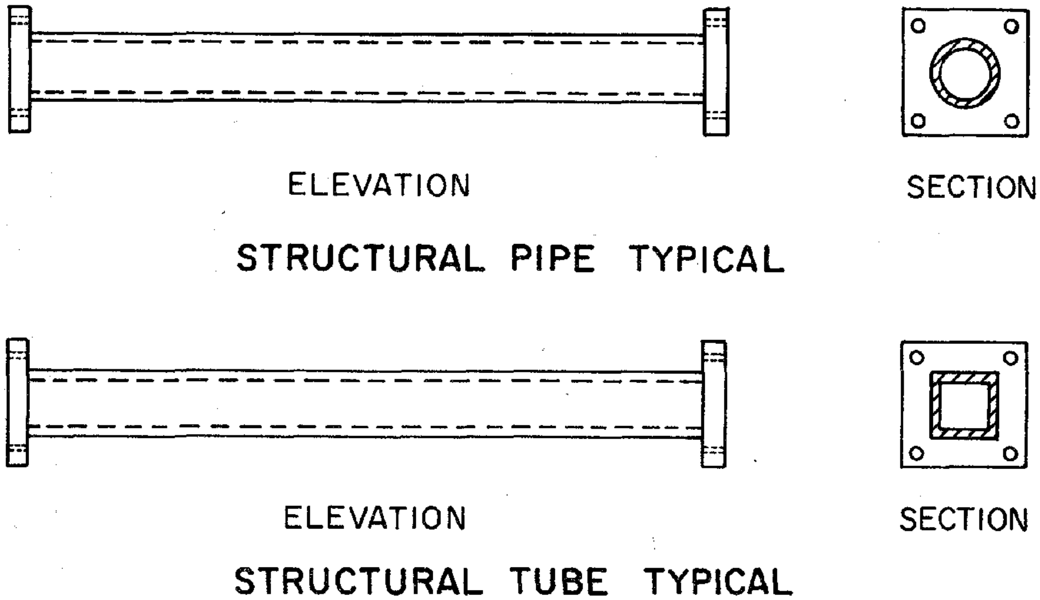

FIG. 2 TYPICAL TEST STRUTS - PIPES AND TUBES

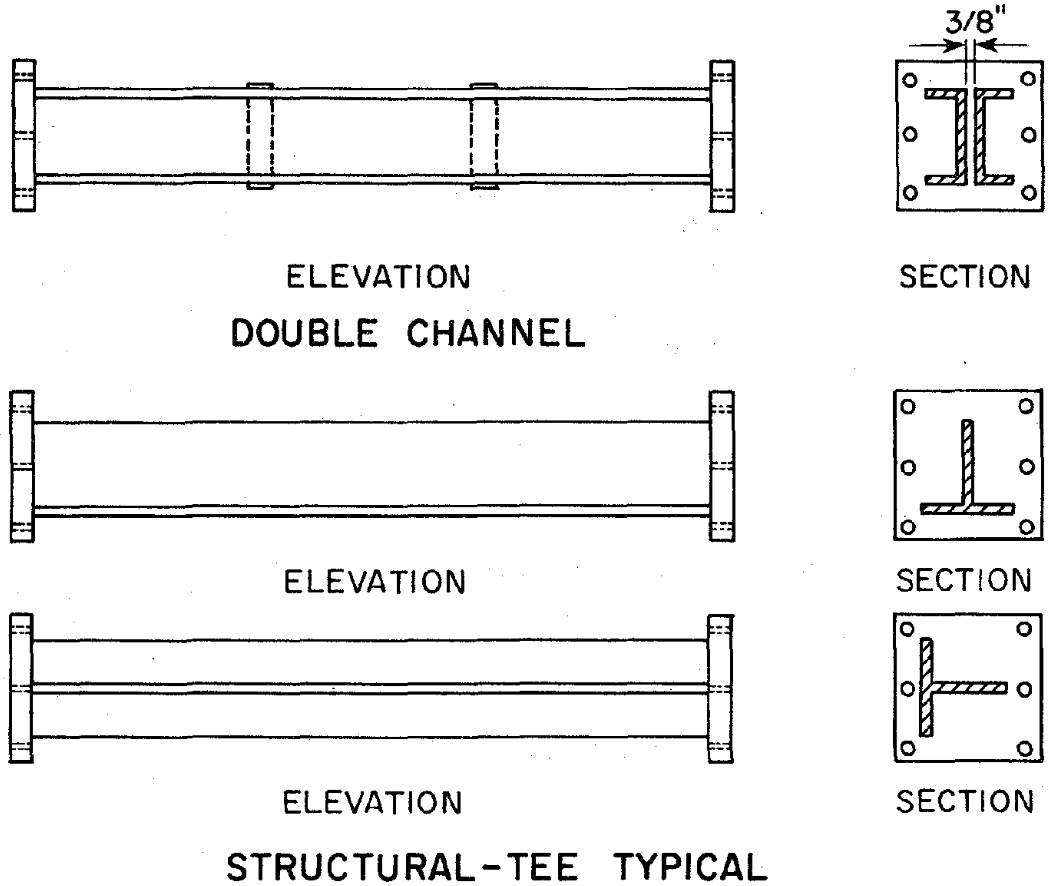

FIG. 3 TYPICAL TEST STRUTS - DOUBLE CHANNEL AND STRUCTURAL TEES

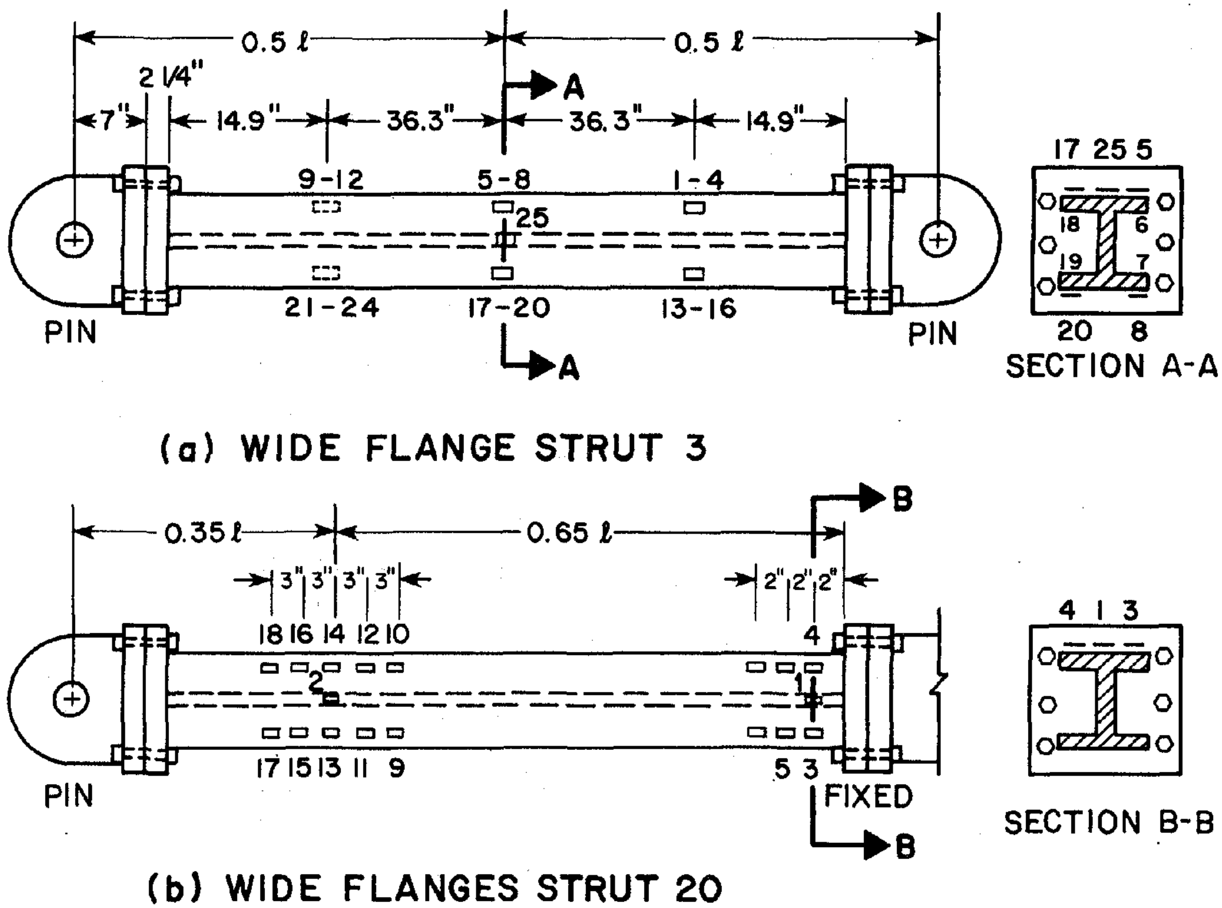

FIG. 4 TEST SPECIMENS WITH EXAMPLES OF STRAIN GAGE ARRANGEMENTS

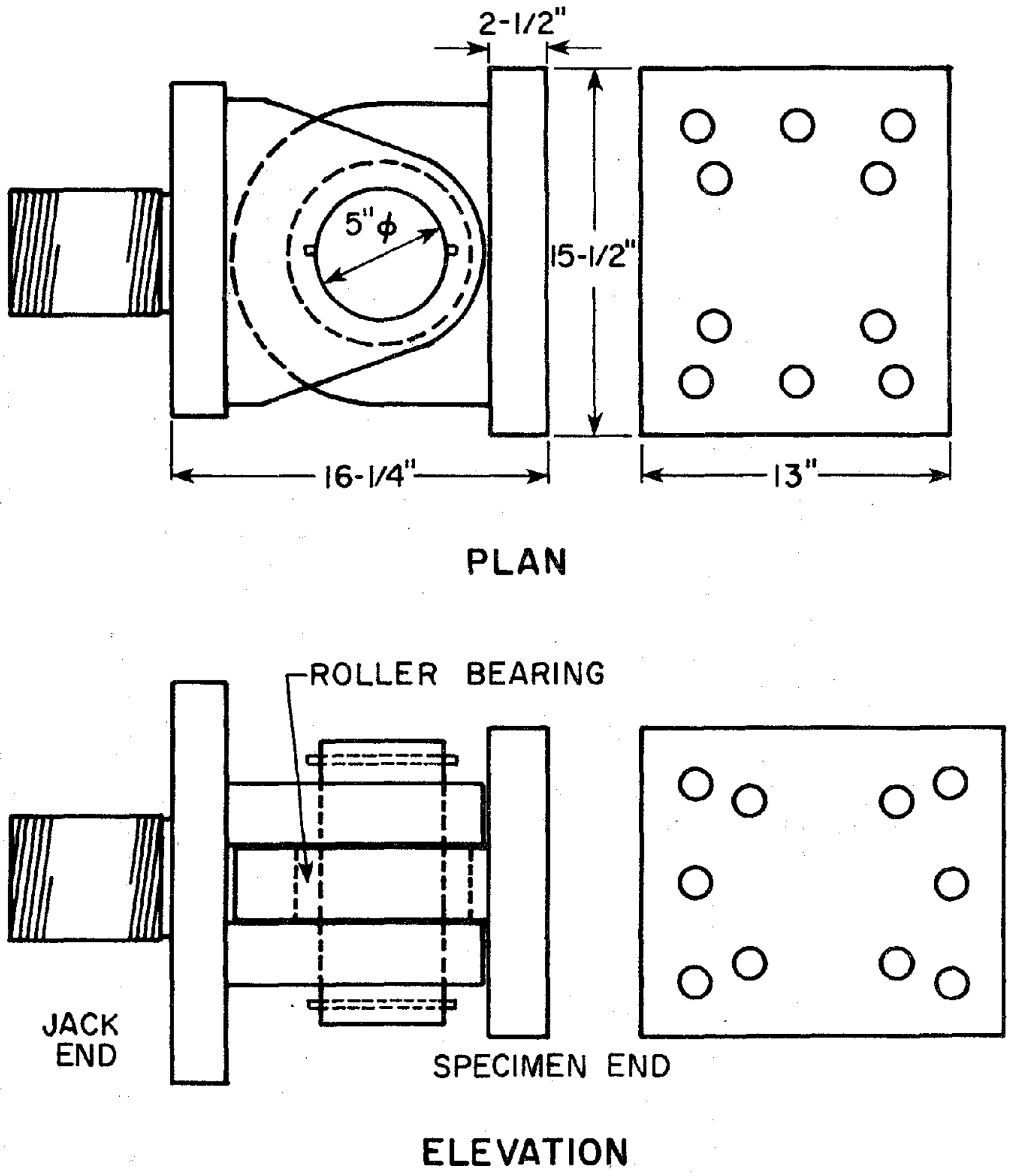

FIG. 5 CLEVIS DETAILS

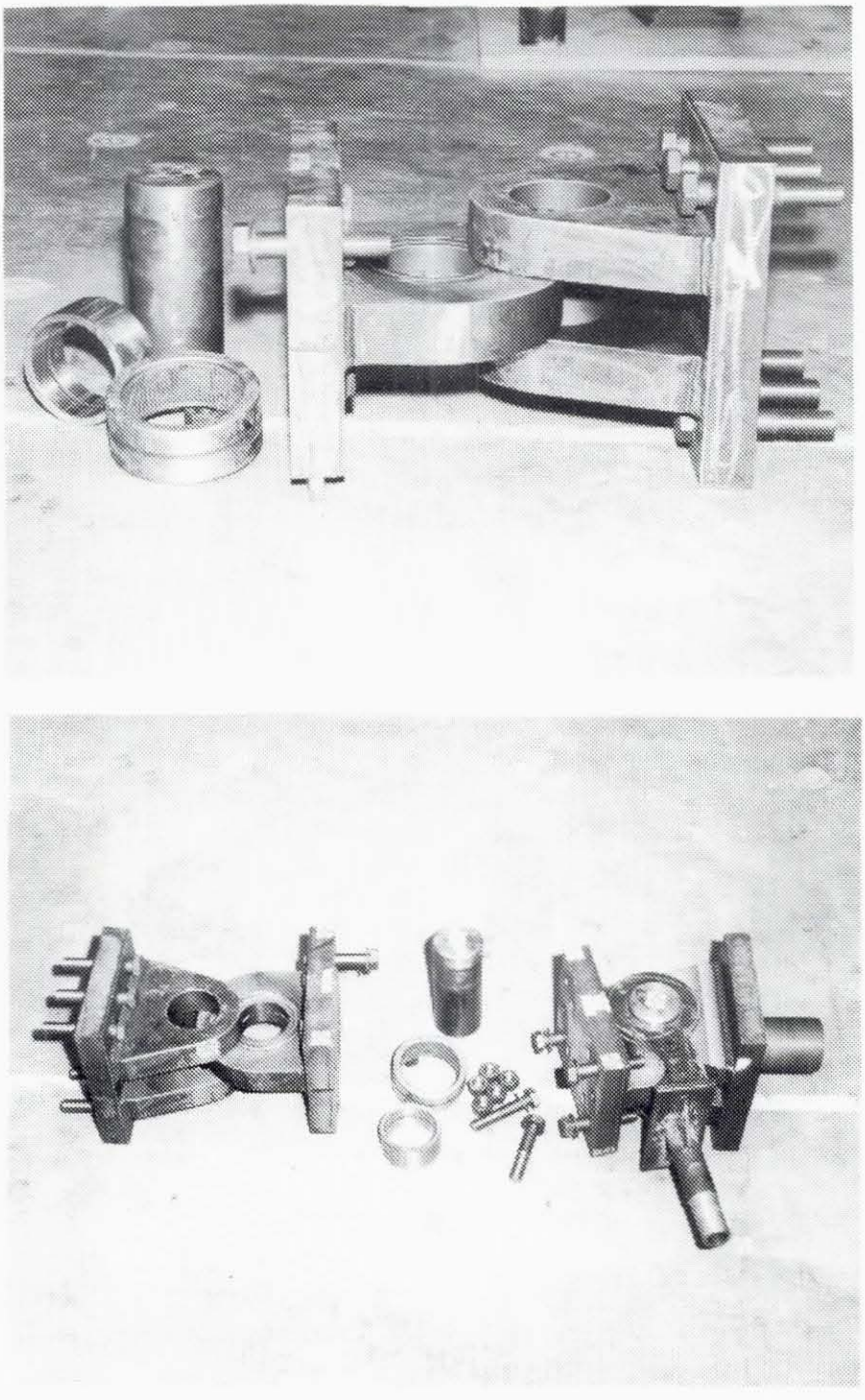

FIG. 6 EXPLODED VIEWS OF END CELVISES

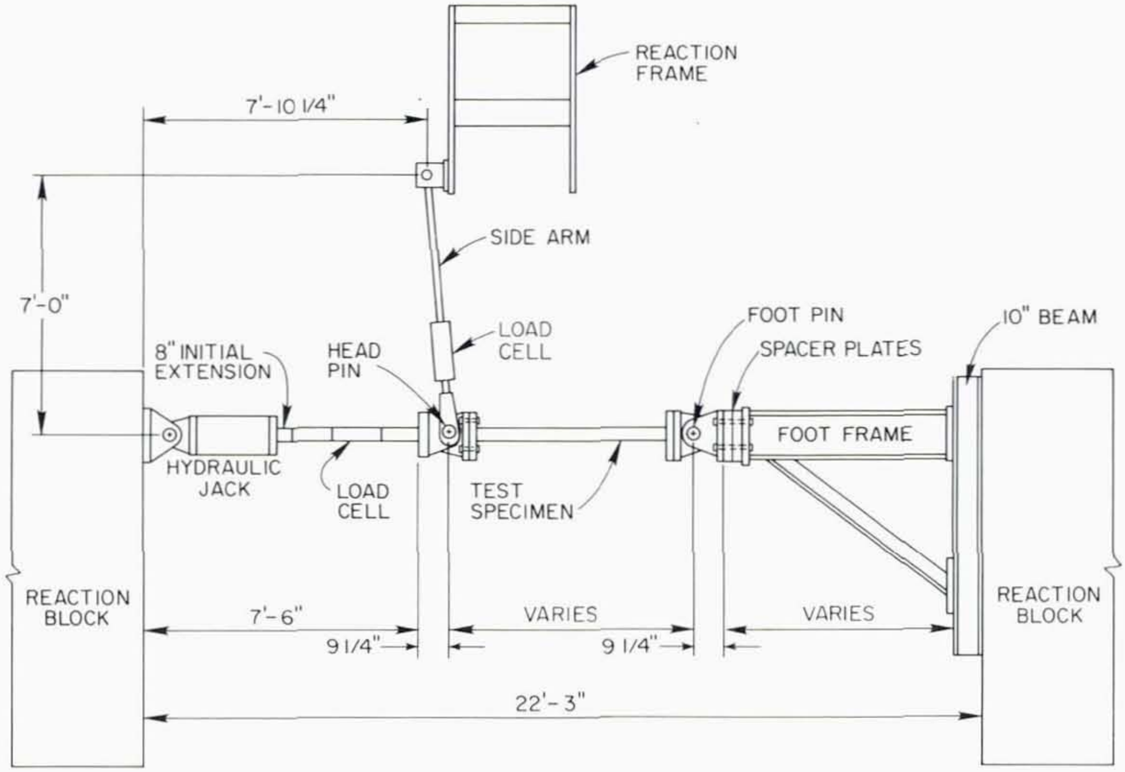

FIG. 7 PINNED-PINNED TEST LAYOUT

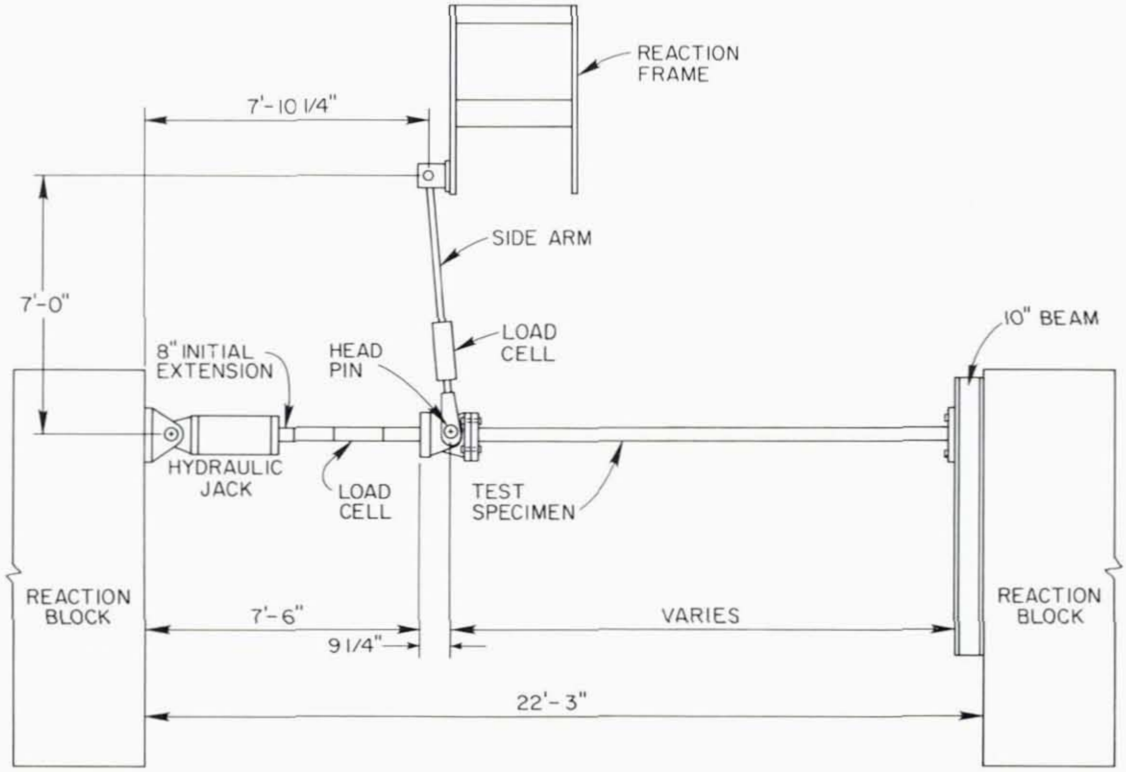

FIG. 8 FIXED-PINNED TEST LAYOUT

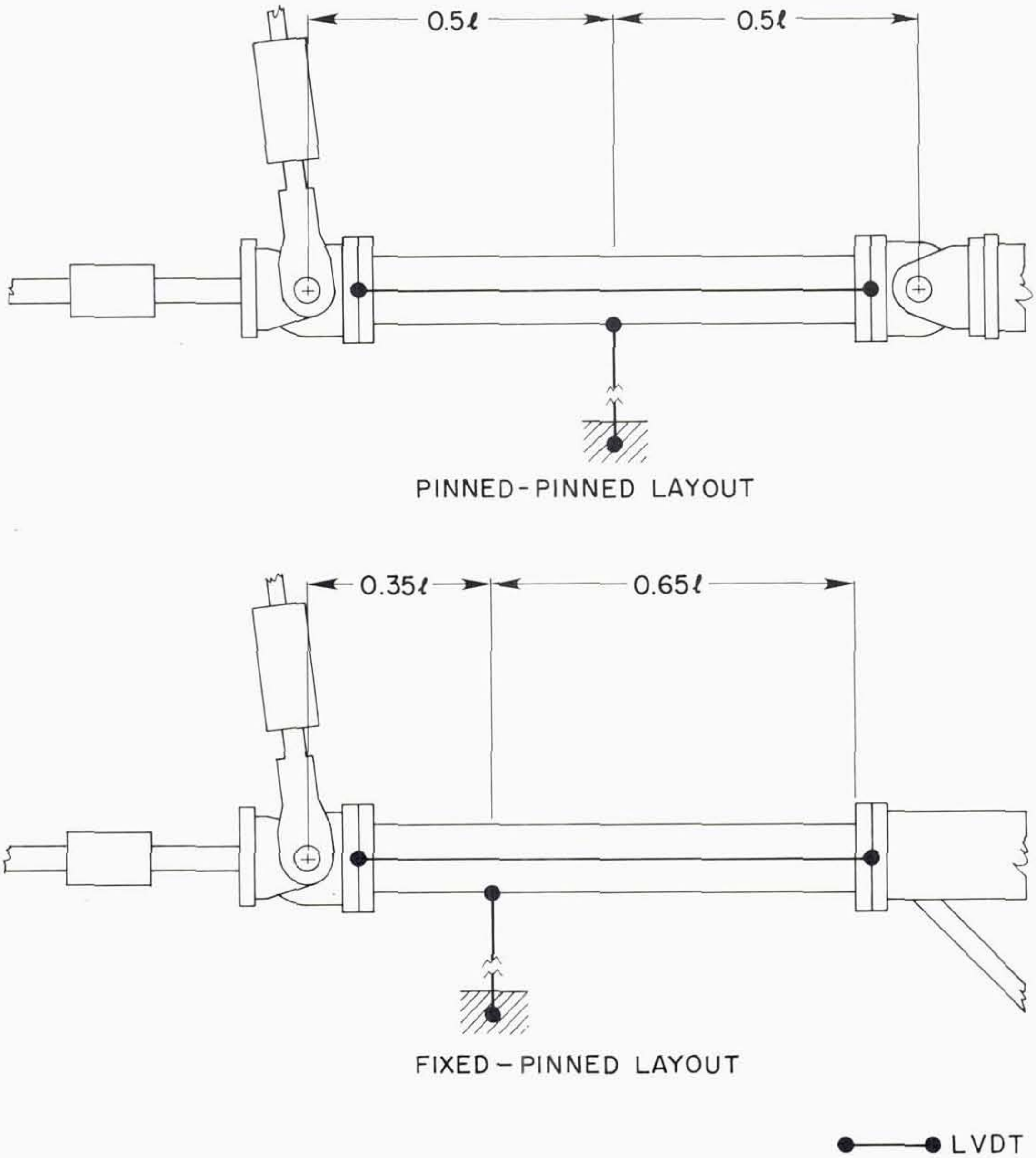

FIG. 9 LOCATION OF LVDT'S

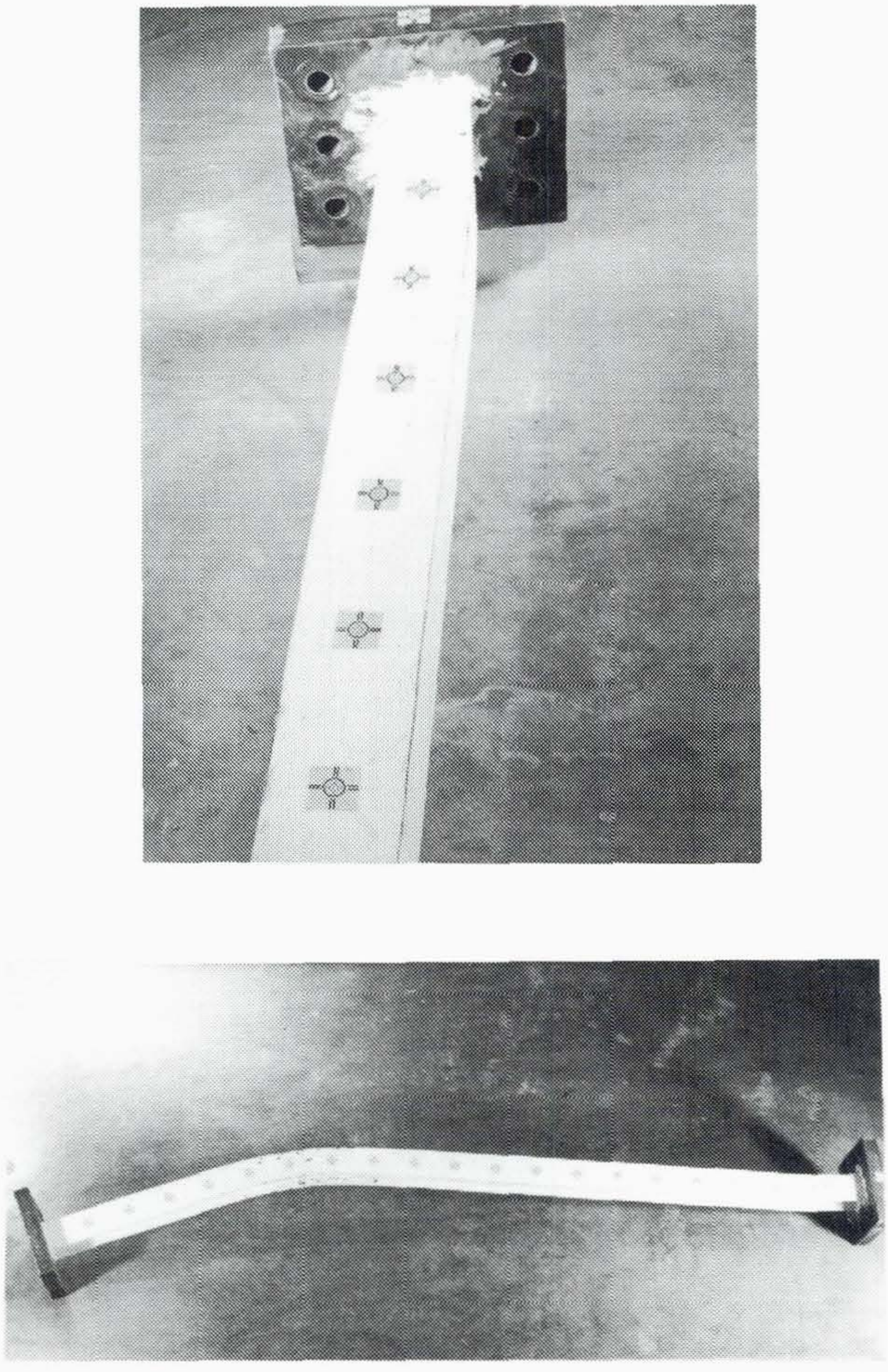

FIG. 10 STRUT 23 AFTER TEST - NOTE GLUED-ON PHOTOGRAMMETRIC TARGETS

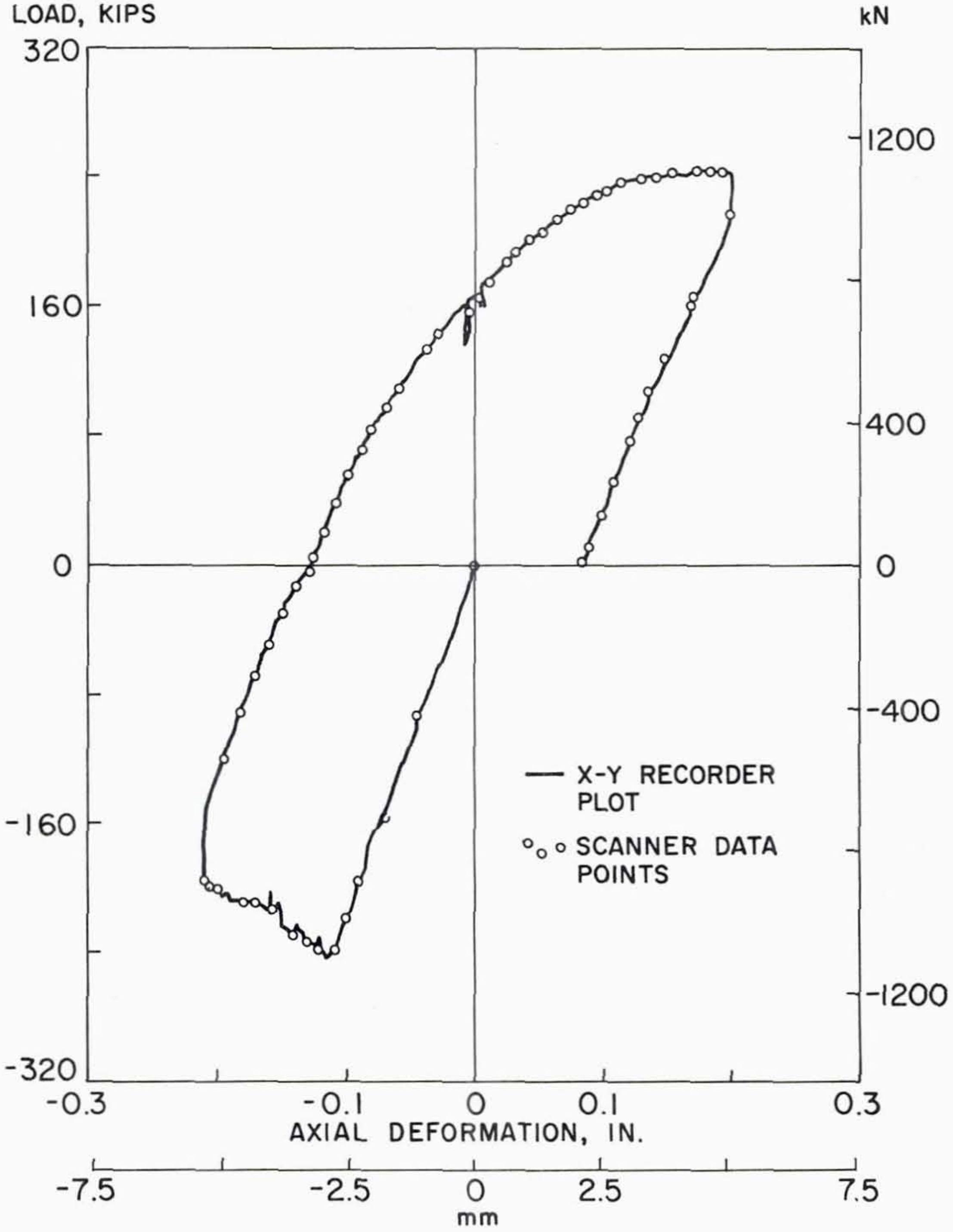

FIG. 11 X-Y RECORDER PLOT COMPARED WITH SCANNER OUTPUT - STRUT 19, CYCLE 1

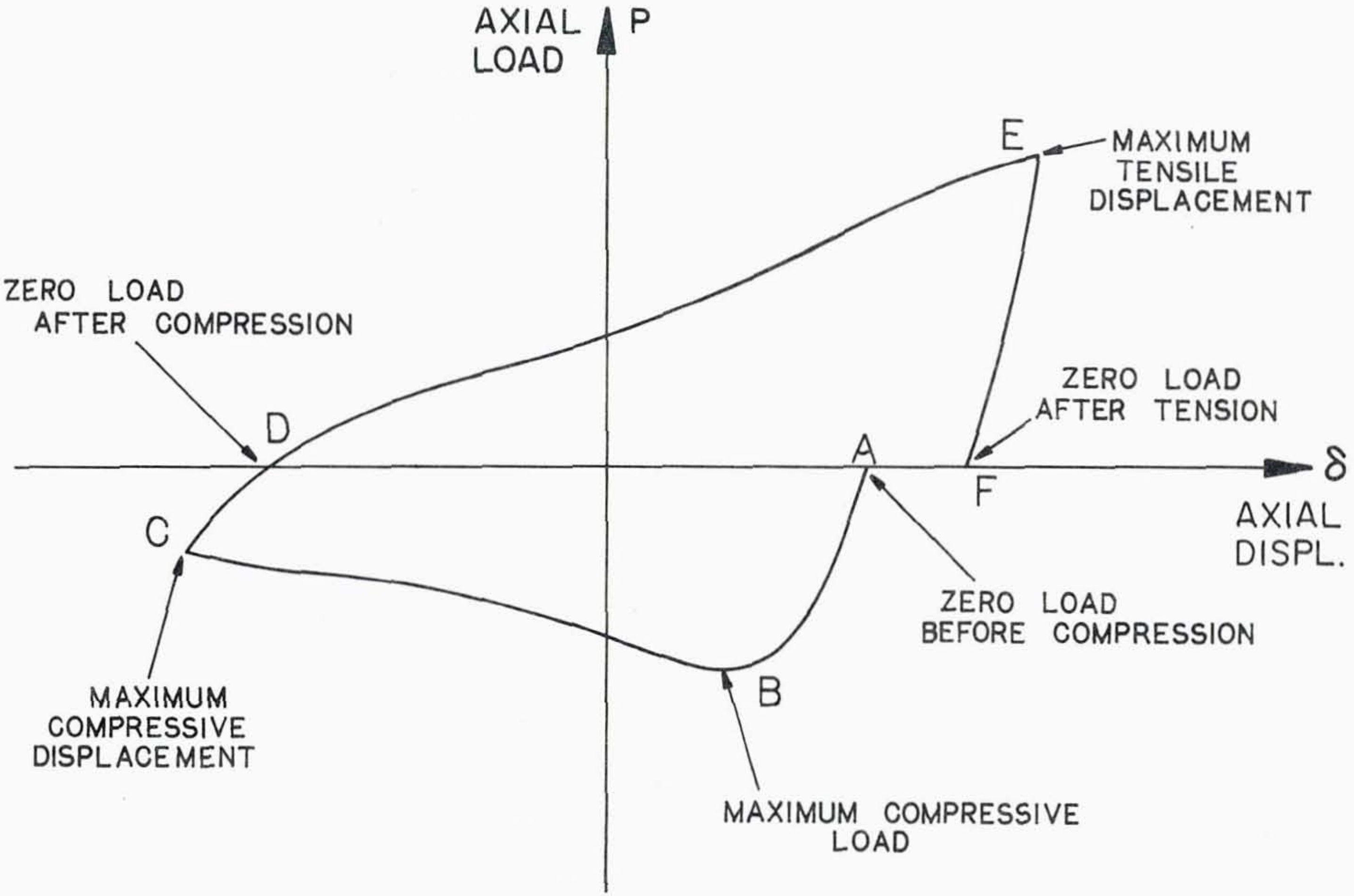

FIG. 12 DESIGNATION OF REFERENCE POINTS

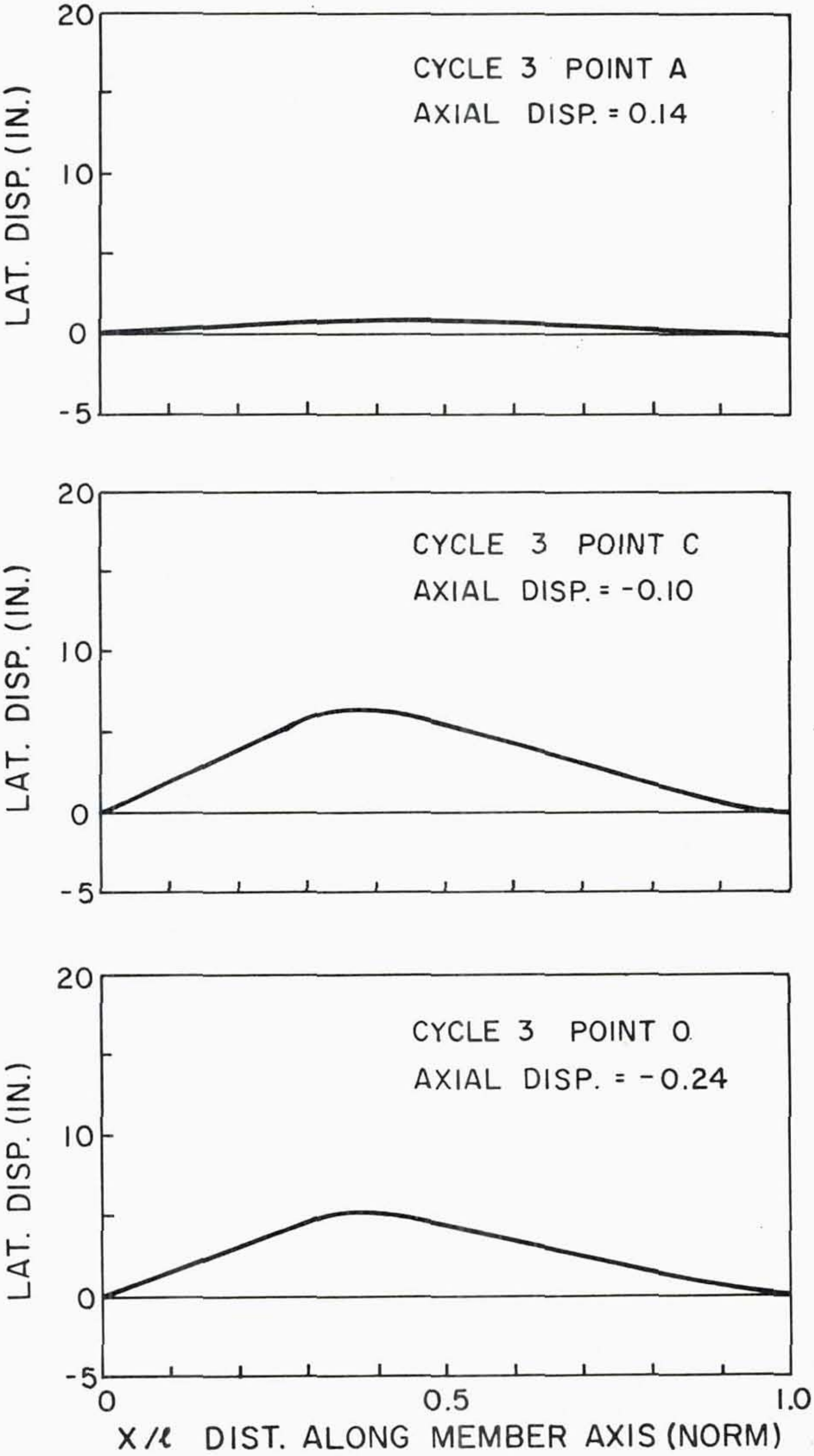

FIG. 13 LATERAL DISPLACEMENTS FROM PHOTOGRAMMETRIC DATA - STRUT 23 - COMPRESSIVE CYCLE

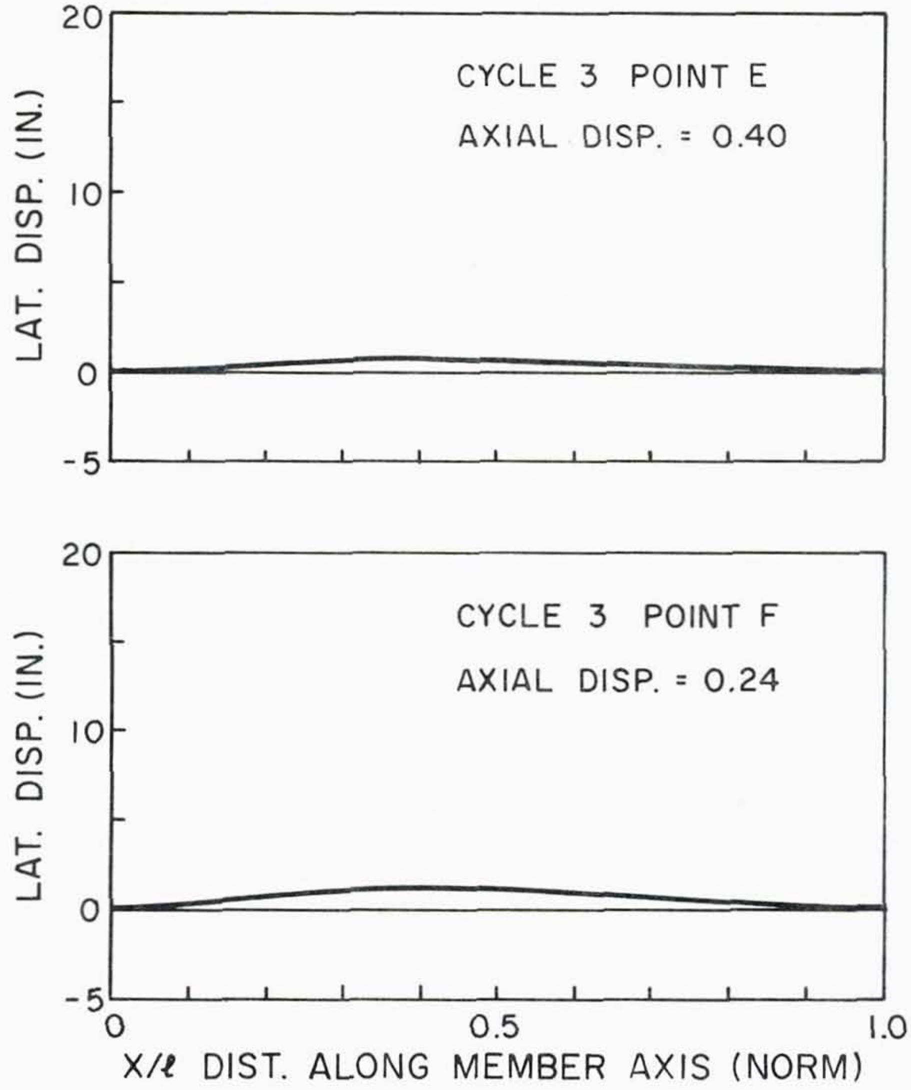

FIG. 14 LATERAL DISPLACEMENTS FROM PHOTOGRAMMETRIC DATA - STRUT 23 - (a) AT MAXIMUM AXIAL PULL; (b) RESIDUAL DISPLACEMENTS AFTER RELEASE OF TENSILE FORCE

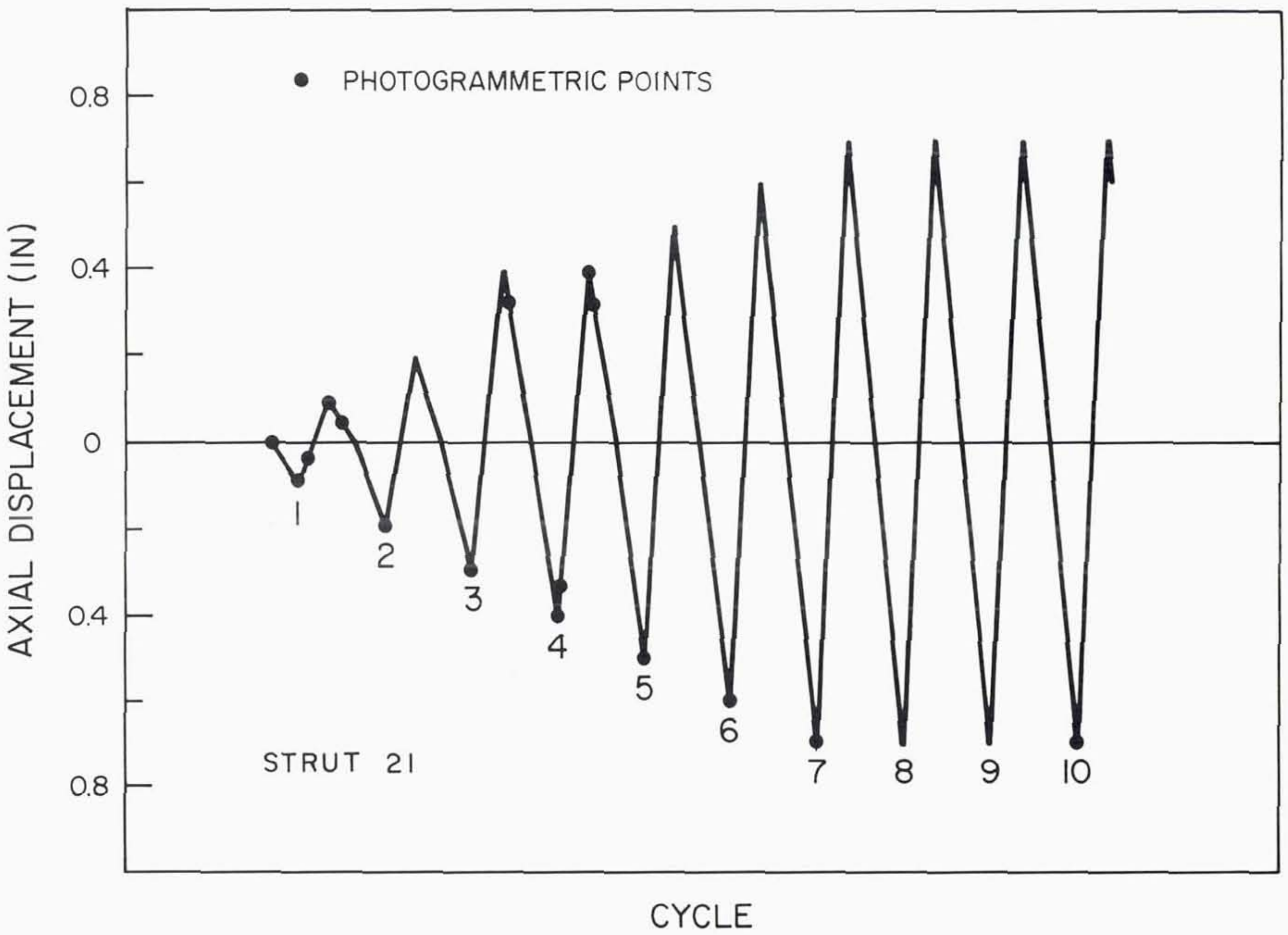

FIG. 15 LOADING SEQUENCE AND PHOTOGRAMMETRIC POINTS FOR STRUT 21

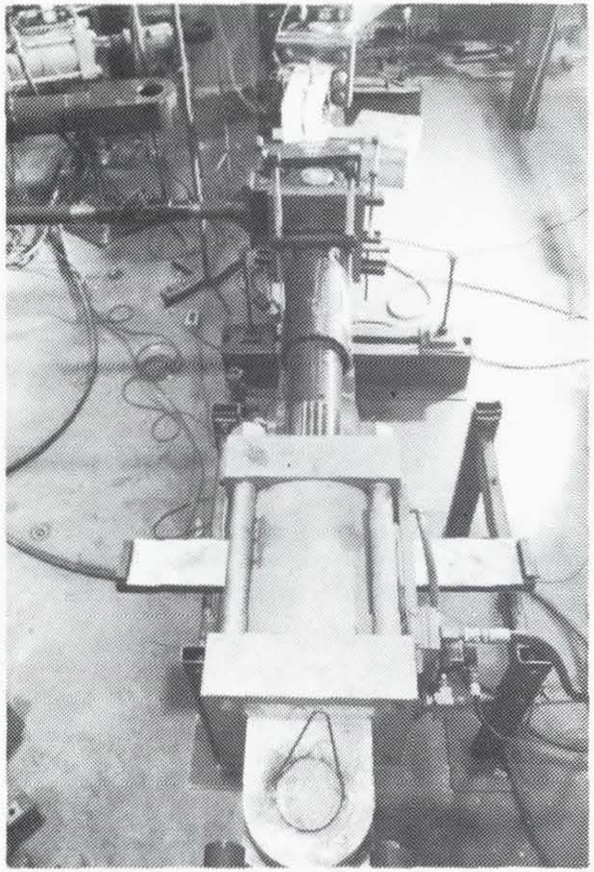

FIG. 16 LOADING CYLINDER WITH A SPECIMEN IN-PLACE

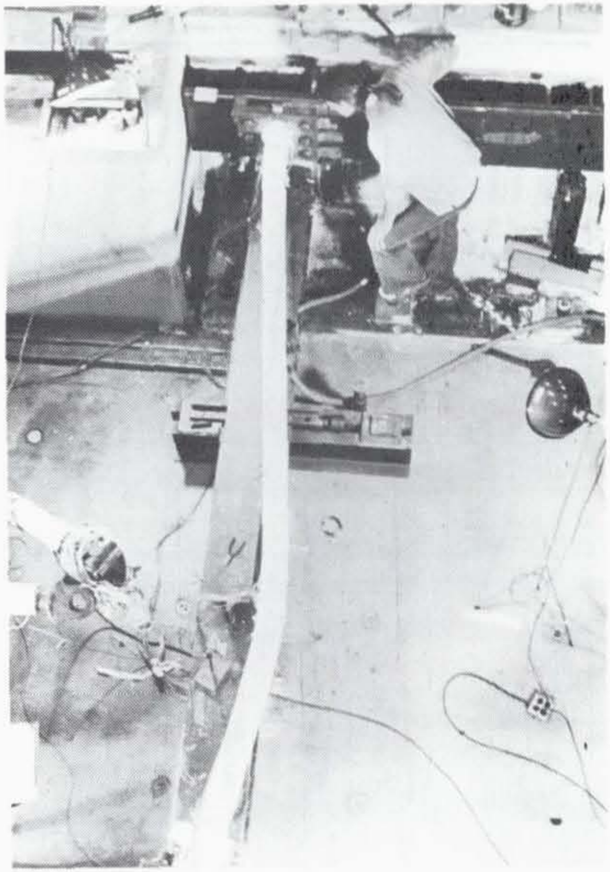

FIG. 17 STRUT 22 IN TESTING BAY

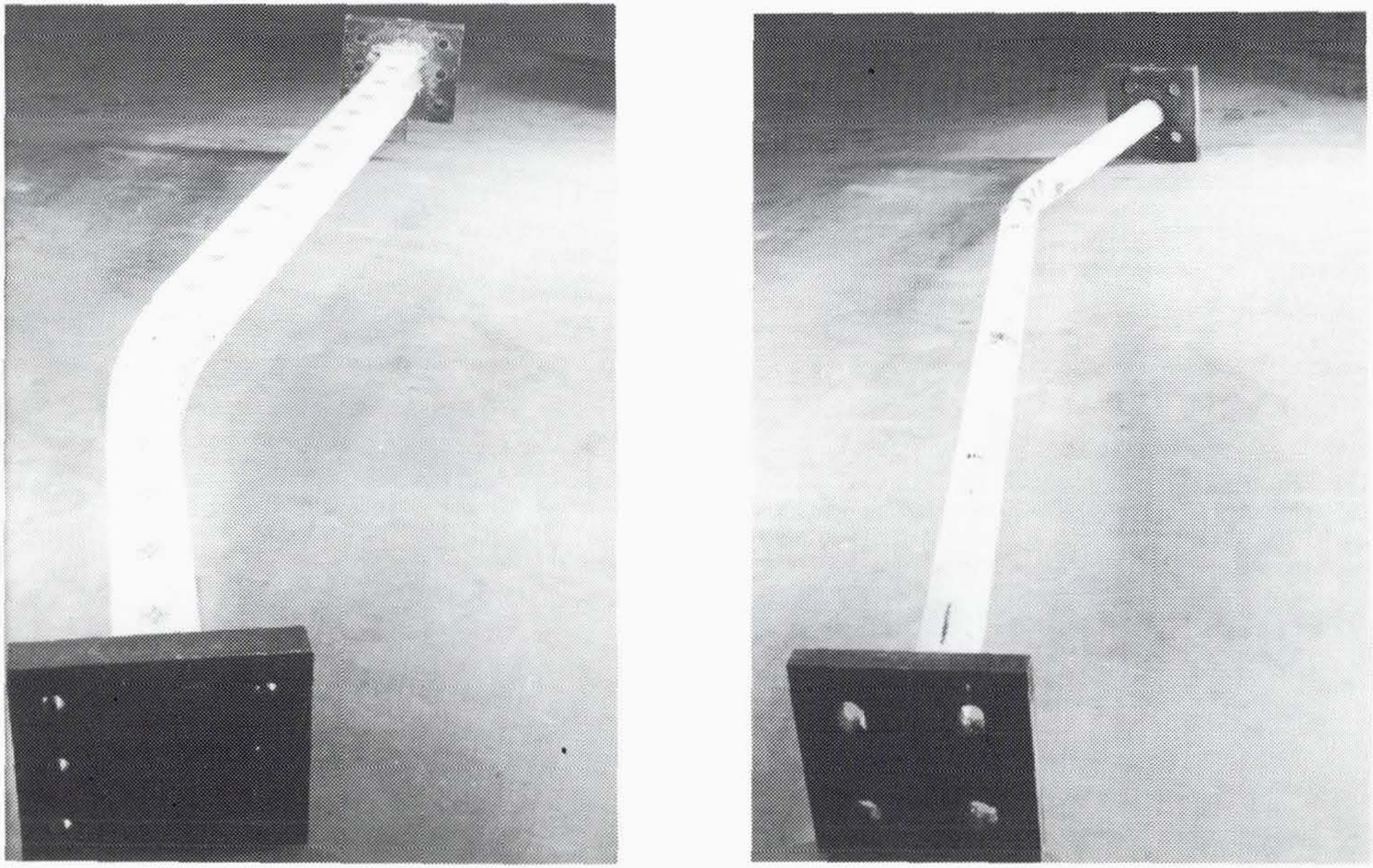

FIG. 18 STRUTS 23 AND 24 AFTER TEST

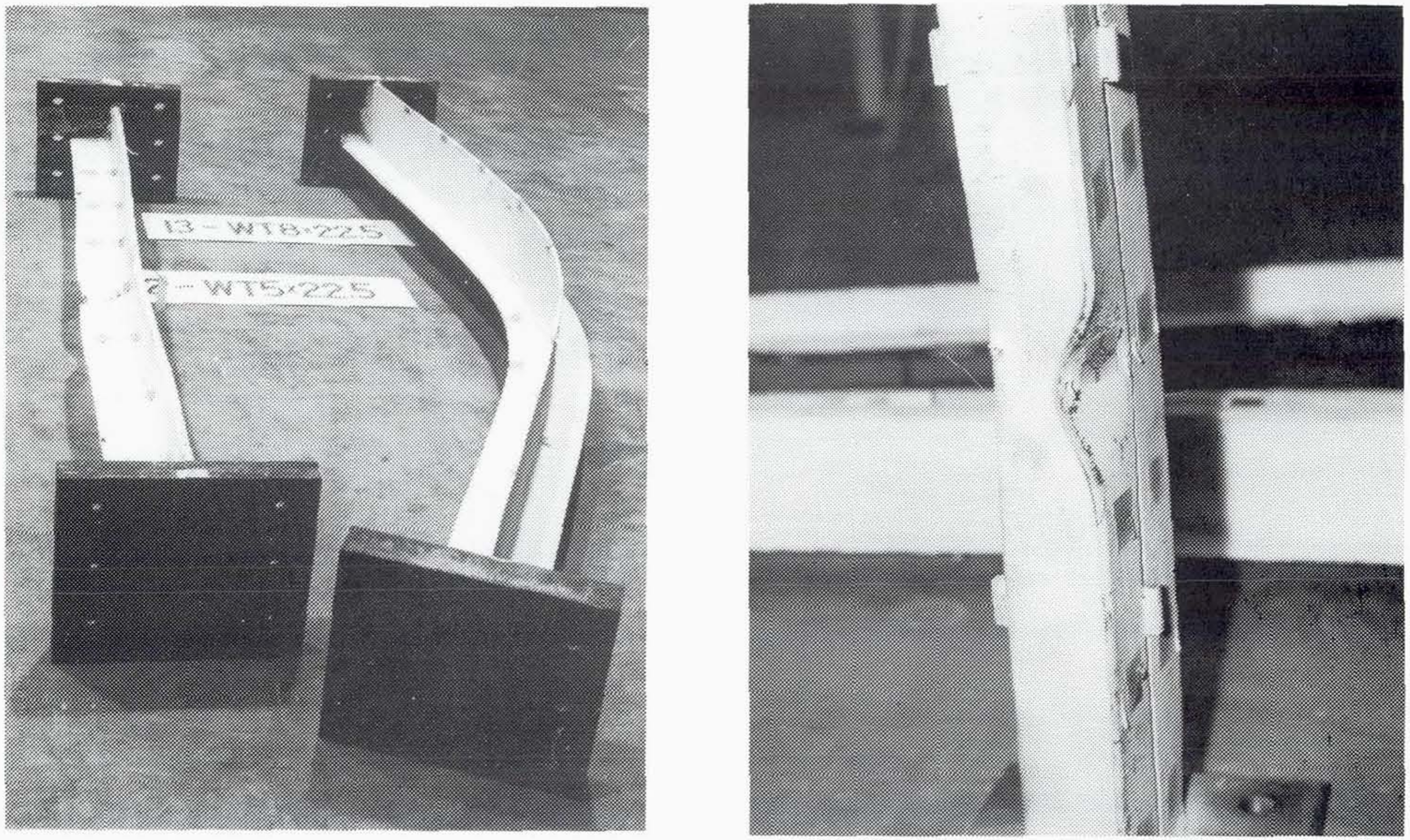

FIG. 19 STRUTS 12, 13 AND 9 AFTER TEST

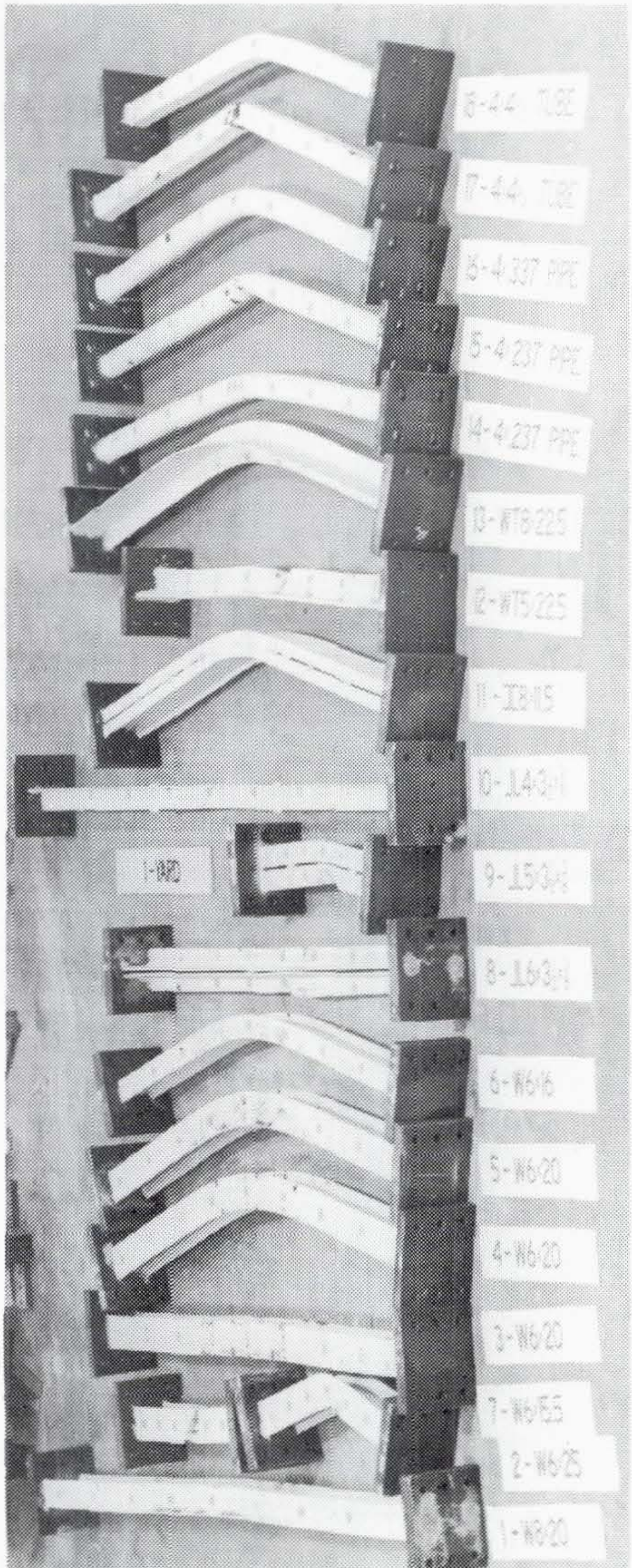

FIG. 20 PIN-ENDED SPECIMENS AFTER TESTS

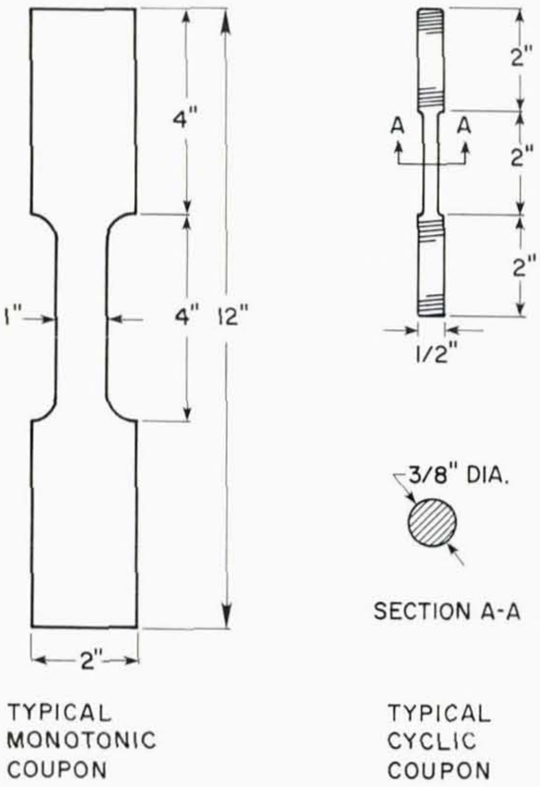

FIG. 21 TEST COUPON DETAILS

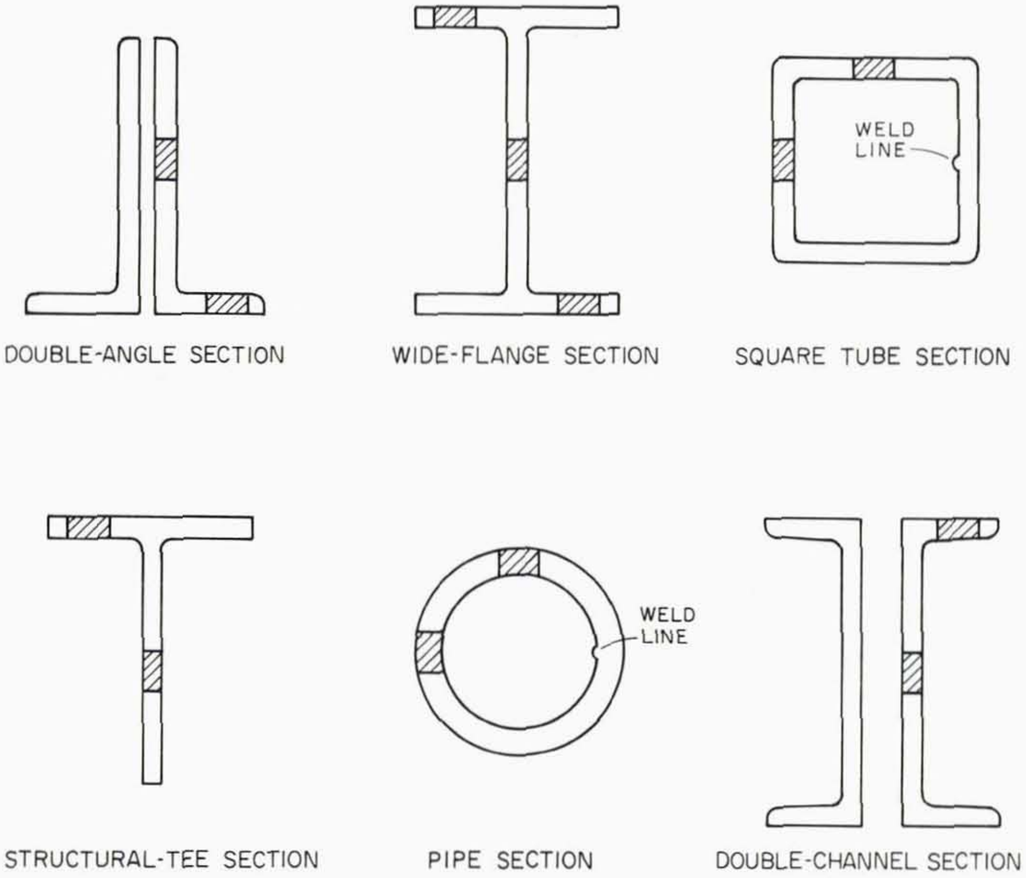

FIG. 22 TYPICAL LOCATIONS OF TENSILE COUPONS

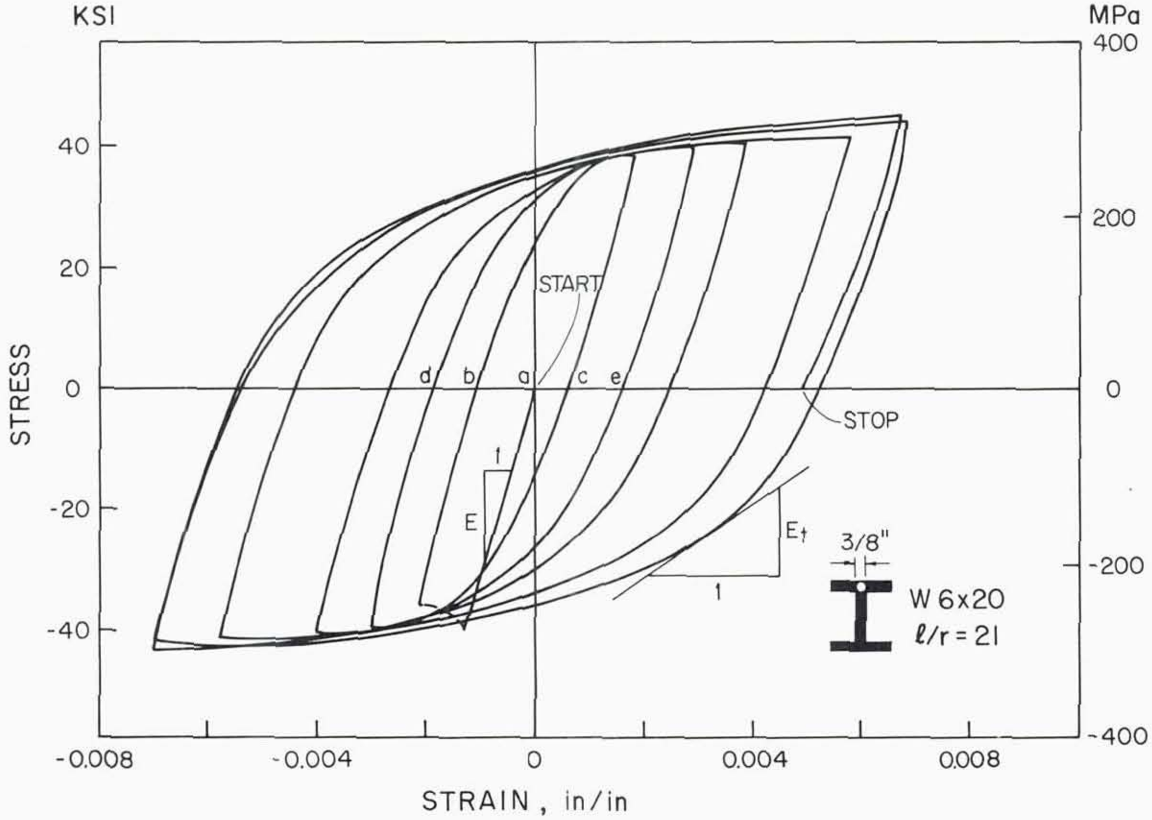

FIG. 23 HYSTERETIC CURVES FROM A CYCLIC COUPON TEST

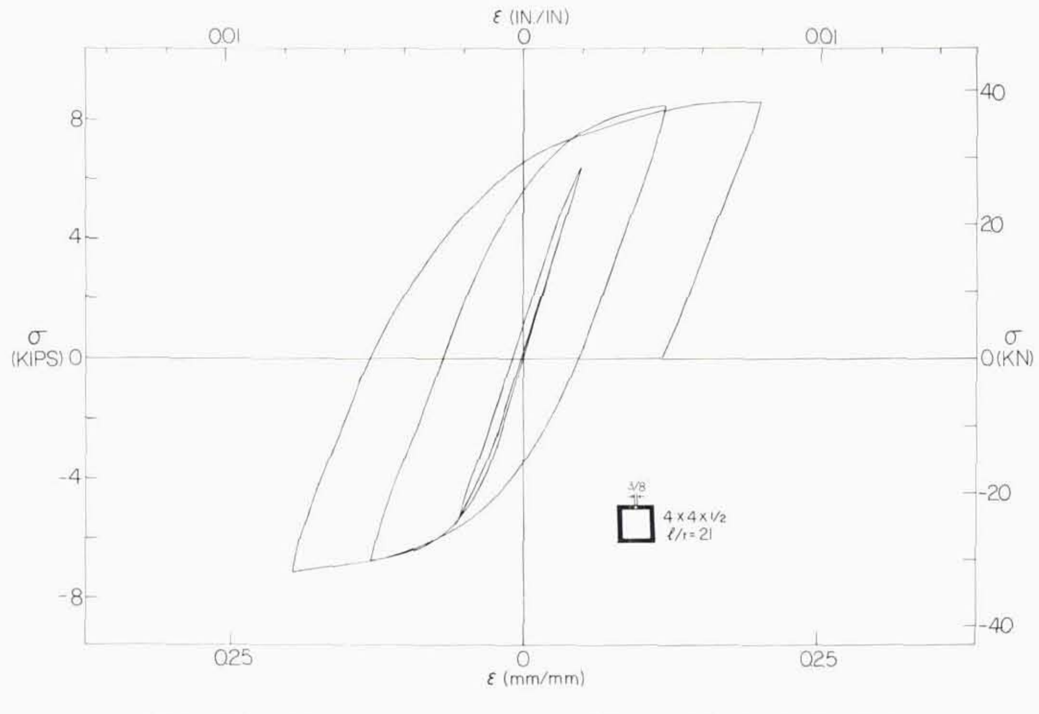

FIG. 24 HYSTERETIC CURVES FROM A CYCLIC COUPON TEST

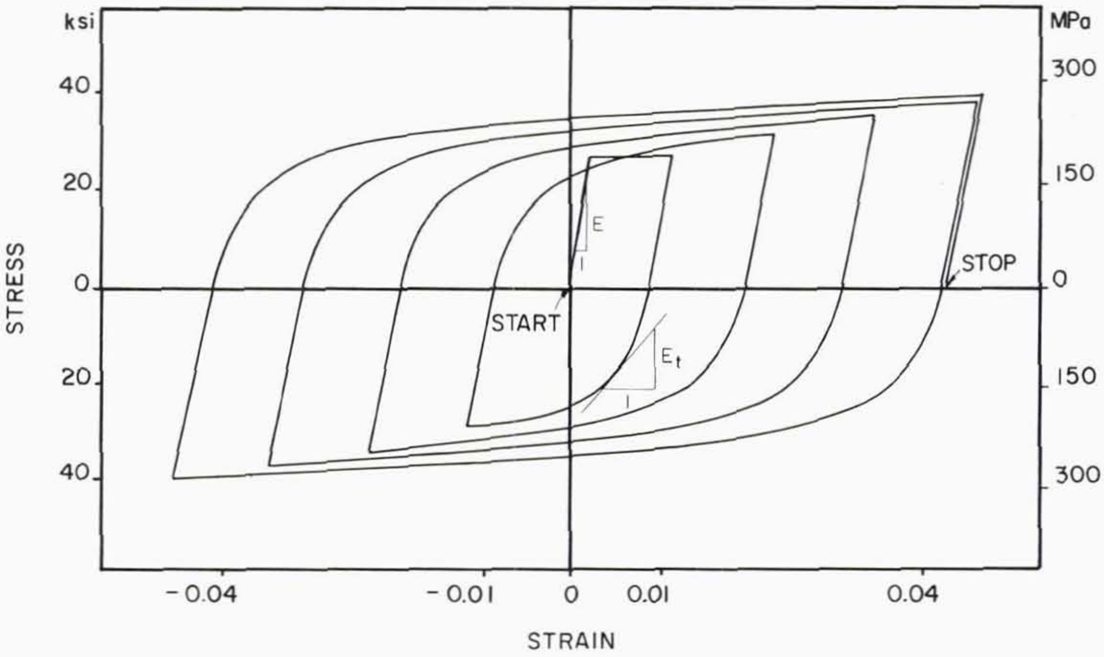

FIG. 25 HYSTERETIC CURVES - CYCLIC COUPON INITIALLY YIELDED IN TENSION [12]

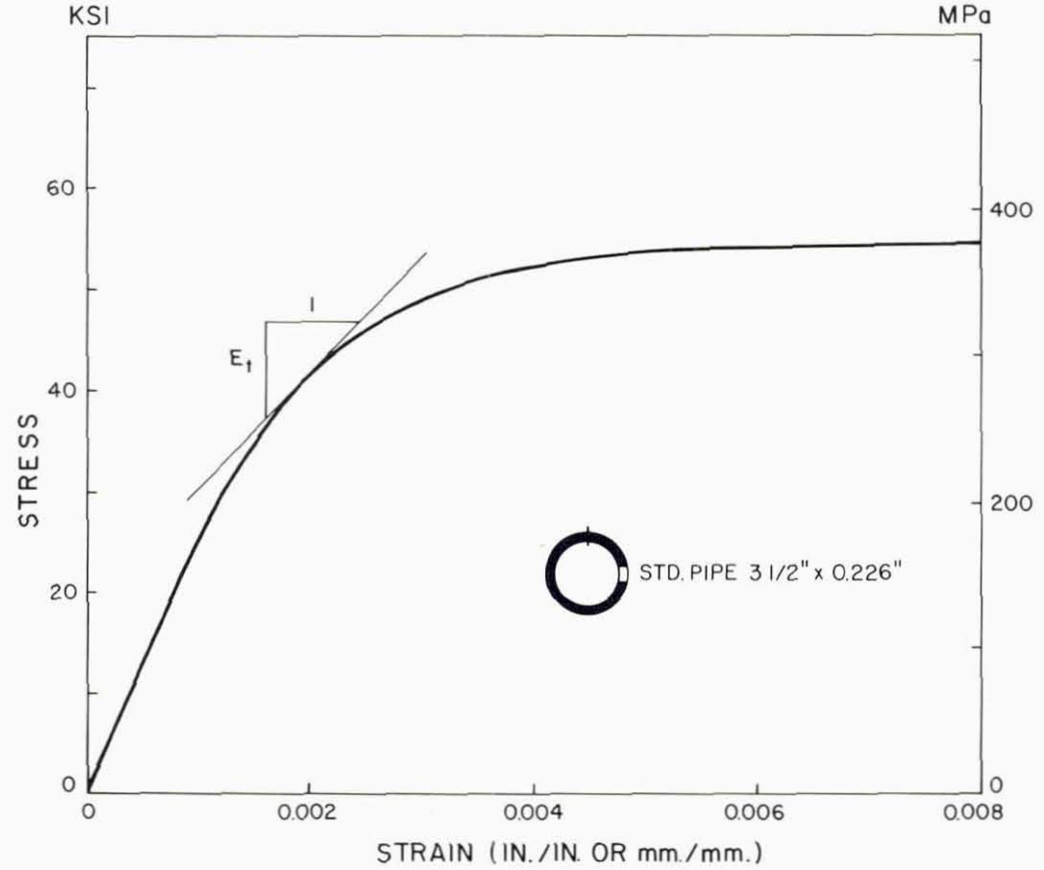

FIG. 26 MONOTONIC COUPON TEST

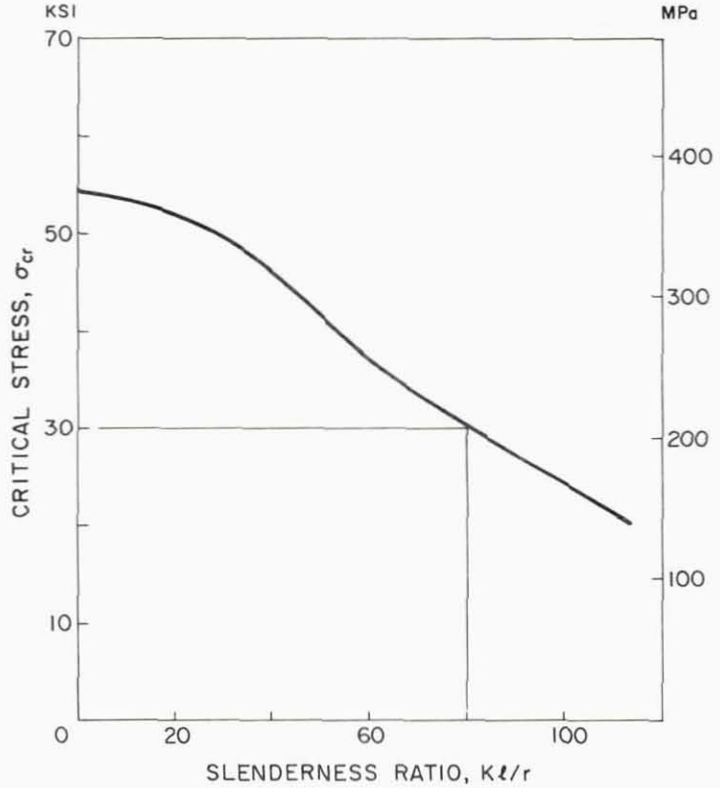

FIG. 27 CRITICAL BUCKLING STRESS VERSUS SLENDERNESS RATIO FOR STRUT 24

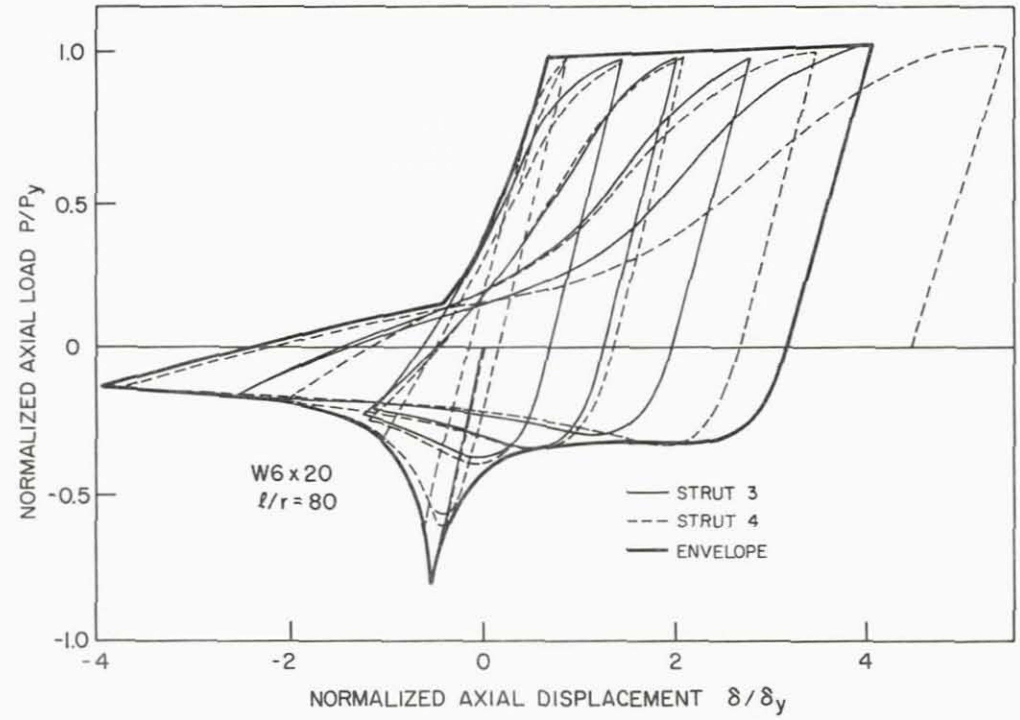

FIG. 28 HYSTERETIC ENVELOPES FOR STRUTS 3 AND 4

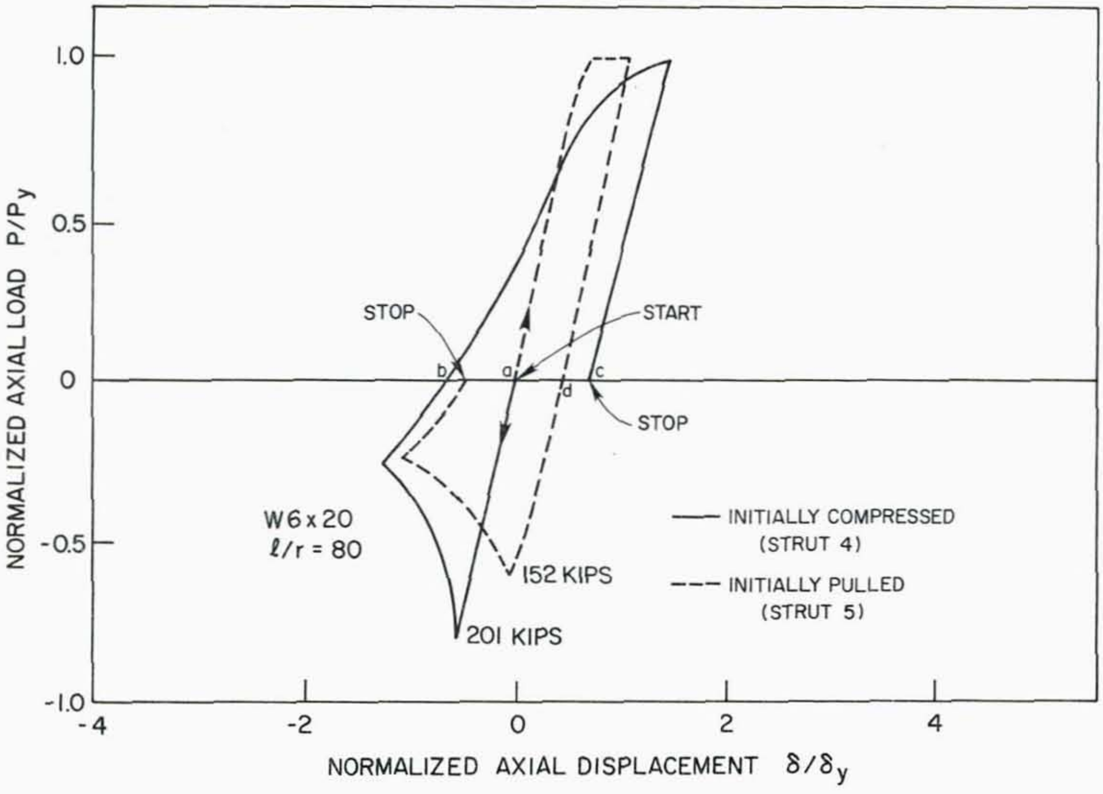

FIG. 29 HYSTERETIC CURVES FOR TWO IDENTICAL STRUTS

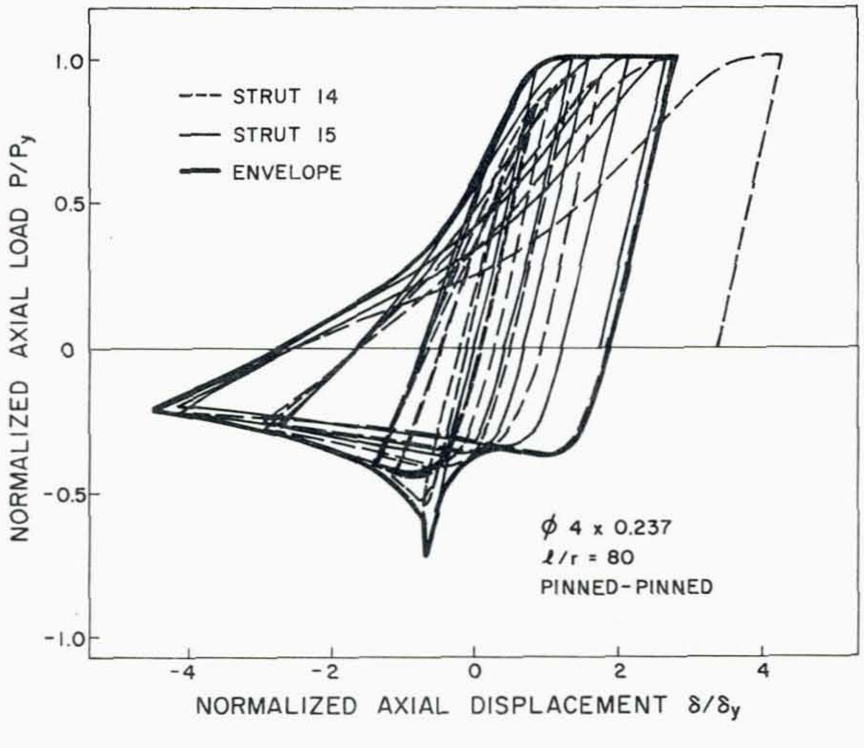

FIG. 30 HYSTERETIC ENVELOPE FOR STRUTS 14 AND 15

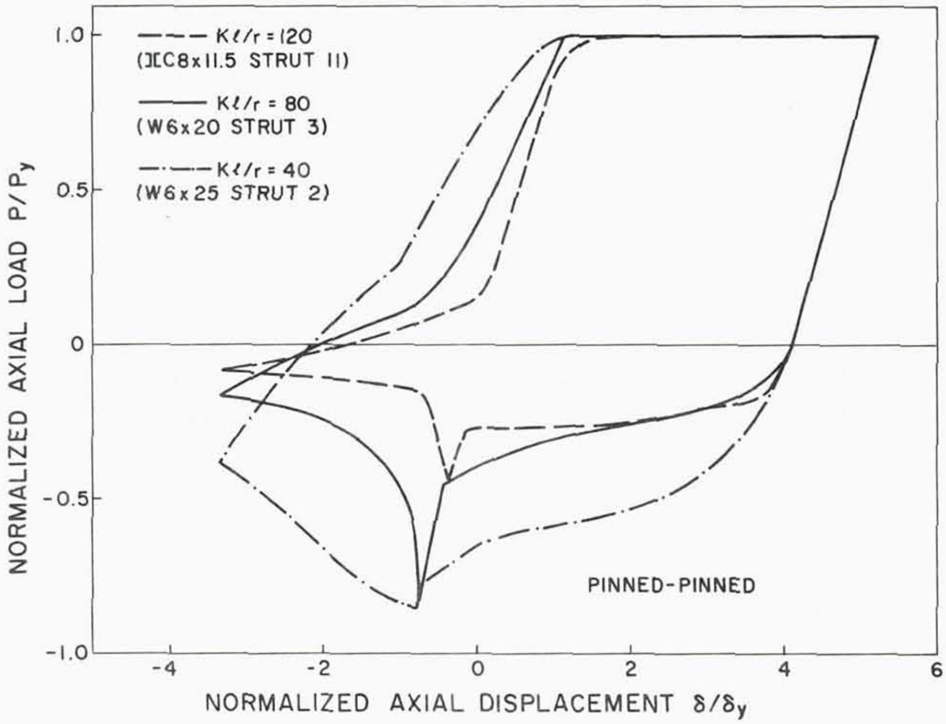

FIG. 31 HYSTERETIC ENVELOPES FOR STRUTS WITH DIFFERENT SLENDERNESS RATIOS

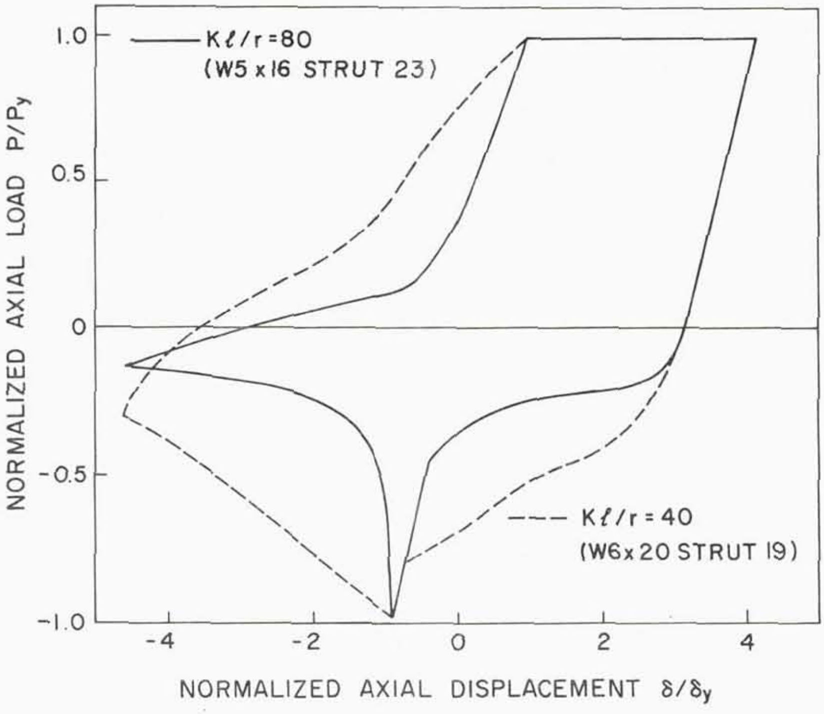

FIG. 32 HYSTERETIC ENVELOPES FOR STRUTS WITH DIFFERENT SLENDERNESS RATIOS

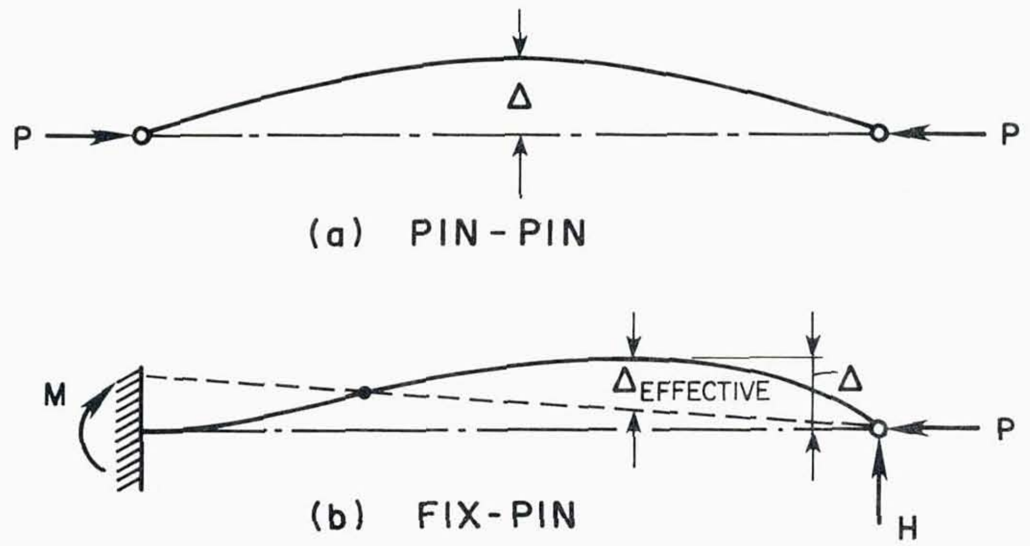

FIG. 33 DEFLECTED ELASTIC CURVES FOR BUCKLED STRUTS WITH DIFFERENT BOUNDARY CONDITIONS

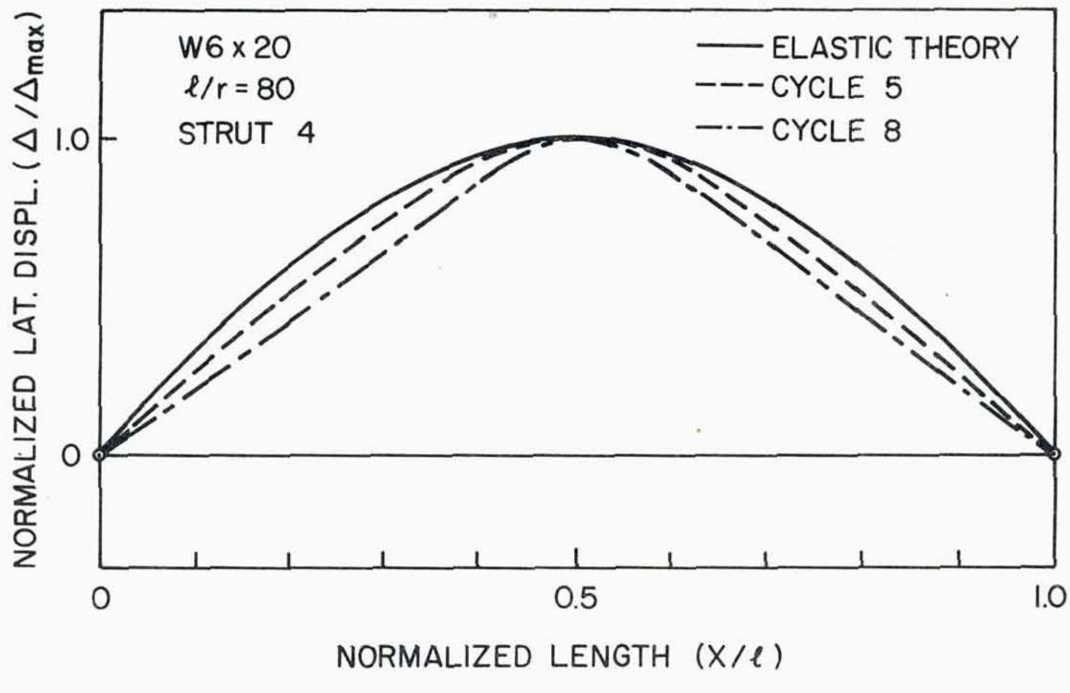

FIG. 34 INELASTIC BUCKLED SHAPES COMPARED WITH ELASTIC CURVE FOR A STRUT WITH PINNED ENDS

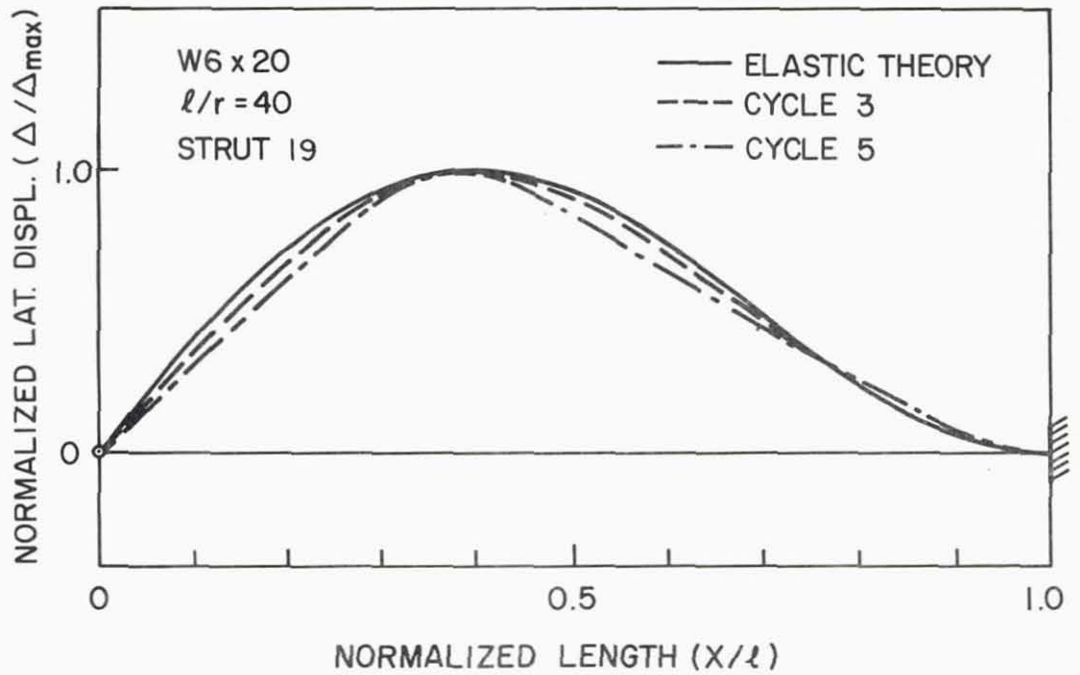

FIG. 35 INELASTIC BUCKLED SHAPES COMPARED WITH ELASTIC CURVE FOR A STRUT PINNED AT ONE AND FIXED AT THE OTHER

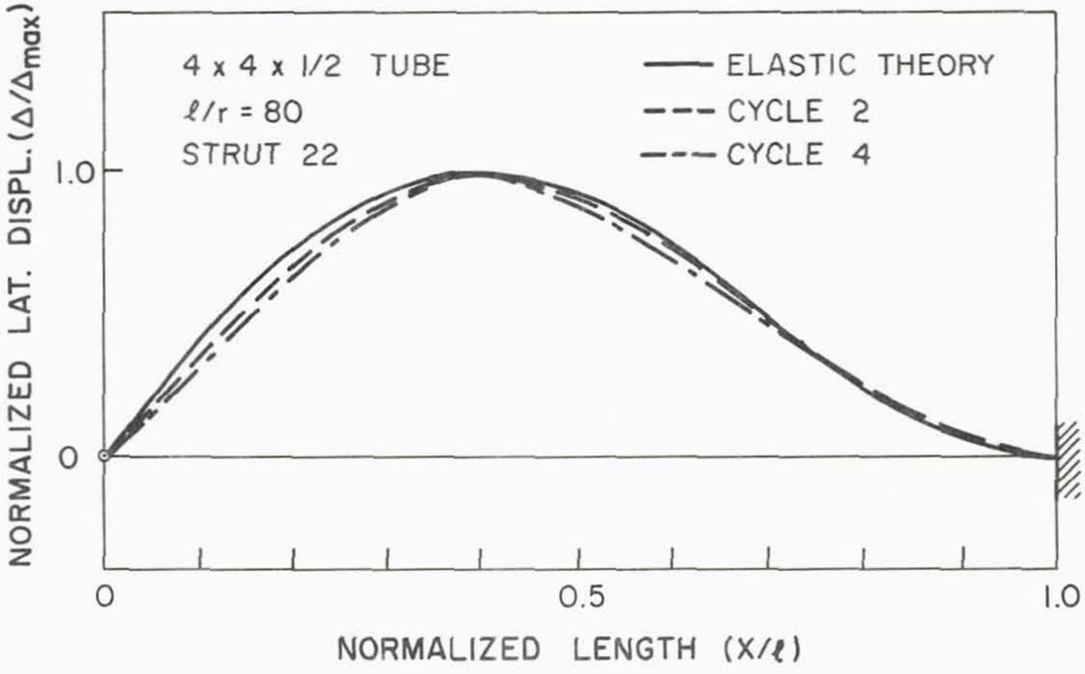

FIG. 36 INELASTIC BUCKLED SHAPES COMPARED WITH ELASTIC CURVE

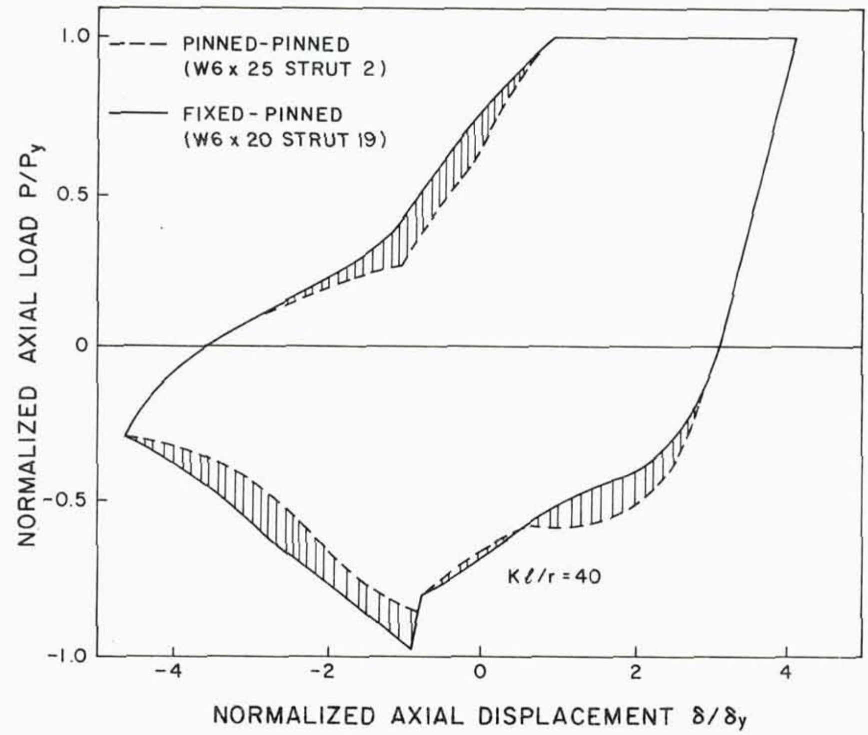

FIG. 37 COMPARISON OF HYSTERETIC ENVELOPES FOR STRUTS WITH DIFFERENT BOUNDARY CONDITIONS

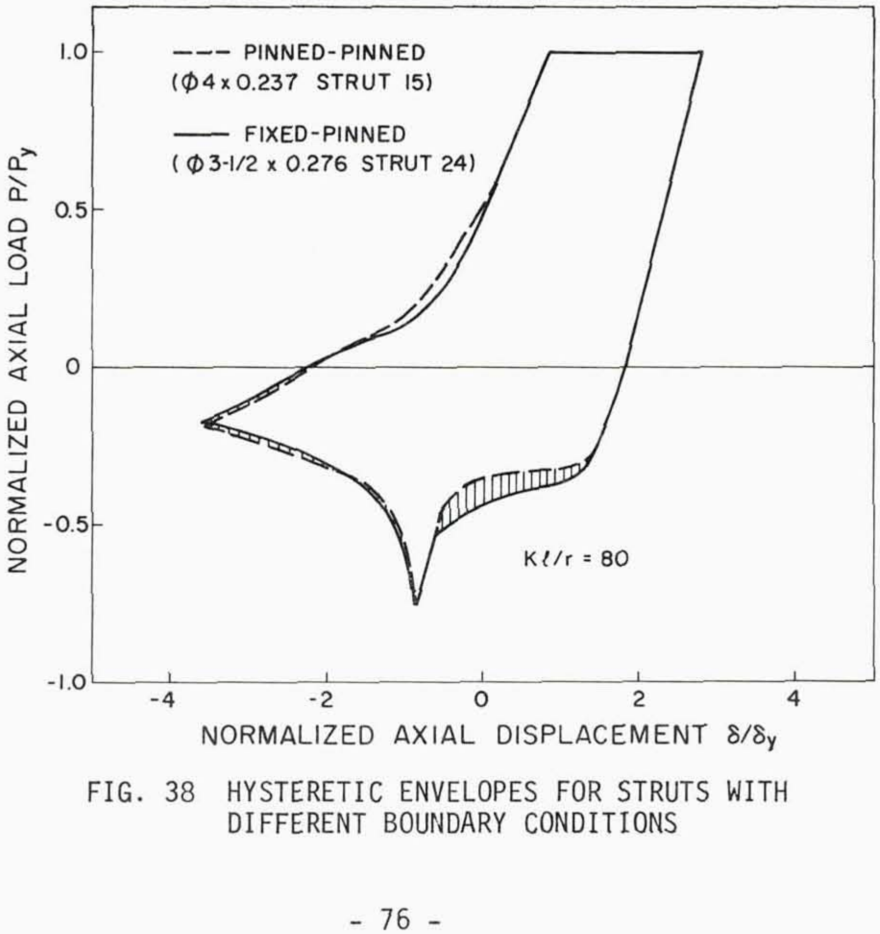

FIG. 38 HYSTERETIC ENVELOPES FOR STRUTS WITH DIFFERENT BOUNDARY CONDITIONS

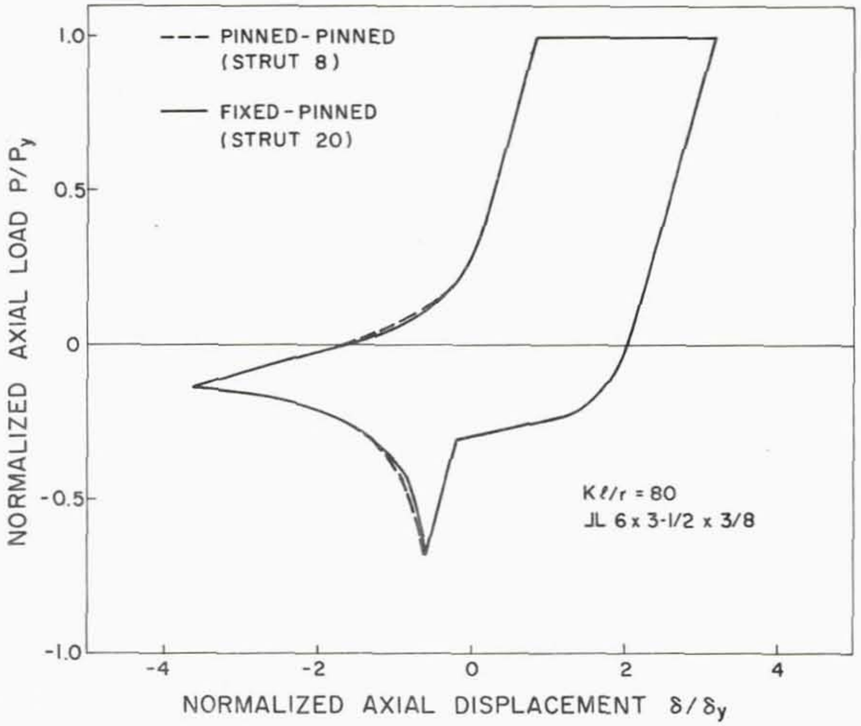

FIG. 39 HYSTERETIC ENVELOPES FOR STRUTS WITH DIFFERENT BOUNDARY CONDITIONS

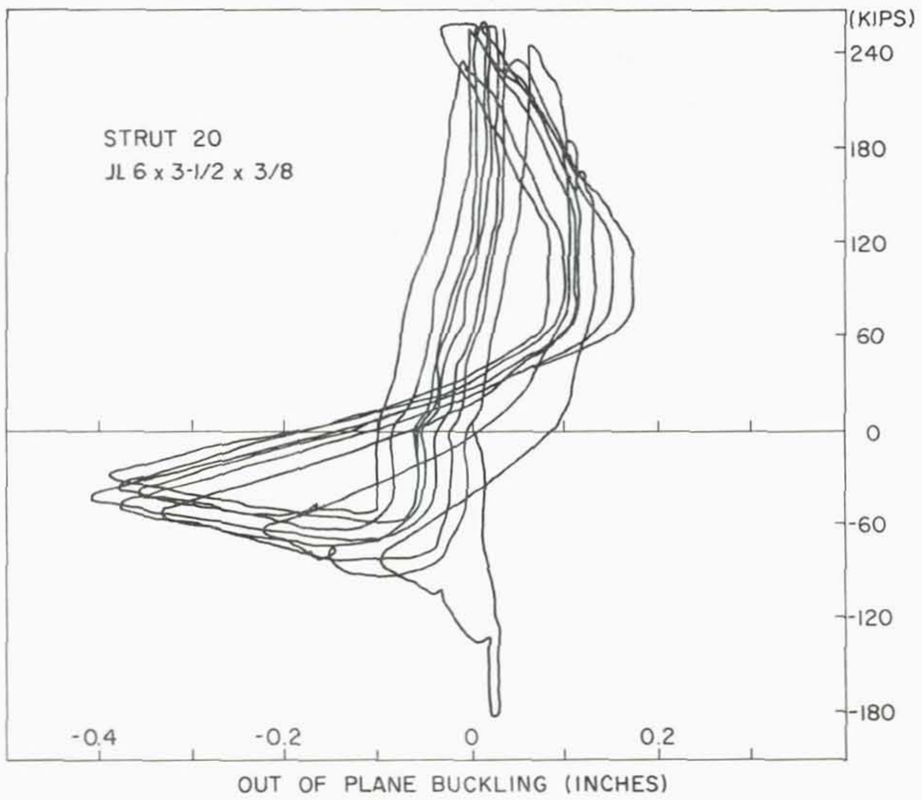

FIG. 40 PLOT OF VERTICAL LATERAL DISPLACEMENT - STRUT 20

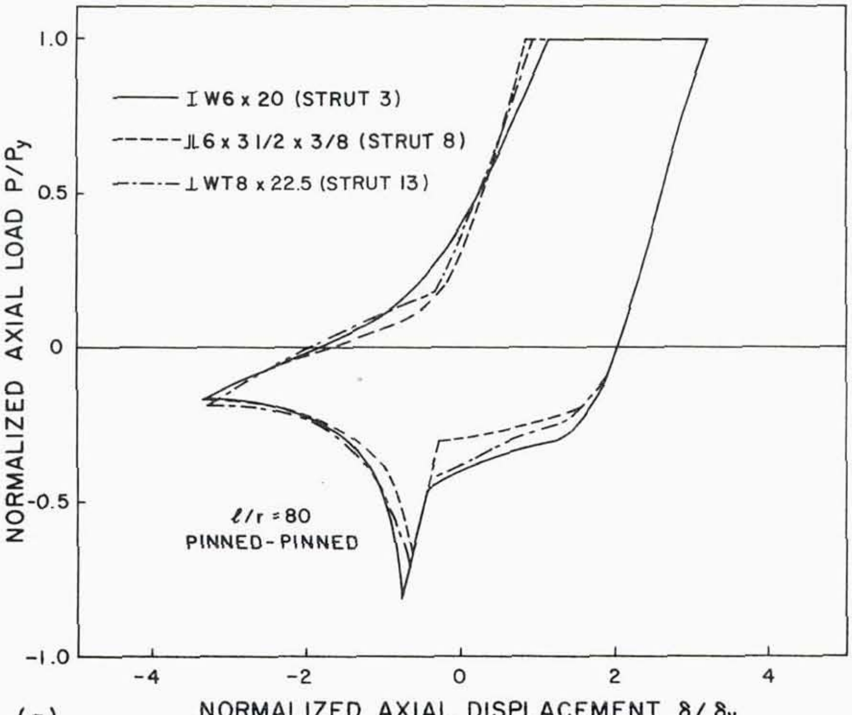

(a)

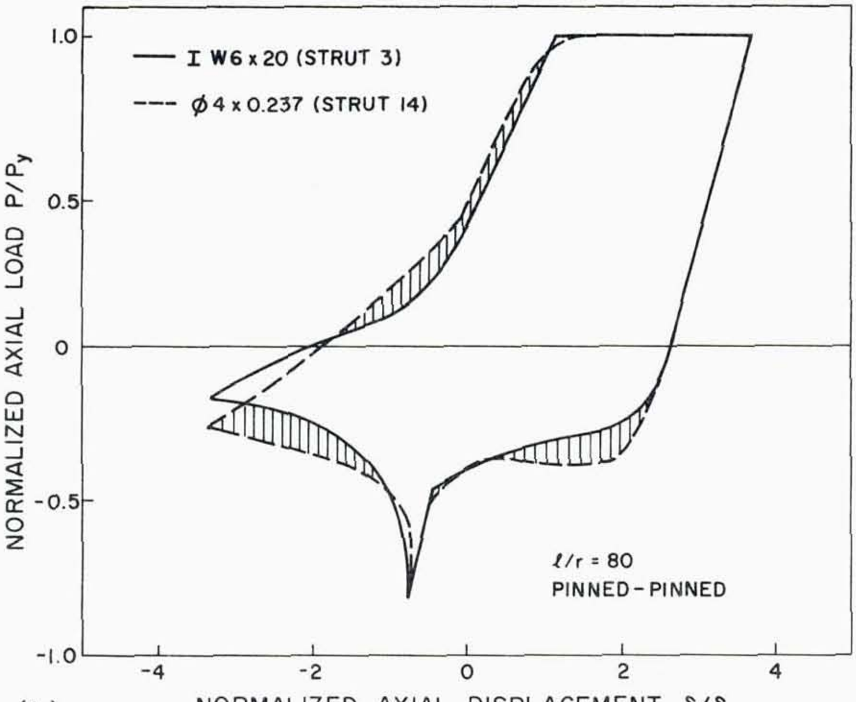

(b)

FIG. 41 HYSTERETIC ENVELOPES FOR STRUTS WITH DIFFERENT CROSS-SECTIONAL SHAPES

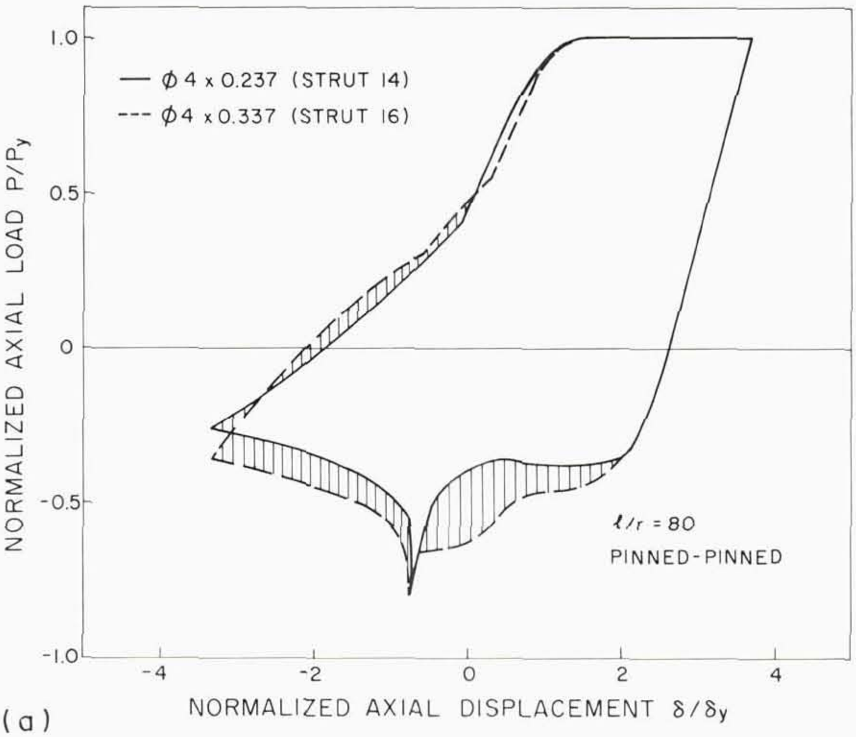

(a)

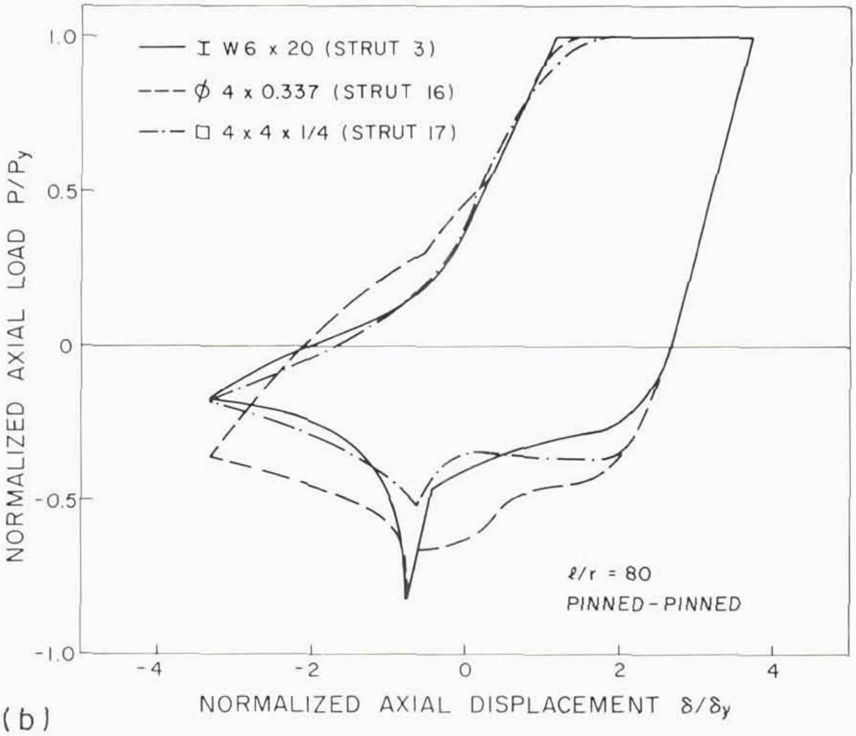

(b)

FIG. 42 HYSTERETIC ENVELOPES FOR STRUTS WITH DIFFERENT CROSS-SECTIONAL SHAPES

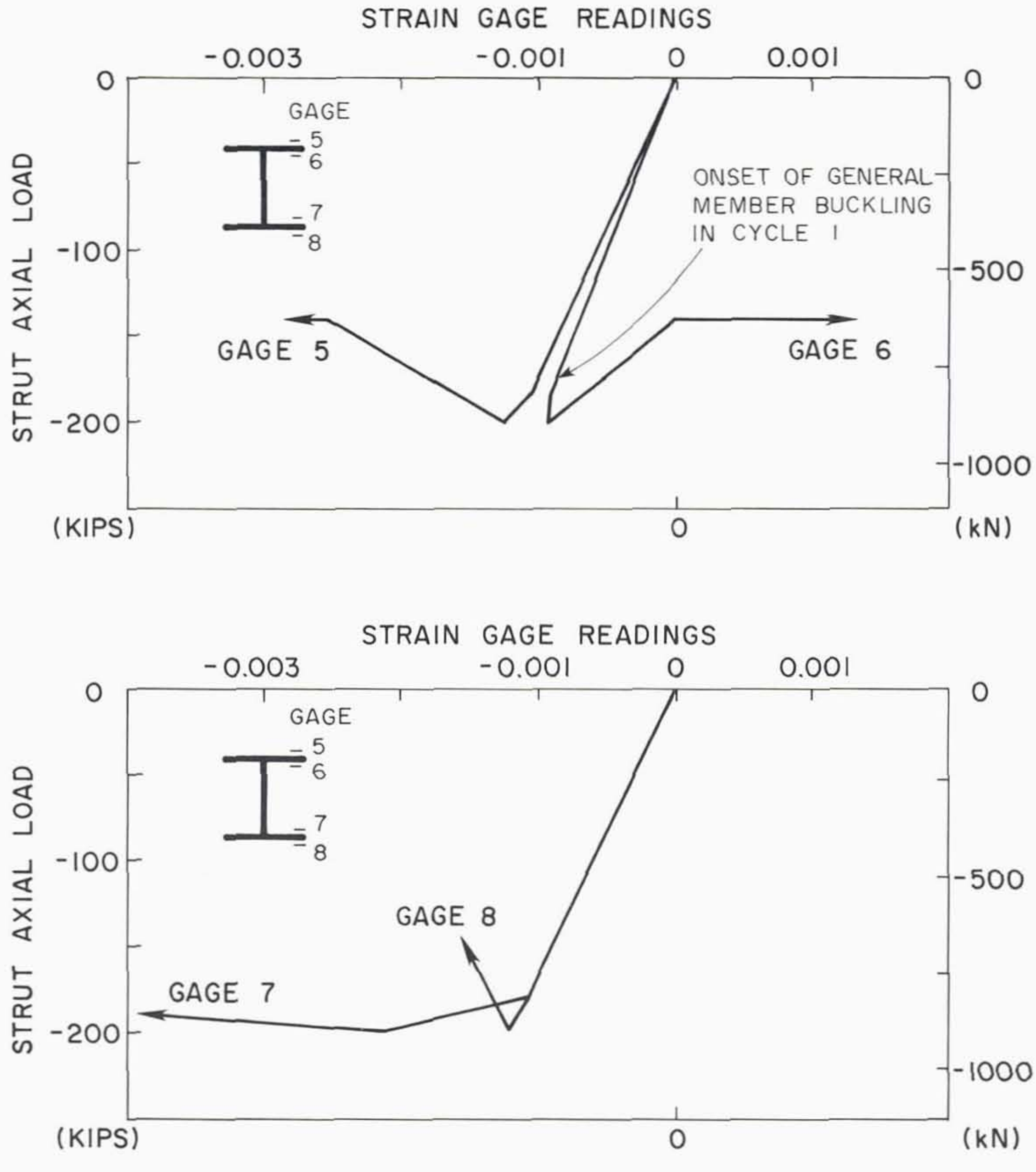

FIG. 43 GAGE DATA FOR DETERMINING LOCAL FLANGE BUCKLING - STRUT 19

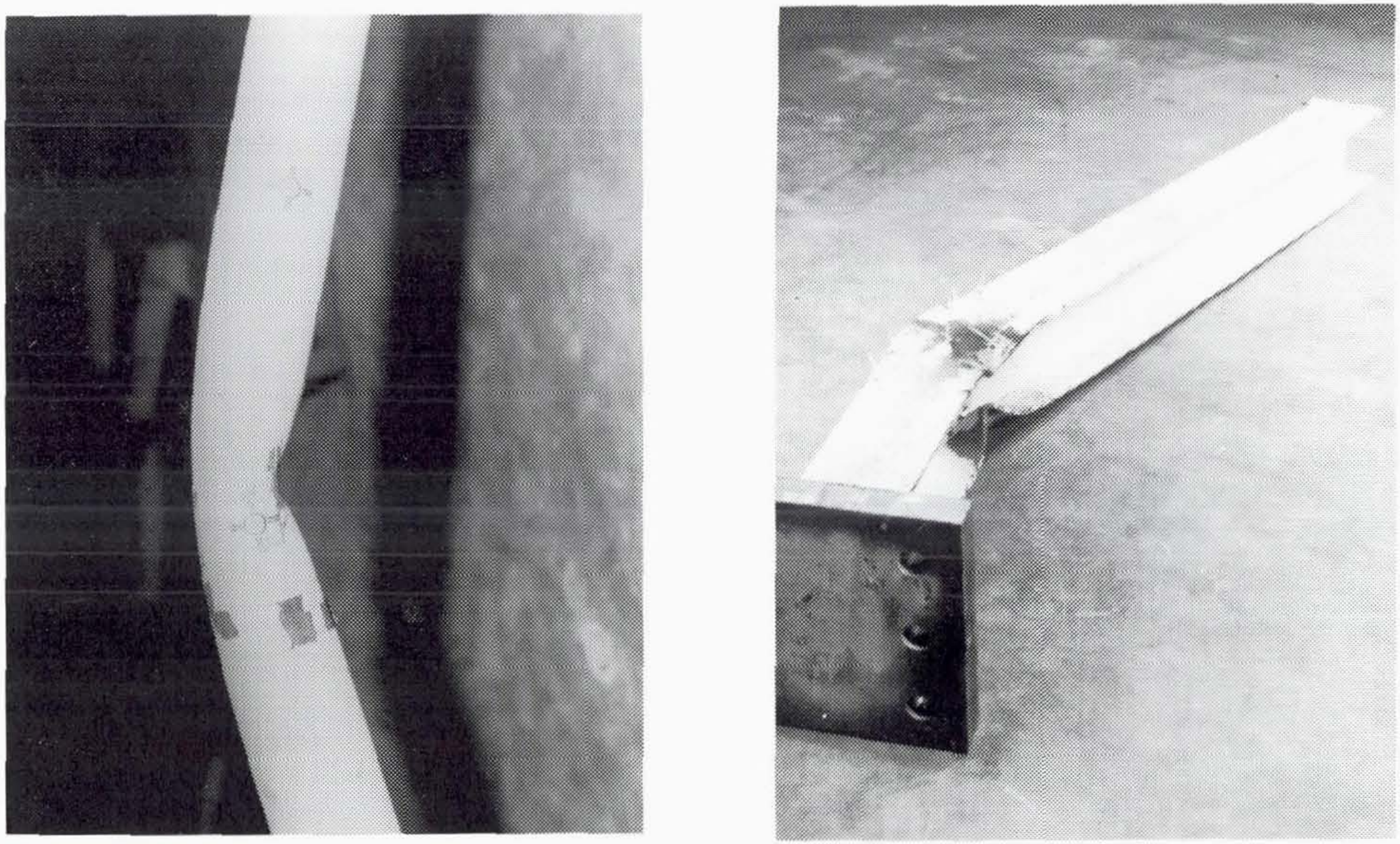

FIG. 44 LOCAL BUCKLING AT LARGE LATERAL DISPLACEMENTS

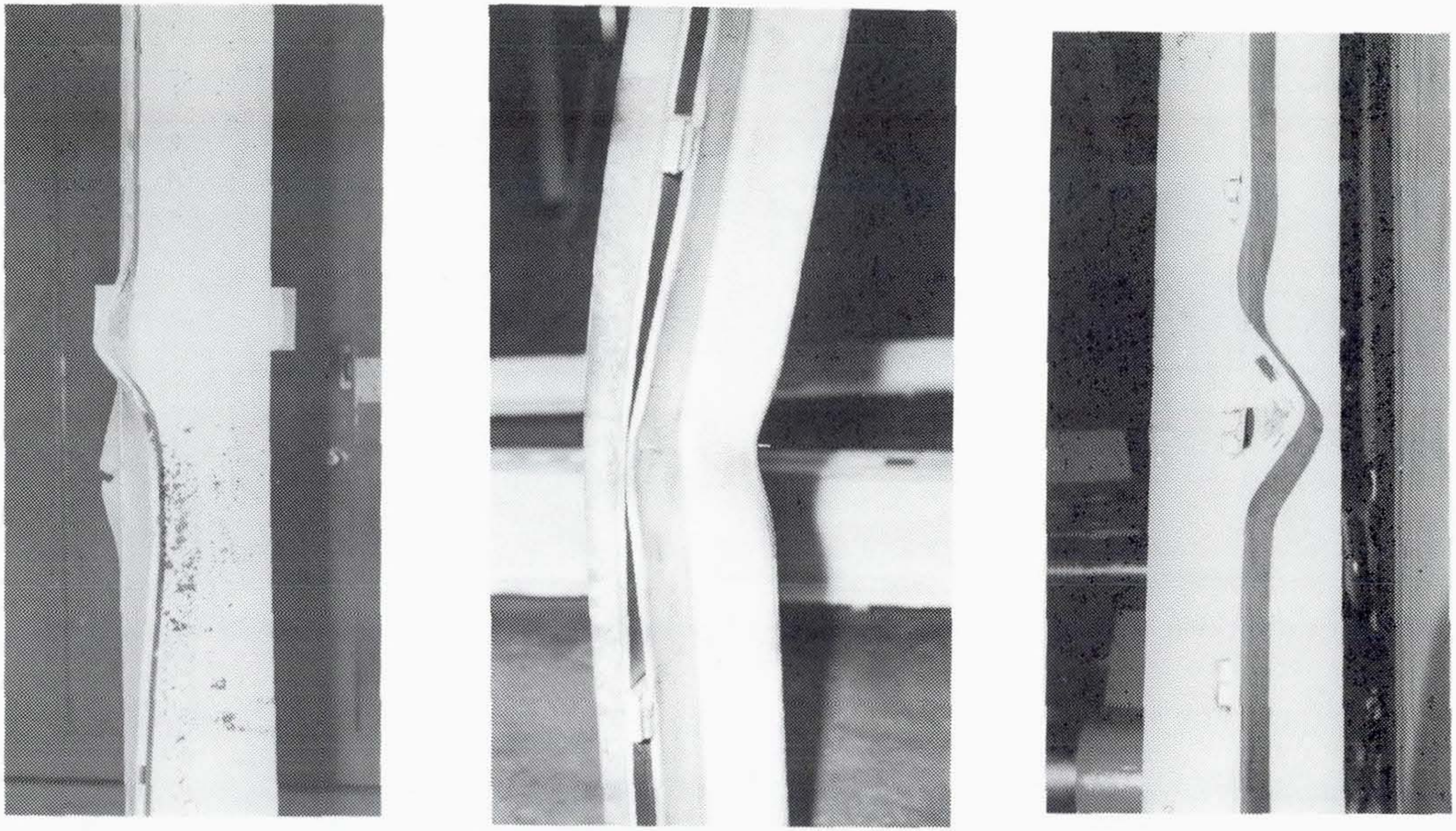

FIG. 45 LOCAL BUCKLING OF DOUBLE-ANGLE STRUTS 8 AND 9, AND OF TEE STRUT 12

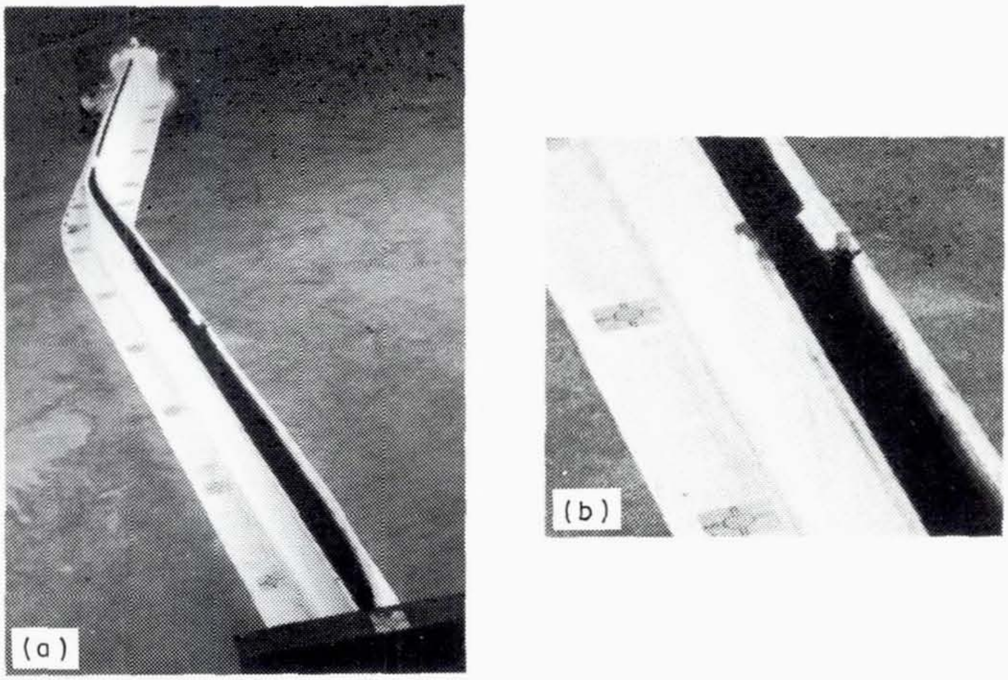

FIG. 46 STITCH FAILURE OF STRUT 20
(a) GENERAL VIEW, (b) DETAIL

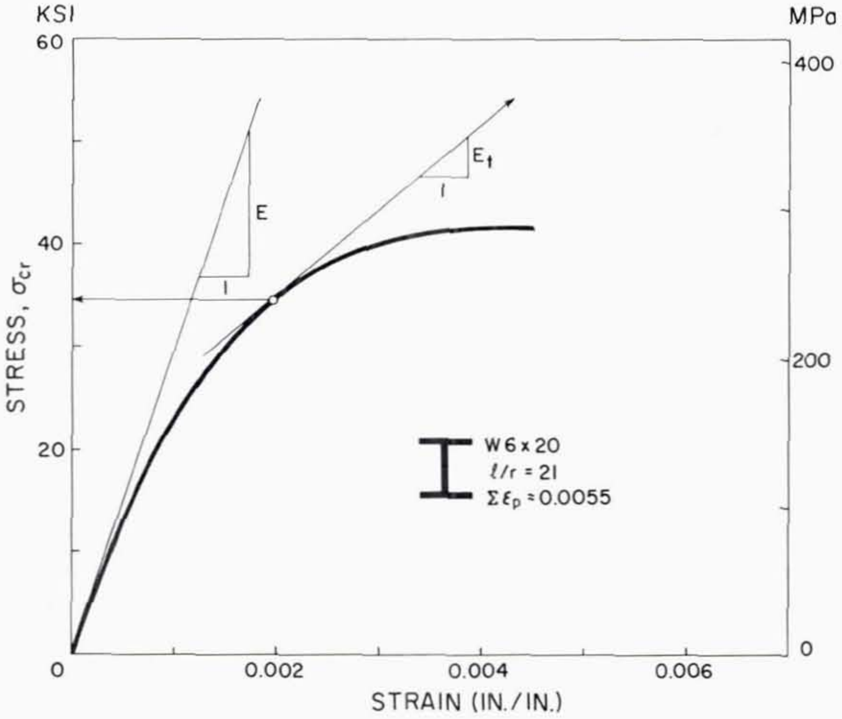

FIG. 47 TENSILE LOADING BRANCH OF CYCLIC
COUPON TEST IN CYCLE 2

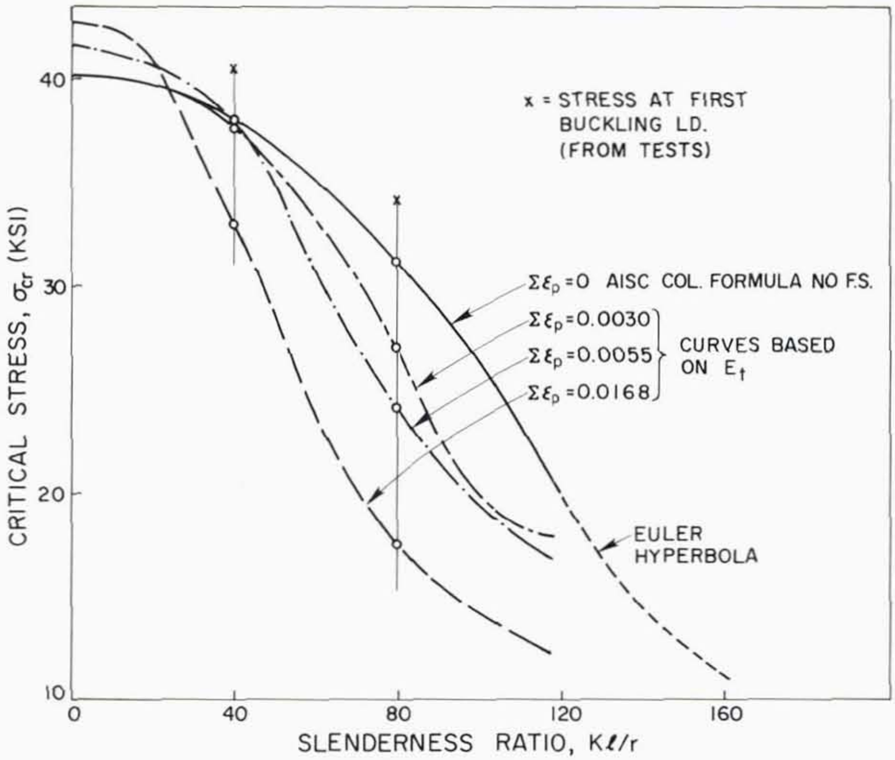

FIG. 48 COLUMN BUCKLING CURVES BASED ON TANGENT MODULUS - W6 × 20 MATERIAL

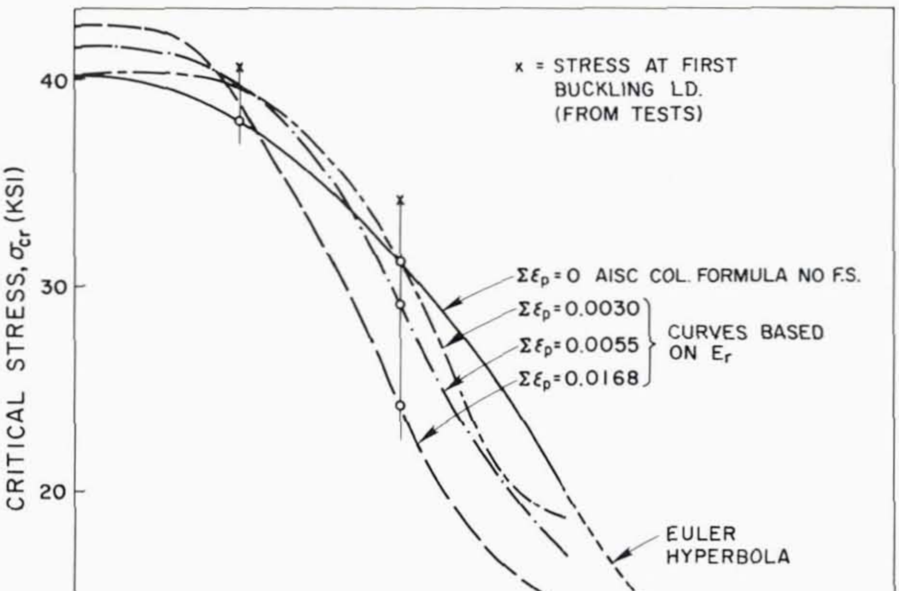

FIG. 49 COLUMN BUCKLING CURVES BASED ON REDUCED MODULUS - W6 × 20 MATERIAL

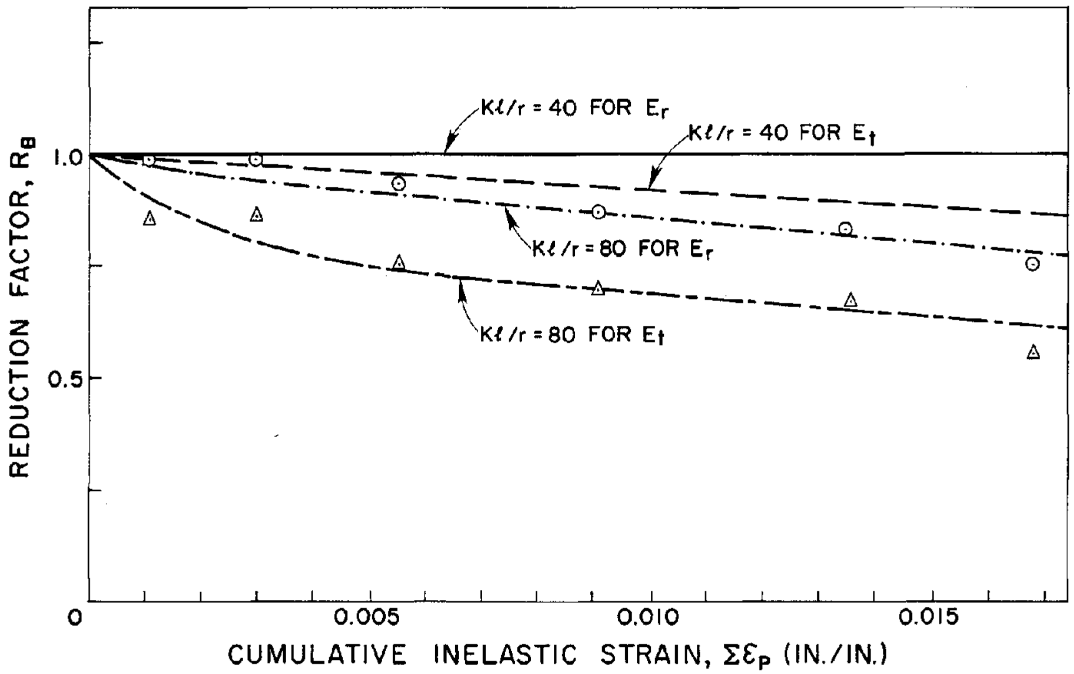

FIG. 50 COLUMN BUCKLING REDUCTION FACTORS DUE TO BAUSCHINGER EFFECT ON TWO BASES: TANGENT MODULUS AND REDUCED MODULUS

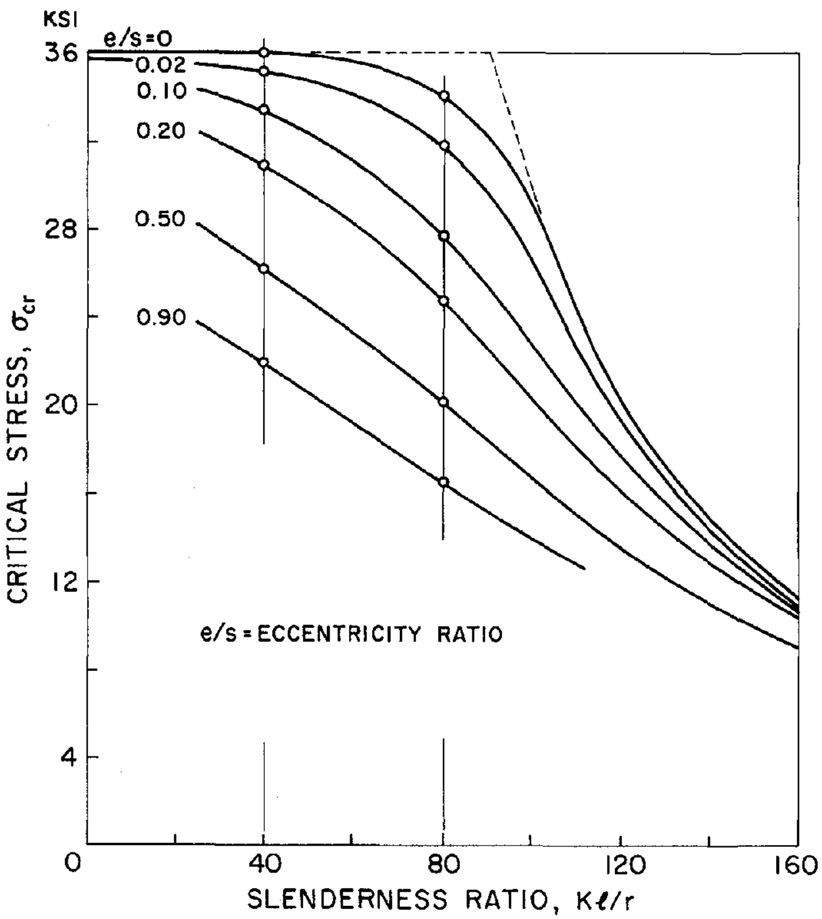

FIG. 51 COLUMN BUCKLING CURVES FOR ECCENTRIC LOADINGS [17]

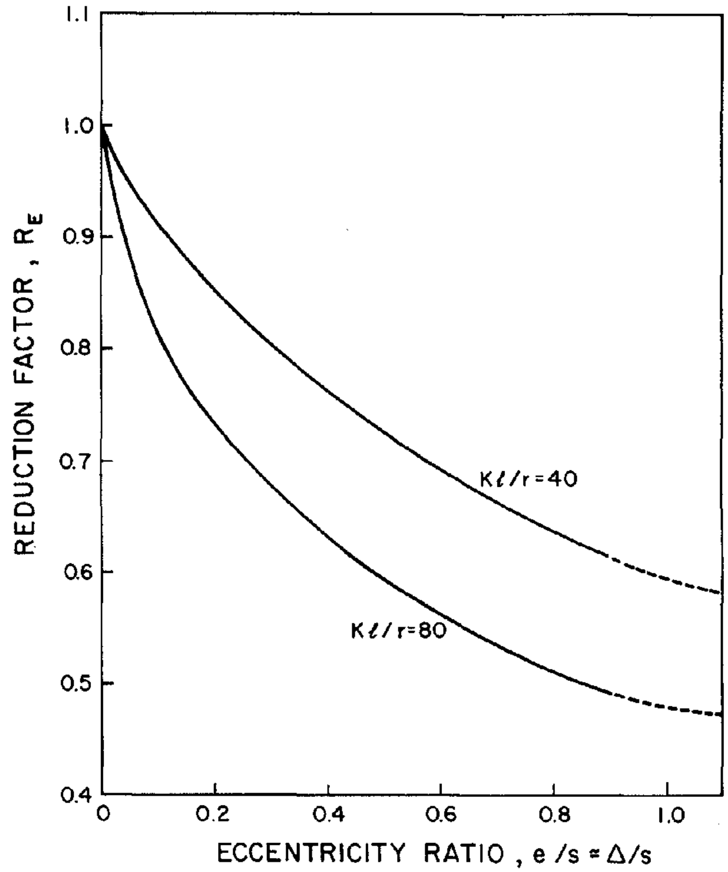

FIG. 52 COLUMN BUCKLING REDUCTION FACTOR DUE TO ECCENTRICITY EFFECT

APPENDIX A

MATERIAL PROPERTIES

In this Appendix, the stress-strain diagrams resulting from monotonic coupon tests for the material of each specimen shape are assembled.

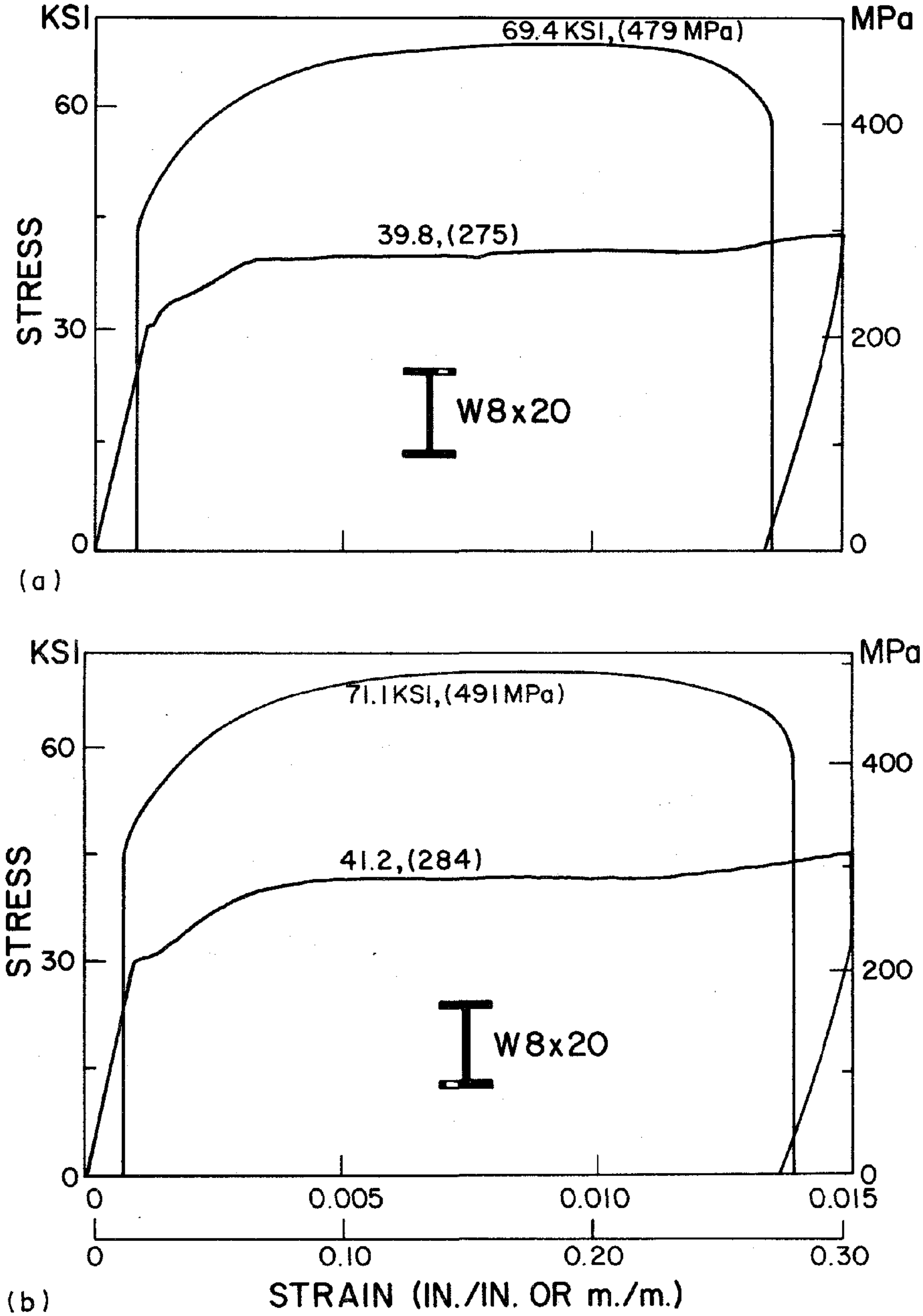

FIG. A1 STRESS-STRAIN DIAGRAMS FOR W8 × 20 MATERIAL

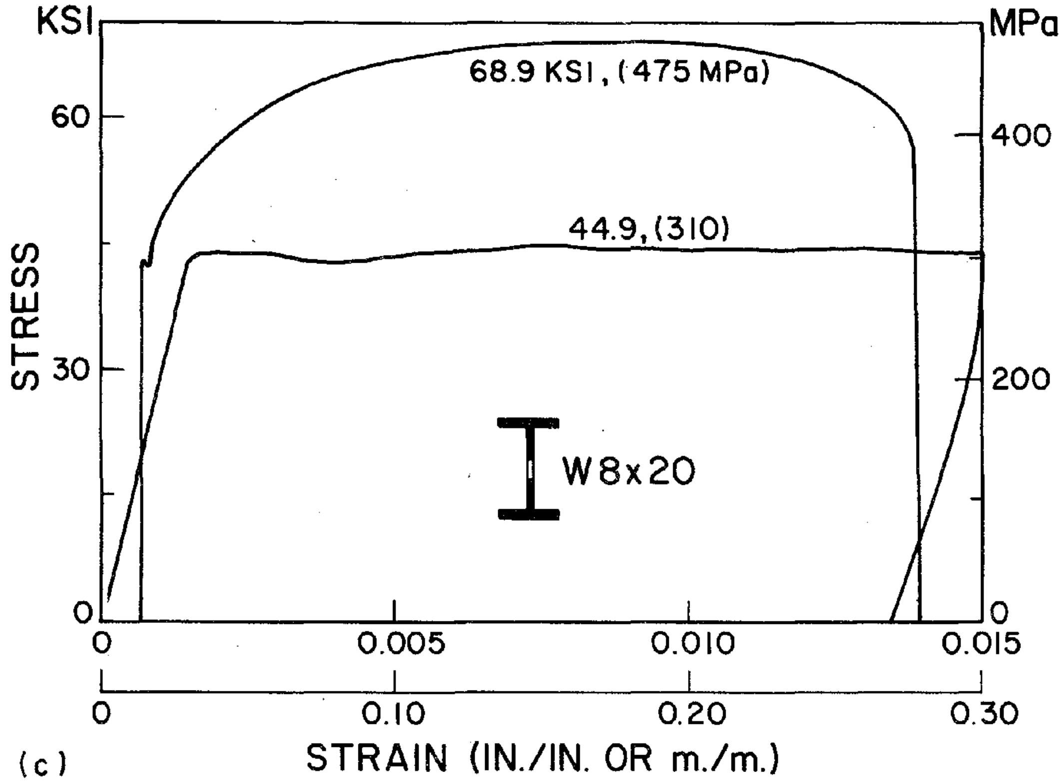

FIG. A1 STRESS-STRAIN DIAGRAMS FOR W8 × 20 MATERIAL

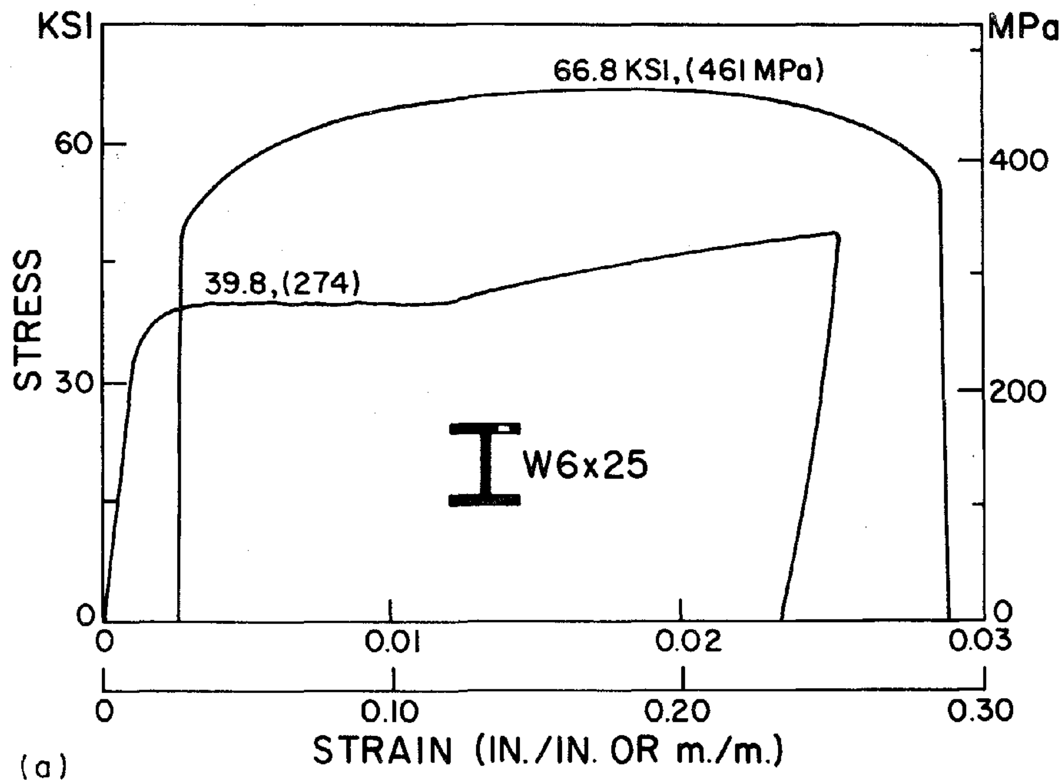

FIG. A2 STRESS-STRAIN DIAGRAMS FOR W6 × 25 MATERIAL

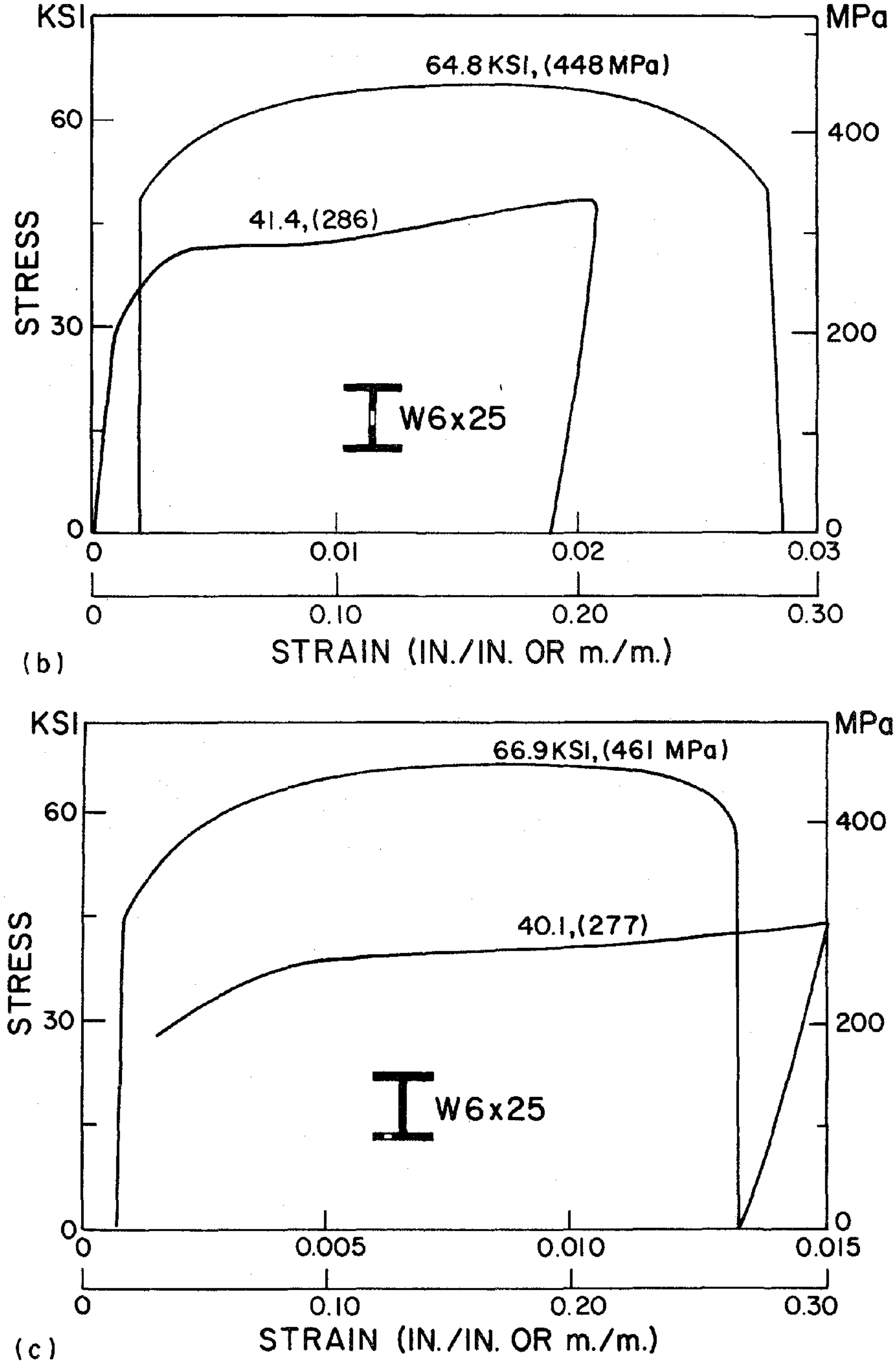

FIG. A2 STRESS-STRAIN DIAGRAMS FOR W6 × 25 MATERIAL

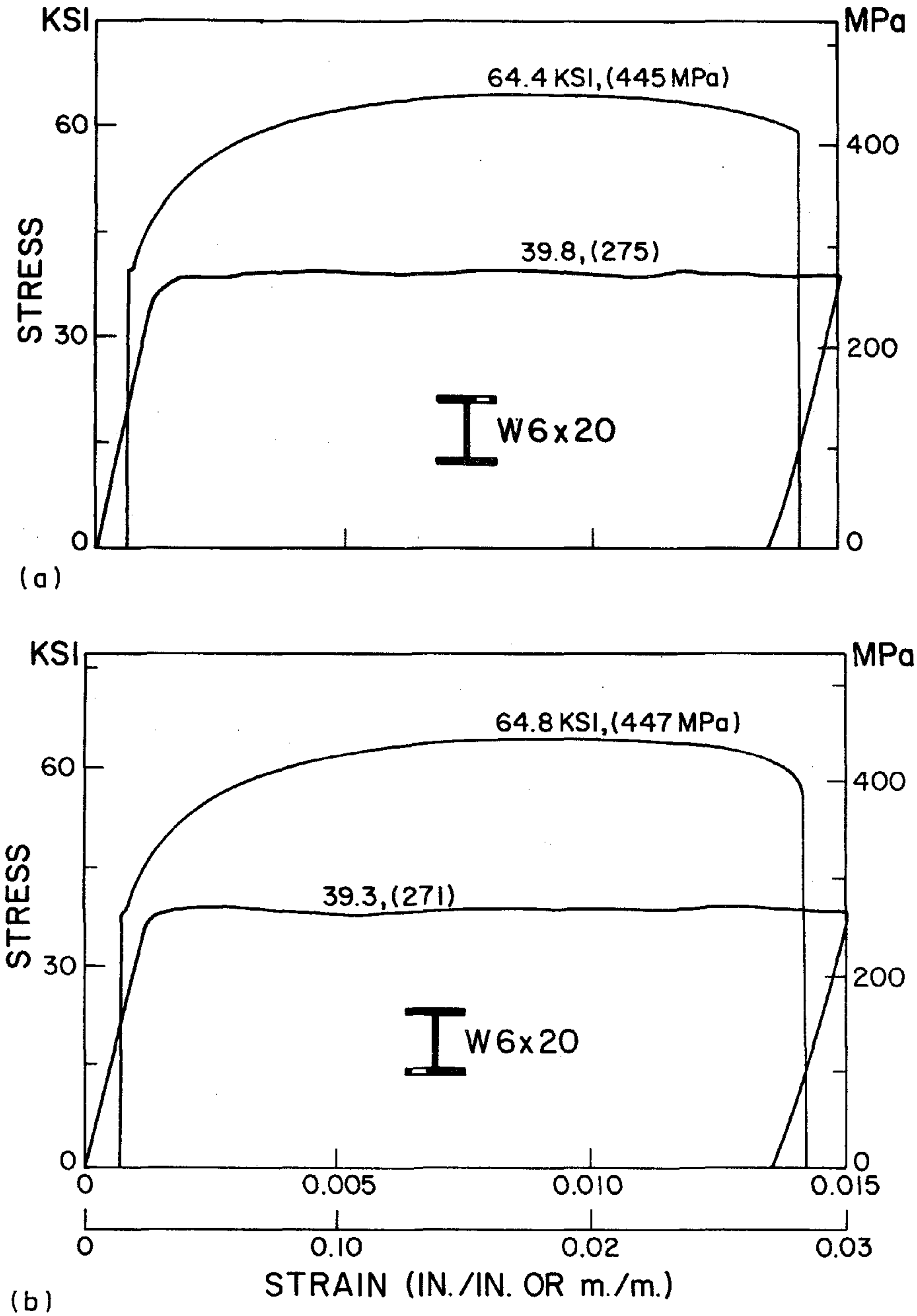

FIG. A3 STRESS-STRAIN DIAGRAMS FOR W6 × 20 MATERIAL

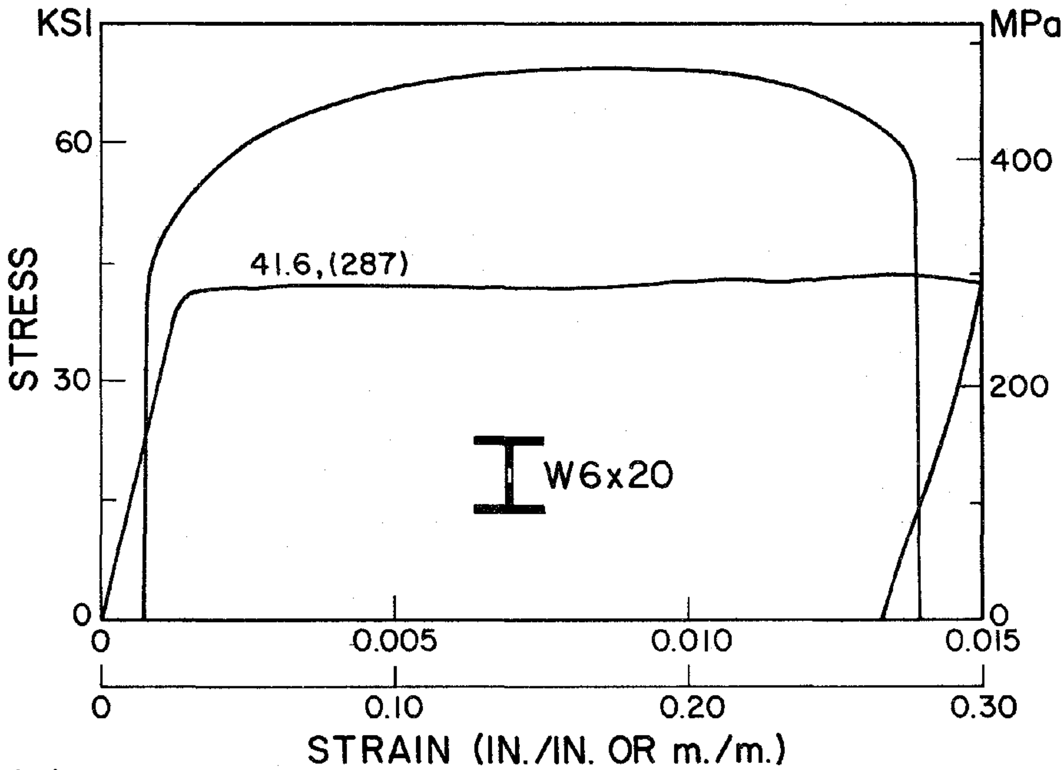

(c)

FIG. A3 STRESS-STRAIN DIAGRAMS FOR W6 × 20 MATERIAL

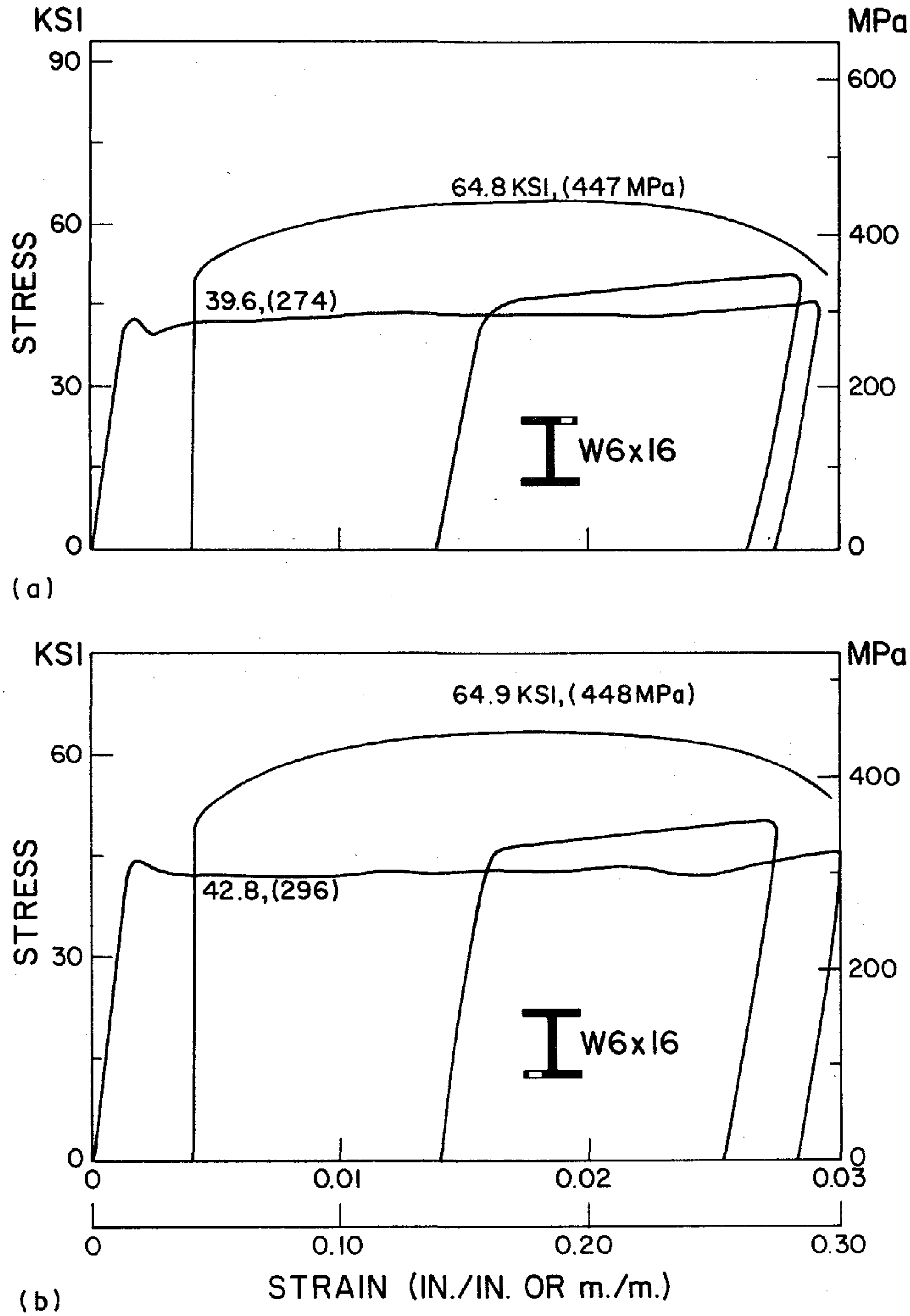

FIG. A4 STRESS-STRAIN DIAGRAMS FOR W6 × 16 MATERIAL

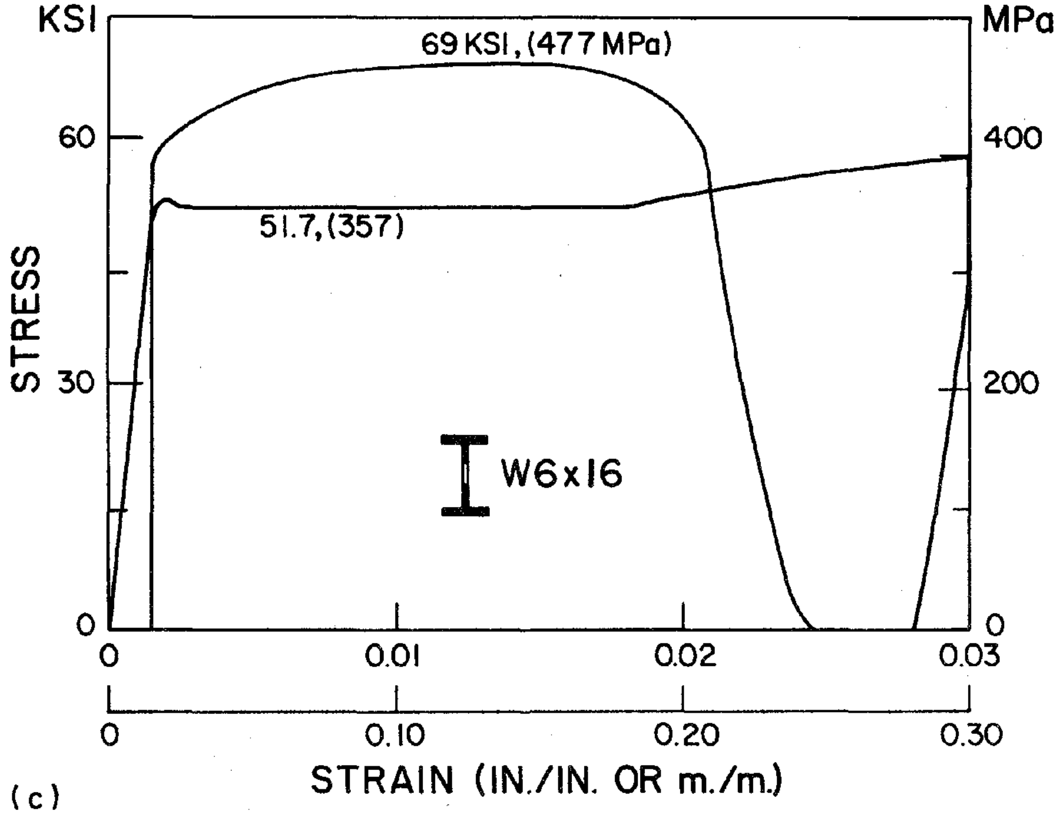

FIG. A4 STRESS-STRAIN DIAGRAMS FOR W6 × 16 MATERIAL

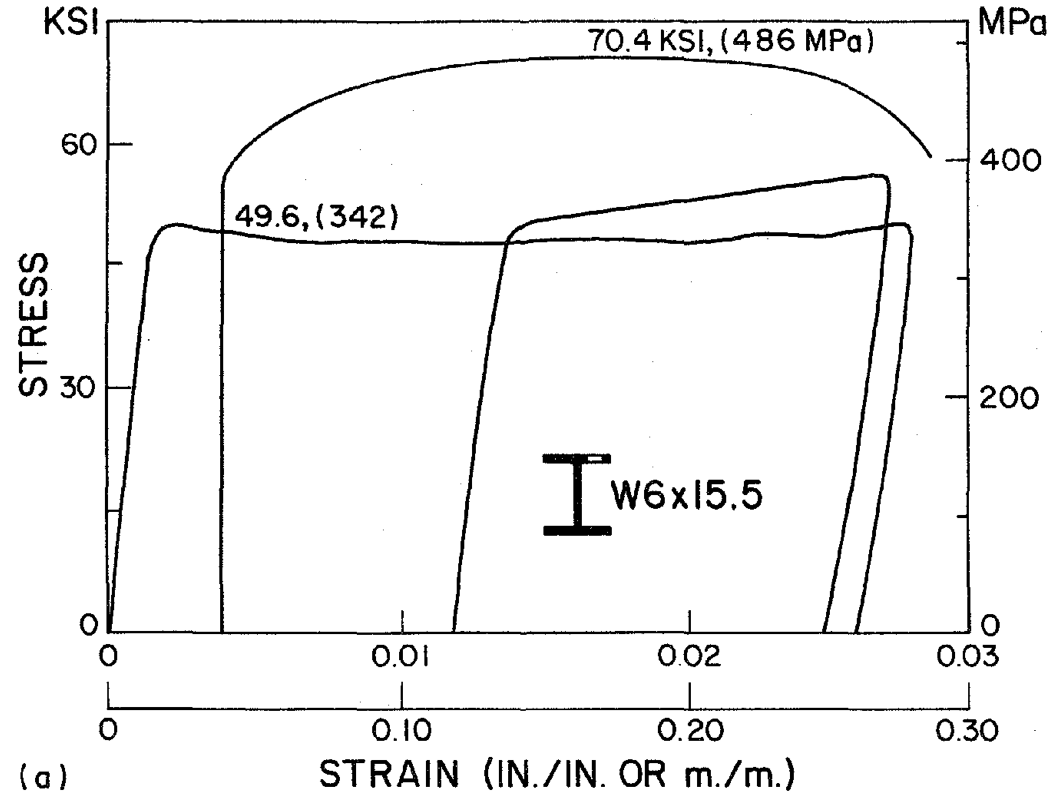

FIG. A5 STRESS-STRAIN DIAGRAMS FOR W6 × 15.5 MATERIAL

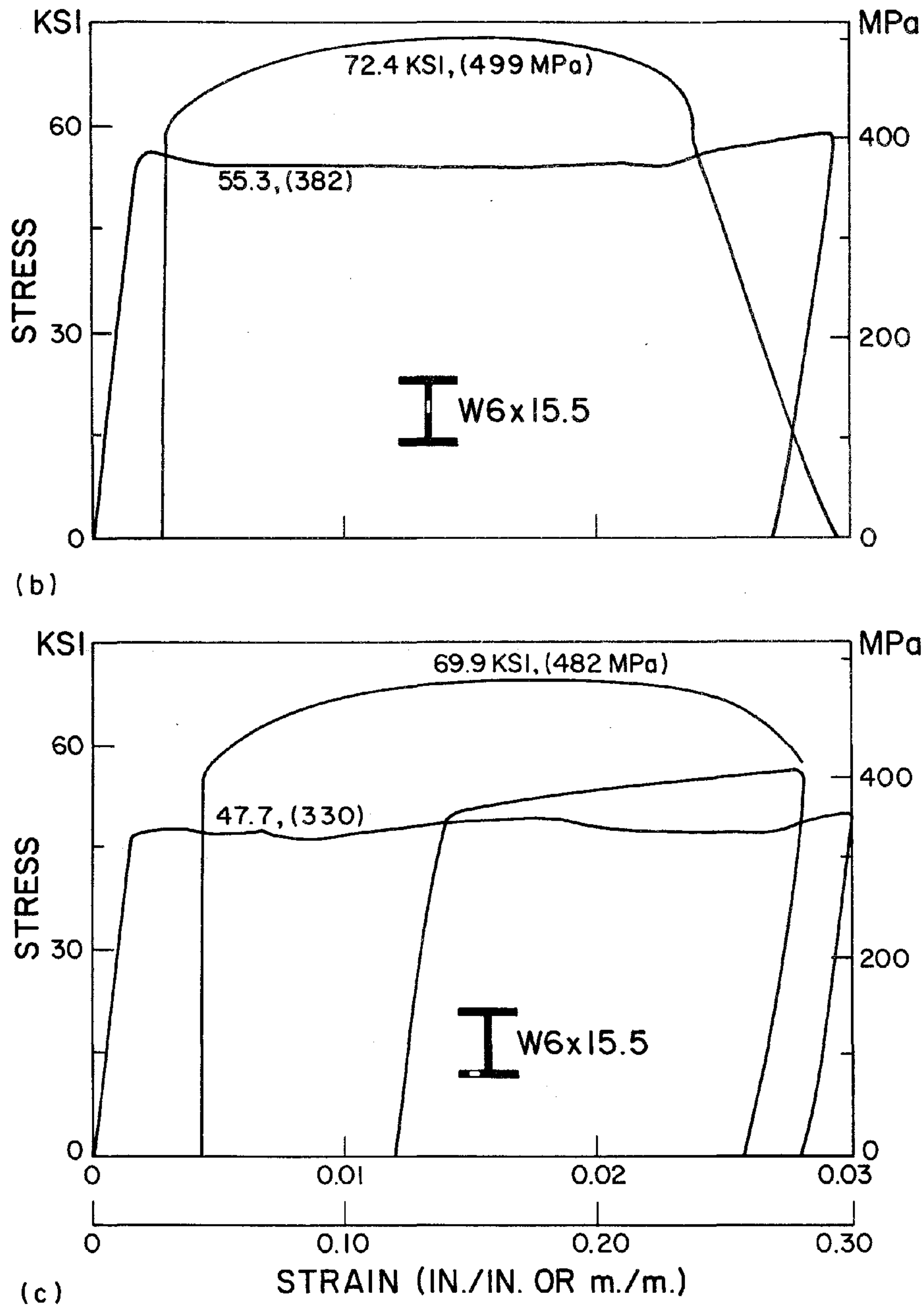

FIG. A5 STRESS-STRAIN DIAGRAMS FOR W6 × 15.5 MATERIAL

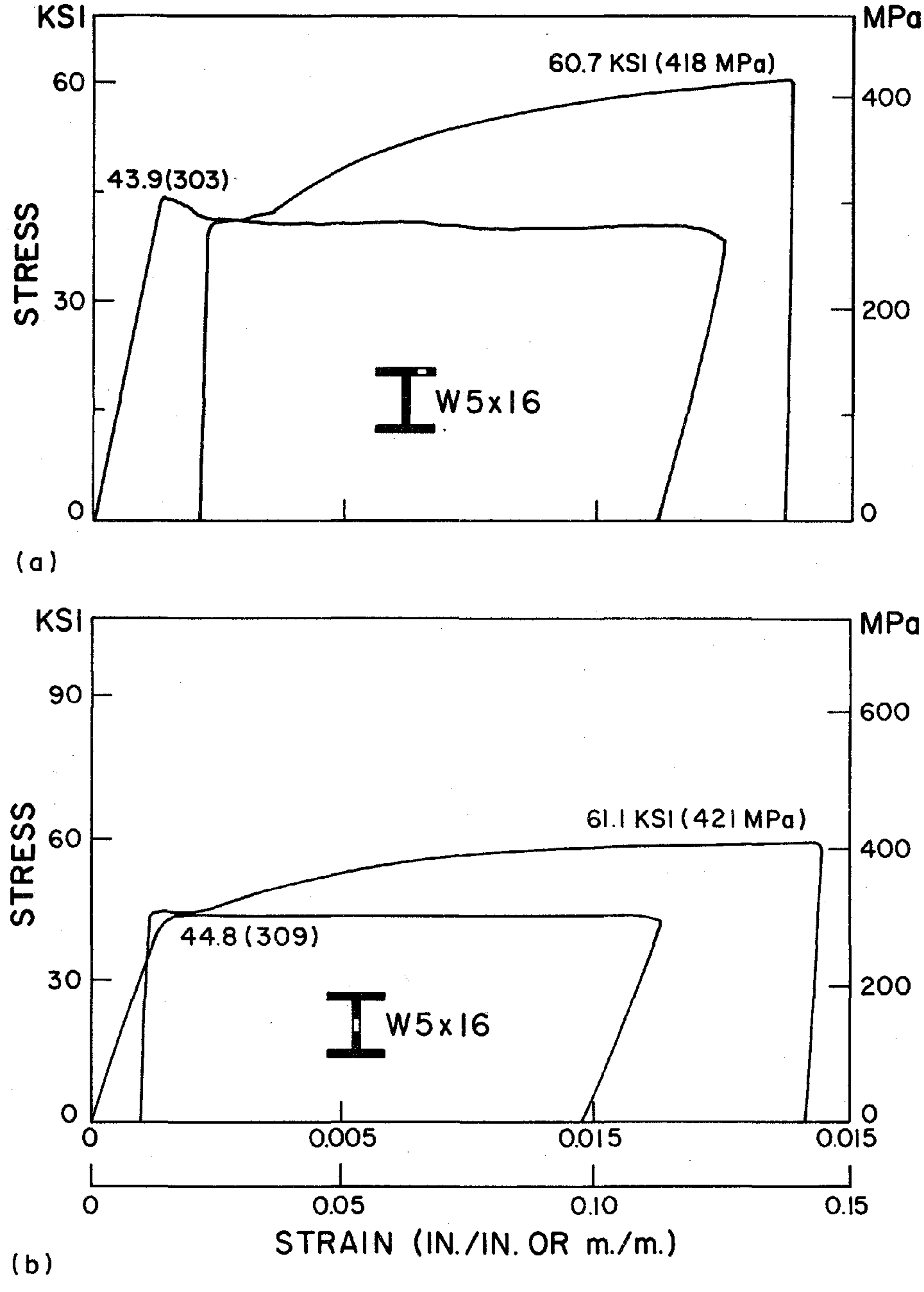

FIG. A6 STRESS-STRAIN DIAGRAMS FOR W5 × 16 MATERIAL

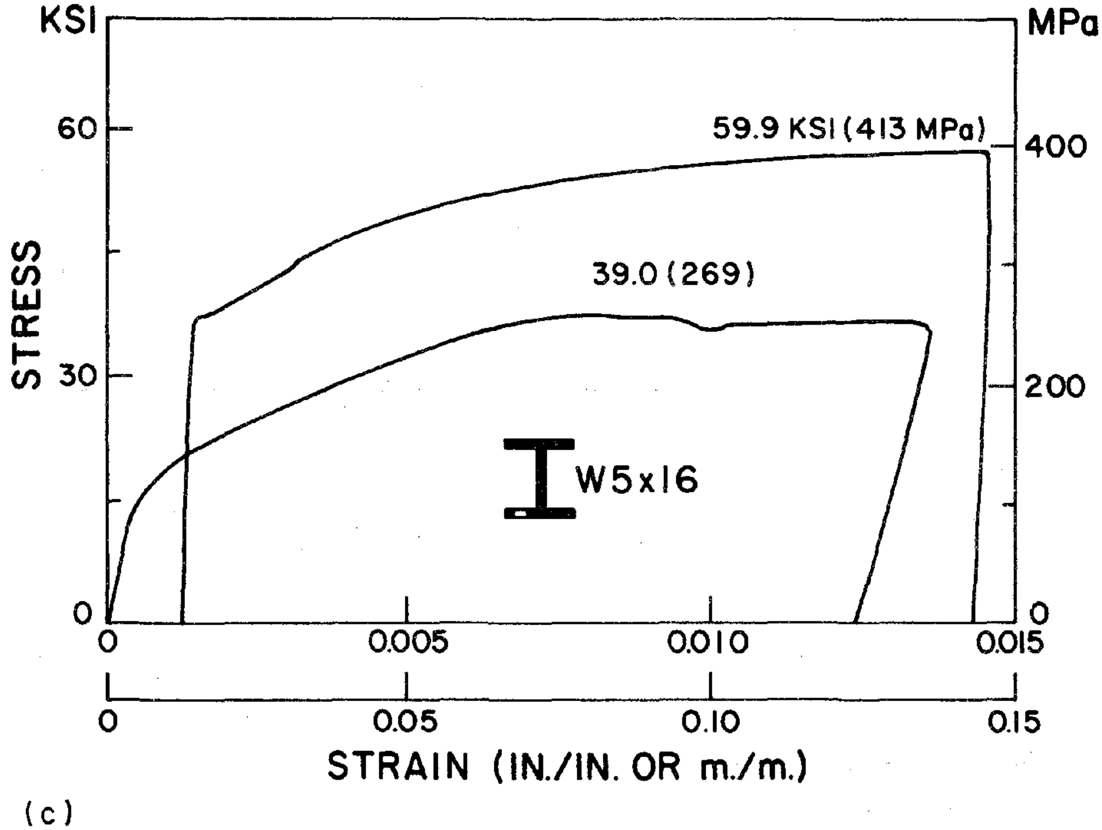

FIG. A6 STRESS-STRAIN DIAGRAMS FOR W5 × 16 MATERIAL

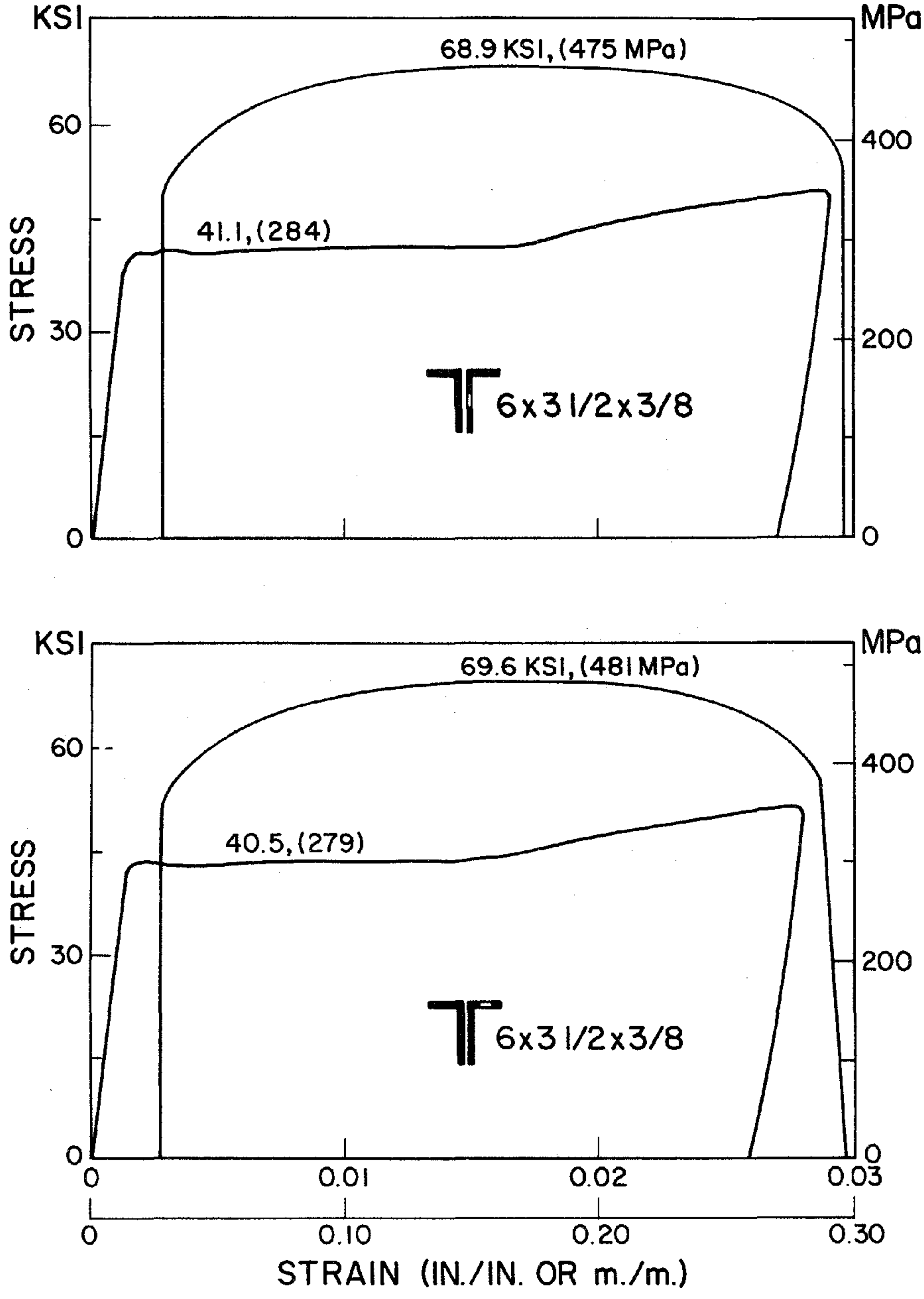

FIG. A7 STRESS-STRAIN DIAGRAMS FOR MATERIAL FROM $6 \times 3\frac{1}{2} \times \frac{3}{8}$ ANGLES.

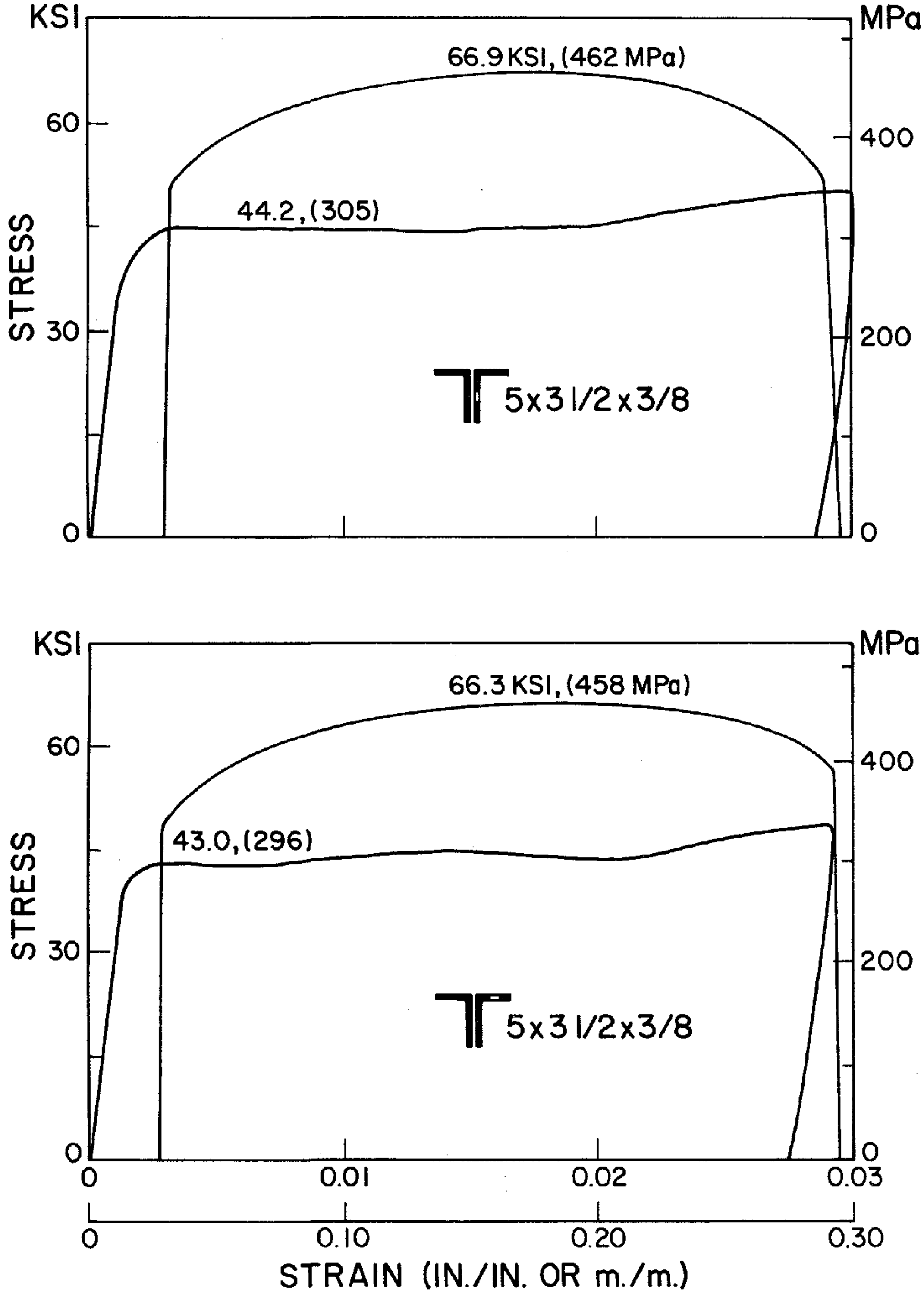

FIG. A8 STRESS-STRAIN DIAGRAMS FOR MATERIAL FROM $5 \times 3\frac{1}{2} \times \frac{3}{8}$ ANGLES

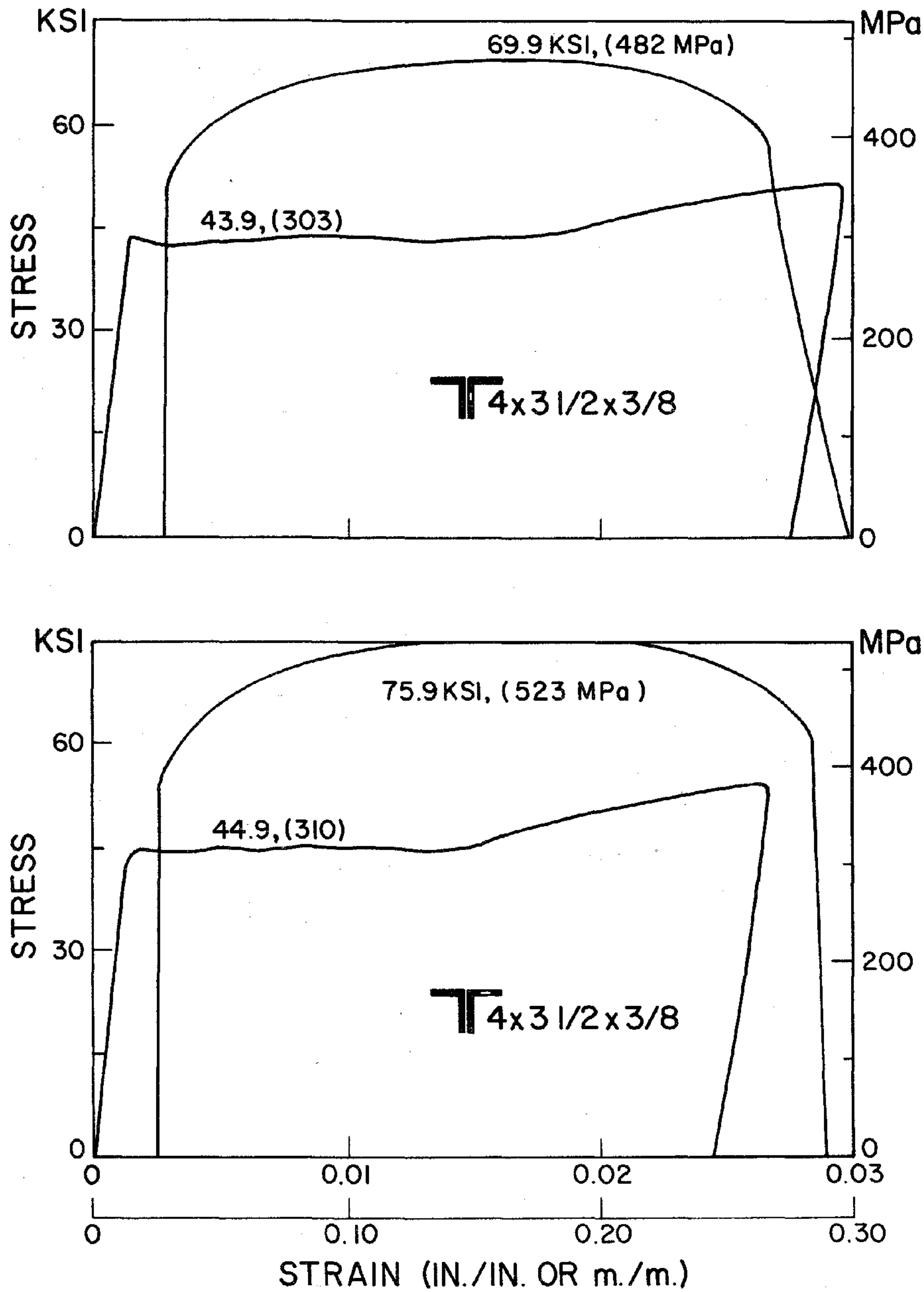

FIG. A9 STRESS-STRAIN DIAGRAMS FOR MATERIAL FROM $4 \times 3\,\frac{1}{2} \times \frac{3}{8}$ ANGLES

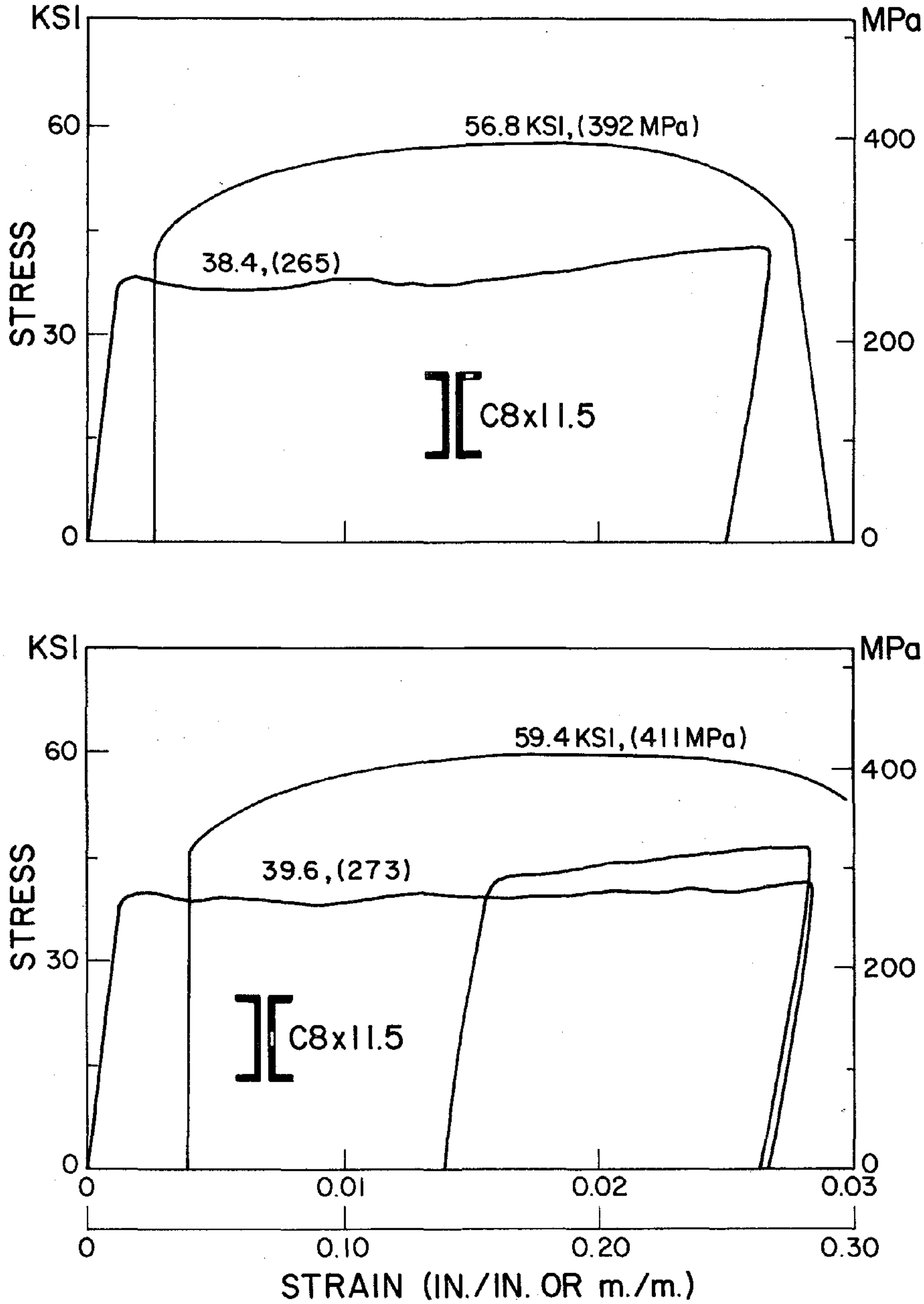

FIG. A10 STRESS-STRAIN DIAGRAMS FOR MATERIAL FROM C8 × 11.5

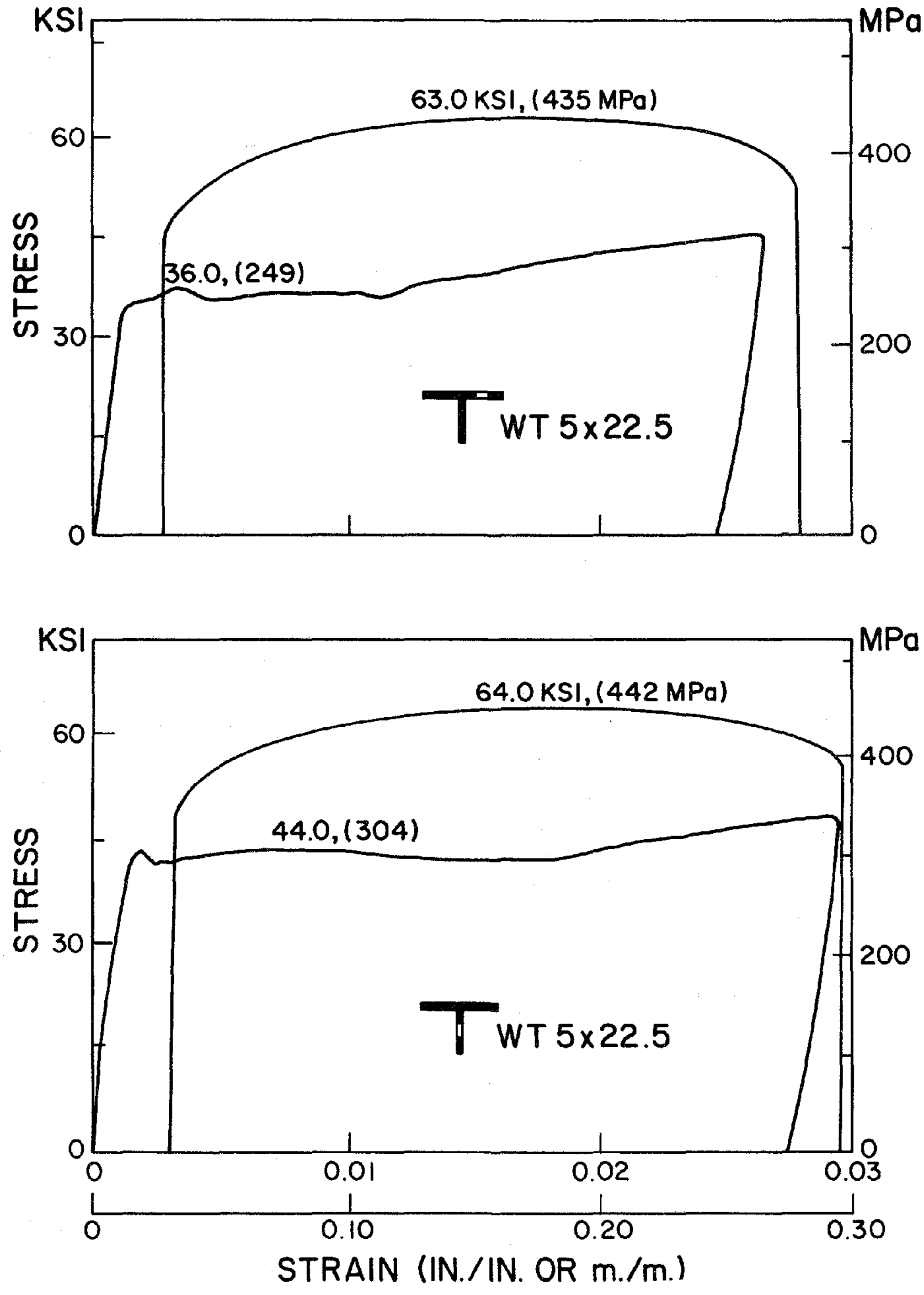

FIG. A11 STRESS-STRAIN DIAGRAMS FOR MATERIAL FROM WT5 × 22.5

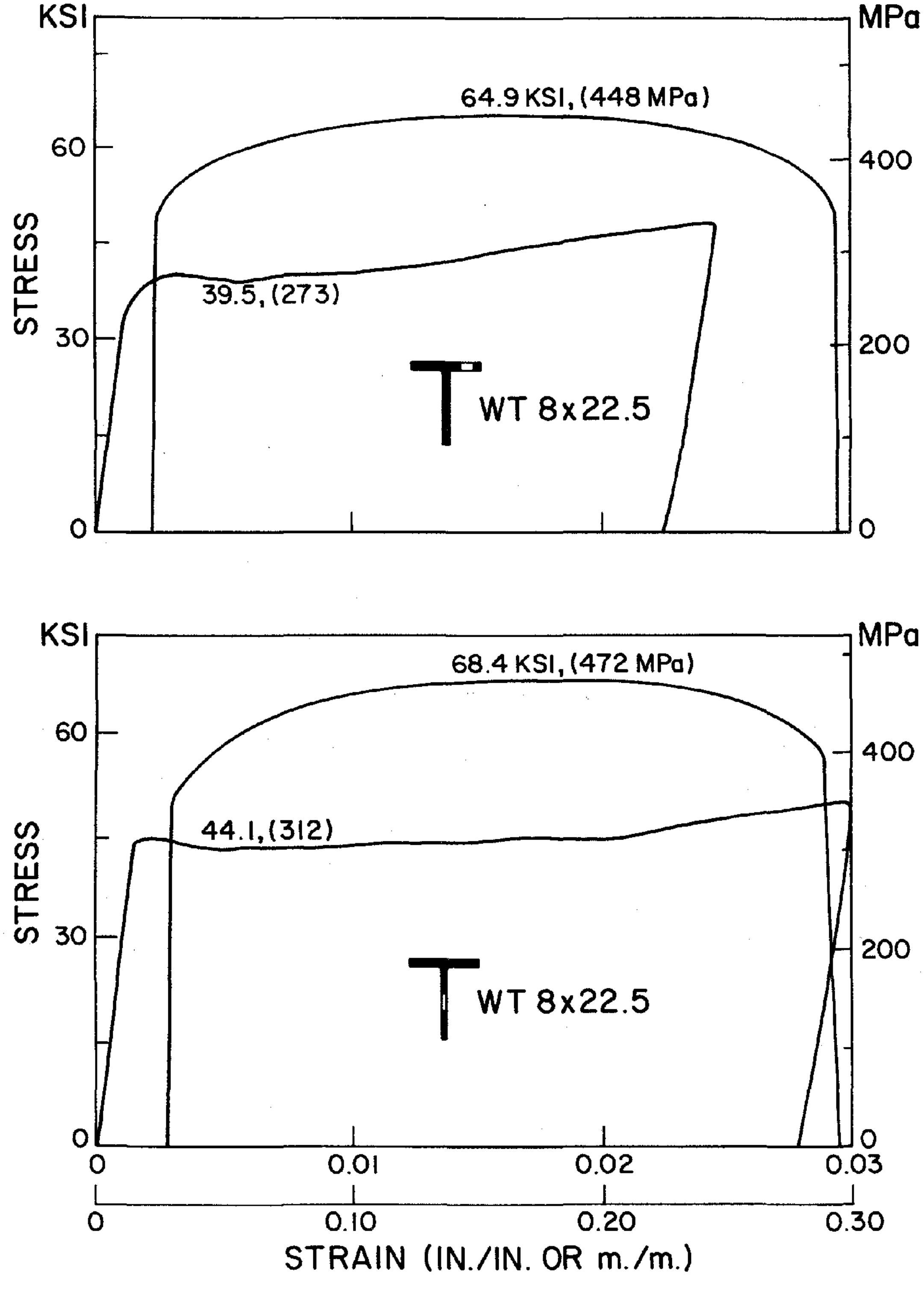

FIG. A12 STRESS-STRAIN DIAGRAMS FOR MATERIAL FROM WT8 × 22.5

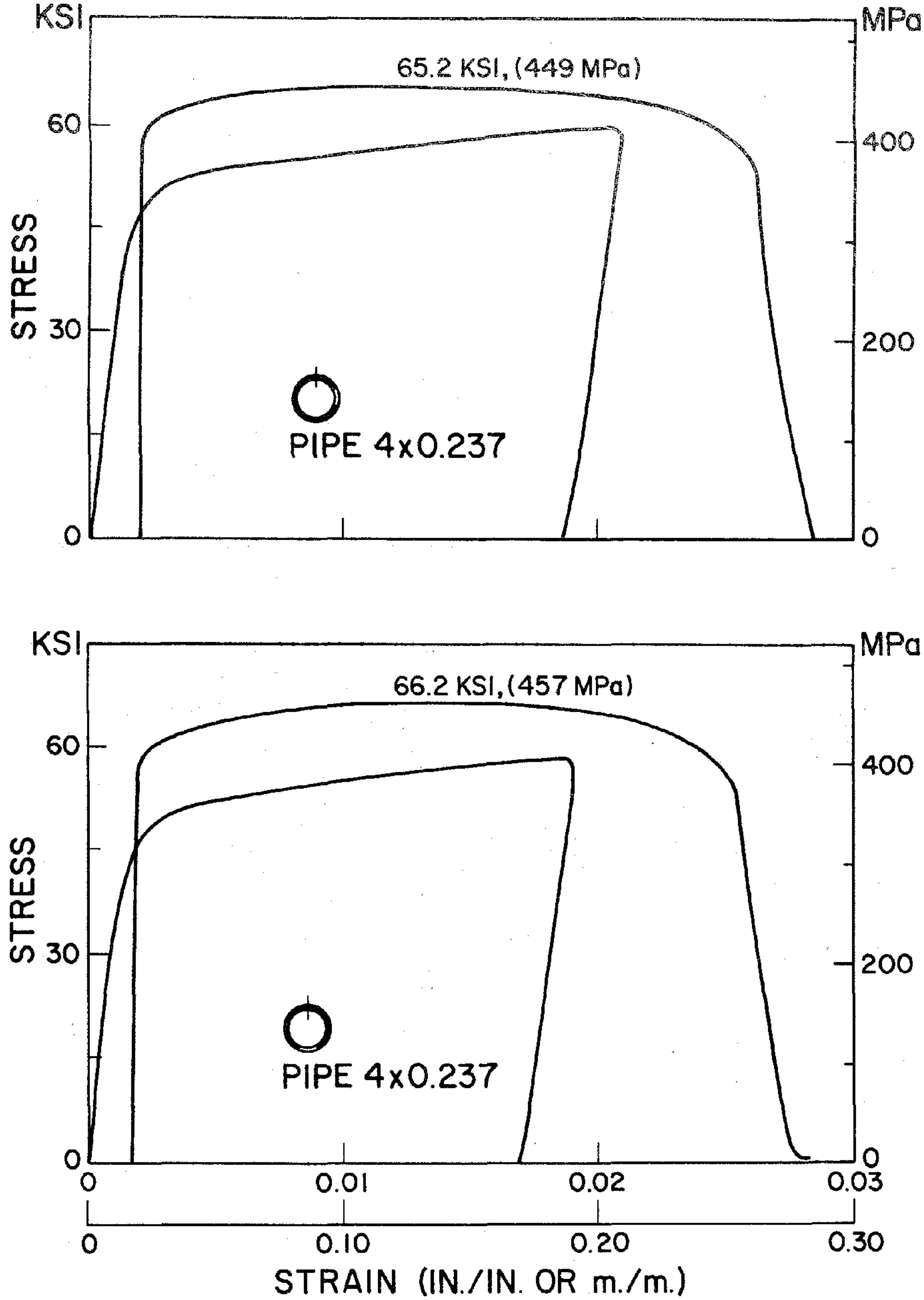

FIG. A13 STRESS-STRAIN DIAGRAMS FOR MATERIAL FROM 4 IN. STANDARD WEIGHT PIPE

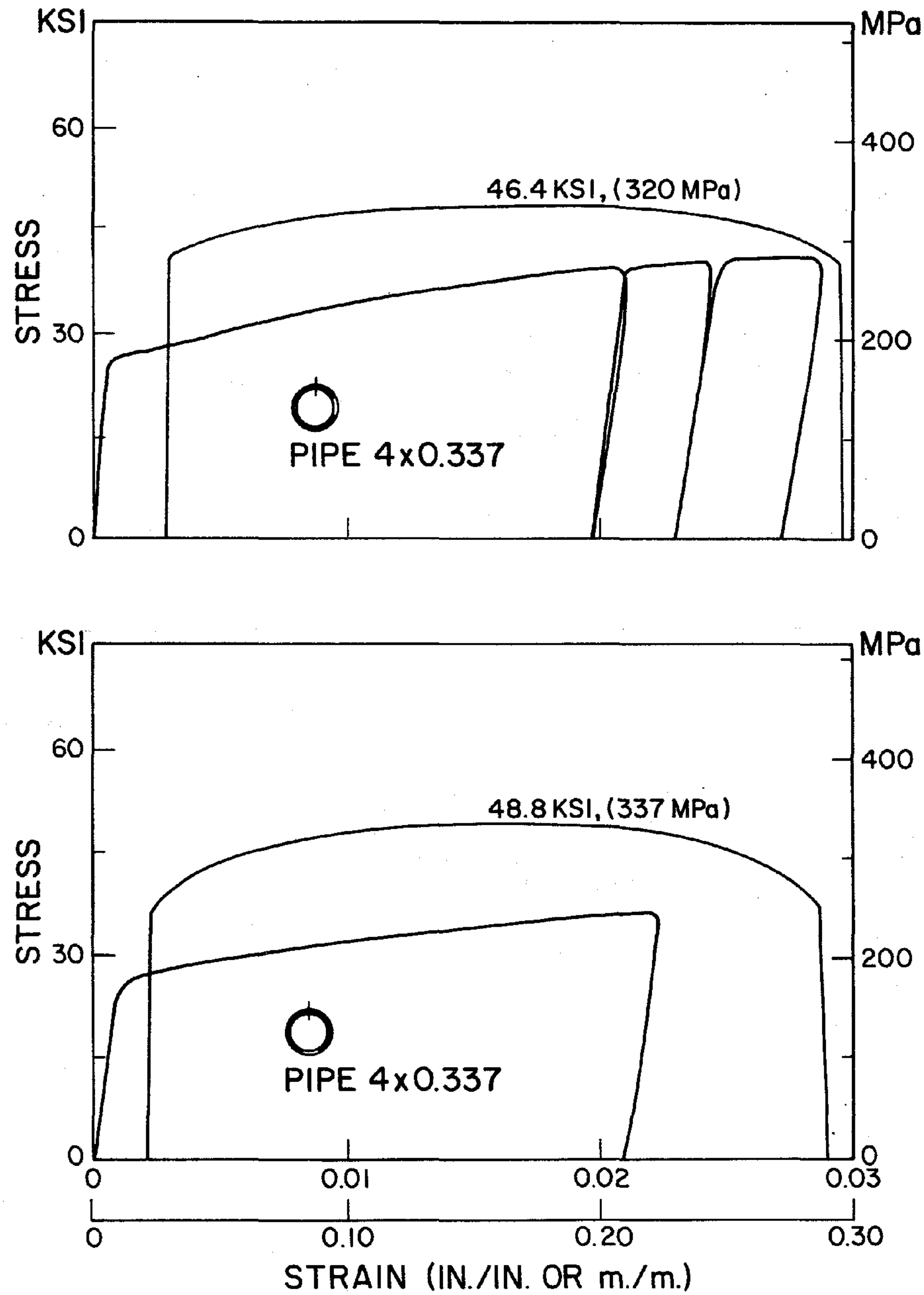

FIG. A14 STRESS-STRAIN DIAGRAMS FOR MATERIAL FROM 4 IN. EXTRA STRONG PIPE

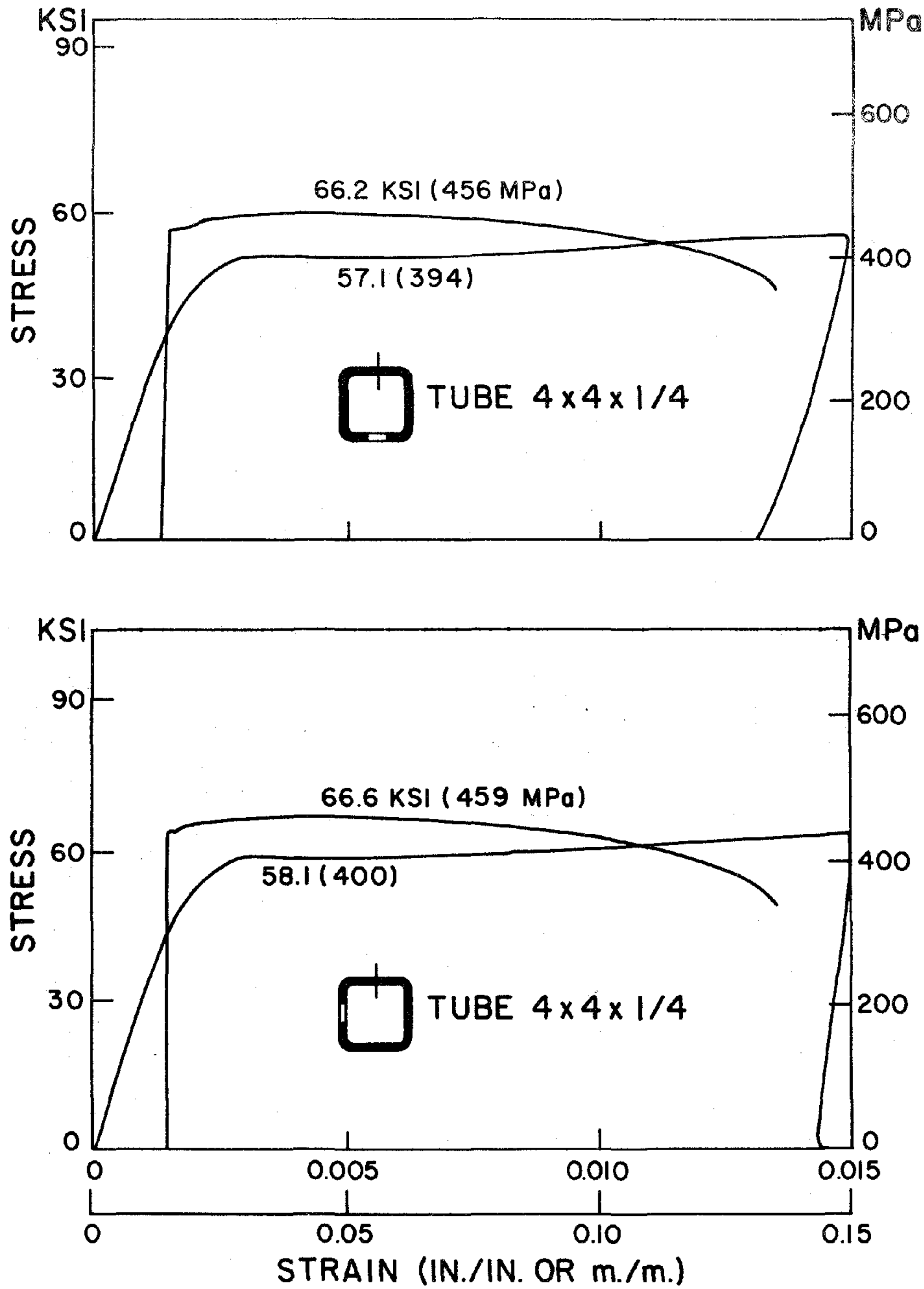

FIG. A15 STRESS-STRAIN DIAGRAMS FOR MATERIAL FROM $4 \times 4 \times \frac{1}{4}$ TUBE

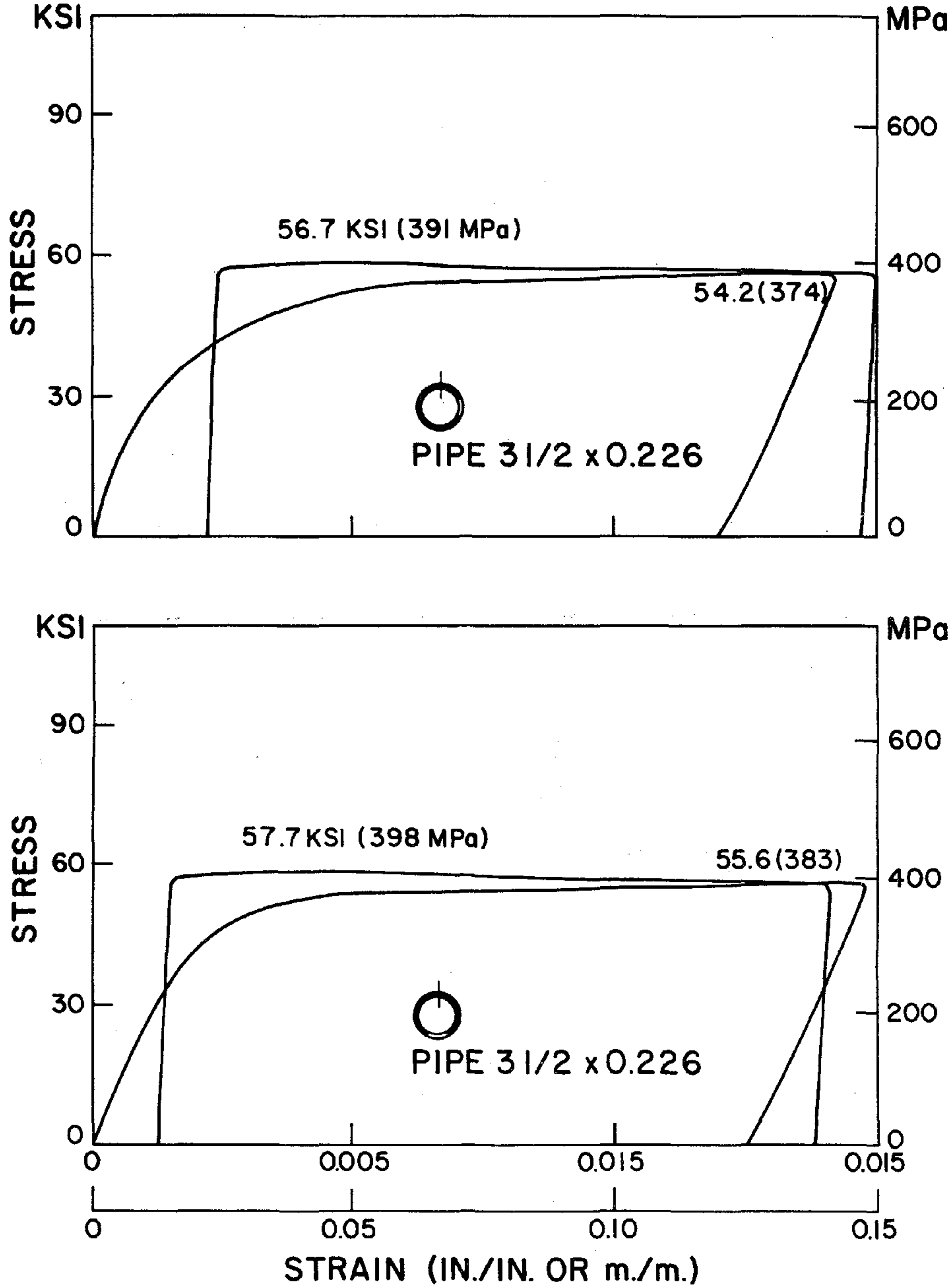

FIG. A16 STRESS-STRAIN DIAGRAMS FOR MATERIAL FROM 3 $\frac{1}{2}$ IN. STANDARD WEIGHT PIPE

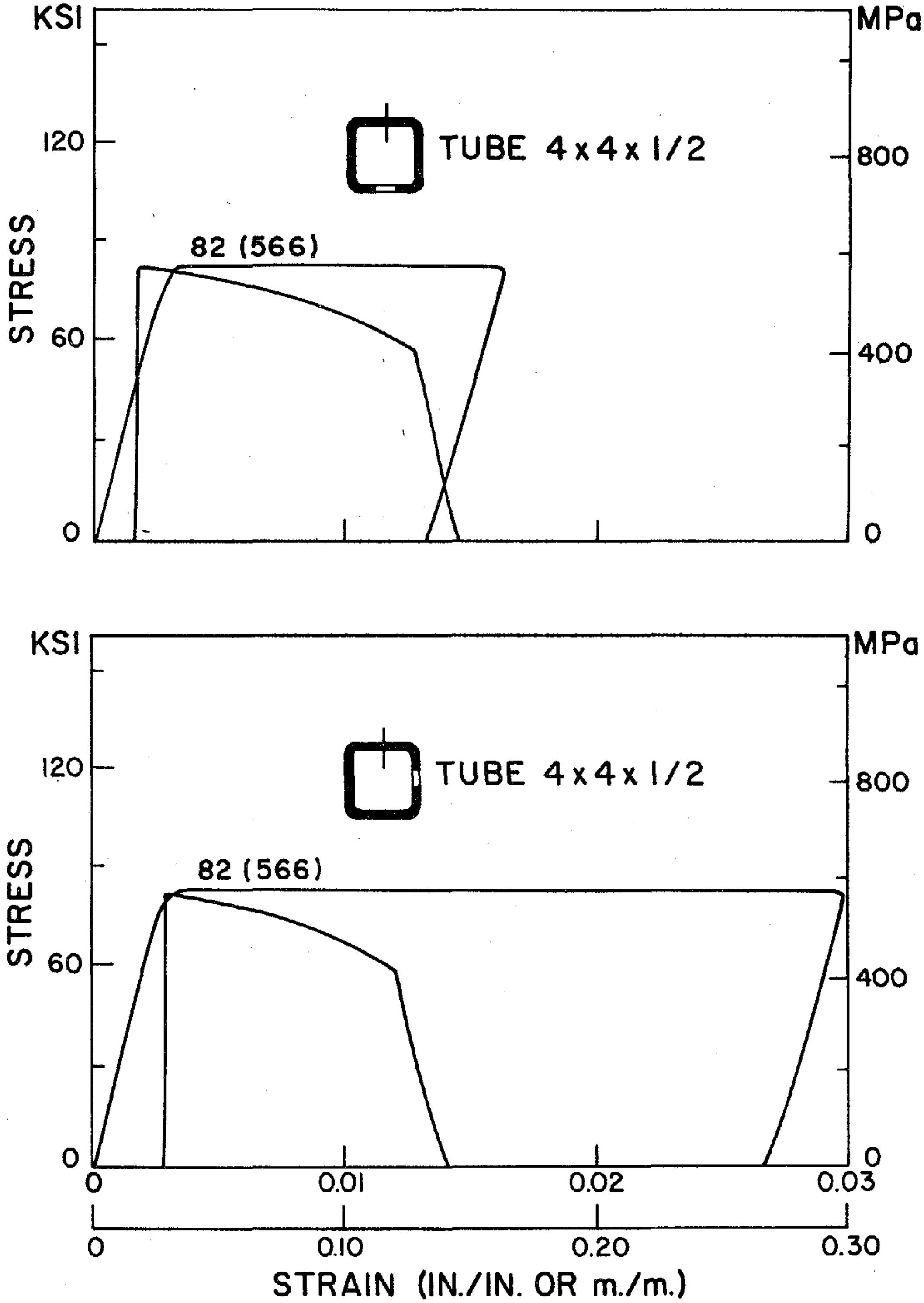

FIG. A17 STRESS-STRAIN DIAGRAMS FOR MATERIAL FROM $4 \times 4 \times \frac{1}{2}$ TUBE

APPENDIX B

EXPERIMENTAL HYSTERETIC CURVES

In this Appendix, two kinds of hysteretic diagrams are presented for all of the tested specimens. In one of the groups, the hysteretic P-δ curves are shown, which give the relationship of the axially applied force to the axial displacement. In the second group, the P-Δ diagrams are exhibited relating the axial force with the maximum lateral displacement (see Fig. 33).

The curves shown have been corrected for the two principal errors commonly encountered in this type of testing. These are the frictional effects of the moving parts, and mechanical backlash of the displacement measuring apparatus. To illustrate the procedure used, consider somewhat of an extreme case shown in Fig. B1, where the recorderd hysteretic P-δ plot for Strut 21 is shown. Here one can note that at any number of points of load reversal, an apparent change in the applied force occurs with no corresponding change in the axial displacement. These regions have been identified with an asterisk in the figure. At least a part of this effect is due to the frictional forces that must be overcome. The nature of these forces is illustrated in Fig. B2. Based on some measurements of these forces a typical hysteretic loop is modified as shown in Fig. B3.

The second cause contributing to the error in recorded hysteretic loops was due to the mechanical backlash which resulted in a delay in the displacement record. Therefore, the top curve corrected for the frictional effects is extrapolated on the left, and moved as a whole to the right, Fig. B4. On this basis, the corrected hysteretic loop in relation to the recorded data looks as shown in Fig. B5. Because of the uncertainties involved, other adjustments of the data are possible. However, since the basic shape of the curves corrected for frictional effects is essentially correct, the corrected curves found in the above manner give an essentially correct picture of the strut behavior. In a number of the available reports, the corrections discussed above are not considered, which may lead to erroneous conclusions.

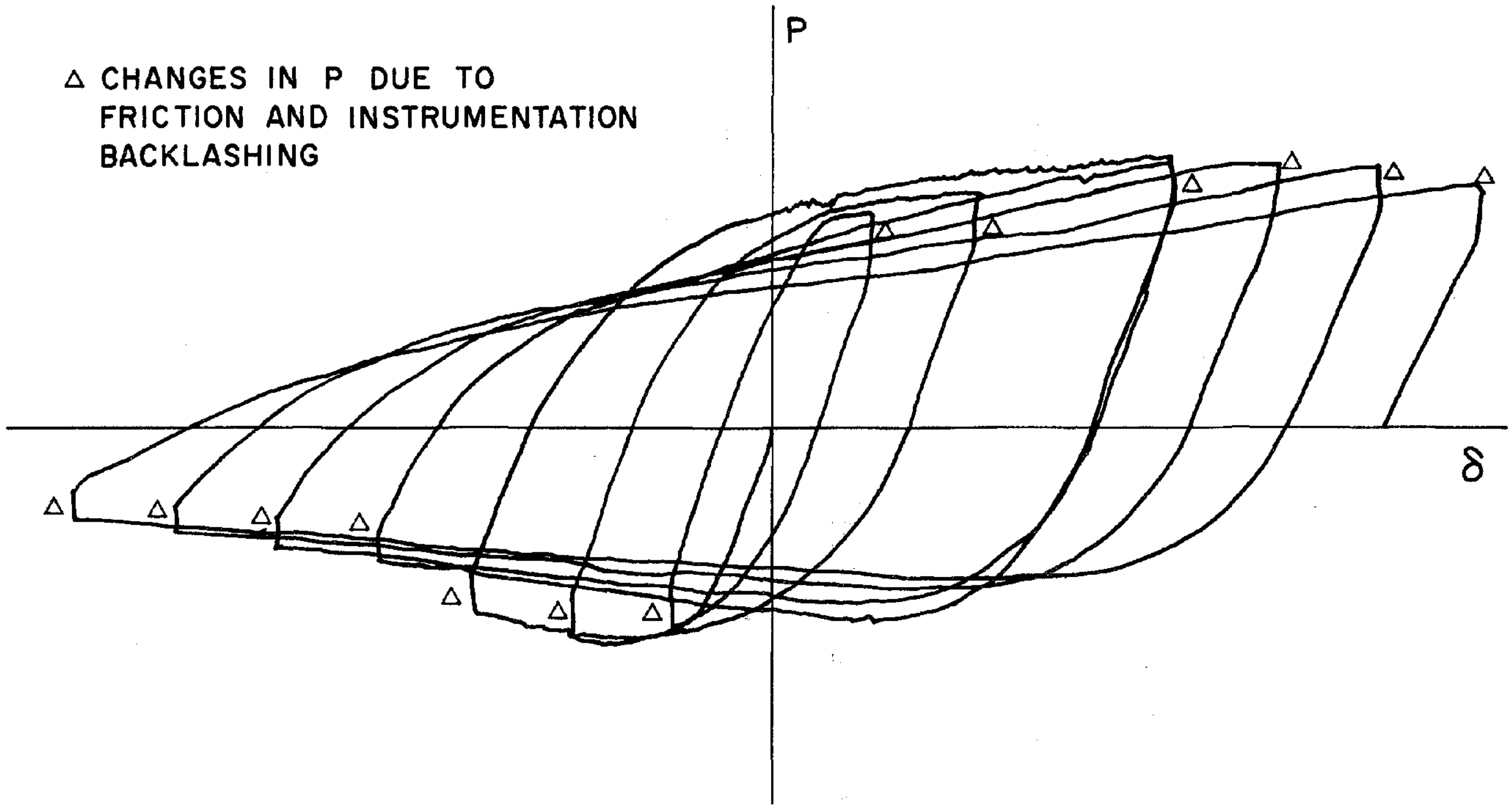

FIG. B1 RECORDED HYSTERETIC PLOT FOR STRUT 21

F_S = ACTUAL LOAD EXPERIENCED BY SPECIMEN

F_J = MEASURED JACK LOAD

F_F = FRICTIONAL FORCE

LOADING IN COMPRESSION

$$F_S = F_J - F_F$$

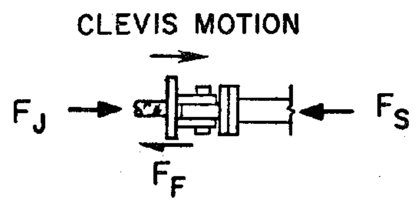

UNLOADING IN COMPRESSION

$$F_S = F_J + F_F$$

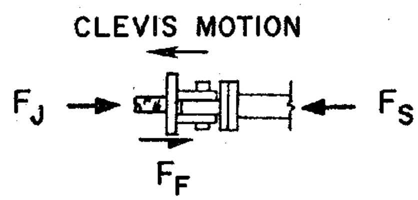

LOADING IN TENSION

$$F_S = F_J - F_F$$

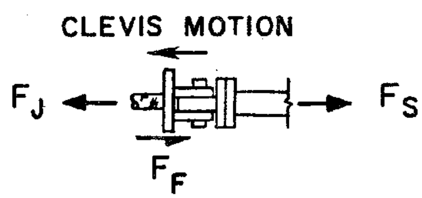

UNLOADING IN TENSION

$$F_S = F_J + F_F$$

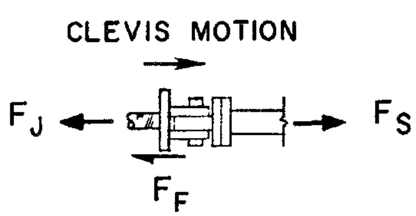

FIG. B2 EFFECT OF FRICTION ON MEASURED LOAD

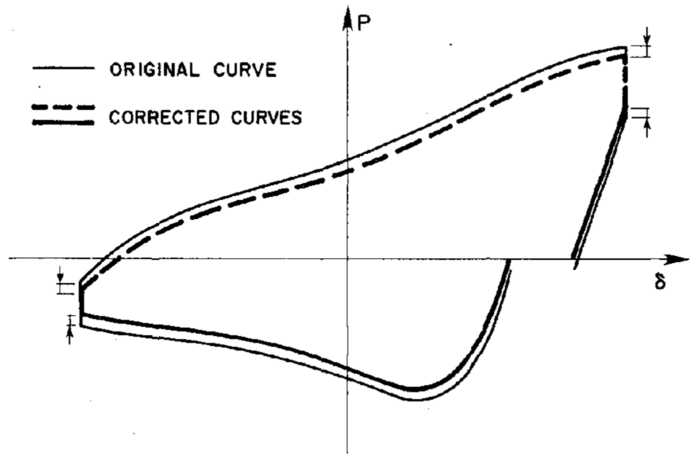

FIG. B3 CORRECTION FOR FRICTION

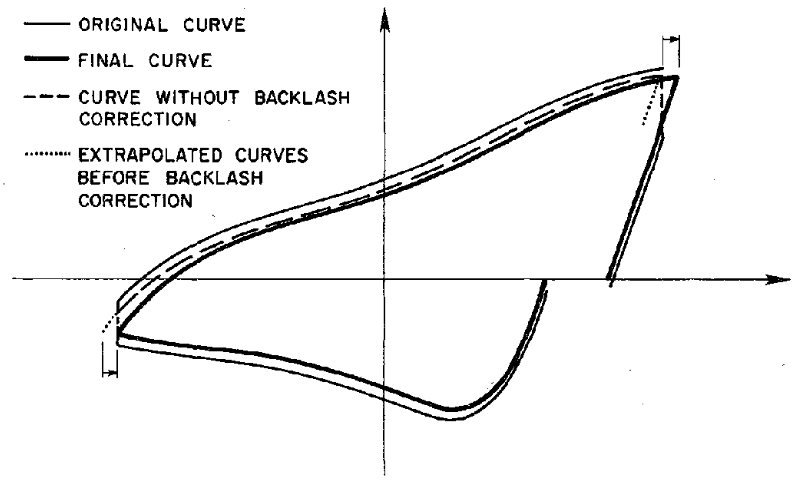

FIG. B4 CORRECTION FOR BACKLASH

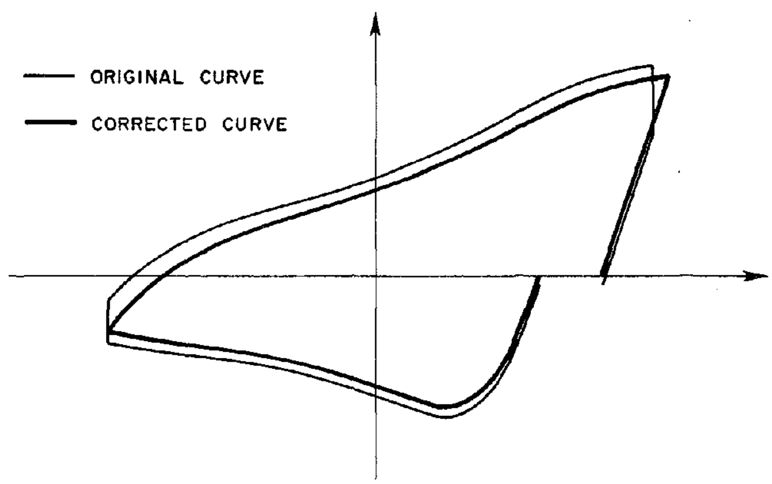

FIG. B5 COMPARISON OF RECORDED CURVE WITH FINAL CURVE CORRECTED FOR FRICTIONAL EFFECTS AND DISPLACEMENT BACKLASH

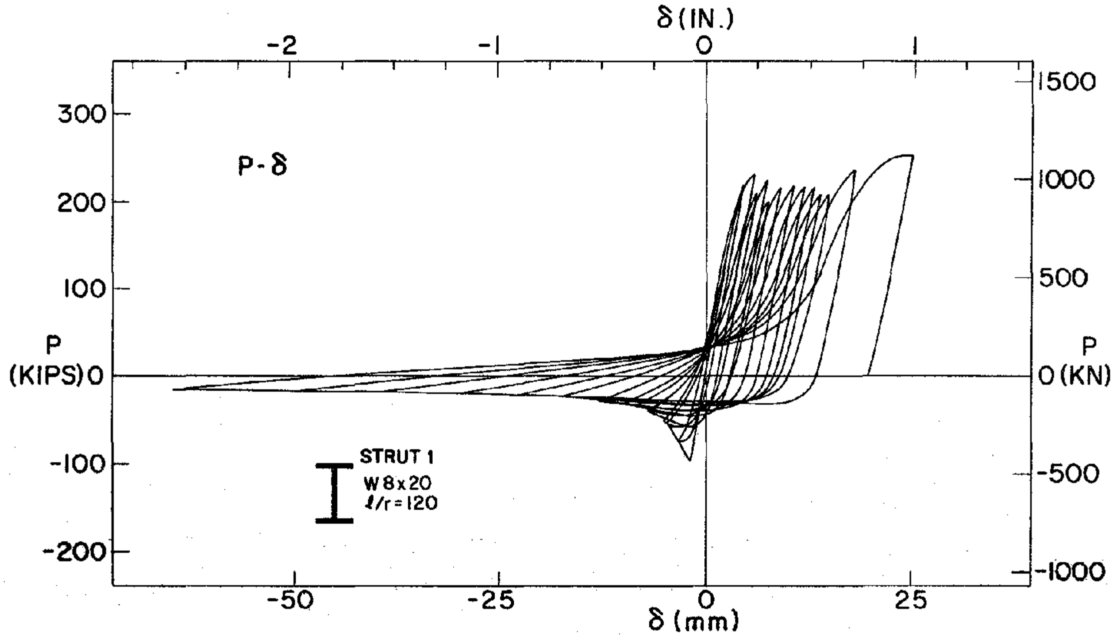

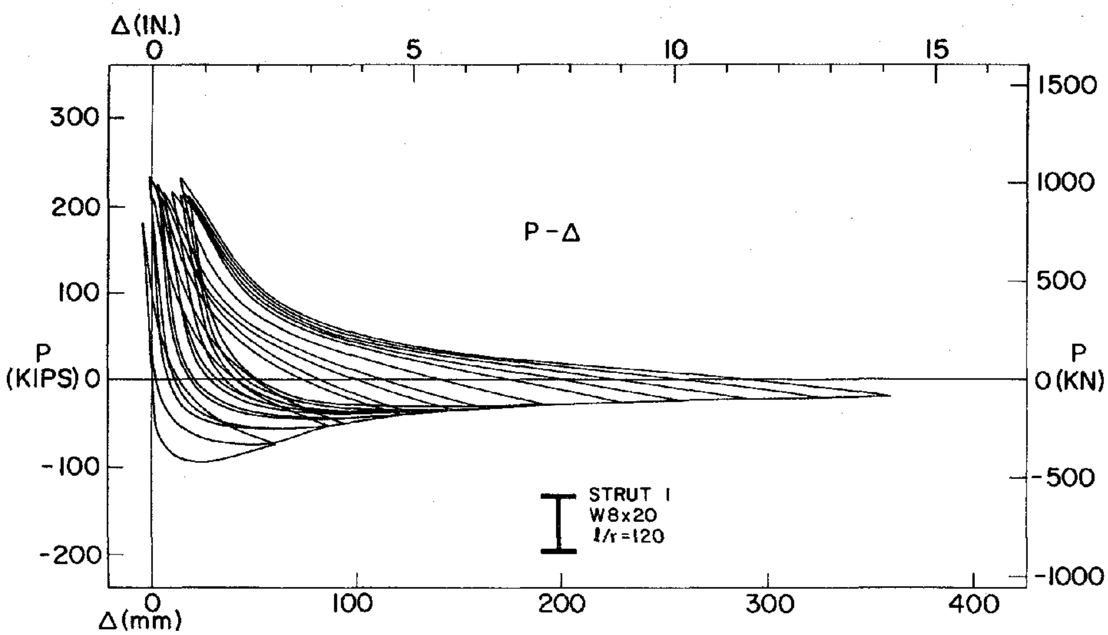

FIG. B6 P-δ AND P-Δ CURVES FOR STRUT 1

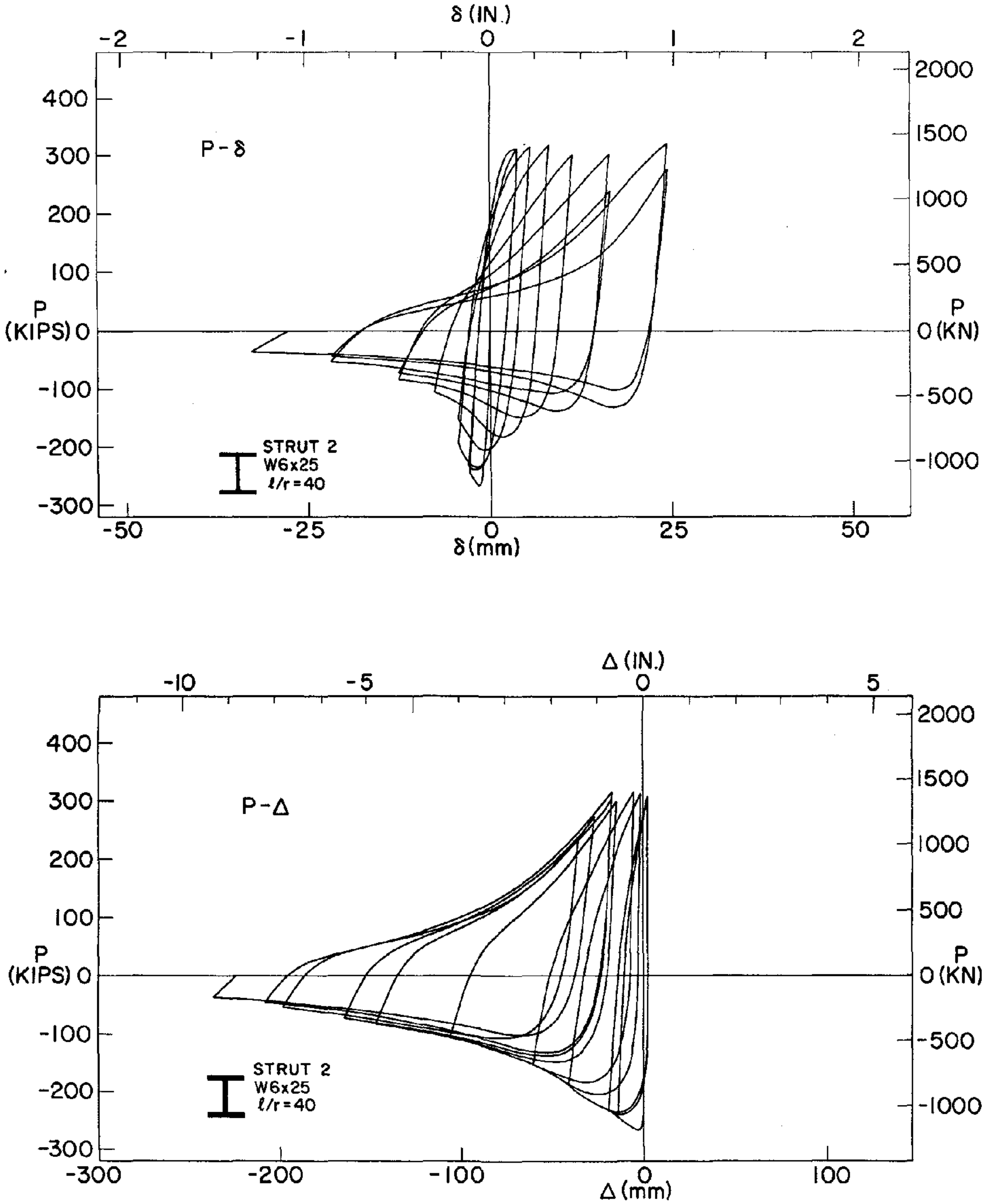

FIG. B7 P-δ AND P-Δ CURVES FOR STRUT 2

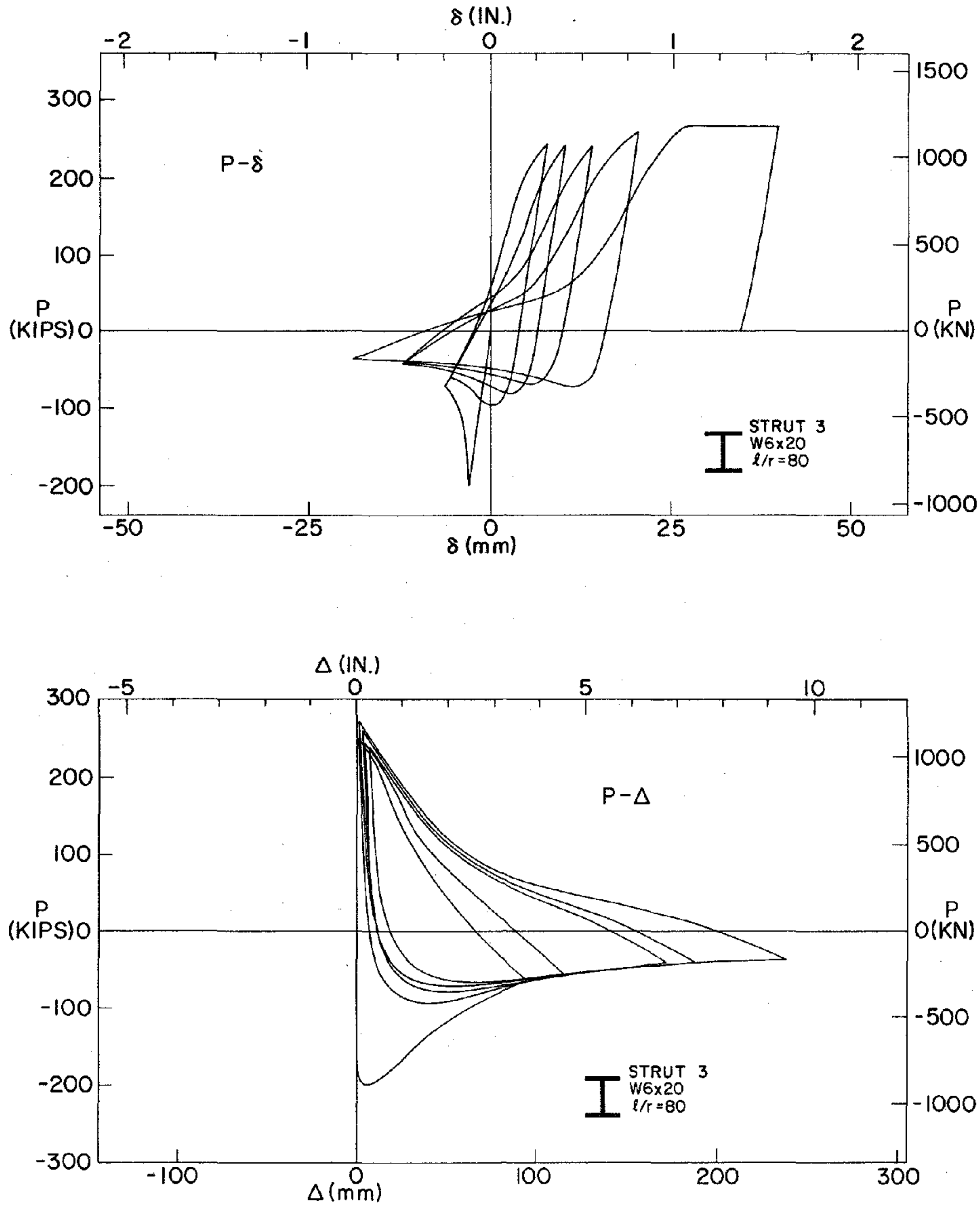

FIG. B8 P-δ AND P-Δ CURVES FOR STRUT 3

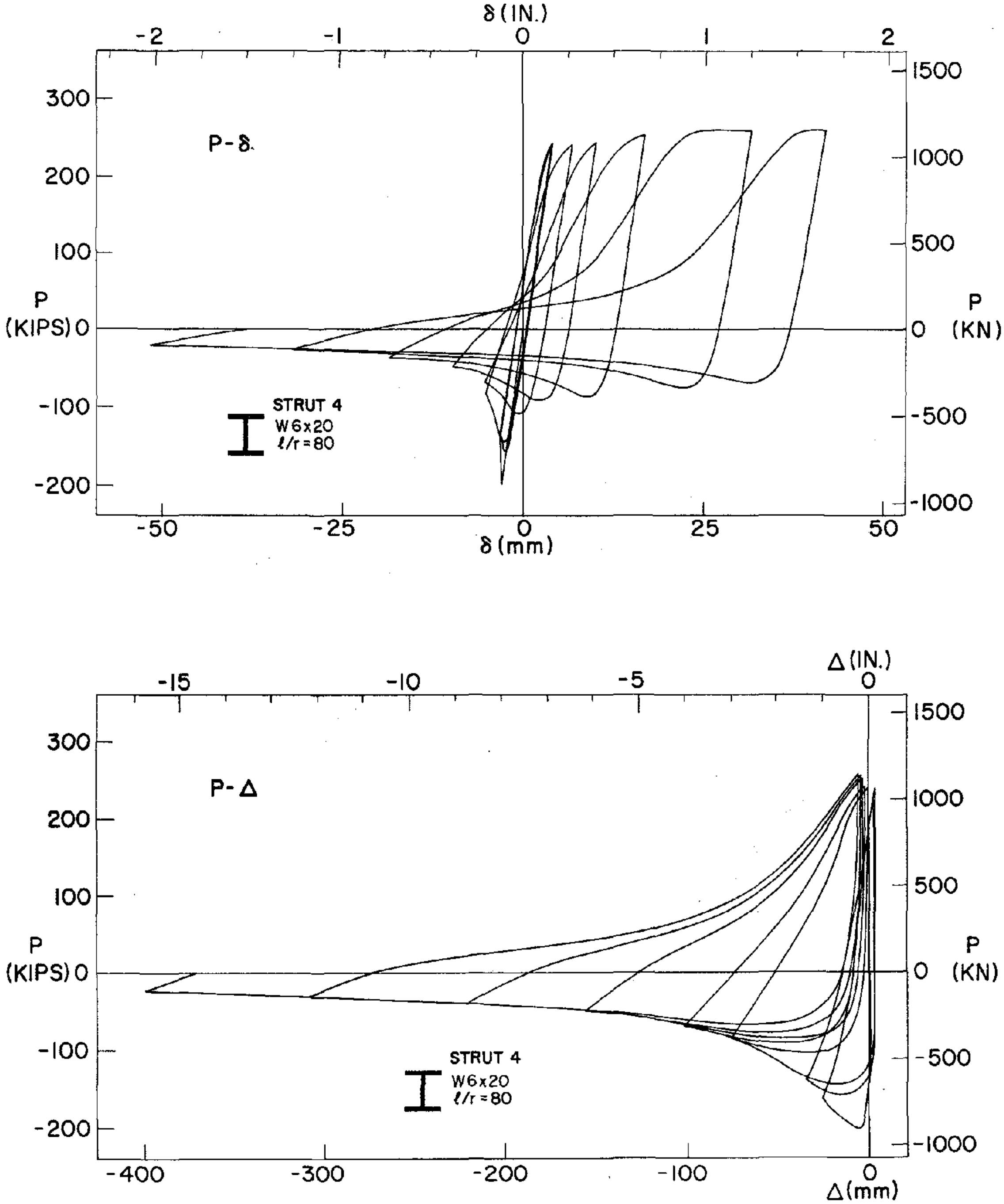

FIG. B9 P-δ AND P-Δ CURVES FOR STRUT 4

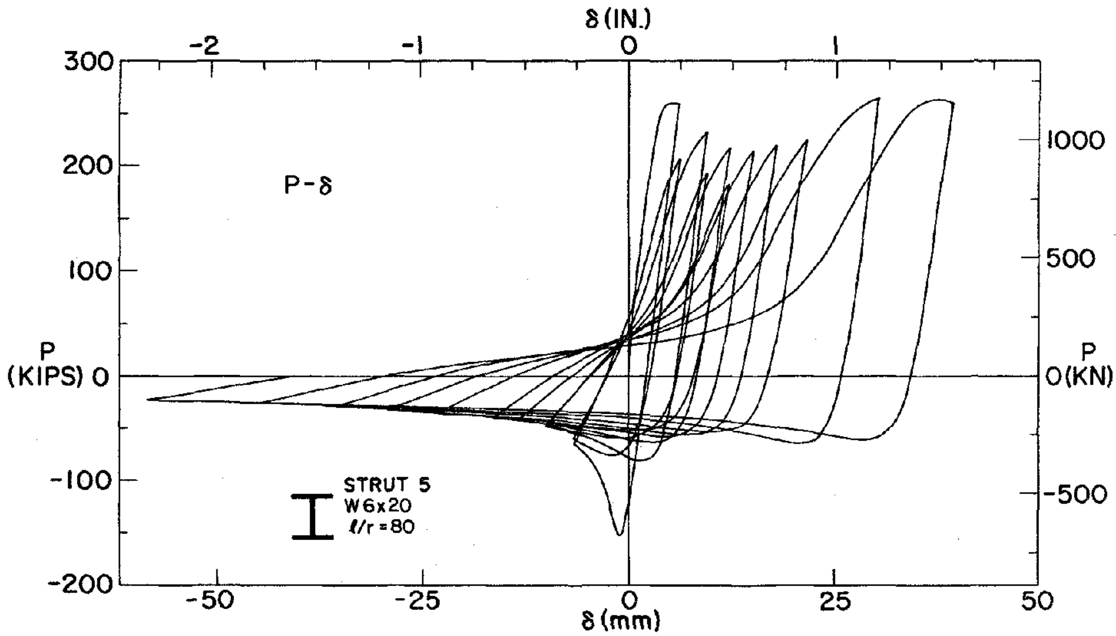

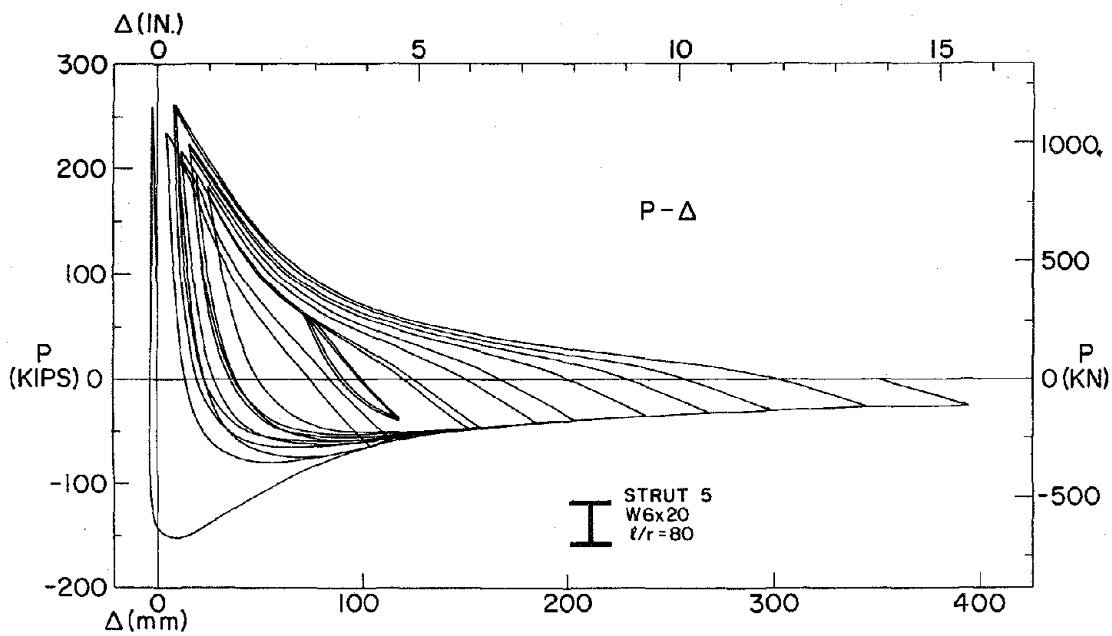

FIG. B10 P-δ AND P-Δ CURVES FOR STRUT 5

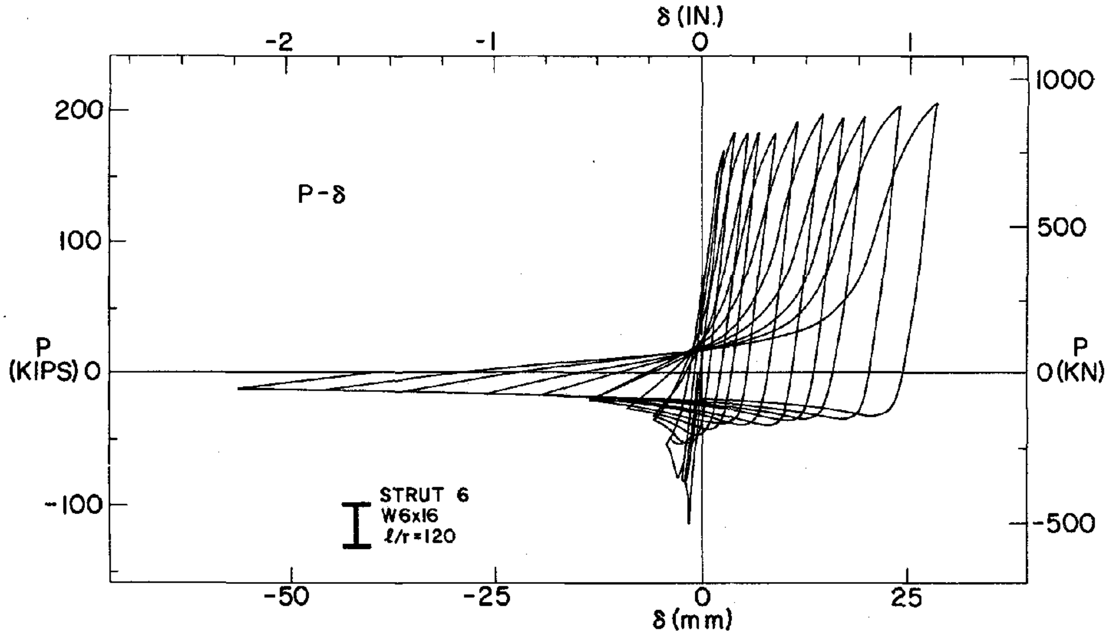

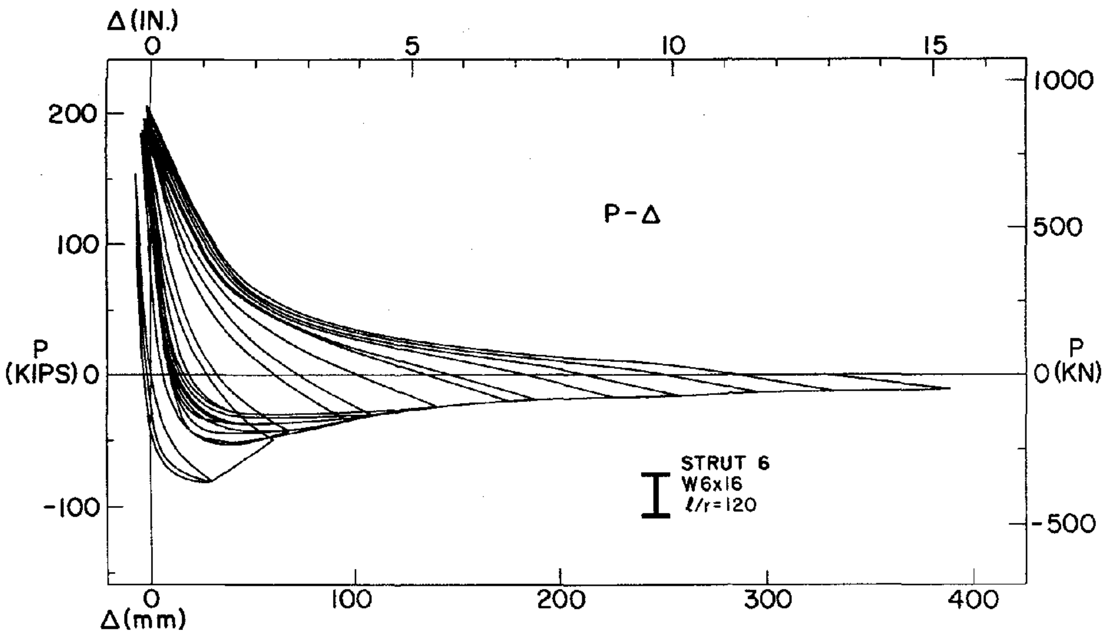

FIG. B11 P-δ AND P-Δ CURVES FOR STRUT 6

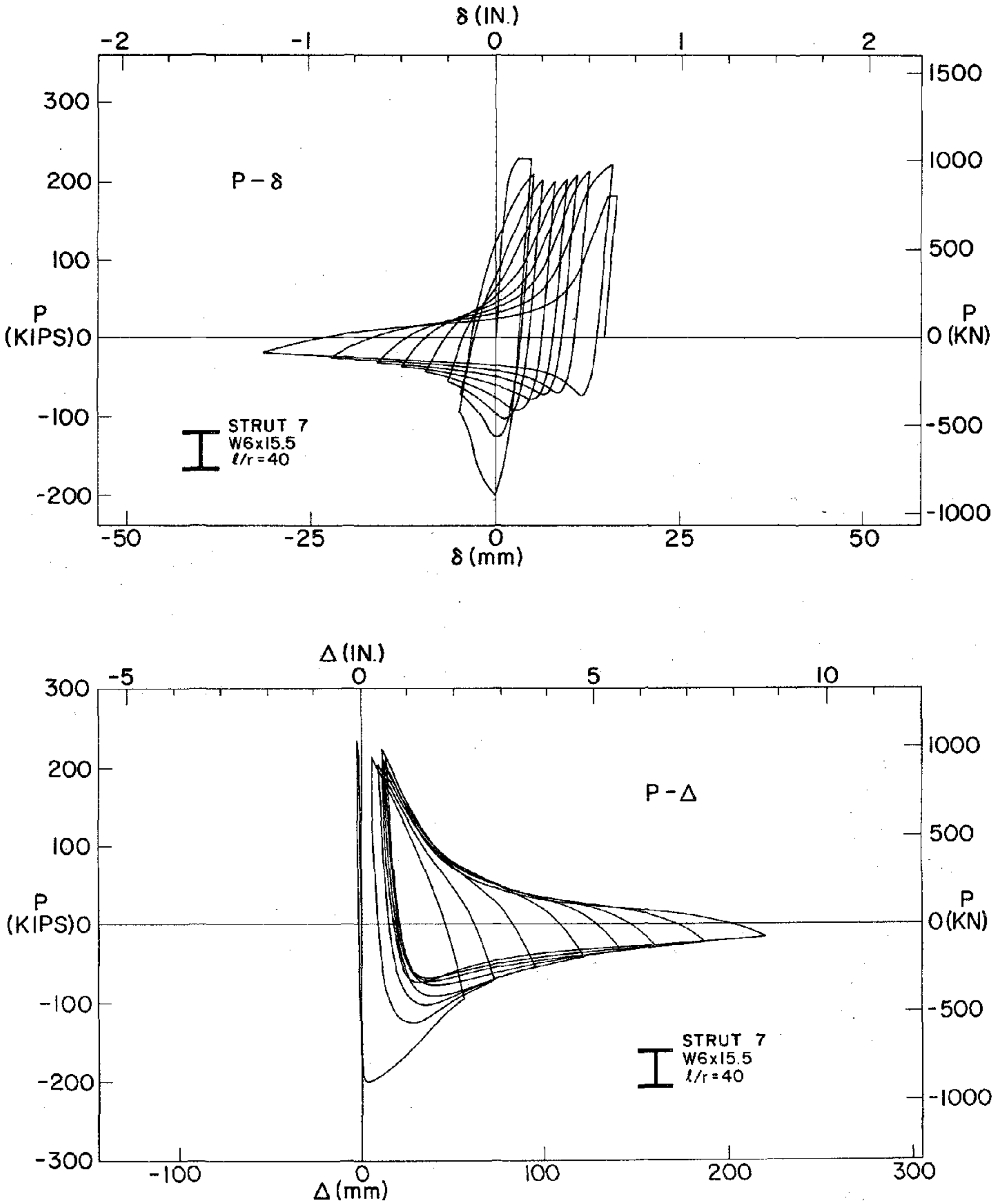

FIG. B12 P-δ AND P-Δ CURVES FOR STRUT 7

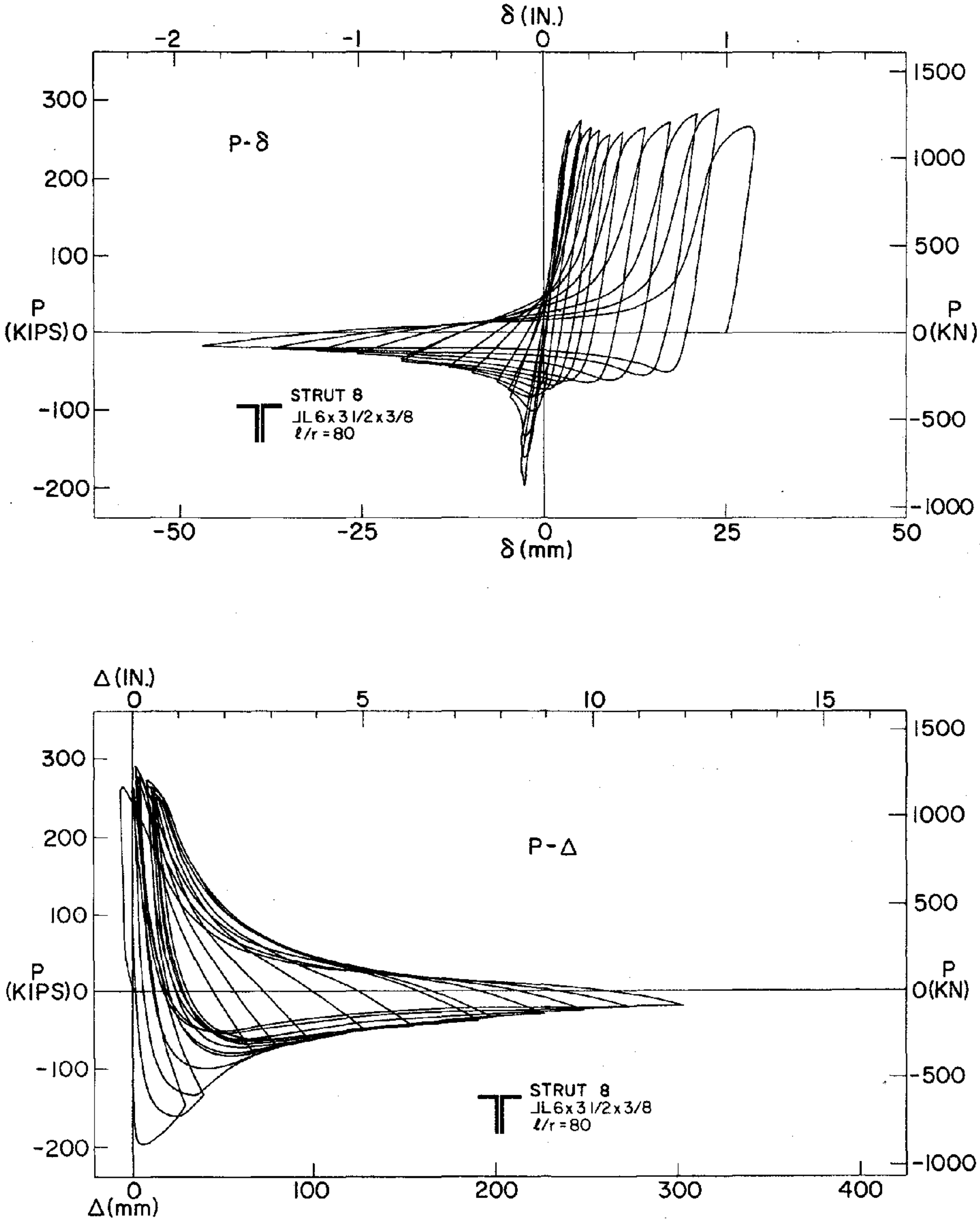

FIG. B13 P-δ AND P-Δ CURVES FOR STRUT 8

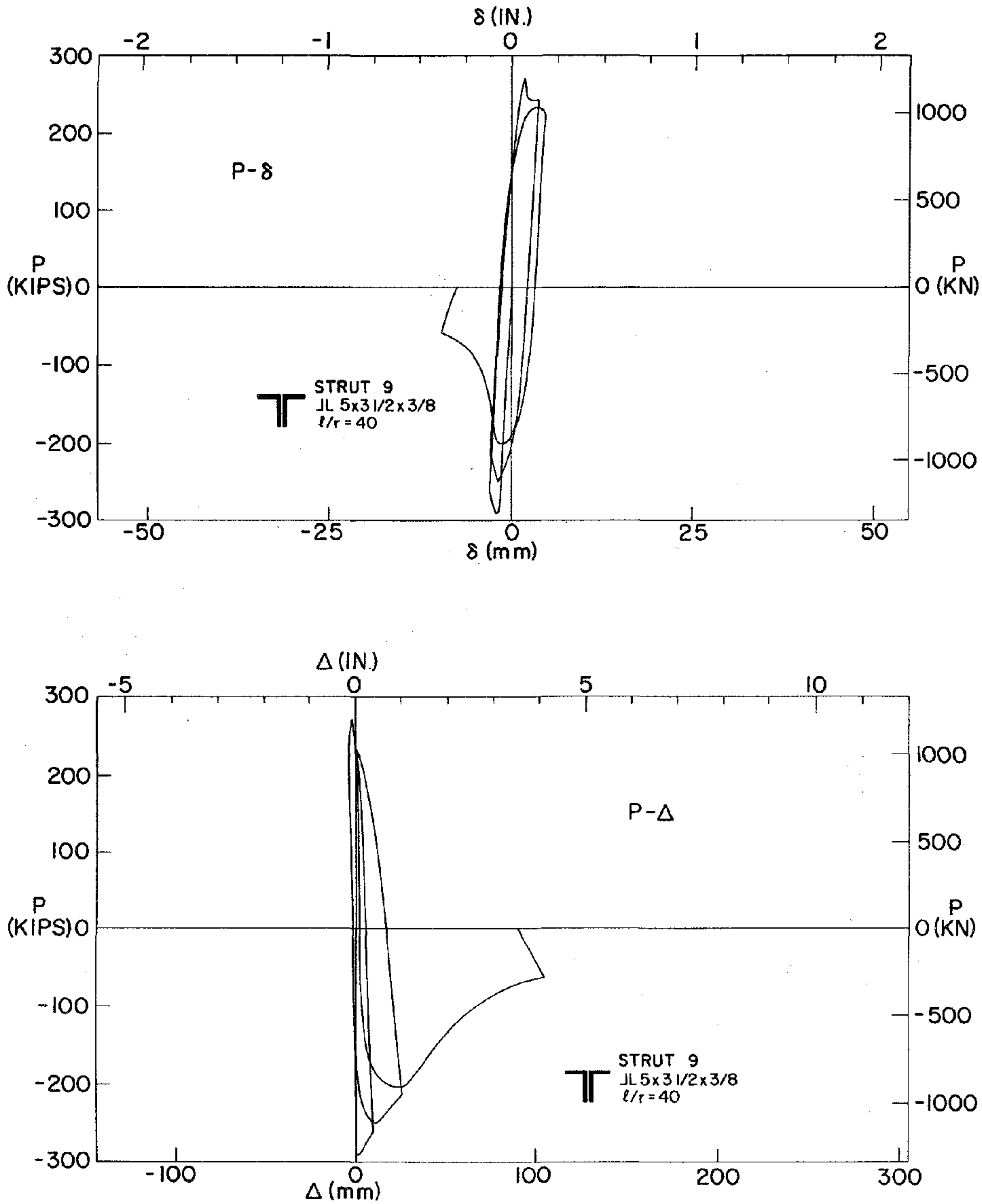

FIG. B14 P-δ AND P-Δ CURVES FOR STRUT 9

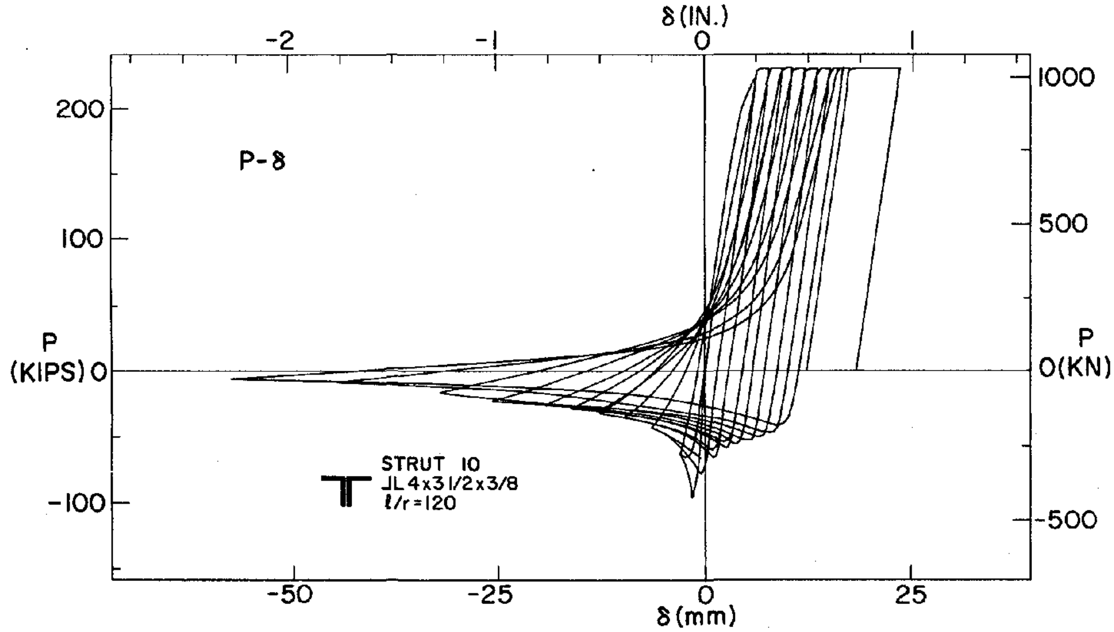

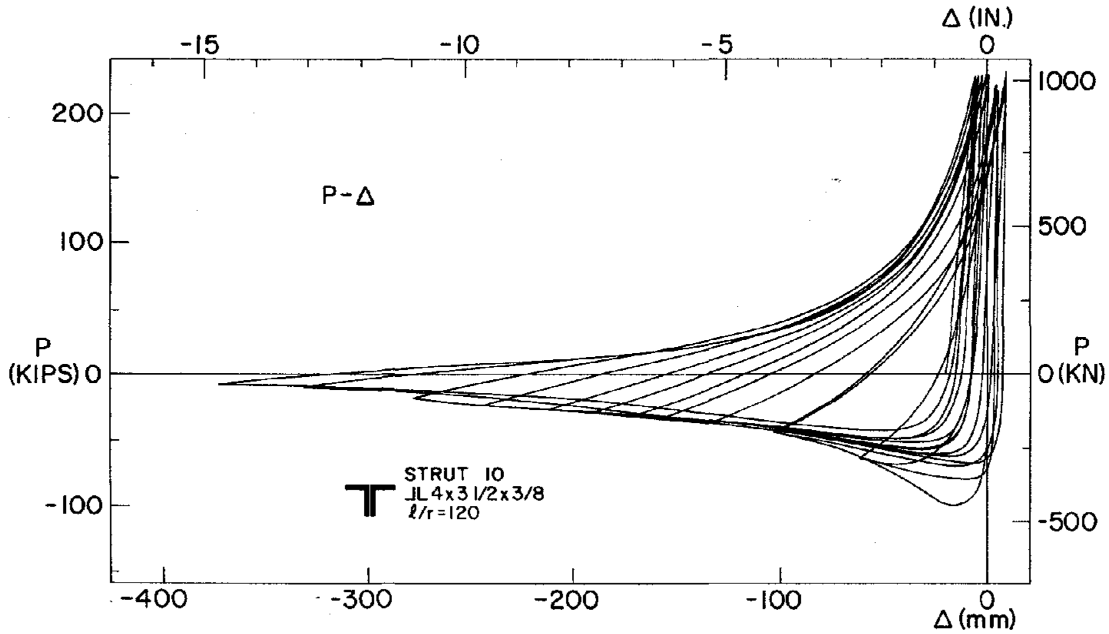

FIG. B15 P-δ AND P-Δ CURVES FOR STRUT 10

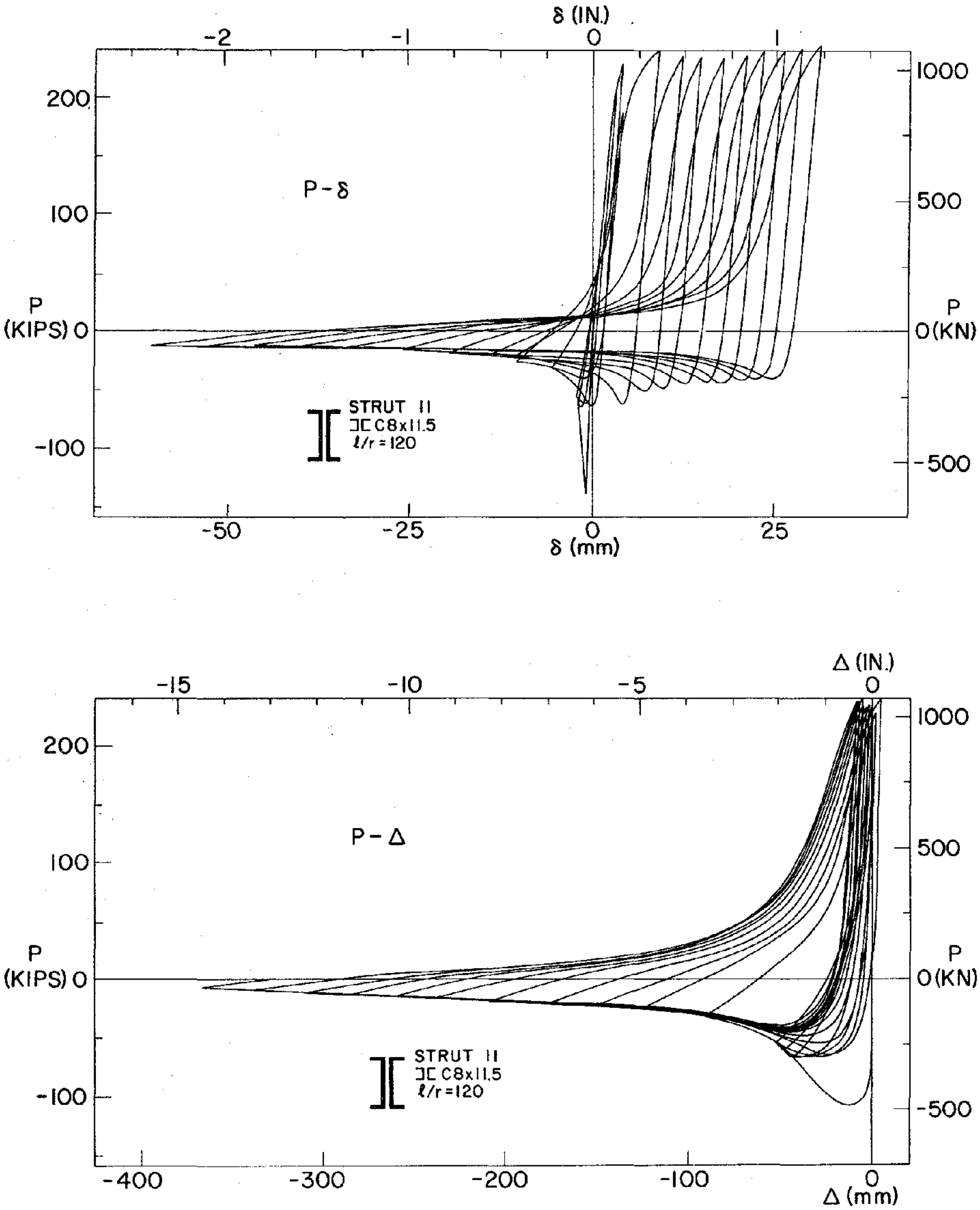

FIG. B16 P-δ AND P-Δ CURVES FOR STRUT 11

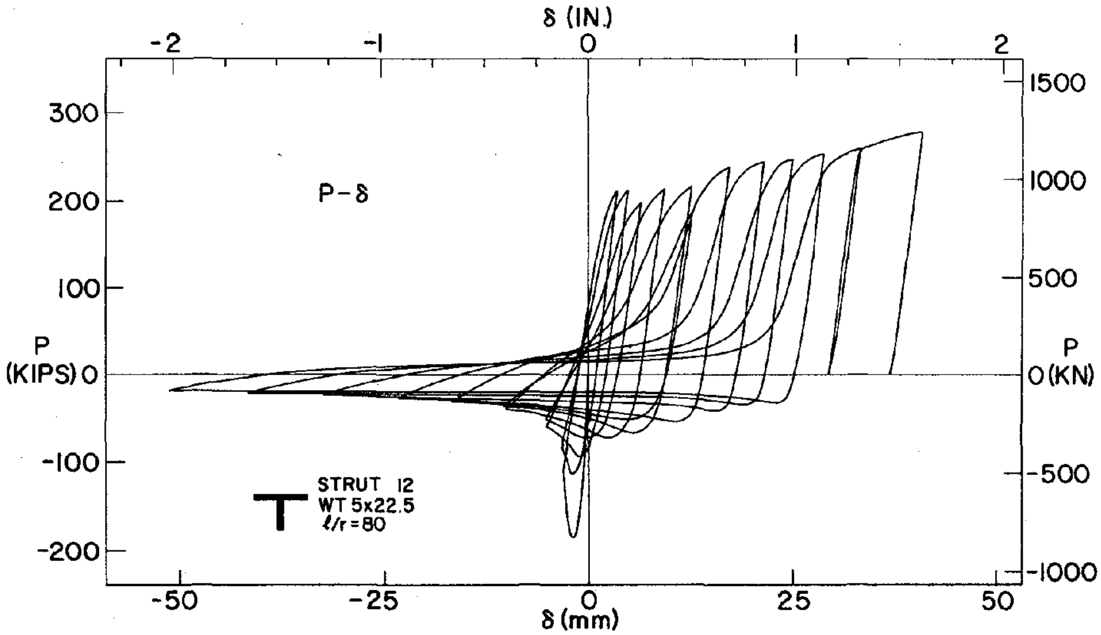

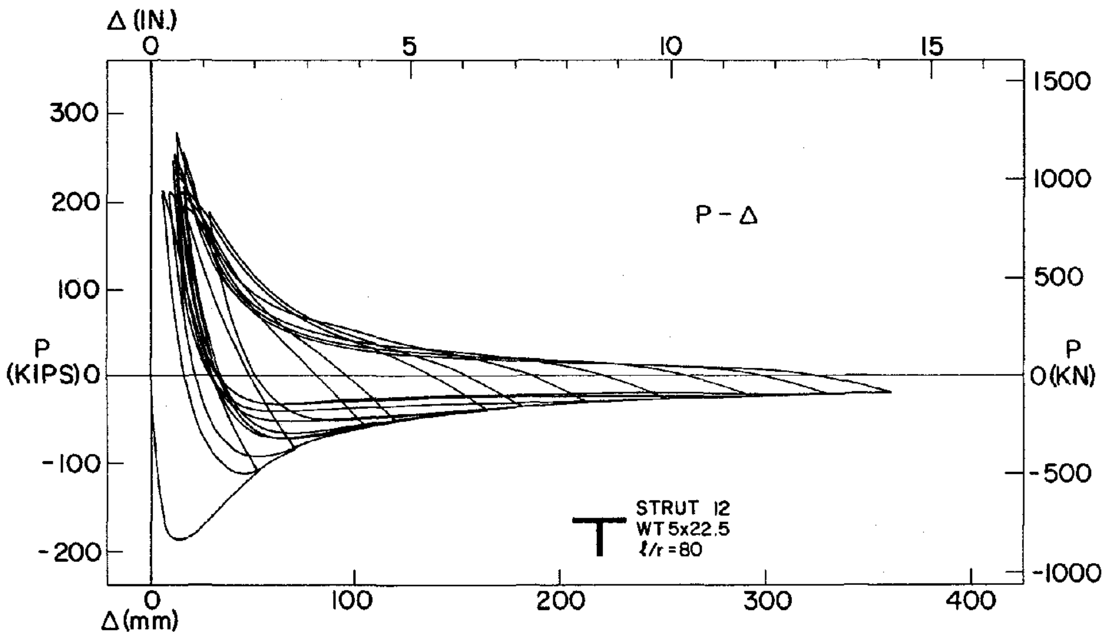

FIG. B17 P-δ AND P-Δ CURVES FOR STRUT 12

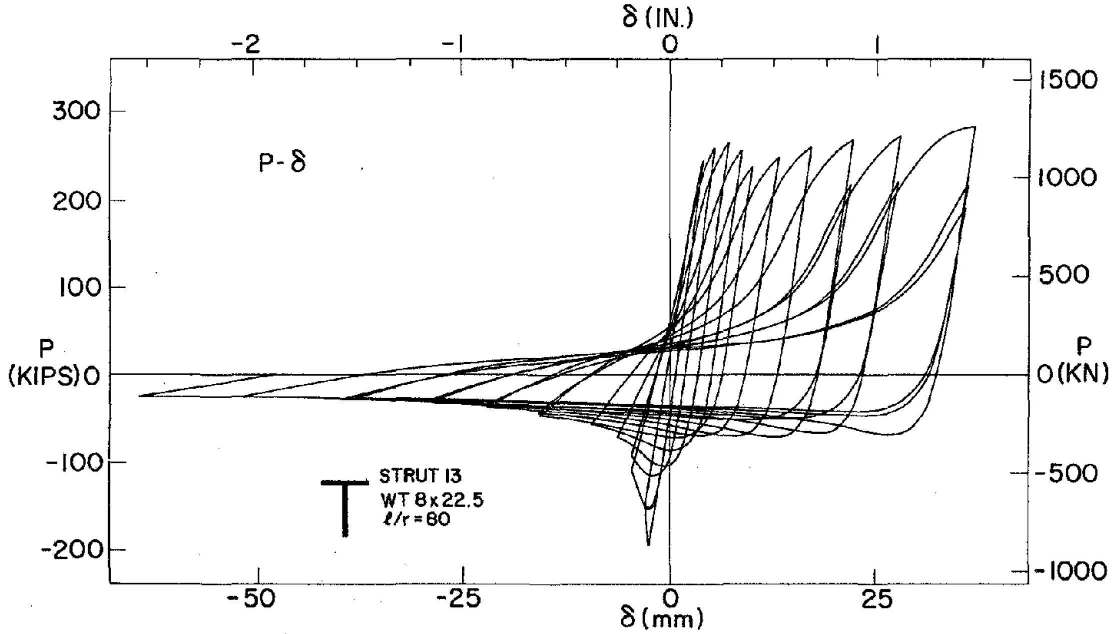

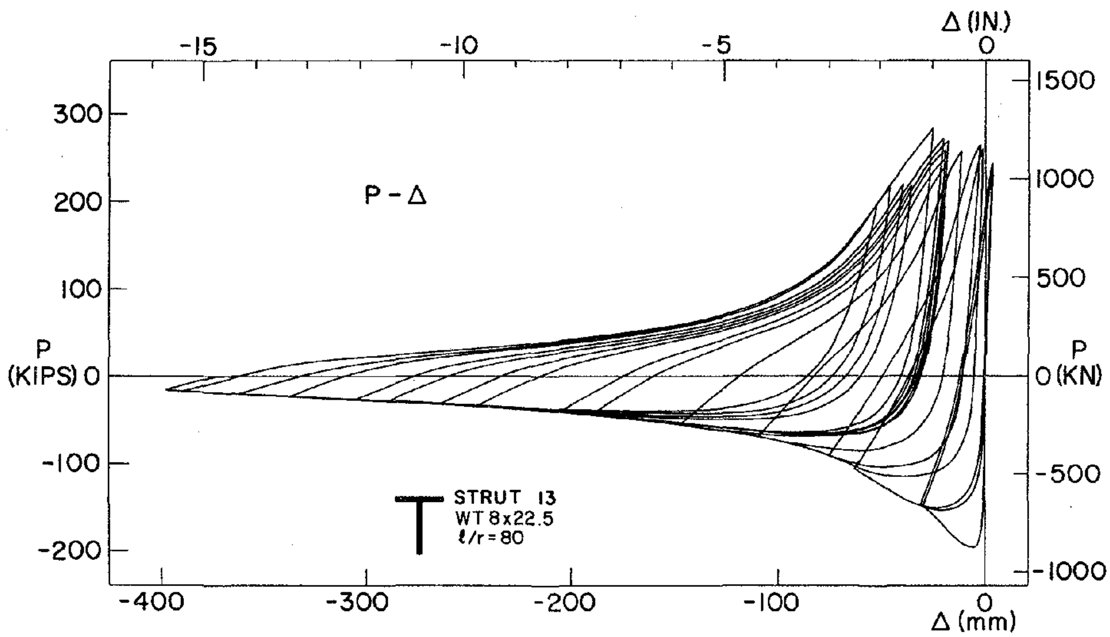

FIG. B18 P-δ AND P-Δ CURVES FOR STRUT 13

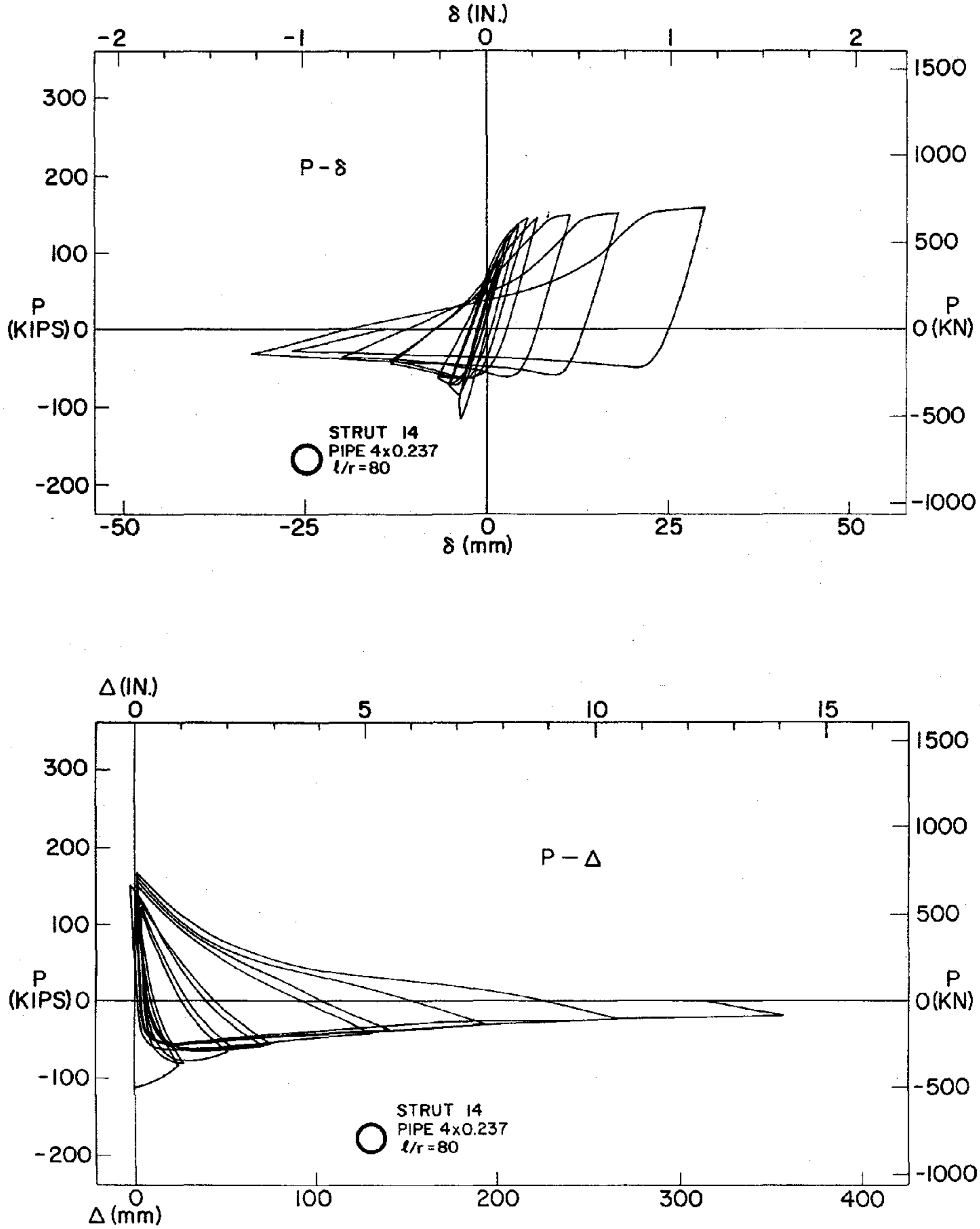

FIG. B19 P-δ AND P-Δ CURVES FOR STRUT 14

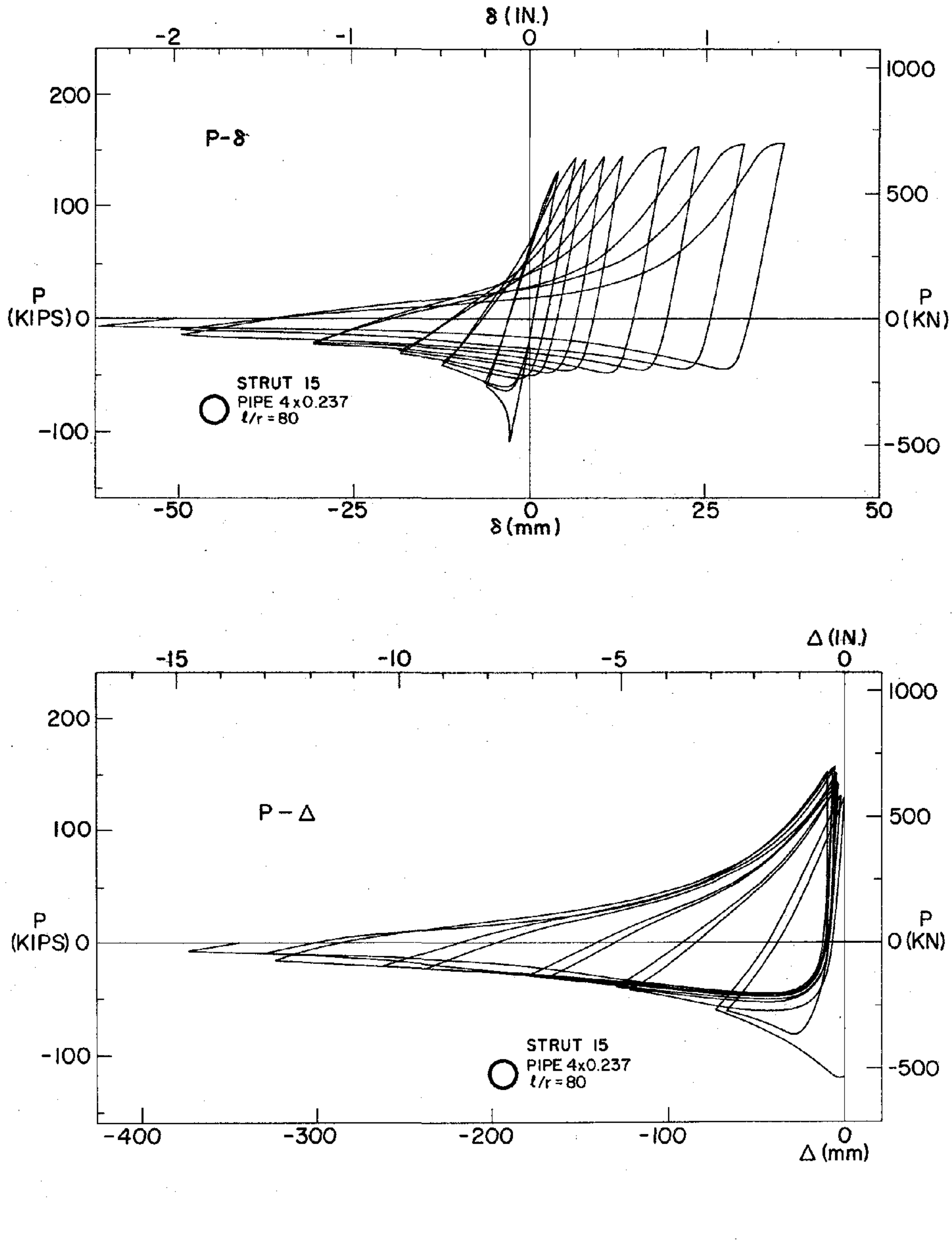

FIG. B20 P-δ AND P-Δ CURVES FOR STRUT 15

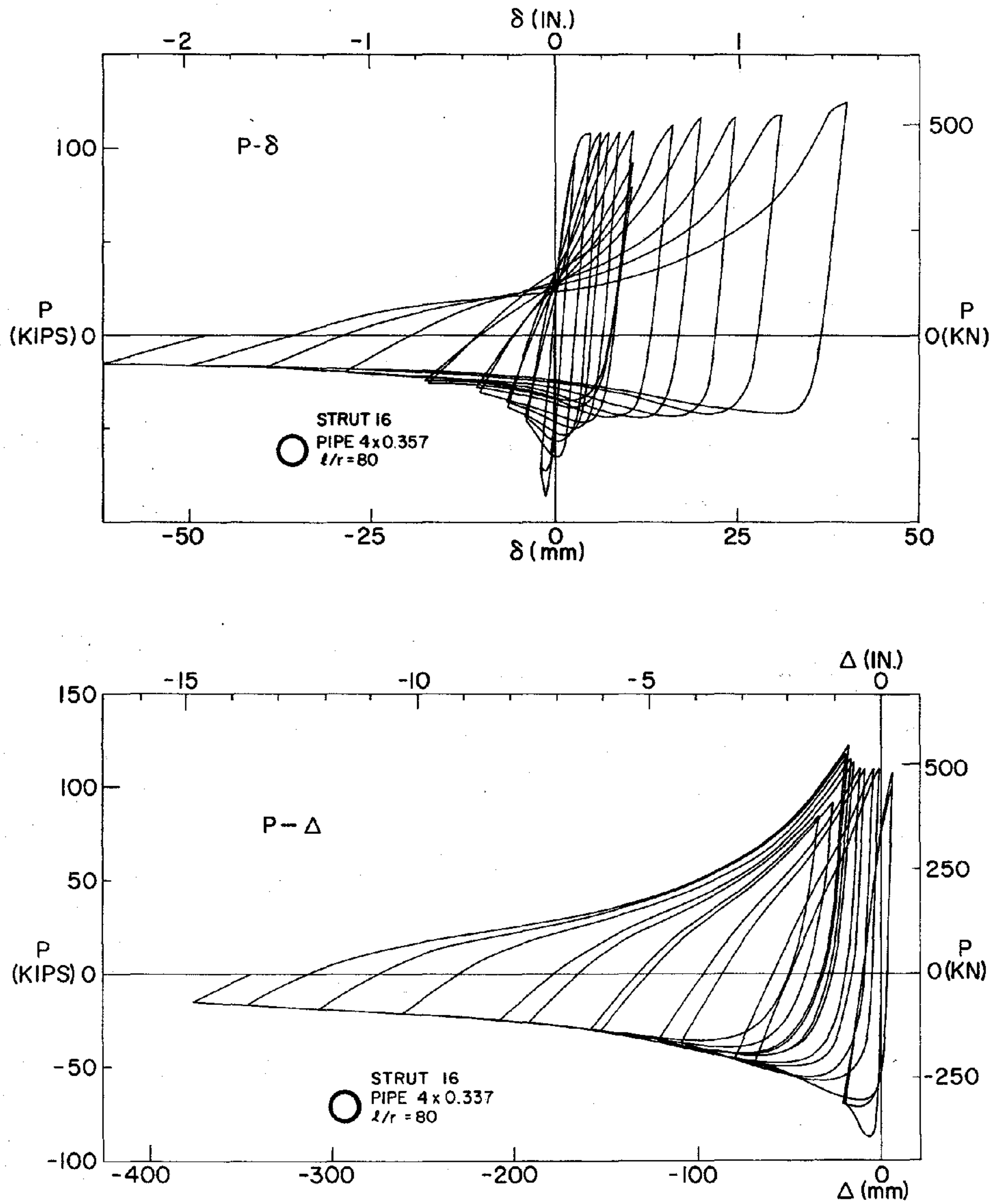

FIG. B21 P-δ AND P-Δ CURVES FOR STRUT 16

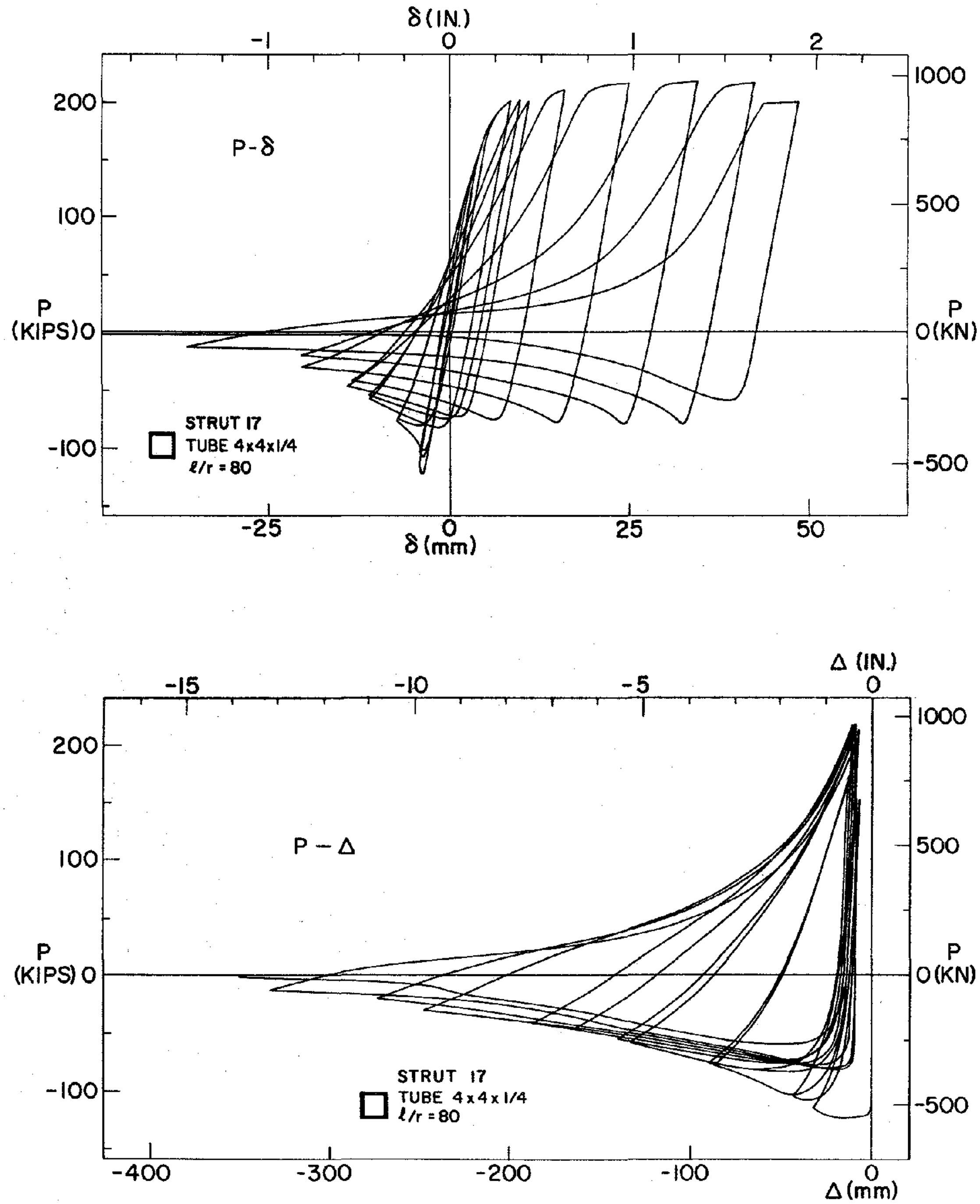

FIG. B22 P-δ AND P-Δ CURVES FOR STRUT 17

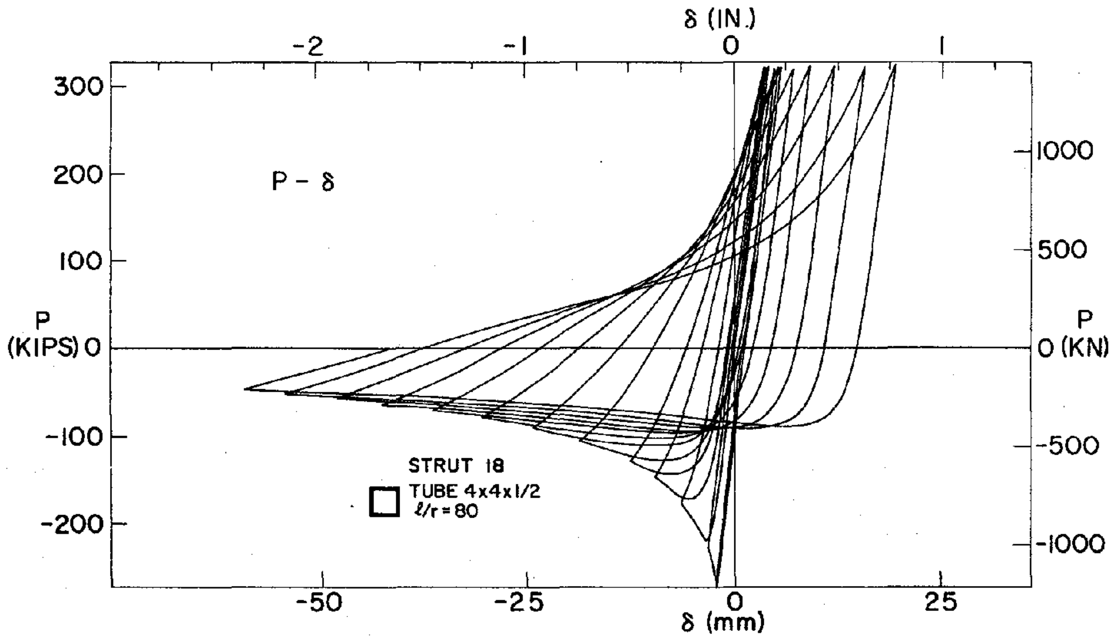

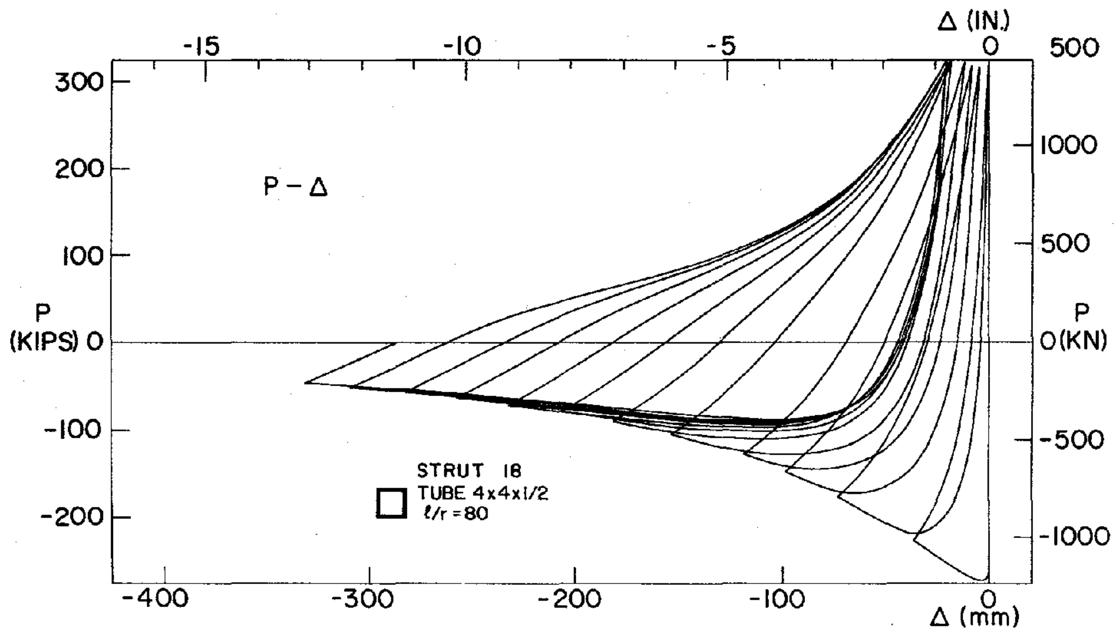

FIG. B23 P-δ AND P-Δ CURVES FOR STRUT 18

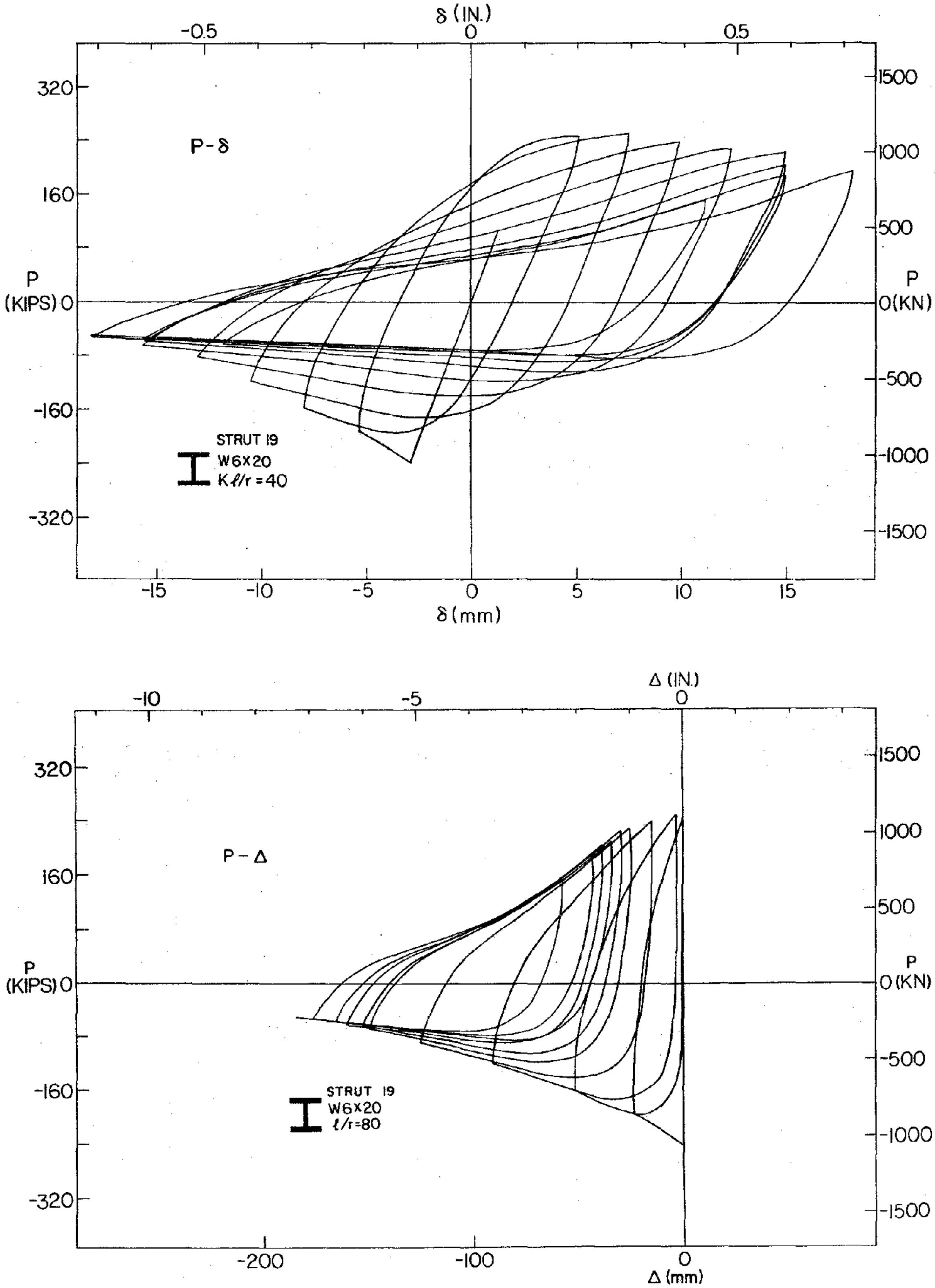

FIG. B24 P-δ AND P-Δ CURVES FOR STRUT 19

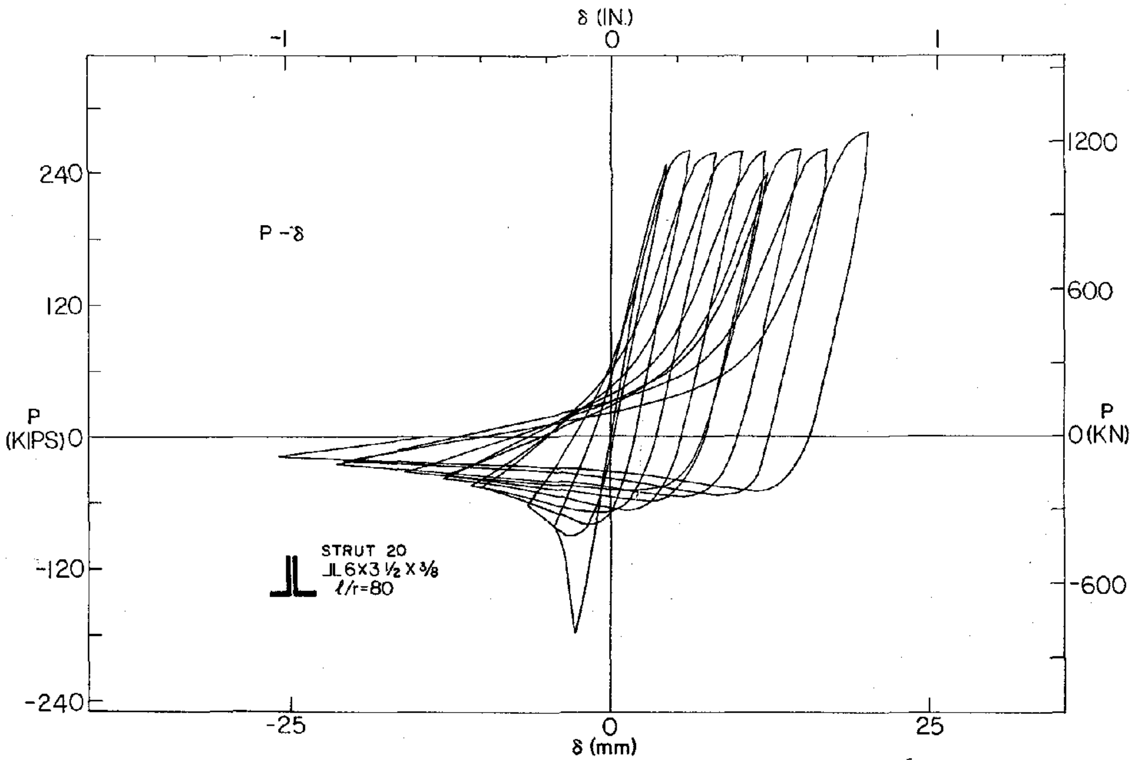

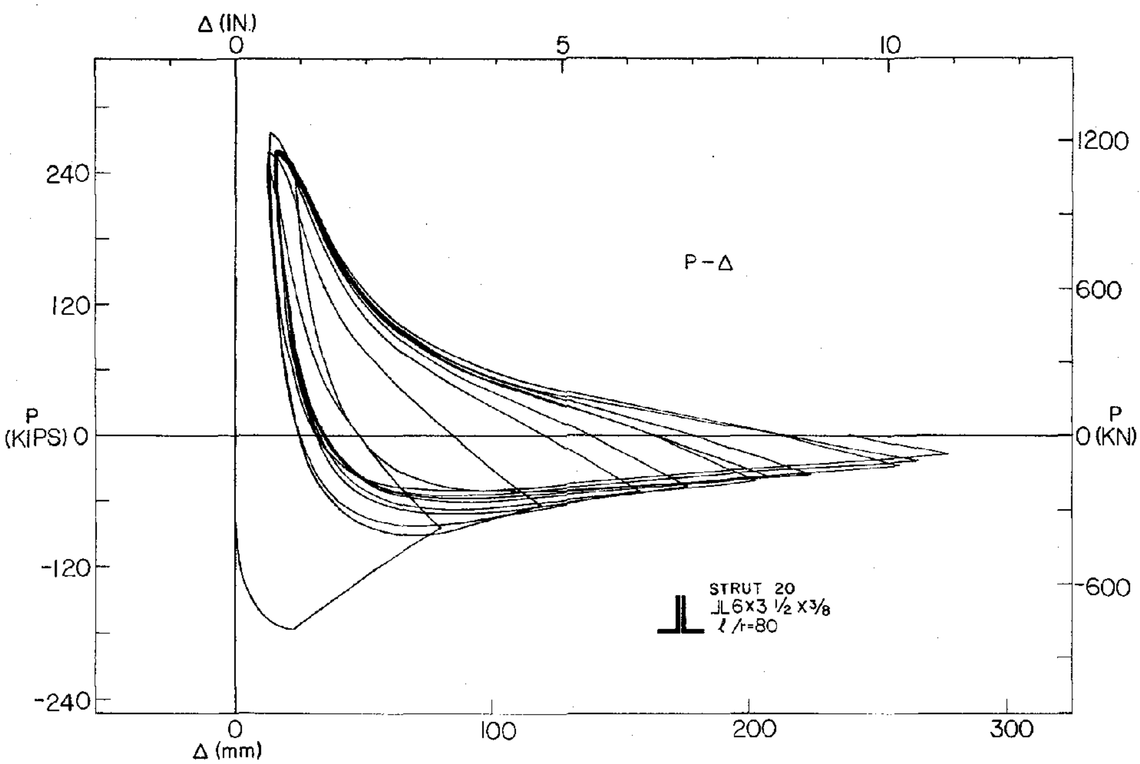

FIG. B25 P-δ AND P-Δ CURVES FOR STRUT 20

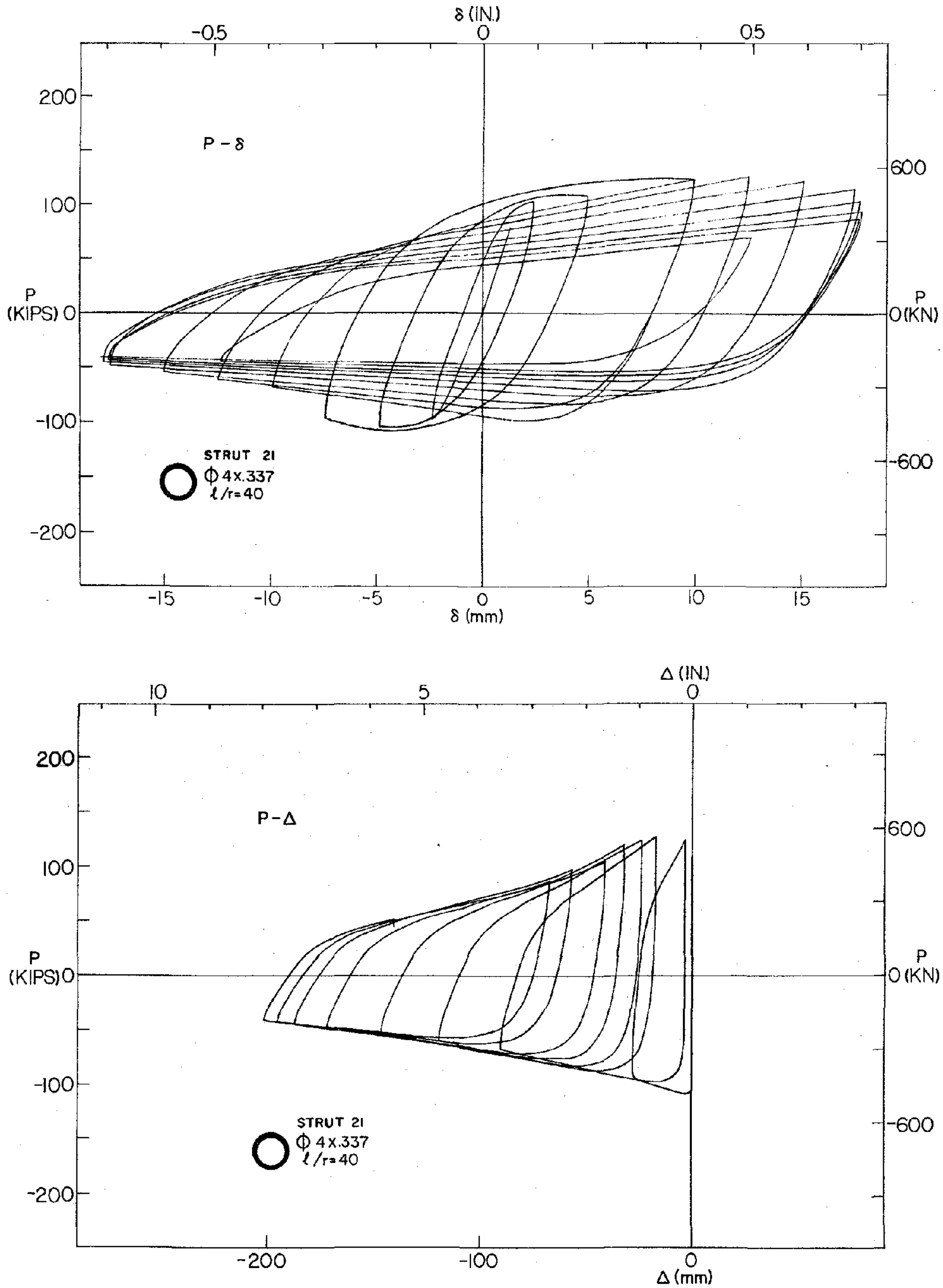

FIG. B26 P-δ AND P-Δ CURVES FOR STRUT 21

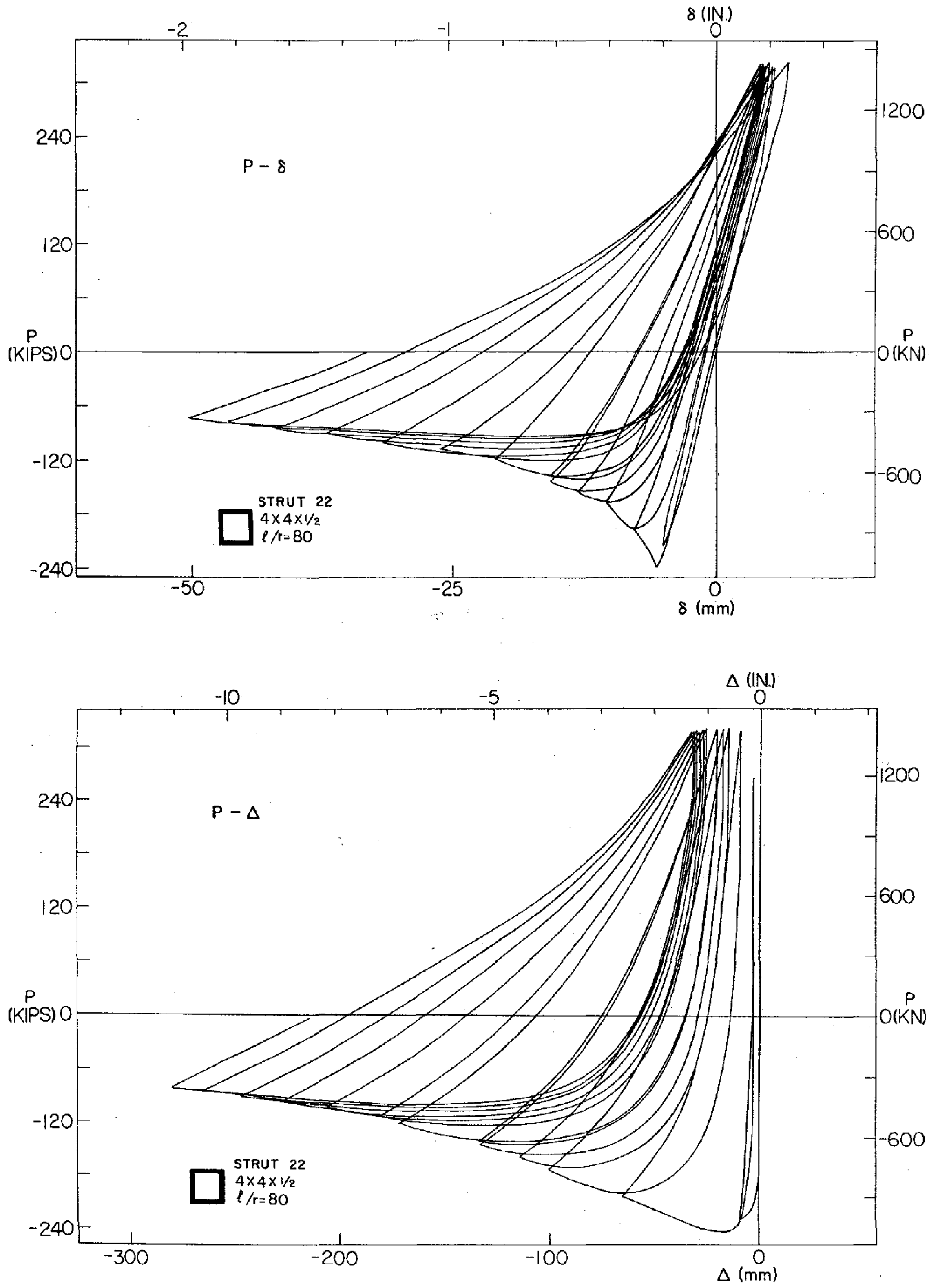

FIG. B27 P-δ AND P-Δ CURVES FOR STRUT 22

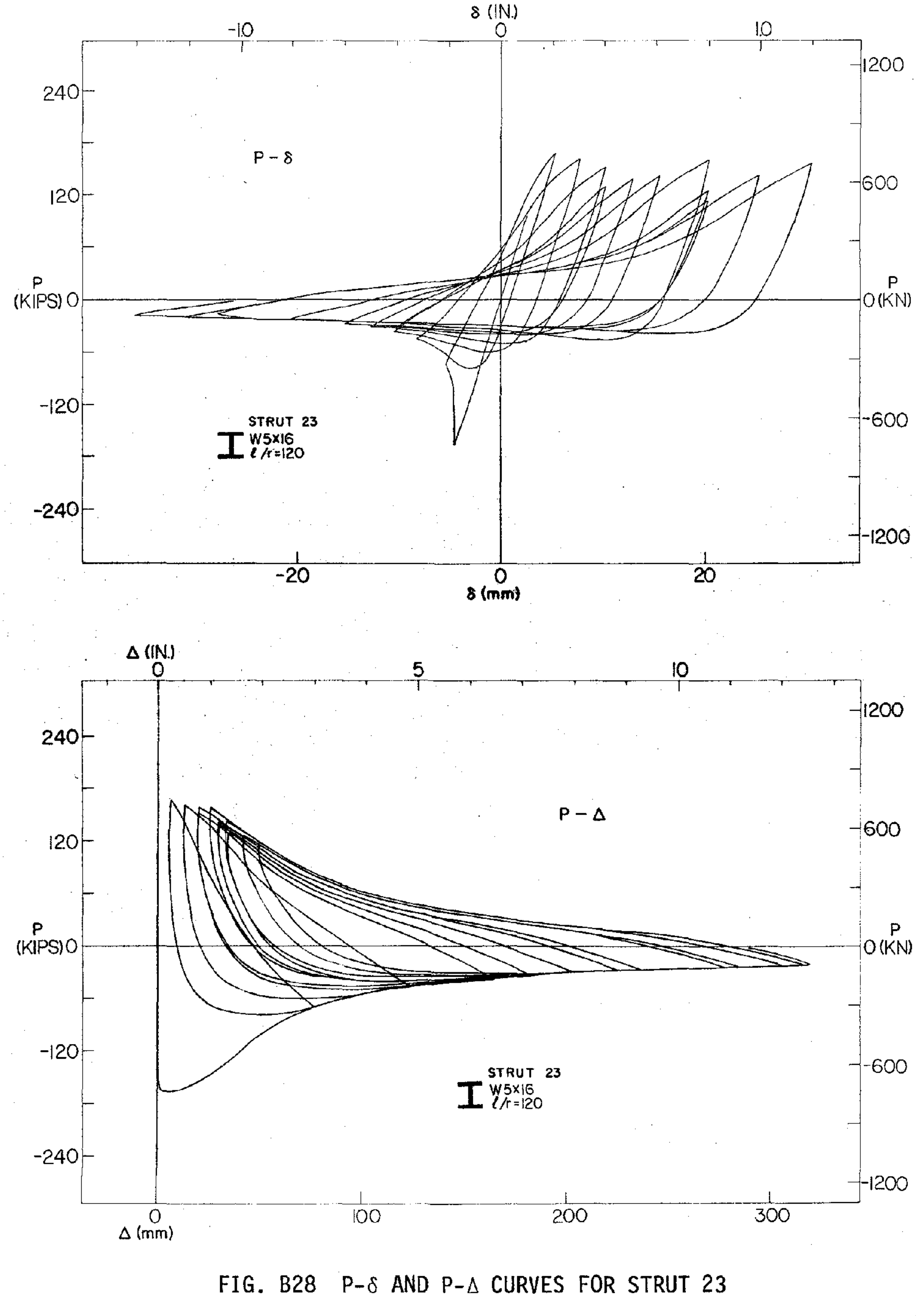

FIG. B28 P-δ AND P-Δ CURVES FOR STRUT 23

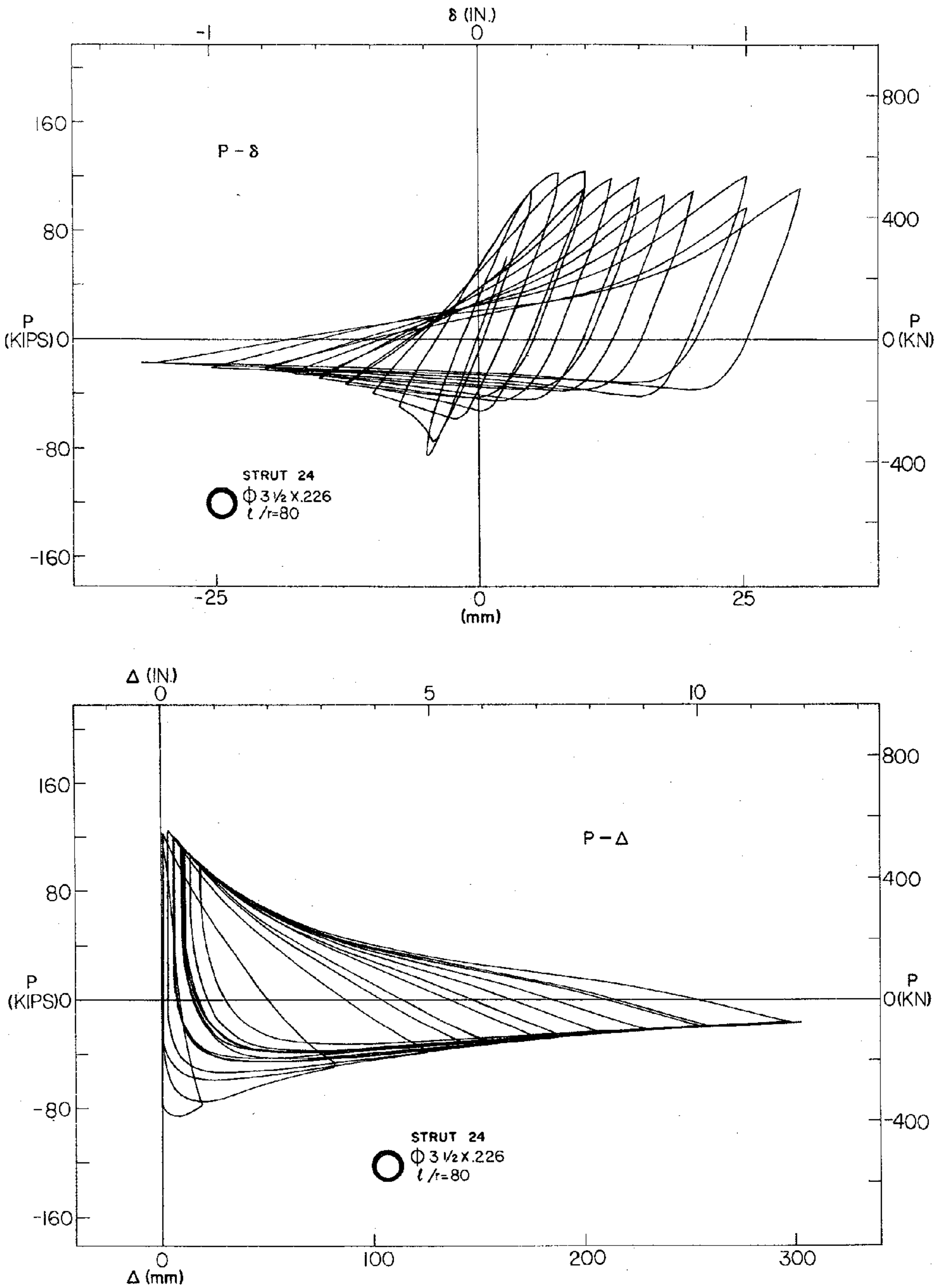

FIG. B29 P-δ AND P-Δ CURVES FOR STRUT 24

APPENDIX C

NORMALIZED HYSTERETIC CURVES

Normalized P-δ hysteretic curves for all but Strut 1 are given in this Appendix. The processed data have not been corrected in the manner discussed in Appendix B. Therefore, any effort to analytically mimic the vertical rises and drops at load reversal points is not warranted.

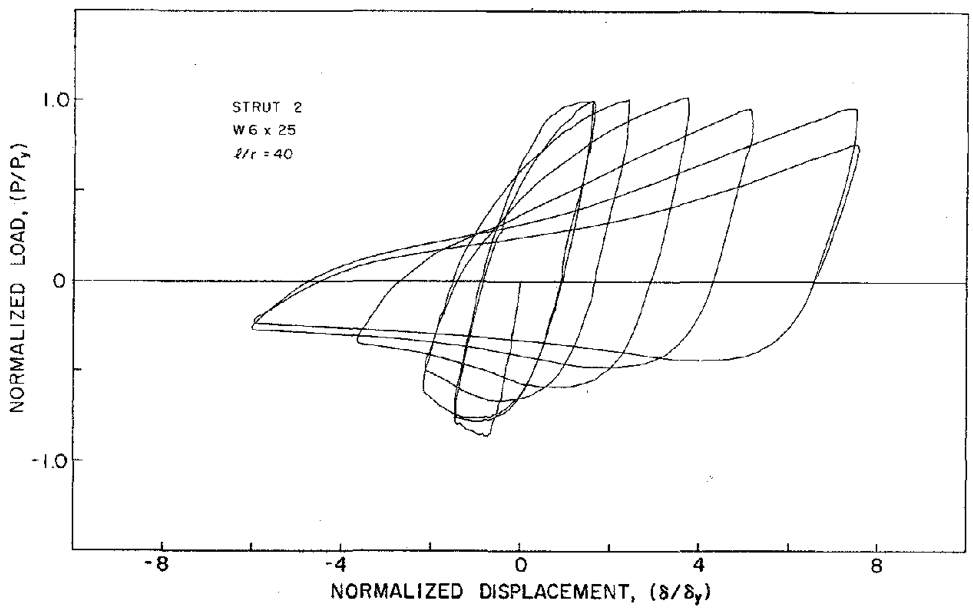

FIG. C1 NORMALIZED P-δ CURVES FOR STRUT 2

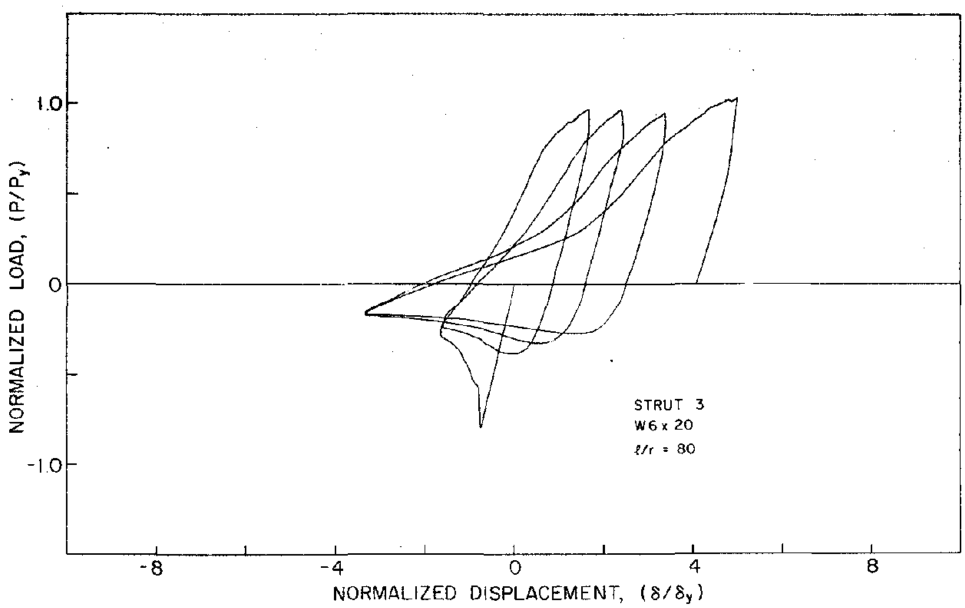

FIG. C2 NORMALIZED P-δ CURVES FOR STRUT 3

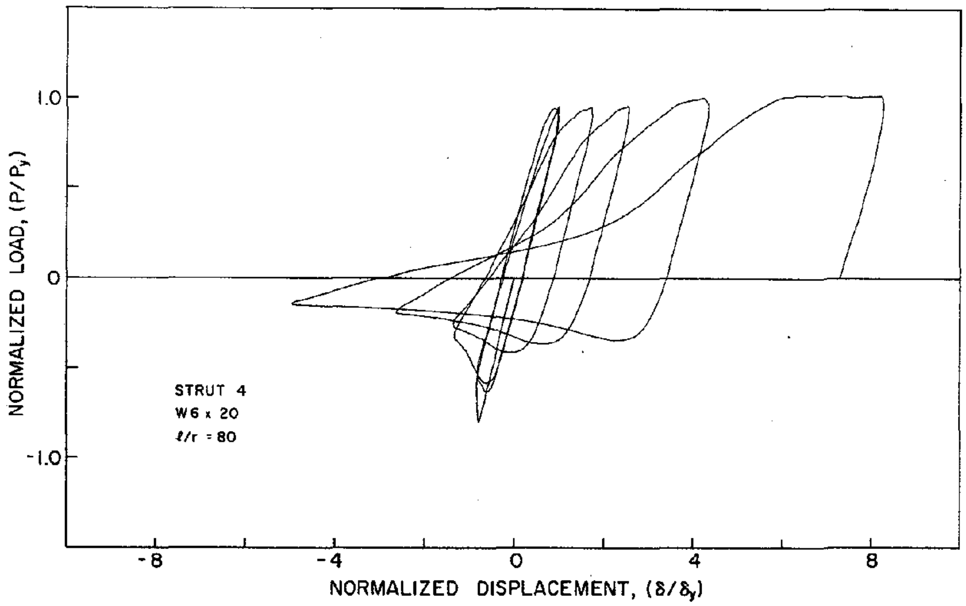

FIG. C3 NORMALIZED P-δ CURVES FOR STRUT 4

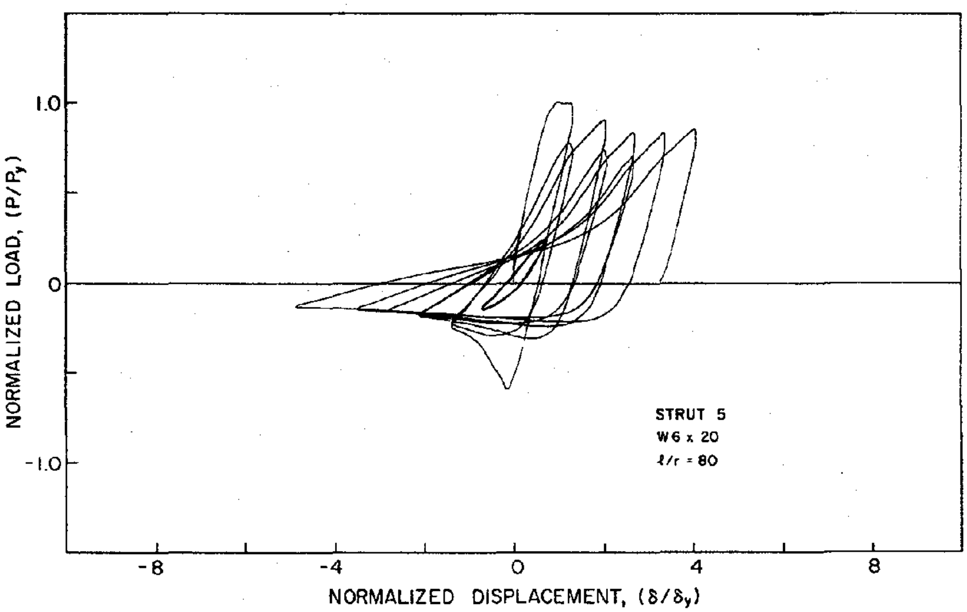

FIG. C4 NORMALIZED P-δ CURVES FOR STRUT 5

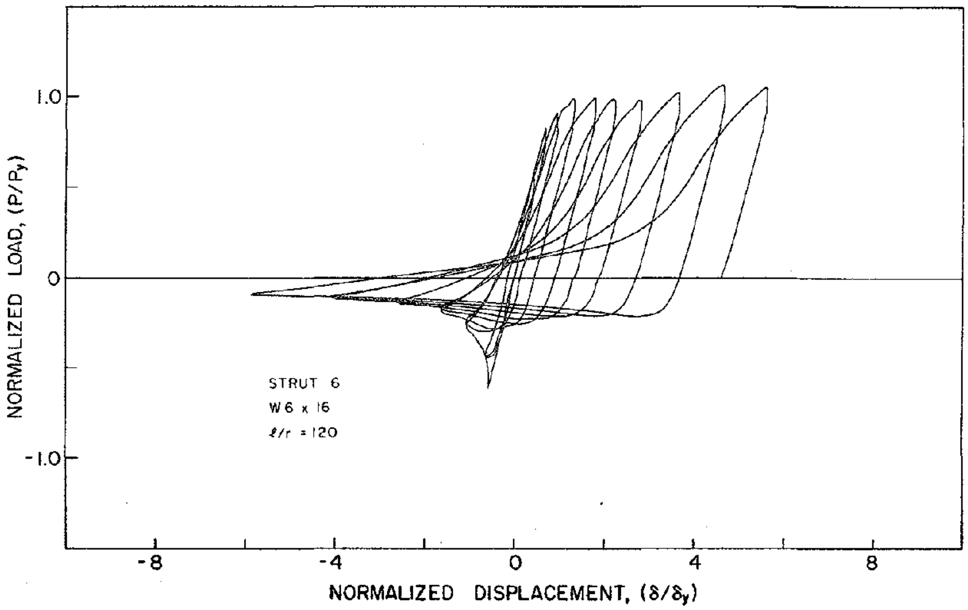

FIG. C5 NORMALIZED P-δ CURVES FOR STRUT 6

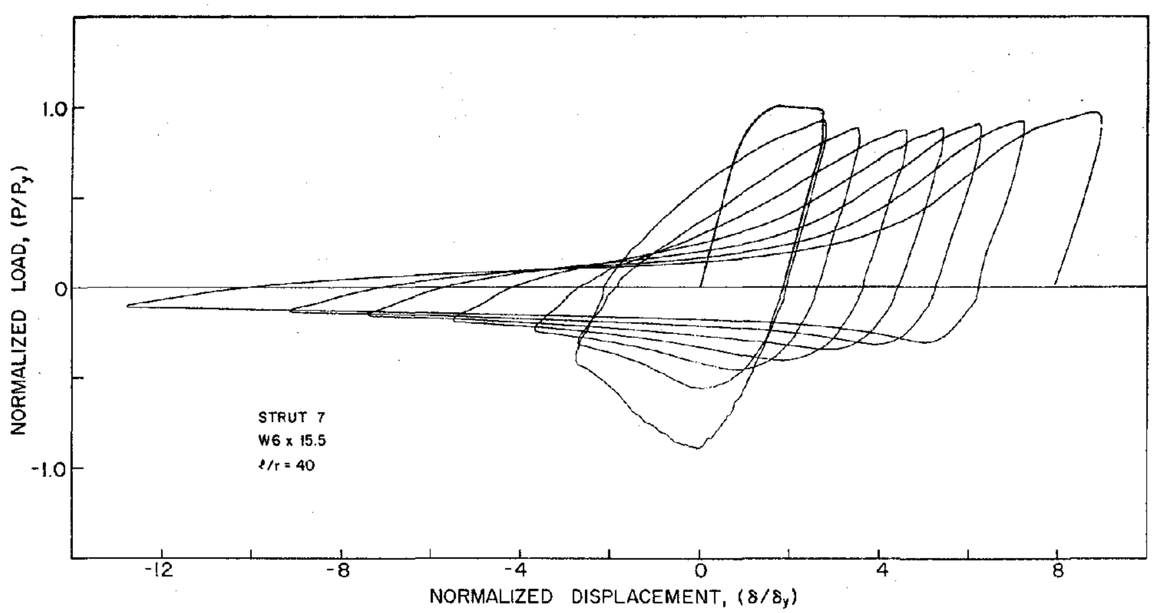

FIG. C6 NORMALIZED P-δ CURVES FOR STRUT 7

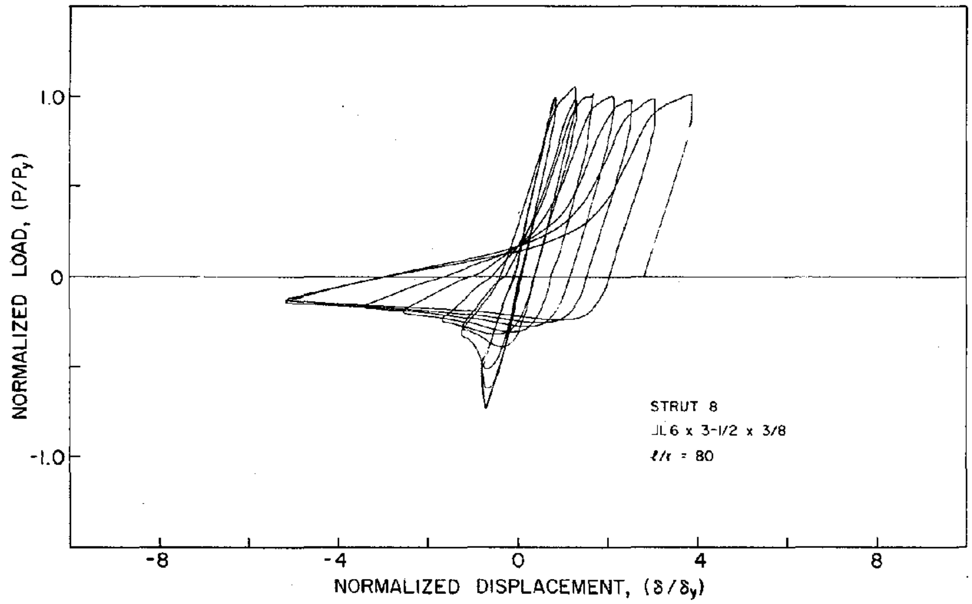

FIG. C7 NORMALIZED P-δ CURVES FOR STRUT 8

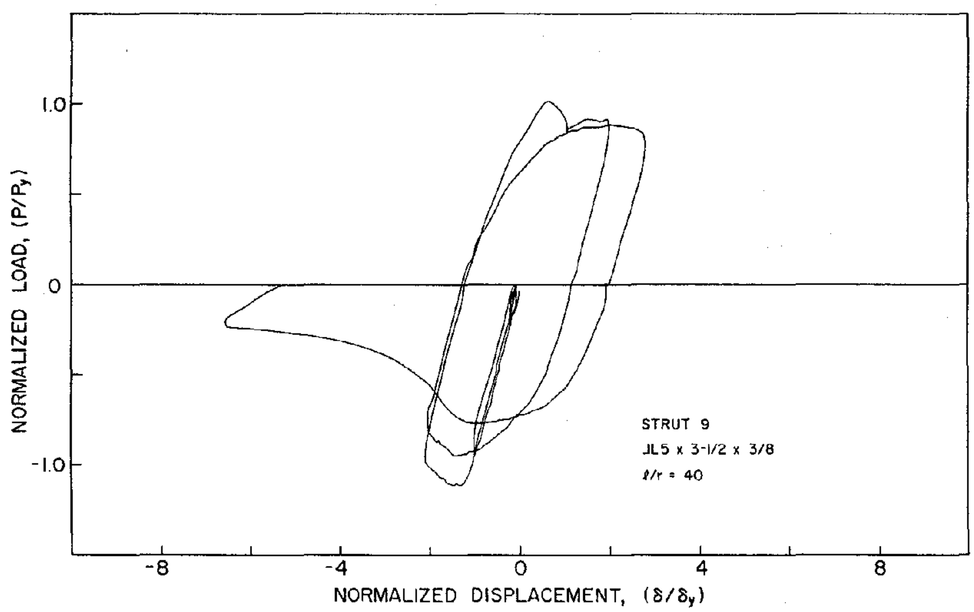

FIG. C8 NORMALIZED P-δ CURVES FOR STRUT 9

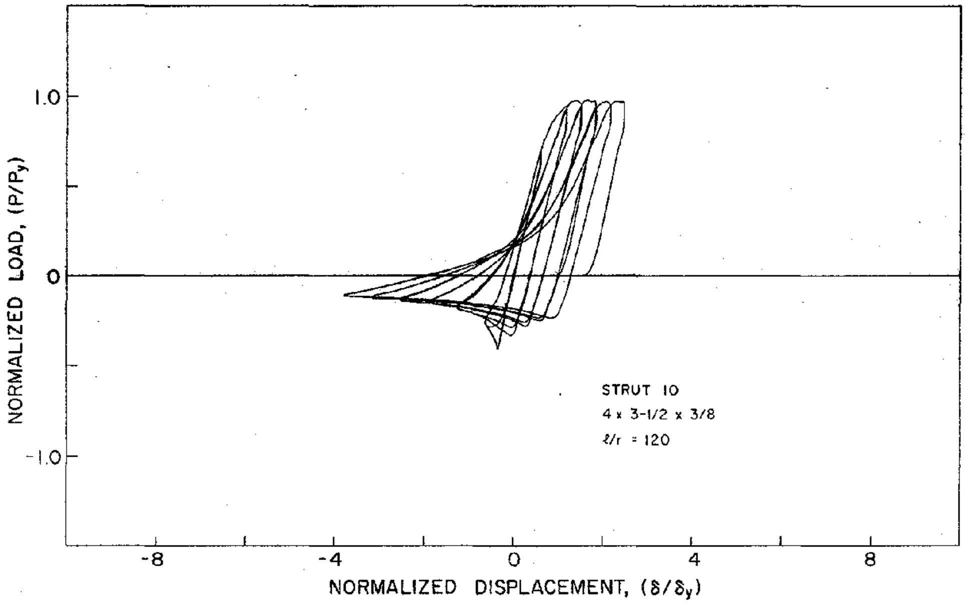

FIG. C9 NORMALIZED P-δ CURVES FOR STRUT 10

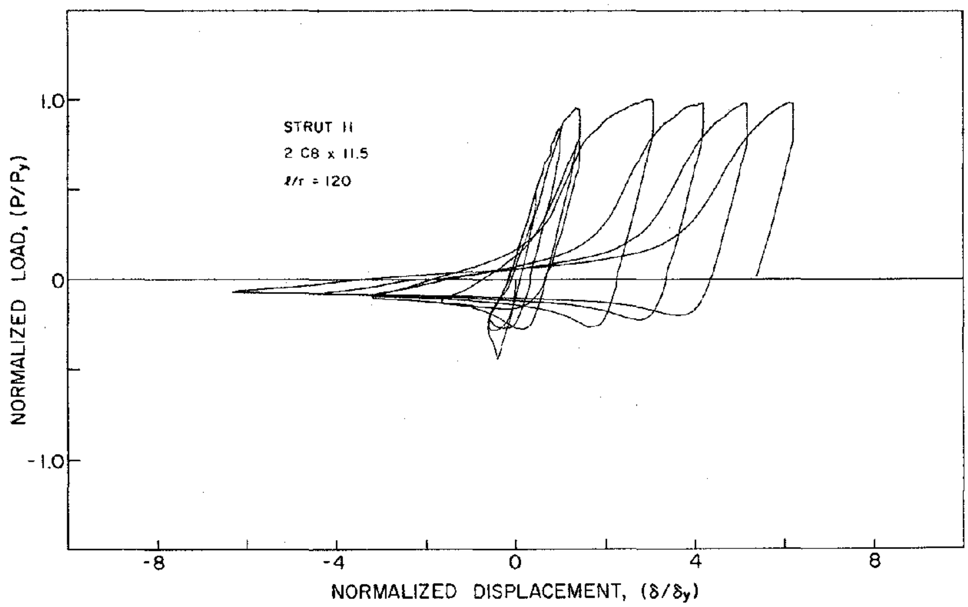

FIG. C10 NORMALIZED P-δ CURVES FOR STRUT 11

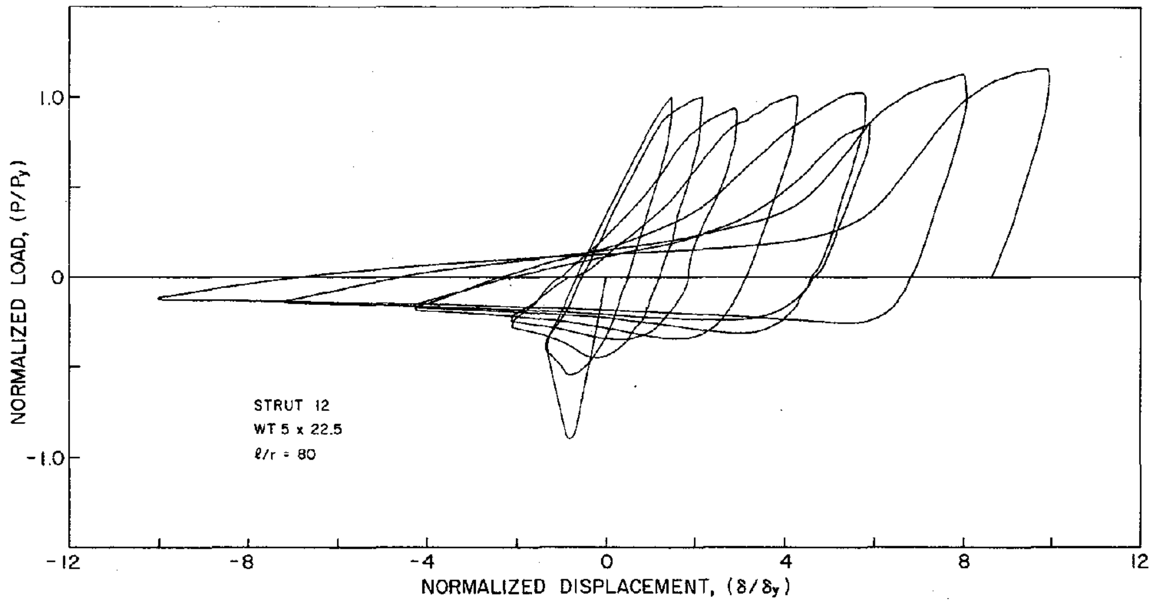

FIG. C11 NORMALIZED P-δ CURVES FOR STRUT 12

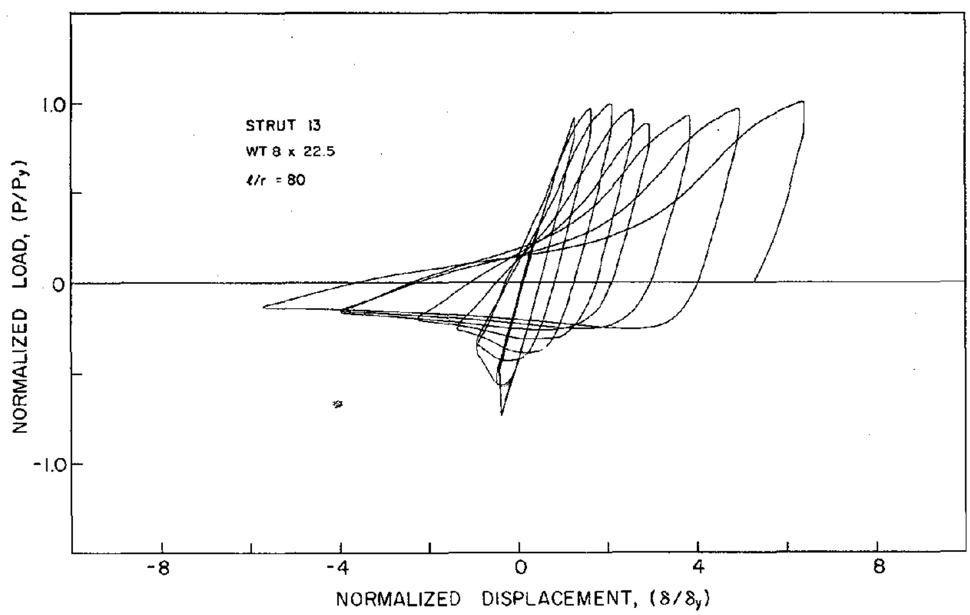

FIG. C12 NORMALIZED P-δ CURVES FOR STRUT 13

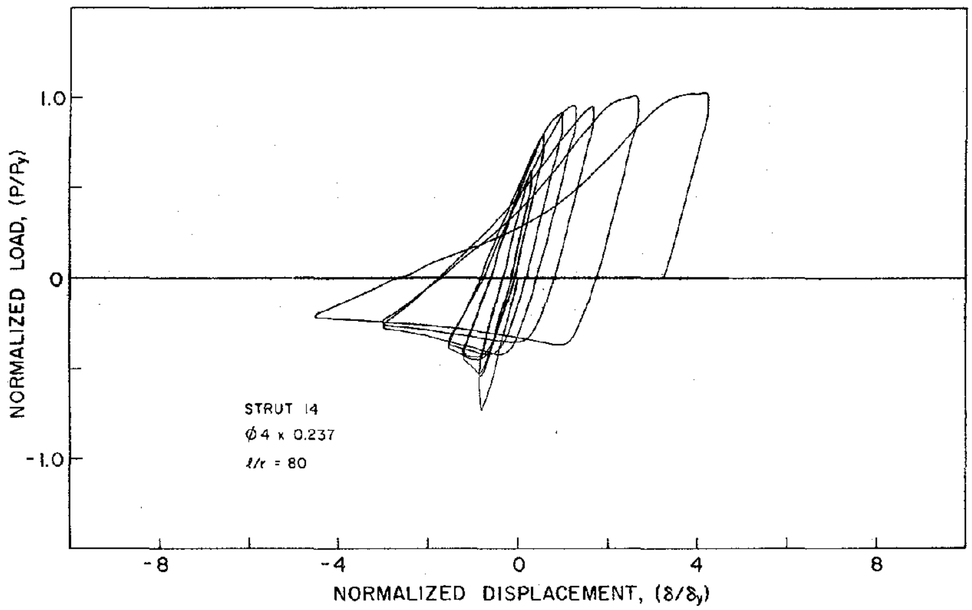

FIG. C13 NORMALIZED P-δ CURVES FOR STRUT 14

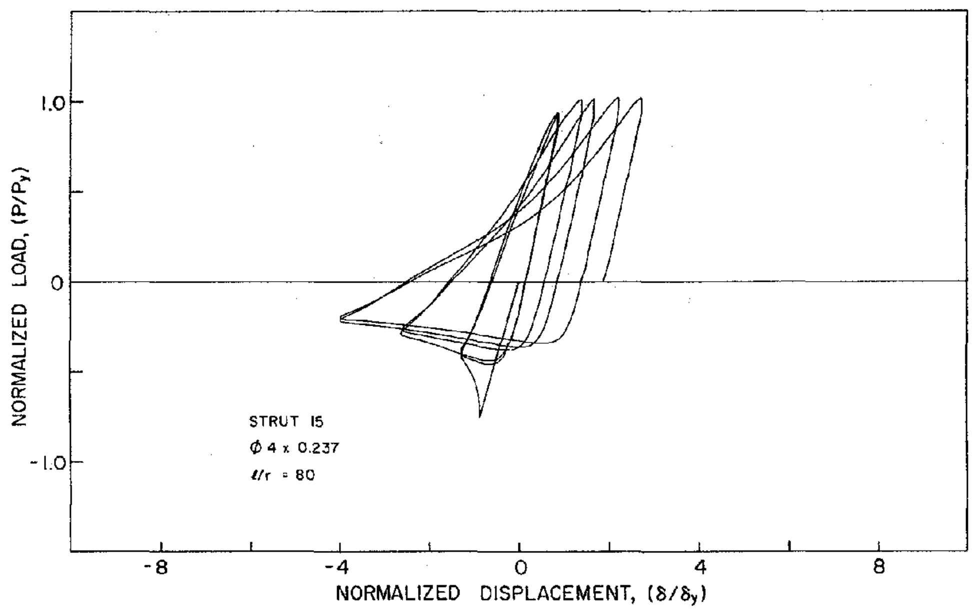

FIG. C14 NORMALIZED P-δ CURVES FOR STRUT 15

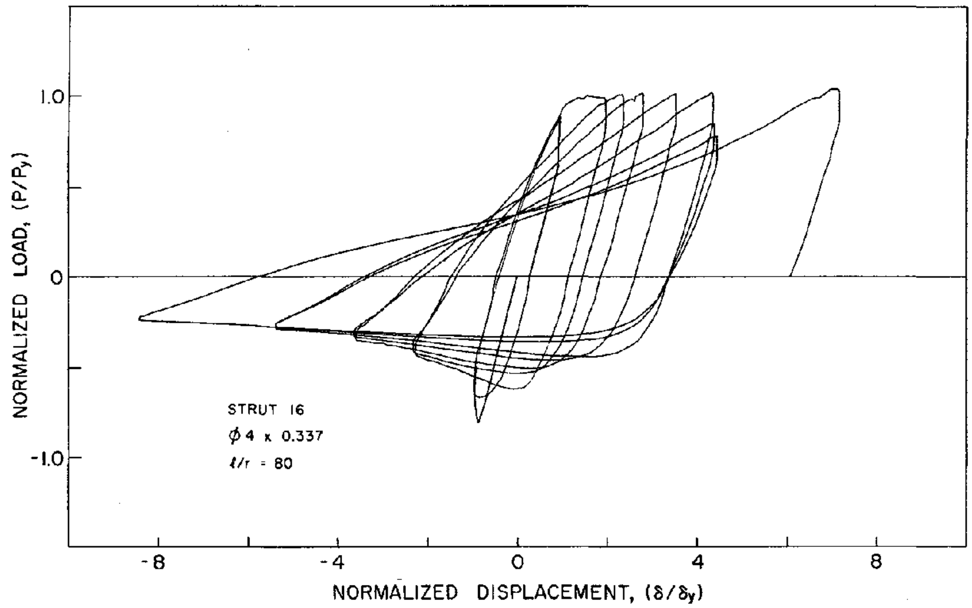

FIG. C15 NORMALIZED P-δ CURVES FOR STRUT 16

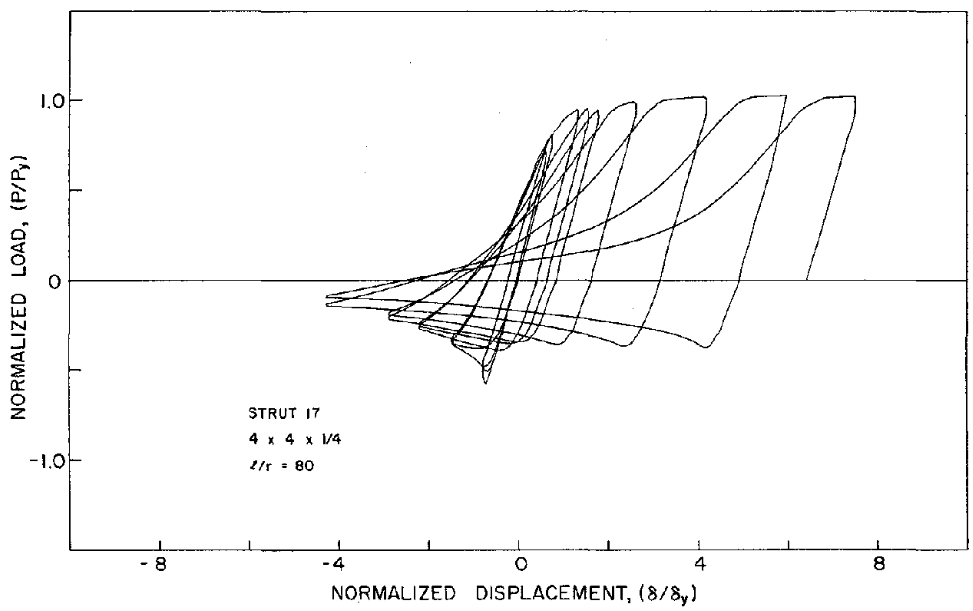

FIG. C16 NORMALIZED P-δ CURVES FOR STRUT 17

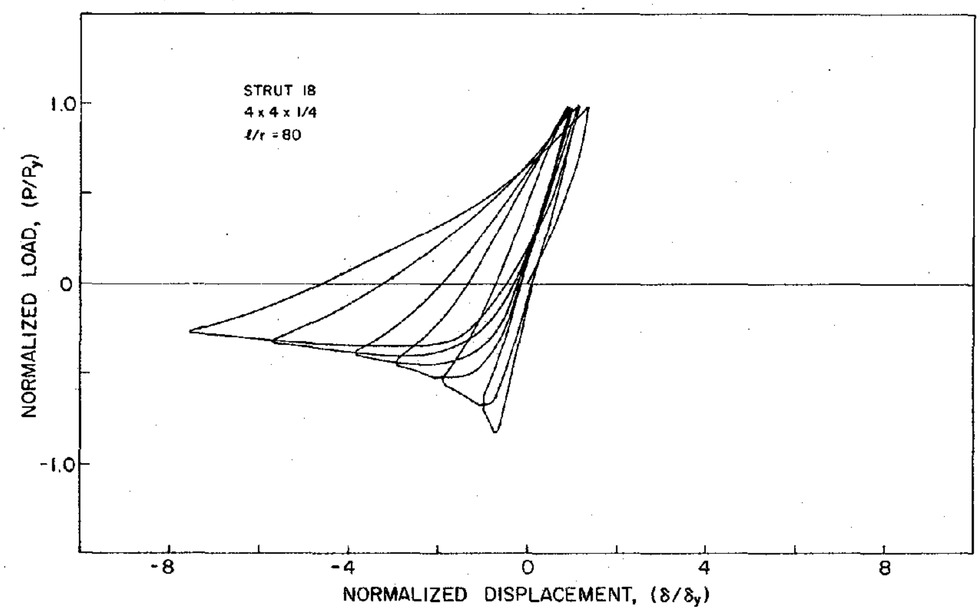

FIG. C17 NORMALIZED P-δ CURVES FOR STRUT 18

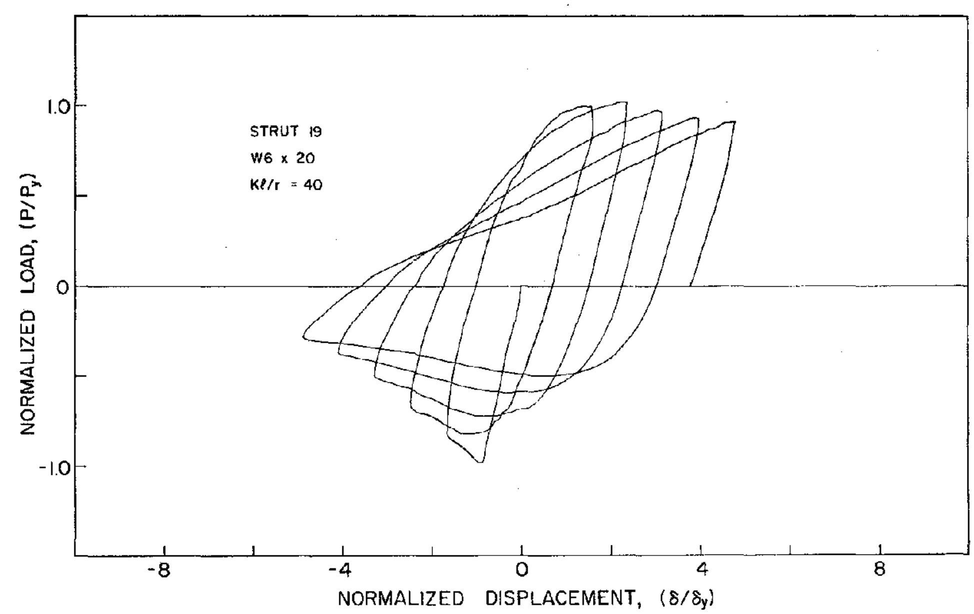

FIG. C18 NORMALIZED P-δ CURVES FOR STRUT 19

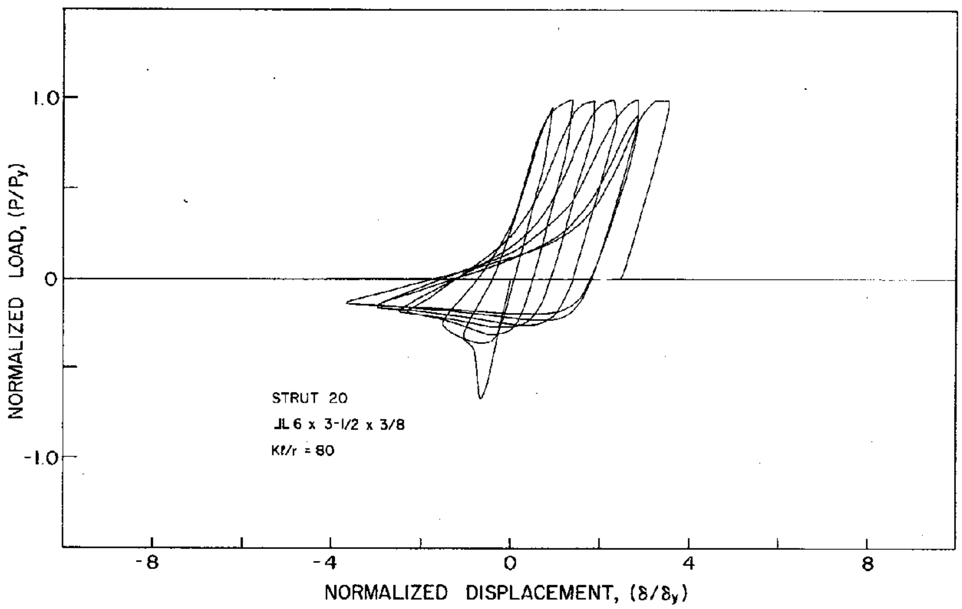

FIG. C19 NORMALIZED P-δ CURVES FOR STRUT 20

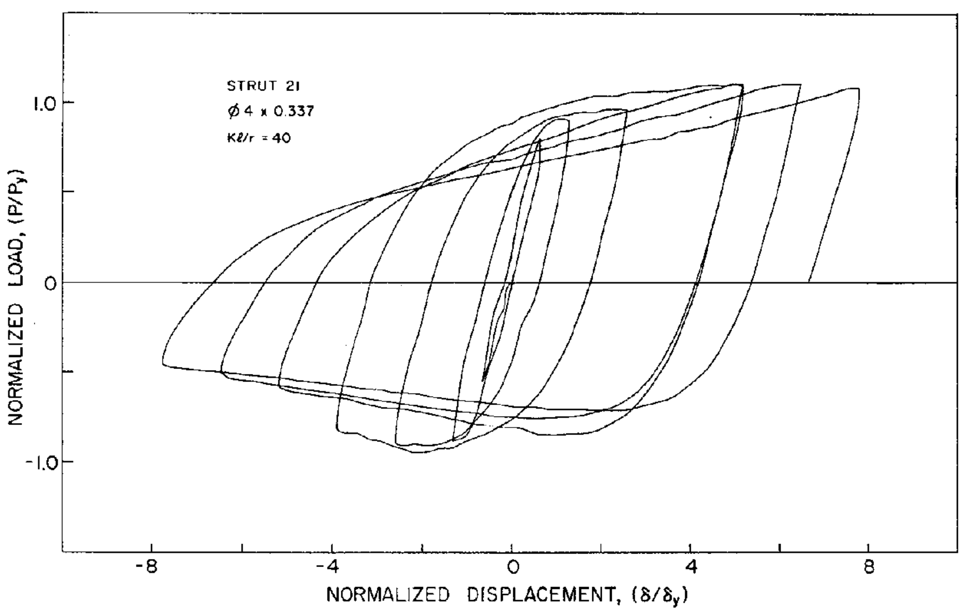

FIG. C20 NORMALIZED P-δ CURVES FOR STRUT 21

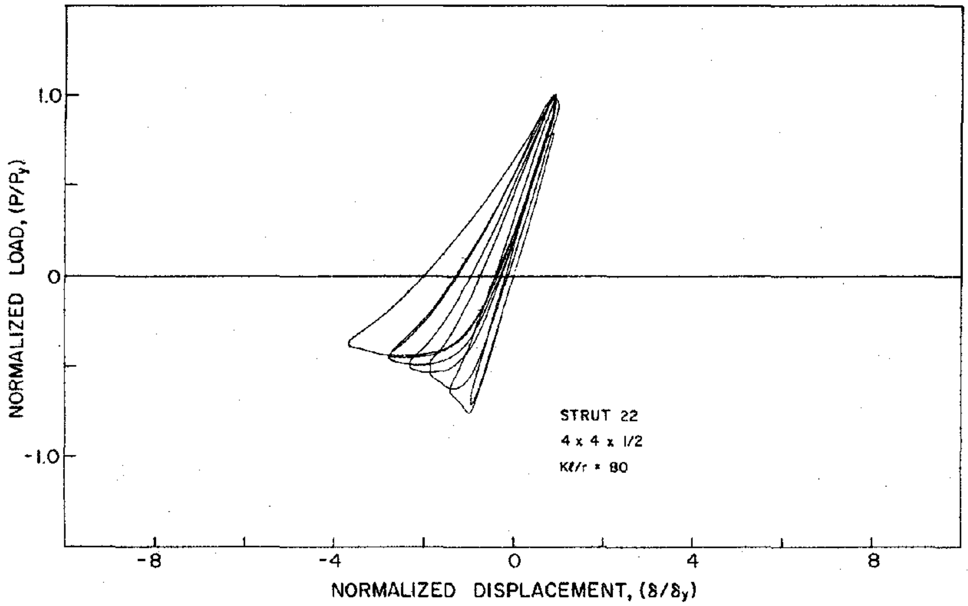

FIG. C21 NORMALIZED P-δ CURVES FOR STRUT 22

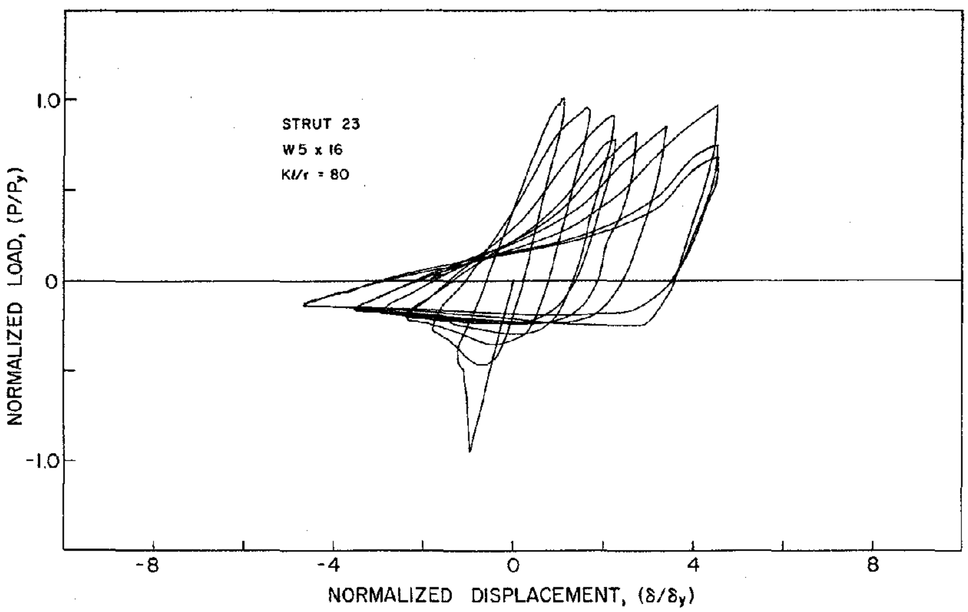

FIG. C22 NORMALIZED P-δ CURVES FOR STRUT 23

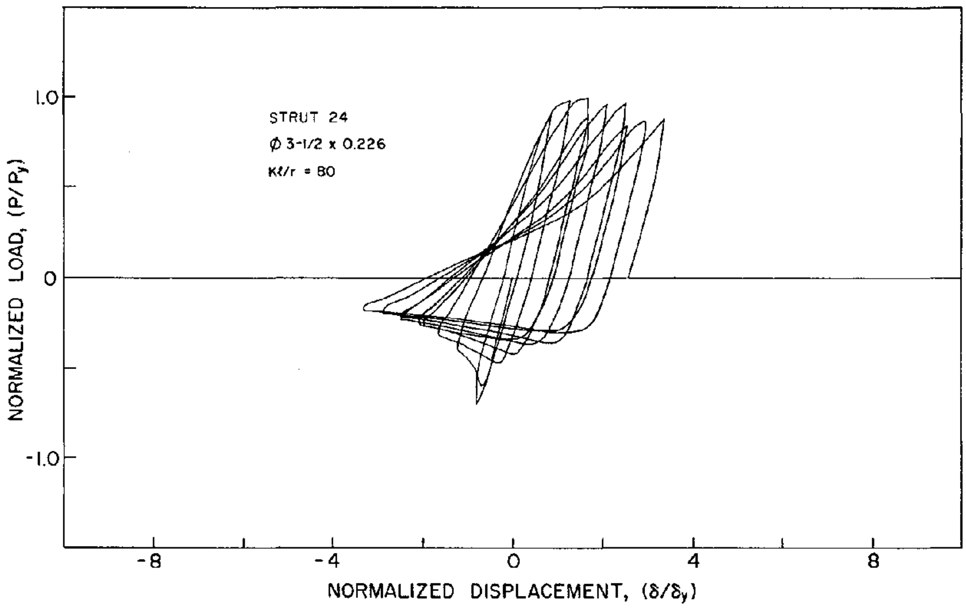

FIG. C23 NORMALIZED P-δ CURVES FOR STRUT 24

EARTHQUAKE ENGINEERING RESEARCH CENTER REPORTS

NOTE: Numbers in parenthesis are Accession Numbers assigned by the National Technical Information Service; these are followed by a price code. Copies of the reports may be ordered from the National Technical Information Service, 5285 Port Royal Road, Springfield, Virginia, 22161. Accession Numbers should be quoted on orders for reports (PB --- ---) and remittance must accompany each order. Reports without this information were not available at time of printing. Upon request, EERC will mail inquirers this information when it becomes available.

EERC 67-1 "Feasibility Study Large-Scale Earthquake Simulator Facility," by J. Penzien, J.G. Bouwkamp, R.W. Clough and D. Rea - 1967 (PB 187 905)A07

EERC 68-1 Unassigned

EERC 68-2 "Inelastic Behavior of Beam-to-Column Subassemblages Under Repeated Loading," by V.V. Bertero - 1968 (PB 184 888)A05

EERC 68-3 "A Graphical Method for Solving the Wave Reflection-Refraction Problem," by H.D. McNiven and Y. Mengi - 1968 (PB 187 943)A03

EERC 68-4 "Dynamic Properties of McKinley School Buildings," by D. Rea, J.G. Bouwkamp and R.W. Clough - 1968 (PB 187 902)A07

EERC 68-5 "Characteristics of Rock Motions During Earthquakes," by H.B. Seed, I.M. Idriss and F.W. Kiefer - 1968 (PB 188 338)A03

EERC 69-1 "Earthquake Engineering Research at Berkeley," - 1969 (PB 187 906)A11

EERC 69-2 "Nonlinear Seismic Response of Earth Structures," by M. Dibaj and J. Penzien - 1969 (PB 187 904)A08

EERC 69-3 "Probabilistic Study of the Behavior of Structures During Earthquakes," by R. Ruiz and J. Penzien - 1969 (PB 187 886)A06

EERC 69-4 "Numerical Solution of Boundary Value Problems in Structural Mechanics by Reduction to an Initial Value Formulation," by N. Distefano and J. Schujman - 1969 (PB 187 942)A02

EERC 69-5 "Dynamic Programming and the Solution of the Biharmonic Equation," by N. Distefano - 1969 (PB 187 941)A03

EERC 69-6 "Stochastic Analysis of Offshore Tower Structures," by A.K. Malhotra and J. Penzien - 1969 (PB 187 903)A09

EERC 69-7 "Rock Motion Accelerograms for High Magnitude Earthquakes," by H.B. Seed and I.M. Idriss - 1969 (PB 187 940)A02

EERC 69-8 "Structural Dynamics Testing Facilities at the University of California, Berkeley," by R.M. Stephen, J.G. Bouwkamp, R.W. Clough and J. Penzien - 1969 (PB 189 111)A04

EERC 69-9 "Seismic Response of Soil Deposits Underlain by Sloping Rock Boundaries," by H. Dezfulian and H.B. Seed 1969 (PB 189 114)A03

EERC 69-10 "Dynamic Stress Analysis of Axisymmetric Structures Under Arbitrary Loading," by S. Ghosh and E.L. Wilson 1969 (PB 189 026)A10

EERC 69-11 "Seismic Behavior of Multistory Frames Designed by Different Philosophies," by J.C. Anderson and V. V. Bertero - 1969 (PB 190 662)A10

EERC 69-12 "Stiffness Degradation of Reinforcing Concrete Members Subjected to Cyclic Flexural Moments," by V.V. Bertero, B. Bresler and H. Ming Liao - 1969 (PB 202 942)A07

EERC 69-13 "Response of Non-Uniform Soil Deposits to Travelling Seismic Waves," by H. Dezfulian and H.B. Seed - 1969 (PB 191 023)A03

EERC 69-14 "Damping Capacity of a Model Steel Structure," by D. Rea, R.W. Clough and J.G. Bouwkamp - 1969 (PB 190 663)A06

EERC 69-15 "Influence of Local Soil Conditions on Building Damage Potential during Earthquakes," by H.B. Seed and I.M. Idriss - 1969 (PB 191 036)A03

EERC 69-16 "The Behavior of Sands Under Seismic Loading Conditions," by M.L. Silver and H.B. Seed - 1969 (AD 714 982)A07

EERC 70-1 "Earthquake Response of Gravity Dams," by A.K. Chopra - 1970 (AD 709 640)A03

EERC 70-2 "Relationships between Soil Conditions and Building Damage in the Caracas Earthquake of July 29, 1967," by H.B. Seed, I.M. Idriss and H. Dezfulian - 1970 (PB 195 762)A05

EERC 70-3 "Cyclic Loading of Full Size Steel Connections," by E.P. Popov and R.M. Stephen - 1970 (PB 213 545)A04

EERC 70-4 "Seismic Analysis of the Charaima Building, Caraballeda, Venezuela," by Subcommittee of the SEAONC Research Committee: V.V. Bertero, P.F. Fratessa, S.A. Mahin, J.H. Sexton, A.C. Scordelis, E.L. Wilson, L.A. Wyllie, H.B. Seed and J. Penzien, Chairman - 1970 (PB 201 455)A06

EERC 70-5 "A Computer Program for Earthquake Analysis of Dams," by A.K. Chopra and P. Chakrabarti - 1970 (AD 723 994)A05

EERC 70-6 "The Propagation of Love Waves Across Non-Horizontally Layered Structures," by J. Lysmer and L.A. Drake 1970 (PB 197 896)A03

EERC 70-7 "Influence of Base Rock Characteristics on Ground Response," by J. Lysmer, H.B. Seed and P.B. Schnabel 1970 (PB 197 897)A03

EERC 70-8 "Applicability of Laboratory Test Procedures for Measuring Soil Liquefaction Characteristics under Cyclic Loading," by H.B. Seed and W.H. Peacock - 1970 (PB 198 016)A03

EERC 70-9 "A Simplified Procedure for Evaluating Soil Liquefaction Potential," by H.B. Seed and I.M. Idriss - 1970 (PB 198 009)A03

EERC 70-10 "Soil Moduli and Damping Factors for Dynamic Response Analysis," by H.B. Seed and I.M. Idriss - 1970 (PB 197 869)A03

EERC 71-1 "Koyna Earthquake of December 11, 1967 and the Performance of Koyna Dam," by A.K. Chopra and P. Chakrabarti 1971 (AD 731 496)A06

EERC 71-2 "Preliminary In-Situ Measurements of Anelastic Absorption in Soils Using a Prototype Earthquake Simulator," by R.D. Borcherdt and P.W. Rodgers - 1971 (PB 201 454)A03

EERC 71-3 "Static and Dynamic Analysis of Inelastic Frame Structures," by F.L. Porter and G.H. Powell - 1971 (PB 210 135)A06

EERC 71-4 "Research Needs in Limit Design of Reinforced Concrete Structures," by V.V. Bertero - 1971 (PB 202 943)A04

EERC 71-5 "Dynamic Behavior of a High-Rise Diagonally Braced Steel Building," by D. Rea, A.A. Shah and J.G. Bouwkamp 1971 (PB 203 584)A06

EERC 71-6 "Dynamic Stress Analysis of Porous Elastic Solids Saturated with Compressible Fluids," by J. Ghaboussi and E. L. Wilson - 1971 (PB 211 396)A06

EERC 71-7 "Inelastic Behavior of Steel Beam-to-Column Subassemblages," by H. Krawinkler, V.V. Bertero and E.P. Popov 1971 (PB 211 335)A14

EERC 71-8 "Modification of Seismograph Records for Effects of Local Soil Conditions," by P. Schnabel, H.B. Seed and J. Lysmer - 1971 (PB 214 450)A03

EERC 72-1 "Static and Earthquake Analysis of Three Dimensional Frame and Shear Wall Buildings," by E.L. Wilson and H.H. Dovey - 1972 (PB 212 904)A05

EERC 72-2 "Accelerations in Rock for Earthquakes in the Western United States," by P.B. Schnabel and H.B. Seed - 1972 (PB 213 100)A03

EERC 72-3 "Elastic-Plastic Earthquake Response of Soil-Building Systems," by T. Minami - 1972 (PB 214 868)A08

EERC 72-4 "Stochastic Inelastic Response of Offshore Towers to Strong Motion Earthquakes," by M.K. Kaul - 1972 (PB 215 713)A05

EERC 72-5 "Cyclic Behavior of Three Reinforced Concrete Flexural Members with High Shear," by E.P. Popov, V.V. Bertero and H. Krawinkler - 1972 (PB 214 555)A05

EERC 72-6 "Earthquake Response of Gravity Dams Including Reservoir Interaction Effects," by P. Chakrabarti and A.K. Chopra - 1972 (AD 762 330)A08

EERC 72-7 "Dynamic Properties of Pine Flat Dam," by D. Rea, C.Y. Liaw and A.K. Chopra - 1972 (AD 763 928)A05

EERC 72-8 "Three Dimensional Analysis of Building Systems," by E.L. Wilson and H.H. Dovey - 1972 (PB 222 438)A06

EERC 72-9 "Rate of Loading Effects on Uncracked and Repaired Reinforced Concrete Members," by S. Mahin, V.V. Bertero, D. Rea and M. Atalay - 1972 (PB 224 520)A08

EERC 72-10 "Computer Program for Static and Dynamic Analysis of Linear Structural Systems," by E.L. Wilson, K.-J. Bathe, J.E. Peterson and H.H.Dovey - 1972 (PB 220 437)A04

EERC 72-11 "Literature Survey - Seismic Effects on Highway Bridges," by T. Iwasaki, J. Penzien and R.W. Clough - 1972 (PB 215 613)A19

EERC 72-12 "SHAKE-A Computer Program for Earthquake Response Analysis of Horizontally Layered Sites," by P.B. Schnabel and J. Lysmer - 1972 (PB 220 207)A06

EERC 73-1 "Optimal Seismic Design of Multistory Frames," by V.V. Bertero and H. Kamil - 1973

EERC 73-2 "Analysis of the Slides in the San Fernando Dams During the Earthquake of February 9, 1971," by H.B. Seed, K.L. Lee, I.M. Idriss and F. Makdisi - 1973 (PB 223 402)A14

EERC 73-3 "Computer Aided Ultimate Load Design of Unbraced Multistory Steel Frames," by M.B. El-Hafez and G.H. Powell 1973 (PB 248 315)A09

EERC 73-4 "Experimental Investigation into the Seismic Behavior of Critical Regions of Reinforced Concrete Components as Influenced by Moment and Shear," by M. Celebi and J. Penzien - 1973 (PB 215 884)A09

EERC 73-5 "Hysteretic Behavior of Epoxy-Repaired Reinforced Concrete Beams," by M. Celebi and J. Penzien - 1973 (PB 239 568)A03

EERC 73-6 "General Purpose Computer Program for Inelastic Dynamic Response of Plane Structures," by A. Kanaan and G.H. Powell - 1973 (PB 221 260)A08

EERC 73-7 "A Computer Program for Earthquake Analysis of Gravity Dams Including Reservoir Interaction," by P. Chakrabarti and A.K. Chopra - 1973 (AD 766 271)A04

EERC 73-8 "Behavior of Reinforced Concrete Deep Beam-Column Subassemblages Under Cyclic Loads," by O. Küstü and J.G. Bouwkamp - 1973 (PB 246 117)A12

EERC 73-9 "Earthquake Analysis of Structure-Foundation Systems," by A.K. Vaish and A.K. Chopra - 1973 (AD 766 272)A07

EERC 73-10 "Deconvolution of Seismic Response for Linear Systems," by R.B. Reimer - 1973 (PB 227 179)A08

EERC 73-11 "SAP IV: A Structural Analysis Program for Static and Dynamic Response of Linear Systems," by K.-J. Bathe, E.L. Wilson and F.E. Peterson - 1973 (PB 221 967)A09

EERC 73-12 "Analytical Investigations of the Seismic Response of Long, Multiple Span Highway Bridges," by W.S. Tseng and J. Penzien - 1973 (PB 227 816)A10

EERC 73-13 "Earthquake Analysis of Multi-Story Buildings Including Foundation Interaction," by A.K. Chopra and J.A. Gutierrez - 1973 (PB 222 970)A03

EERC 73-14 "ADAP: A Computer Program for Static and Dynamic Analysis of Arch Dams," by R.W. Clough, J.M. Raphael and S. Mojtahedi - 1973 (PB 223 763)A09

EERC 73-15 "Cyclic Plastic Analysis of Structural Steel Joints," by R.B. Pinkney and R.W. Clough - 1973 (PB 226 843)A08

EERC 73-16 "QUAD-4: A Computer Program for Evaluating the Seismic Response of Soil Structures by Variable Damping Finite Element Procedures," by I.M. Idriss, J. Lysmer, R. Hwang and H.B. Seed - 1973 (PB 229 424)A05

EERC 73-17 "Dynamic Behavior of a Multi-Story Pyramid Shaped Building," by R.M. Stephen, J.P. Hollings and J.G. Bouwkamp - 1973 (PB 240 718)A06

EERC 73-18 "Effect of Different Types of Reinforcing on Seismic Behavior of Short Concrete Columns," by V.V. Bertero, J. Hollings, O. Küstü, R.M. Stephen and J.G. Bouwkamp - 1973

EERC 73-19 "Olive View Medical Center Materials Studies, Phase I," by B. Bresler and V.V. Bertero - 1973 (PB 235 986)A06

EERC 73-20 "Linear and Nonlinear Seismic Analysis Computer Programs for Long Multiple-Span Highway Bridges," by W.S. Tseng and J. Penzien - 1973

EERC 73-21 "Constitutive Models for Cyclic Plastic Deformation of Engineering Materials," by J.M. Kelly and P.P. Gillis 1973 (PB 226 024)A03

EERC 73-22 "DRAIN - 2D User's Guide," by G.H. Powell - 1973 (PB 227 016)A05

EERC 73-23 "Earthquake Engineering at Berkeley - 1973," (PB 226 033)A11

EERC 73-24 Unassigned

EERC 73-25 "Earthquake Response of Axisymmetric Tower Structures Surrounded by Water," by C.Y. Liaw and A.K. Chopra 1973 (AD 773 052)A09

EERC 73-26 "Investigation of the Failures of the Olive View Stairtowers During the San Fernando Earthquake and Their Implications on Seismic Design," by V.V. Bertero and R.G. Collins - 1973 (PB 235 106)A13

EERC 73-27 "Further Studies on Seismic Behavior of Steel Beam-Column Subassemblages," by V.V. Bertero, H. Krawinkler and E.P. Popov - 1973 (PB 234 172)A06

EERC 74-1 "Seismic Risk Analysis," by C.S. Oliveira - 1974 (PB 235 920)A06

EERC 74-2 "Settlement and Liquefaction of Sands Under Multi-Directional Shaking," by R. Pyke, C.K. Chan and H.B. Seed 1974

EERC 74-3 "Optimum Design of Earthquake Resistant Shear Buildings," by D. Ray, K.S. Pister and A.K. Chopra - 1974 (PB 231 172)A06

EERC 74-4 "LUSH - A Computer Program for Complex Response Analysis of Soil-Structure Systems," by J. Lysmer, T. Udaka, H.B. Seed and R. Hwang - 1974 (PB 236 796)A05

EERC 74-5 "Sensitivity Analysis for Hysteretic Dynamic Systems: Applications to Earthquake Engineering," by D. Ray 1974 (PB 233 213)A06

EERC 74-6 "Soil Structure Interaction Analyses for Evaluating Seismic Response," by H.B. Seed, J. Lysmer and R. Hwang 1974 (PB 236 519)A04

EERC 74-7 Unassigned

EERC 74-8 "Shaking Table Tests of a Steel Frame - A Progress Report," by R.W. Clough and D. Tang - 1974 (PB 240 869)A03

EERC 74-9 "Hysteretic Behavior of Reinforced Concrete Flexural Members with Special Web Reinforcement," by V.V. Bertero, E.P. Popov and T.Y. Wang - 1974 (PB 236 797)A07

EERC 74-10 "Applications of Reliability-Based, Global Cost Optimization to Design of Earthquake Resistant Structures," by E. Vitiello and K.S. Pister - 1974 (PB 237 231)A06

EERC 74-11 "Liquefaction of Gravelly Soils Under Cyclic Loading Conditions," by R.T. Wong, H.B. Seed and C.K. Chan 1974 (PB 242 042)A03

EERC 74-12 "Site-Dependent Spectra for Earthquake-Resistant Design," by H.B. Seed, C. Ugas and J. Lysmer - 1974 (PB 240 953)A03

EERC 74-13 "Earthquake Simulator Study of a Reinforced Concrete Frame," by P. Hidalgo and R.W. Clough - 1974 (PB 241 944)A13

EERC 74-14 "Nonlinear Earthquake Response of Concrete Gravity Dams," by N. Pal - 1974 (AD/A 006 583)A06

EERC 74-15 "Modeling and Identification in Nonlinear Structural Dynamics - I. One Degree of Freedom Models," by N. Distefano and A. Rath - 1974 (PB 241 548)A06

EERC 75-1 "Determination of Seismic Design Criteria for the Dumbarton Bridge Replacement Structure, Vol. I: Description, Theory and Analytical Modeling of Bridge and Parameters," by F. Baron and S.-H. Pang - 1975 (PB 259 407)A15

EERC 75-2 "Determination of Seismic Design Criteria for the Dumbarton Bridge Replacement Structure, Vol. II: Numerical Studies and Establishment of Seismic Design Criteria," by F. Baron and S.-H. Pang - 1975 (PB 259 408)A11 (For set of EERC 75-1 and 75-2 (PB 259 406))

EERC 75-3 "Seismic Risk Analysis for a Site and a Metropolitan Area," by C.S. Oliveira - 1975 (PB 248 134)A09

EERC 75-4 "Analytical Investigations of Seismic Response of Short, Single or Multiple-Span Highway Bridges," by M.-C. Chen and J. Penzien - 1975 (PB 241 454)A09

EERC 75-5 "An Evaluation of Some Methods for Predicting Seismic Behavior of Reinforced Concrete Buildings," by S.A. Mahin and V.V. Bertero - 1975 (PB 246 306)A16

EERC 75-6 "Earthquake Simulator Study of a Steel Frame Structure, Vol. I: Experimental Results," by R.W. Clough and D.T. Tang - 1975 (PB 243 981)A13

EERC 75-7 "Dynamic Properties of San Bernardino Intake Tower," by D. Rea, C.-Y. Liaw and A.K. Chopra - 1975 (AD/A008 406) A05

EERC 75-8 "Seismic Studies of the Articulation for the Dumbarton Bridge Replacement Structure, Vol. I: Description, Theory and Analytical Modeling of Bridge Components," by F. Baron and R.E. Hamati - 1975 (PB 251 539)A07

EERC 75-9 "Seismic Studies of the Articulation for the Dumbarton Bridge Replacement Structure, Vol. 2: Numerical Studies of Steel and Concrete Girder Alternates," by F. Baron and R.E. Hamati - 1975 (PB 251 540)A10

EERC 75-10 "Static and Dynamic Analysis of Nonlinear Structures," by D.P. Mondkar and G.H. Powell - 1975 (PB 242 434)A08

EERC 75-11 "Hysteretic Behavior of Steel Columns," by E.P. Popov, V.V. Bertero and S. Chandramouli - 1975 (PB 252 365)A11

EERC 75-12 "Earthquake Engineering Research Center Library Printed Catalog," - 1975 (PB 243 711)A26

EERC 75-13 "Three Dimensional Analysis of Building Systems (Extended Version)," by E.L. Wilson, J.P. Hollings and H.H. Dovey - 1975 (PB 243 989)A07

EERC 75-14 "Determination of Soil Liquefaction Characteristics by Large-Scale Laboratory Tests," by P. De Alba, C.K. Chan and H.B. Seed - 1975 (NUREG 0027)A08

EERC 75-15 "A Literature Survey - Compressive, Tensile, Bond and Shear Strength of Masonry," by R.L. Mayes and R.W. Clough - 1975 (PB 246 292)A10

EERC 75-16 "Hysteretic Behavior of Ductile Moment Resisting Reinforced Concrete Frame Components," by V.V. Bertero and E.P. Popov - 1975 (PB 246 388)A05

EERC 75-17 "Relationships Between Maximum Acceleration, Maximum Velocity, Distance from Source, Local Site Conditions for Moderately Strong Earthquakes," by H.B. Seed, R. Murarka, J. Lysmer and I.M. Idriss - 1975 (PB 248 172)A03

EERC 75-18 "The Effects of Method of Sample Preparation on the Cyclic Stress-Strain Behavior of Sands," by J. Mulilis, C.K. Chan and H.B. Seed - 1975 (Summarized in EERC 75-28)

EERC 75-19 "The Seismic Behavior of Critical Regions of Reinforced Concrete Components as Influenced by Moment, Shear and Axial Force," by M.B. Atalay and J. Penzien - 1975 (PB 258 842)A11

EERC 75-20 "Dynamic Properties of an Eleven Story Masonry Building," by R.M. Stephen, J.P. Hollings, J.G. Bouwkamp and D. Jurukovski - 1975 (PB 246 945)A04

EERC 75-21 "State-of-the-Art in Seismic Strength of Masonry - An Evaluation and Review," by R.L. Mayes and R.W. Clough 1975 (PB 249 040)A07

EERC 75-22 "Frequency Dependent Stiffness Matrices for Viscoelastic Half-Plane Foundations," by A.K. Chopra, P. Chakrabarti and G. Dasgupta - 1975 (PB 248 121)A07

EERC 75-23 "Hysteretic Behavior of Reinforced Concrete Framed Walls," by T.Y. Wong, V.V. Bertero and E.P. Popov - 1975

EERC 75-24 "Testing Facility for Subassemblages of Frame-Wall Structural Systems," by V.V. Bertero, E.P. Popov and T. Endo - 1975

EERC 75-25 "Influence of Seismic History on the Liquefaction Characteristics of Sands," by H.B. Seed, K. Mori and C.K. Chan - 1975 (Summarized in EERC 75-28)

EERC 75-26 "The Generation and Dissipation of Pore Water Pressures during Soil Liquefaction," by H.B. Seed, P.P. Martin and J. Lysmer - 1975 (PB 252 648)A03

EERC 75-27 "Identification of Research Needs for Improving Aseismic Design of Building Structures," by V.V. Bertero 1975 (PB 248 136)A05

EERC 75-28 "Evaluation of Soil Liquefaction Potential during Earthquakes," by H.B. Seed, I. Arango and C.K. Chan - 1975 (NUREG 0026)A13

EERC 75-29 "Representation of Irregular Stress Time Histories by Equivalent Uniform Stress Series in Liquefaction Analyses," by H.B. Seed, I.M. Idriss, F. Makdisi and N. Banerjee - 1975 (PB 252 635)A03

EERC 75-30 "FLUSH - A Computer Program for Approximate 3-D Analysis of Soil-Structure Interaction Problems," by J. Lysmer, T. Udaka, C.-F. Tsai and H.B. Seed - 1975 (PB 259 332)A07

EERC 75-31 "ALUSH - A Computer Program for Seismic Response Analysis of Axisymmetric Soil-Structure Systems," by E. Berger, J. Lysmer and H.B. Seed - 1975

EERC 75-32 "TRIP and TRAVEL - Computer Programs for Soil-Structure Interaction Analysis with Horizontally Travelling Waves," by T. Udaka, J. Lysmer and H.B. Seed - 1975

EERC 75-33 "Predicting the Performance of Structures in Regions of High Seismicity," by J. Penzien - 1975 (PB 248 130)A03

EERC 75-34 "Efficient Finite Element Analysis of Seismic Structure - Soil - Direction," by J. Lysmer, H.B. Seed, T. Udaka, R.N. Hwang and C.-F. Tsai - 1975 (PB 253 570)A03

EERC 75-35 "The Dynamic Behavior of a First Story Girder of a Three-Story Steel Frame Subjected to Earthquake Loading," by R.W. Clough and L.-Y. Li - 1975 (PB 248 841)A05

EERC 75-36 "Earthquake Simulator Study of a Steel Frame Structure, Volume II - Analytical Results," by D.T. Tang - 1975 (PB 252 926)A10

EERC 75-37 "ANSR-I General Purpose Computer Program for Analysis of Non-Linear Structural Response," by D.P. Mondkar and G.H. Powell - 1975 (PB 252 386)A08

EERC 75-38 "Nonlinear Response Spectra for Probabilistic Seismic Design and Damage Assessment of Reinforced Concrete Structures," by M. Murakami and J. Penzien - 1975 (PB 259 530)A05

EERC 75-39 "Study of a Method of Feasible Directions for Optimal Elastic Design of Frame Structures Subjected to Earthquake Loading," by N.D. Walker and K.S. Pister - 1975 (PB 257 781)A06

EERC 75-40 "An Alternative Representation of the Elastic-Viscoelastic Analogy," by G. Dasgupta and J.L. Sackman - 1975 (PB 252 173)A03

EERC 75-41 "Effect of Multi-Directional Shaking on Liquefaction of Sands," by H.B. Seed, R. Pyke and G.R. Martin - 1975 (PB 258 781)A03

EERC 76-1 "Strength and Ductility Evaluation of Existing Low-Rise Reinforced Concrete Buildings - Screening Method," by T. Okada and B. Bresler - 1976 (PB 257 906)A11

EERC 76-2 "Experimental and Analytical Studies on the Hysteretic Behavior of Reinforced Concrete Rectangular and T-Beams," by S.-Y.M. Ma, E.P. Popov and V.V. Bertero - 1976 (PB 260 843)A12

EERC 76-3 "Dynamic Behavior of a Multistory Triangular-Shaped Building," by J. Petrovski, R.M. Stephen, E. Gartenbaum and J.G. Bouwkamp - 1976 (PB 273 279)A07

EERC 76-4 "Earthquake Induced Deformations of Earth Dams," by N. Serff, H.B. Seed, F.I. Makdisi & C.-Y. Chang - 1976 (PB 292 065)A08

EERC 76-5 "Analysis and Design of Tube-Type Tall Building Structures," by H. de Clercq and G.H. Powell - 1976 (PB 252 220) A10

EERC 76-6 "Time and Frequency Domain Analysis of Three-Dimensional Ground Motions, San Fernando Earthquake," by T. Kubo and J. Penzien (PB 260 556)A11

EERC 76-7 "Expected Performance of Uniform Building Code Design Masonry Structures," by R.L. Mayes, Y. Omote, S.W. Chen and R.W. Clough - 1976 (PB 270 098)A05

EERC 76-8 "Cyclic Shear Tests of Masonry Piers, Volume 1 - Test Results," by R.L. Mayes, Y. Omote, R.W. Clough - 1976 (PB 264 424)A06

EERC 76-9 "A Substructure Method for Earthquake Analysis of Structure - Soil Interaction," by J.A. Gutierrez and A.K. Chopra - 1976 (PB 257 783)A08

EERC 76-10 "Stabilization of Potentially Liquefiable Sand Deposits using Gravel Drain Systems," by H.B. Seed and J.R. Booker - 1976 (PB 258 820)A04

EERC 76-11 "Influence of Design and Analysis Assumptions on Computed Inelastic Response of Moderately Tall Frames," by G.H. Powell and D.G. Row - 1976 (PB 271 409)A06

EERC 76-12 "Sensitivity Analysis for Hysteretic Dynamic Systems: Theory and Applications," by D. Ray, K.S. Pister and E. Polak - 1976 (PB 262 859)A04

EERC 76-13 "Coupled Lateral Torsional Response of Buildings to Ground Shaking," by C.L. Kan and A.K. Chopra - 1976 (PB 257 907)A09

EERC 76-14 "Seismic Analyses of the Banco de America," by V.V. Bertero, S.A. Mahin and J.A. Hollings - 1976

EERC 76-15 "Reinforced Concrete Frame 2: Seismic Testing and Analytical Correlation," by R.W. Clough and J. Gidwani - 1976 (PB 261 323)A08

EERC 76-16 "Cyclic Shear Tests of Masonry Piers, Volume 2 - Analysis of Test Results," by R.L. Mayes, Y. Omote and R.W. Clough - 1976

EERC 76-17 "Structural Steel Bracing Systems: Behavior Under Cyclic Loading," by E.P. Popov, K. Takanashi and C.W. Roeder - 1976 (PB 260 715)A05

EERC 76-18 "Experimental Model Studies on Seismic Response of High Curved Overcrossings," by D. Williams and W.G. Godden - 1976 (PB 269 548)A08

EERC 76-19 "Effects of Non-Uniform Seismic Disturbances on the Dumbarton Bridge Replacement Structure," by F. Baron and R.E. Hamati - 1976 (PB 282 981)A16

EERC 76-20 "Investigation of the Inelastic Characteristics of a Single Story Steel Structure Using System Identification and Shaking Table Experiments," by V.C. Matzen and H.D. McNiven - 1976 (PB 258 453)A07

EERC 76-21 "Capacity of Columns with Splice Imperfections," by E.P. Popov, R.M. Stephen and R. Philbrick - 1976 (PB 260 378)A04

EERC 76-22 "Response of the Olive View Hospital Main Building during the San Fernando Earthquake," by S. A. Mahin, V.V. Bertero, A.K. Chopra and R. Collins - 1976 (PB 271 425)A14

EERC 76-23 "A Study on the Major Factors Influencing the Strength of Masonry Prisms," by N.M. Mostaghel, R.L. Mayes, R. W. Clough and S.W. Chen - 1976 (Not published)

EERC 76-24 "GADFLEA - A Computer Program for the Analysis of Pore Pressure Generation and Dissipation during Cyclic or Earthquake Loading," by J.R. Booker, M.S. Rahman and H.B. Seed - 1976 (PB 263 947)A04

EERC 76-25 "Seismic Safety Evaluation of a R/C School Building," by B. Bresler and J. Axley - 1976

EERC 76-26 "Correlative Investigations on Theoretical and Experimental Dynamic Behavior of a Model Bridge Structure," by K. Kawashima and J. Penzien - 1976 (PB 263 388)A11

EERC 76-27 "Earthquake Response of Coupled Shear Wall Buildings," by T. Srichatrapimuk - 1976 (PB 265 157)A07

EERC 76-28 "Tensile Capacity of Partial Penetration Welds," by E.P. Popov and R.M. Stephen - 1976 (PB 262 899)A03

EERC 76-29 "Analysis and Design of Numerical Integration Methods in Structural Dynamics," by H.M. Hilber - 1976 (PB 264 410)A06

EERC 76-30 "Contribution of a Floor System to the Dynamic Characteristics of Reinforced Concrete Buildings," by L.E. Malik and V.V. Bertero - 1976 (PB 272 247)A13

EERC 76-31 "The Effects of Seismic Disturbances on the Golden Gate Bridge," by F. Baron, M. Arikan and R.E. Hamati - 1976 (PB 272 279)A09

EERC 76-32 "Infilled Frames in Earthquake Resistant Construction," by R.E. Klingner and V.V. Bertero - 1976 - (PB 265 892)A13

UCB/EERC-77/01 "PLUSH - A Computer Program for Probabilistic Finite Element Analysis of Seismic Soil-Structure Interaction," by M.P. Romo Organista, J. Lysmer and H.B. Seed - 1977

UCB/EERC-77/02 "Soil-Structure Interaction Effects at the Humboldt Bay Power Plant in the Ferndale Earthquake of June 7, 1975," by J.E. Valera, H.B. Seed, C.F. Tsai and J. Lysmer - 1977 (PB 265 795)A04

UCB/EERC-77/03 "Influence of Sample Disturbance on Sand Response to Cyclic Loading," by K. Mori, H.B. Seed and C.K. Chan - 1977 (PB 267 352)A04

UCB/EERC-77/04 "Seismological Studies of Strong Motion Records," by J. Shoja-Taheri - 1977 (PB 269 655)A10

UCB/EERC-77/05 "Testing Facility for Coupled-Shear Walls," by L. Li-Hyung, V.V. Bertero and E.P. Popov - 1977

UCB/EERC-77/06 "Developing Methodologies for Evaluating the Earthquake Safety of Existing Buildings," by No. 1 - B. Bresler; No. 2 - B. Bresler, T. Okada and D. Zisling; No. 3 - T. Okada and B. Bresler; No. 4 - V.V. Bertero and B. Bresler - 1977 (PB 267 354)A08

UCB/EERC-77/07 "A Literature Survey - Transverse Strength of Masonry Walls," by Y. Omote, R.L. Mayes, S.W. Chen and R.W. Clough - 1977 (PB 277 933)A07

UCB/EERC-77/08 "DRAIN-TABS: A Computer Program for Inelastic Earthquake Response of Three Dimensional Buildings," by R. Guendelman-Israel and G.H. Powell - 1977 (PB 270 693)A07

UCB/EERC-77/09 "SUBWALL: A Special Purpose Finite Element Computer Program for Practical Elastic Analysis and Design of Structural Walls with Substructure Option," by D.Q. Le, H. Peterson and E.P. Popov - 1977 (PB 270 567)A05

UCB/EERC-77/10 "Experimental Evaluation of Seismic Design Methods for Broad Cylindrical Tanks," by D.P. Clough (PB 272 280)A13

UCB/EERC-77/11 "Earthquake Engineering Research at Berkeley - 1976," - 1977 (PB 273 507)A09

UCB/EERC-77/12 "Automated Design of Earthquake Resistant Multistory Steel Building Frames," by N.D. Walker, Jr. - 1977 (PB 276 526)A09

UCB/EERC-77/13 "Concrete Confined by Rectangular Hoops Subjected to Axial Loads," by J. Vallenas, V.V. Bertero and E.P. Popov - 1977 (PB 275 165)A06

UCB/EERC-77/14 "Seismic Strain Induced in the Ground During Earthquakes," by Y. Sugimura - 1977 (PB 284 201)A04

UCB/EERC-77/15 "Bond Deterioration under Generalized Loading," by V.V. Bertero, E.P. Popov and S. Viwathanatepa - 1977

UCB/EERC-77/16 "Computer Aided Optimum Design of Ductile Reinforced Concrete Moment Resisting Frames," by S.W. Zagajeski and V.V. Bertero - 1977 (PB 280 137)A07

UCB/EERC-77/17 "Earthquake Simulation Testing of a Stepping Frame with Energy-Absorbing Devices," by J.M. Kelly and D.F. Tsztoo - 1977 (PB 273 506)A04

UCB/EERC-77/18 "Inelastic Behavior of Eccentrically Braced Steel Frames under Cyclic Loadings," by C.W. Roeder and E.P. Popov - 1977 (PB 275 526)A15

UCB/EERC-77/19 "A Simplified Procedure for Estimating Earthquake-Induced Deformations in Dams and Embankments," by F.I. Makdisi and H.B. Seed - 1977 (PB 276 820)A04

UCB/EERC-77/20 "The Performance of Earth Dams during Earthquakes," by H.B. Seed, F.I. Makdisi and P. de Alba - 1977 (PB 276 821)A04

UCB/EERC-77/21 "Dynamic Plastic Analysis Using Stress Resultant Finite Element Formulation," by P. Lukkunapvasit and J.M. Kelly - 1977 (PB 275 453)A04

UCB/EERC-77/22 "Preliminary Experimental Study of Seismic Uplift of a Steel Frame," by R.W. Clough and A.A. Huckelbridge 1977 (PB 278 769)A08

UCB/EERC-77/23 "Earthquake Simulator Tests of a Nine-Story Steel Frame with Columns Allowed to Uplift," by A.A. Huckelbridge - 1977 (PB 277 944)A09

UCB/EERC-77/24 "Nonlinear Soil-Structure Interaction of Skew Highway Bridges," by M.-C. Chen and J. Penzien - 1977 (PB 276 176)A07

UCB/EERC-77/25 "Seismic Analysis of an Offshore Structure Supported on Pile Foundations," by D.D.-N. Liou and J. Penzien 1977 (PB 283 180)A06

UCB/EERC-77/26 "Dynamic Stiffness Matrices for Homogeneous Viscoelastic Half-Planes," by G. Dasgupta and A.K. Chopra - 1977 (PB 279 654)A06

UCB/EERC-77/27 "A Practical Soft Story Earthquake Isolation System," by J.M. Kelly, J.M. Eidinger and C.J. Derham - 1977 (PB 276 814)A07

UCB/EERC-77/28 "Seismic Safety of Existing Buildings and Incentives for Hazard Mitigation in San Francisco: An Exploratory Study," by A.J. Meltsner - 1977 (PB 281 970)A05

UCB/EERC-77/29 "Dynamic Analysis of Electrohydraulic Shaking Tables," by D. Rea, S. Abedi-Hayati and Y. Takahashi 1977 (PB 282 569)A04

UCB/EERC-77/30 "An Approach for Improving Seismic - Resistant Behavior of Reinforced Concrete Interior Joints," by B. Galunic, V.V. Bertero and E.P. Popov - 1977 (PB 290 870)A06

UCB/EERC-78/01 "The Development of Energy-Absorbing Devices for Aseismic Base Isolation Systems," by J.M. Kelly and D.F. Tsztoo - 1978 (PB 284 978)A04

UCB/EERC-78/02 "Effect of Tensile Prestrain on the Cyclic Response of Structural Steel Connections, by J.G. Bouwkamp and A. Mukhopadhyay - 1978

UCB/EERC-78/03 "Experimental Results of an Earthquake Isolation System using Natural Rubber Bearings," by J.M. Eidinger and J.M. Kelly - 1978 (PB 281 686)A04

UCB/EERC-78/04 "Seismic Behavior of Tall Liquid Storage Tanks," by A. Niwa - 1978 (PB 284 017)A14

UCB/EERC-78/05 "Hysteretic Behavior of Reinforced Concrete Columns Subjected to High Axial and Cyclic Shear Forces," by S.W. Zagajeski, V.V. Bertero and J.G. Bouwkamp - 1978 (PB 283 858)A13

UCB/EERC-78/06 "Inelastic Beam-Column Elements for the ANSR-I Program," by A. Riahi, D.G. Row and G.H. Powell - 1978

UCB/EERC-78/07 "Studies of Structural Response to Earthquake Ground Motion," by O.A. Lopez and A.K. Chopra - 1978 (PB 282 790)A05

UCB/EERC-78/08 "A Laboratory Study of the Fluid-Structure Interaction of Submerged Tanks and Caissons in Earthquakes," by R.C. Byrd - 1978 (PB 284 957)A08

UCB/EERC-78/09 "Model for Evaluating Damageability of Structures," by I. Sakamoto and B. Bresler - 1978

UCB/EERC-78/10 "Seismic Performance of Nonstructural and Secondary Structural Elements," by I. Sakamoto - 1978

UCB/EERC-78/11 "Mathematical Modelling of Hysteresis Loops for Reinforced Concrete Columns," by S. Nakata, T. Sproul and J. Penzien - 1978

UCB/EERC-78/12 "Damageability in Existing Buildings," by T. Blejwas and B. Bresler - 1978

UCB/EERC-78/13 "Dynamic Behavior of a Pedestal Base Multistory Building," by R.M. Stephen, E.L. Wilson, J.G. Bouwkamp and M. Button - 1978 (PB 286 650)A08

UCB/EERC-78/14 "Seismic Response of Bridges - Case Studies," by R.A. Imbsen, V. Nutt and J. Penzien - 1978 (PB 286 503)A10

UCB/EERC-78/15 "A Substructure Technique for Nonlinear Static and Dynamic Analysis," by D.G. Row and G.H. Powell - 1978 (PB 288 077)A10

UCB/EERC-78/16 "Seismic Risk Studies for San Francisco and for the Greater San Francisco Bay Area," by C.S. Oliveira - 1978

UCB/EERC-78/17 "Strength of Timber Roof Connections Subjected to Cyclic Loads," by P. Gülkan, R.L. Mayes and R.W. Clough - 1978

UCB/EERC-78/18 "Response of K-Braced Steel Frame Models to Lateral Loads," by J.G. Bouwkamp, R.M. Stephen and E.P. Popov - 1978

UCB/EERC-78/19 "Rational Design Methods for Light Equipment in Structures Subjected to Ground Motion," by J.L. Sackman and J.M. Kelly - 1978 (PB 292 357)A04

UCB/EERC-78/20 "Testing of a Wind Restraint for Aseismic Base Isolation," by J.M. Kelly and D.E. Chitty - 1978 (PB 292 833)A03

UCB/EERC-78/21 "APOLLO - A Computer Program for the Analysis of Pore Pressure Generation and Dissipation in Horizontal Sand Layers During Cyclic or Earthquake Loading," by P.P. Martin and H.B. Seed - 1978 (PB 292 835)A04

UCB/EERC-78/22 "Optimal Design of an Earthquake Isolation System," by M.A. Bhatti, K.S. Pister and E. Polak - 1978 (PB 294 735)A06

UCB/EERC-78/23 "MASH - A Computer Program for the Non-Linear Analysis of Vertically Propagating Shear Waves in Horizontally Layered Deposits," by P.P. Martin and H.B. Seed - 1978 (PB 293 101)A05

UCB/EERC-78/24 "Investigation of the Elastic Characteristics of a Three Story Steel Frame Using System Identification," by I. Kaya and H.D. McNiven - 1978

UCB/EERC-78/25 "Investigation of the Nonlinear Characteristics of a Three-Story Steel Frame Using System Identification," by I. Kaya and H.D. McNiven - 1978

UCB/EERC-78/26 "Studies of Strong Ground Motion in Taiwan," by Y.M. Hsiung, B.A. Bolt and J. Penzien - 1978

UCB/EERC-78/27 "Cyclic Loading Tests of Masonry Single Piers: Volume 1 - Height to Width Ratio of 2," by P.A. Hidalgo, R.L. Mayes, H.D. McNiven and R.W. Clough - 1978

UCB/EERC-78/28 "Cyclic Loading Tests of Masonry Single Piers: Volume 2 - Height to Width Ratio of 1," by S.-W.J. Chen, P.A. Hidalgo, R.L. Mayes, R.W. Clough and H.D. McNiven - 1978

UCB/EERC-78/29 "Analytical Procedures in Soil Dynamics," by J. Lysmer - 1978

UCB/EERC-79/01 "Hysteretic Behavior of Lightweight Reinforced Concrete Beam-Column Subassemblages," by B. Forzani, E.P. Popov, and V.V. Bertero - 1979

UCB/EERC-79/02 "The Development of a Mathematical Model to Predict the Flexural Response of Reinforced Concrete Beams to Cyclic Loads, Using System Identification," by J.F. Stanton and H.D. McNiven - 1979

UCB/EERC-79/03 "Linear and Nonlinear Earthquake Response of Simple Torsionally Coupled Systems," by C.L. Kan and A.K. Chopra - 1979

UCB/EERC-79/04 "A Mathematical Model of Masonry for Predicting Its Linear Seismic Response Characteristics," by Y. Mengi and H.D. McNiven - 1979

UCB/EERC-79/05 "Mechanical Behavior of Lightweight Concrete Confined by Different Types of Lateral Reinforcement," by M.A. Manrique, V.V. Bertero and E.P. Popov - 1979

UCB/EERC-79/06 "Static Tilt Tests of a Tall Cylindrical Liquid Storage Tank," by R.W. Clough and A. Niwa - 1979

UCB/EERC-79/07 "The Design of Steel Energy Absorbing Restrainers and Their Incorporation Into Nuclear Power Plants for Enhanced Safety: Volume 1 - Summary Report," by P.N. Spencer, V.F. Zackay, and E.R. Parker - 1979

UCB/EERC-79/08 "The Design of Steel Energy Absorbing Restrainers and Their Incorporation Into Nuclear Power Plants for Enhanced Safety: Volume 2 - The Development of Analyses for Reactor System Piping," "Simple Systems" by M.C. Lee, J. Penzien, A.K. Chopra, and K. Suzuki "Complex Systems" by G.H. Powell, E.L. Wilson, R.W. Clough and D.G. Row - 1979

UCB/EERC-79/09 "The Design of Steel Energy Absorbing Restrainers and Their Incorporation Into Nuclear Power Plants for Enhanced Safety: Volume 3 - Evaluation of Commerical Steels," by W.S. Owen, R.M.N. Pelloux, R.O. Ritchie, M. Faral, T. Ohhashi, J. Toplosky, S.J. Hartman, V.F. Zackay, and E.R. Parker - 1979

UCB/EERC-79/10 "The Design of Steel Energy Absorbing Restrainers and Their Incorporation Into Nuclear Power Plants for Enhanced Safety: Volume 4 - A Review of Energy-Absorbing Devices," by J.M. Kelly and M.S. Skinner - 1979

UCB/EERC-79/11 "Conservatism In Summation Rules for Closely Spaced Modes," by J.M. Kelly and J.L. Sackman - 1979

UCB/EERC-79/12	"Cyclic Loading Tests of Masonry Single Piers Volume 3 - Height to Width Ratio of 0.5," by P.A. Hidalgo, R.L. Mayes, H.D. McNiven and R.W. Clough - 1979
UCB/EERC-79/13	"Cyclic Behavior of Dense Coarse-Grained Materials in Relation to the Seismic Stability of Dams," by N.G. Banerjee, H.B. Seed and C.K. Chan - 1979
UCB/EERC-79/14	"Seismic Behavior of Reinforced Concrete Interior Beam-Column Subassemblages," by S. Viwathanatepa, E.P. Popov and V.V. Bertero - 1979
UCB/EERC-79/15	"Optimal Design of Localized Nonlinear Systems with Dual Performance Criteria Under Earthquake Excitations," by M.A. Bhatti - 1979
UCB/EERC-79/16	"OPTDYN - A General Purpose Optimization Program for Problems with or without Dynamic Constraints," by M.A. Bhatti, E. Polak and K.S. Pister - 1979
UCB/EERC-79/17	"ANSR-II, Analysis of Nonlinear Structural Response, Users Manual," by D.P. Mondkar and G.H. Powell - 1979
UCB/EERC-79/18	"Soil Structure Interaction in Different Seismic Environments," A. Gomez-Masso, J. Lysmer, J.-C. Chen and H.B. Seed - 1979
UCB/EERC-79/19	"ARMA Models for Earthquake Ground Motions," by M.K. Chang, J.W. Kwiatkowski, R.F. Nau, R.M. Oliver and K.S. Pister - 1979
UCB/EERC-79/20	"Hysteretic Behavior of Reinforced Concrete Structural Walls," by J.M. Vallenas, V.V. Bertero and E.P. Popov - 1979
UCB/EERC-79/21	"Studies on High-Frequency Vibrations of Buildings I: The Column Effects," by J. Lubliner - 1979
UCB/EERC-79/22	"Effects of Generalized Loadings on Bond Reinforcing Bars Embedded in Confined Concrete Blocks," by S. Viwathanatepa, E.P. Popov and V.V. Bertero - 1979
UCB/EERC-79/23	"Shaking Table Study of Single-Story Masonry Houses, Volume 1: Test Structures 1 and 2," by P. Gülkan, R.L. Mayes and R.W. Clough - 1979
UCB/EERC-79/24	"Shaking Table Study of Single-Story Masonry Houses, Volume 2: Test Structures 3 and 4," by P. Gülkan, R.L. Mayes and R.W. Clough - 1979
UCB/EERC-79/25	"Shaking Table Study of Single-Story Masonry Houses, Volume 3: Summary, Conclusions and Recommendations," by R.W. Clough, R.L. Mayes and P. Gülkan - 1979

UCB/EERC-79/26 "Recommendations for a U.S.-Japan Cooperative Research Program Utilizing Large-Scale Testing Facilities," by U.S.-Japan Planning Group - 1979

UCB/EERC-79/27 "Earthquake-Induced Liquefaction Near Lake Amatitlan, Guatemala," by H.B. Seed, I. Arango, C.K. Chan, A. Gomez-Masso and R. Grant de Ascoli - 1979

UCB/EERC-79/28 "Infill Panels: Their Influence on Seismic Response of Buildings," by J.W. Axley and V.V. Bertero - 1979

UCB/EERC-79/29 "3D Truss Bar Element (Type 1) for the ANSR-II Program," by D.P. Mondkar and G.H. Powell - 1979

UCB/EERC-79/30 "2D Beam-Column Element (Type 5 - Parallel Element Theory) for the ANSR-II Program," by D.G. Row, G.H. Powell and D.P. Mondkar

UCB/EERC-79/31 "3D Beam-Column Element (Type 2 - Parallel Element Theory) for the ANSR-II Program," by A. Riahi, G.H. Powell and D.P. Mondkar - 1979

UCB/EERC-79/32 "On Response of Structures to Stationary Excitation," by A. Der Kiureghian - 1979

UCB/EERC-79/33 "Undisturbed Sampling and Cyclic Load Testing of Sands," by S. Singh, H.B. Seed and C.K. Chan - 1979

UCB/EERC-79/34 "Interaction Effects of Simultaneous Torsional and Compressional Cyclic Loading of Sand," by P.M. Griffin and W.N. Houston - 1979

UCB/EERC-80/01 "Earthquake Response of Concrete Gravity Dams Including Hydrodynamic and Foundation Interaction Effects," by A.K. Chopra, P. Chakrabarti and S. Gupta - 1980

UCB/EERC-80/02 "Rocking Response of Rigid Blocks to Earthquakes," by C.S. Yim, A.K. Chopra and J. Penzien - 1980

UCB/EERC-80/03 "Optimum Inelastic Design of Seismic-Resistant Reinforced Concrete Frame Structures," by S.W. Zagajeski and V.V. Bertero - 1980

UCB/EERC-80/04 "Effects of Amount and Arrangement of Wall-Panel Reinforcement on Hysteretic Behavior of Reinforced Concrete Walls," by R. Iliya and V.V. Bertero - 1980

UCB/EERC-80/05 "Shaking Table Research on Concrete Dam Models," by A. Niwa and R.W. Clough - 1980

UCB/EERC-80/06 "Piping With Energy Absorbing Restrainers: Parameter Study on Small Systems," by G.H. Powell, C. Oughourlian and J. Simons - 1980

UCB/EERC-80/07 "Inelastic Torsional Response of Structures Subjected to Earthquake Ground Motions," by Y. Yamazaki - 1980

UCB/EERC-80/08 "Study of X-Braced Steel Frame Structures Under Earthquake Simulation," by Y. Ghanaat - 1980

UCB/EERC-80/09 "Hybrid Modelling of Soil-Structure Interaction," by S. Gupta, T.W. Lin, J. Penzien and C.S. Yeh - 1980

UCB/EERC-80/10 "General Applicability of a Nonlinear Model of a One Story Steel Frame," by B.I. Sveinsson and H. McNiven - 1980

UCB/EERC-80/11 "A Green-Function Method for Wave Interaction with a Submerged Body," by W. Kioka - 1980

UCB/EERC-80/12 "Hydrodynamic Pressure and Added Mass for Axisymmetric Bodies," by F. Nilrat - 1980

UCB/EERC-80/13 "Treatment of Non-Linear Drag Forces Acting on Offshore Platforms," by B.V. Dao and J. Penzien - 1980

UCB/EERC-80/14 "2D Plane/Axisymmetric Solid Element (Type 3 - Elastic or Elastic-Perfectly Plastic) for the ANSR-II Program," by D.P. Mondkar and G.H. Powell - 1980

UCB/EERC-80/15 "A Response Spectrum Method for Random Vibrations," by A. Der Kiureghian - 1980

UCB/EERC-80/16 "Cyclic Inelastic Buckling of Tubular Steel Braces," by V.A. Zayas, E.P. Popov and S.A. Mahin - June 1980

UCB/EERC-80/17 "Dynamic Response of Simple Arch Dams Including Hydrodynamic Interaction," by C.S. Porter and A.K. Chopra - July 1980

UCB/EERC-80/18 "Experimental Testing of a Friction Damped Aseismic Base Isolation System with Fail-Safe Characteristics," by J.M. Kelly, K.E. Beucke and M.S. Skinner - July 1980

UCB/EERC-80/19 "The Design of Steel Energy-Absorbing Restrainers and their Incorporation into Nuclear Power Plants for Enhanced Safety (Vol 1B): Stochastic Seismic Analyses of Nuclear Power Plant Structures and Piping Systems Subjected to Multiple Support Excitations," by M.C. Lee and J. Penzien - 1980

UCB/EERC-80/20 "The Design of Steel Energy-Absorbing Restrainers and their Incorporation into Nuclear Power Plants for Enhanced Safety (Vol 1C): Numerical Method for Dynamic Substructure Analysis," by J.M. Dickens and E.L. Wilson - 1980

UCB/EERC-80/21 "The Design of Steel Energy-Absorbing Restrainers and their Incorporation into Nuclear Power Plants for Enhanced Safety (Vol 2): Development and Testing of Restraints for Nuclear Piping Systems," by J.M. Kelly and M.S. Skinner - 1980

UCB/EERC-80/22 "3D Solid Element (Type 4-Elastic or Elastic-Perfectly-Plastic) for the ANSR-II Program," by D.P. Mondkar and G.H. Powell - 1980

UCB/EERC-80/23 "Gap-Friction Element (Type 5) for the ANSR-II Program," by D.P. Mondkar and G.H. Powell - 1980

UCB/EERC-80/24 "U-Bar Restraint Element (Type 11) for the ANSR-II Program," C. Oughourlian and G.H. Powell - 1980

UCB/EERC-80/25 "Testing of a Natural Rubber Base Isolation System by an Explosively Simulated Earthquake," by J.M. Kelly 1980

UCB/EERC-80/26 "Input Identification from Structural Vibrational Response," by Y. Hu - 1980

UCB/EERC-80/27 "Cyclic Inelastic Behavior of Steel Offshore Structures," by V.A. Zayas, S.A. Mahin and E.P. Popov - 1980

UCB/EERC-80/28 "Shaking Table Testing of a Reinforced Concrete Frame with Biaxial Response," M.G. Oliva and R.W. Clough 1980

UCB/EERC-80/29 "Dynamic Properties of a Twelve-Story Prefabricated Panel Building," by J.G. Bouwkamp, J.P. Kollegger and R.M. Stephen - 1980

UCB/EERC-80/30 "Dynamic Properties of a Eight-Story Prefabricated Panel Building," by J.G. Bouwkamp, J.P. Kollegger and R.M. Stephen - 1980

UCB/EERC-80/31 "Predictive Dynamic Response of Panel Type Structures Under Earthquakes," by J.P. Kollegger and J.G. Bouwkamp 1980

UCB/EERC-80/32 "The Design of Steel Energy-Absorbing Restrainers and their Incorporation into Nuclear Power Plants for Enhanced Safety: Vol 3, Testing of Commercial Steels in Low-Cycle Torsional Fatigue," by P. Spencer, E.R. Parker, E. Jongewaard and M. Drory - 1980

UCB/EERC-80/33 "The Design of Steel Energy-Absorbing Restrainers and their Incorporation into Nuclear Power Plants for Enhanced Safety: Vol 4, Shaking Table Tests of Piping Systems with Energy-Absorbing Restrainers," by S.F. Stiemer and W.G. Godden - 1980

UCB/EERC-80/34 "The Design of Steel Energy-Absorbing Restrainers and their Incorporation into Nuclear Power Plants for Enhanced Safety: Vol 5, Summary Report," by P. Spencer 1980

UCB/EERC-80/35 "Experimental Testing of an Energy Absorbing Base Isolation System," by J. Kelly, M.S. Skinner and K.E. Beucke - 1980

UCB/EERC-80/36 "Simulating and Analyzing Artificial Non-Stationary Earthquake Ground Motions," by R.F. Nau, R.M. Oliver and K.S. Pister - 1980

UCB/EERC-80/37 "Earthquake Engineering at Berkeley," - 1980

UCB/EERC-80/38 "Inelastic Seismic Analysis of Large Panel Buildings," by V. Schricker and G.H. Powell - 1980

UCB/EERC-80/39 "Dynamic Response of Embankment, Concrete-Gravity and Arch Dams Including Hydrodynamic Interaction," by J.F. Hall and A.K. Chopra - 1980

UCB/EERC-80/40 "Inelastic Buckling of Steel Strut Under Cyclic Load Reversal," by R.G. Black, W.A. Wenger and E.P. Popov - 1980